COMPUTATIONS ON GAS-DYNAMIC AND PLASMA PHENOMENA IN A FLOWING PARTIALLY IONIZED GAS

by

FEDERICO LUIGI ANGELO DELLAFIORA

A Thesis submitted for the Degree of Doctor of Philosophy

in the University of London

Physics Department,
Imperial College of Science & Technology,
London, SW7 2BZ.

January 1981

This Thesis is Dedicated to

My Father,

ANGELO DELLAFIORA,

and to my Grandmother,

ANGIOLINA LUSIGNANI

Two of the most Wonderful

people I have ever known.

CONTENTS

ABSTRACT

In this thesis a two-dimensional, time-dependent, two-temperature fluid model of a partially ionized plasma in an electromagnetic field is developed and used to study the physical phenomena in a closed cycle MHD generator, which utilizes as a working gas an inert (buffer) gas slightly seeded with an alkali metal. A number of assumptions, the most important being a small seeding fraction and negligibly small indirect interaction between the buffer gas and the electromagnetic field, allow the governing equations to be decoupled and two independent systems of equations obtained: the gas-dynamic equations, which govern the gas density, heavy particle temperature and plasma flow velocity; and the plasma-current equations, which govern the electron and neutral seed atom densities, the electron temperature and the current stream function. The latter equations contain terms relating to finite ion and neutral diffusion, arising from both particle transport and turbulent fluctuations, and a term describing turbulent transport of electron energy.

The gas-dynamic equations are solved numerically to describe the steady-state two-dimensional compressible turbulent boundary layer flow on each side wall of a generator channel, assuming quasi three-dimensional flow in the channel. Computed pressure distributions are in close agreement with experiment when finite leakage of gas through the electrode walls is allowed.

Neglecting inlet relaxation effects and assuming quasi-periodic boundary conditions in the flow direction, the plasma-current equations are solved numerically in a single segment of the generator for fixed gas dynamic profiles. The electrode wall boundary conditions are derived

from a collisionless sheath model of the plasma-wall interaction, including the effects of seed particle adsorption and desorption as well as electron emission by the electrodes. Whilst the continuity equations are time dependent, the electron energy equation, like the current stream-function equation, has a steady-state form in accordance with the assumption of instantaneous electron-temperature relaxation. Numerical results showing the temporal development of local plasma and current properties and global generator parameters are presented, thus allowing the effects of the electrothermal instability, plasma-electrode wall interactions and gas-dynamic boundary layers to be studied.

ACKNOWLEDGEMENTS

The work for this thesis was done while the author was a member of the Imperial College Plasma Physics Group.

The author wishes to thank his supervisor, Dr. M.G. Haines, for many helpful discussions. Thanks are also due to his colleagues and friends; in particular, George Fournier and Michael Psimopoulos.

During the course of this work the author was financed by the Science Research Council.

CHAPTER 1

INTRODUCTION

1.1 MHD ELECTRICAL POWER GENERATION

In magneto hydrodynamic (MHD) power generation a heated electrically conducting fluid is accelerated to a high velocity $\underline{u}$ in a nozzle and passed through a channel located in a magnetic field $\underline{B}$ (see fig. 1.1). Forces acting on the charged particles in the fluid cause charge separation, and an induced electric field $\underline{u} \wedge \underline{B}$ is produced which can drive a current through an external load connected across the channel. Denoting the current density in the fluid by $\underline{J}$, the resultant magnetomotive force $\underline{J} \wedge \underline{B}$ retards the motion of the fluid. Electrical energy is therefore produced at the expense of directed energy of motion of the fluid.

These are, of course, the working principles of conventional generators,nearly all of which utilize a solid conductor which is caused to rotate between the poles of a magnet. However, the use of fluid, rather than solid conductors, allows the elimination of large rotating components thereby reducing mechanical strength requirements. This, together with the necessity to employ high temperatures to achieve acceptable levels of ionization in the fluid, means that the optimum operating temperatures for MHD generators are appreciably higher than for conventional power generator systems. As a consequence, MHD generator systems may be capable of operating at higher thermal efficiencies, leading to improved conservation of natural resources, reduced thermal pollution and lower fuel costs.

MHD generators can be divided into three main types, classification being according to the working fluid and anticipated heat source. Open cycle MHD generators utilize fossil or synthetic liquid or gaseous fuels, burned with oxygen or preheated air to provide combustion products at a high temperature (~2500 to 3000^{o}K). The combustion products are seeded with a small amount (about one atomic percent) of an alkali metal, or a compound of an alkali metal, to give a high electrical conductivity. After passage through the generator channel the gas is either exhausted to the atmosphere or passed through a conventional steam raising plant.

Closed cycle inert gas MHD generators utilize an inert gas coolant of an envisaged high temperature (1500 to 2000 ^{o}K) nuclear reactor as the working fluid. The inert gas is seeded with an alkali metal to give a high plasma conductivity and after passing through the generator, and possibly also a steam raising or gas turbine plant, is recycled to the reactor. The equilibrium conductivity of the plasma at a temperature of 1500^{o}K is not sufficiently high, but by the use of pure monatomic gases the electrical conductivity may be significantly enhanced as a result of non-equilibrium ionization. This effect will be considered later in this chapter.

The third type of MHD generator, the closed cycle liquid metal MHD generator, lies outside the scope of this thesis.

Of the two types of MHD generator described above, open cycle MHD generators are closest to practical realization. As long ago as 1965, operation of a 32 MW alcohol-fueled generator with run times up to three minutes was achieved in the United States[1]. In the Soviet Union tests on a 75 MW (25 MW from MHD and 50 MW from steam) pilot plant burning natural gas, the U-25 experiment, began in 1971.

There are several advantages to closed cycle MHD power generation over open cycle. First, a very pure gas system can be used thereby ensuring that the erosion of channel materials by chemical action is kept to a minimum. Second, the operating gas temperature can be comparatively low (1500 to 2000 ^{o}K), an acceptable level of electrical conductivity being achieved by non-equilibrium ionization due to elevation of the electron temperature above the gas temperature (see section 1.3).

However, in contrast to open cycle MHD power generation, much experimental and theoretical research remains to be done before practical realization of closed cycle MHD power generation can be achieved. This is because of the technological problems[2],[3], involved in the continuous operation of a closed cycle MHD power generator, and the difficulties of realization of a high temperature gas cooled reactor with a coolant temperature of at least 1500^{o}K. Also, numerical modelling of closed cycle MHD generators has yet to reach the degree of sophistication achieved in the case of open cycle MHD power generators[5].

Whilst much progress has been made in solving the aforementioned technological problems[3],[4] relatively little progress have been made in the development of numerical models of the degree of sophistication required for the unique interpretation and accurate prediction of results of experiments performed on closed cycle MHD power generators. The main objective of this thesis is to develop a numerical model of closed cycle MHD generators that incorporates much of the relevant physics previously considered only for open cycle generators, and that can be used to interpret and predict results obtained in experiments performed under certain conditions.

where the flow velocity is taken to be uniform and in the x-direction; i.e., $\underline{u} = (u_x, 0, 0)$, so that, $E_x' = E_x$, $E_y' = E_y - u_x B$ and $E_z' = E_z$. The electrodes in fig. 1.1 are taken to be parallel and attention is restricted to two-dimensional current distributions for which $J_z = 0 = E_z'$ and

$$\beta_e = \left| \frac{\underline{J} \wedge \underline{E}'}{\underline{J} \cdot \underline{E}'} \right|$$

so that the current density is inclined to the total electric field $\underline{E}'$ at the Hall angle $\tan^{-1}\beta_e$.

The electrodes shown in fig. 1.1 are segmented, separate loads being connected between opposed electrode pairs. If, instead, the electrodes are continuous, $E_x' = E_x = 0$ and eqns. (1.3a) and (1.3b) yield

$$J_x = -\frac{\sigma_e}{(1+\beta_e^2)} \beta_e E_y' \tag{1.4a}$$

and

$$J_y = \frac{\sigma_e}{(1+\beta_e^2)} E_y' \tag{1.4b}$$

and the maximum power delivered to the external load per unit volume of the generator P_{max} is given by

$$P_{max} = \frac{\sigma_e u_x^2 B^2}{4(1+\beta_e^2)} \tag{1.5}$$

It is clear from eqns. (1.4) and (1.5) that the Hall effect reduces the magnitude of J_y and P_{max} by a factor of $(1+\beta_e^2)^{-1}$ and results in the appearance of a Hall current which flows downstream in the gas and returns upstream through the electrodes. However, if the electrodes are infinitely finely segmented there can be no x-component of current either in the electrodes or in the gas so that $J_x = 0$. From eqn. (1.3a)

1.2 SIMPLE THEORY OF MHD POWER GENERATORS

The basic theory of operation of a closed cycle MHD generator is very simple. We consider an Ohm's law for a uniform plasma in the form

$$\underline{J} = \sigma_e \underline{E}' - \underline{J} \wedge \underline{\beta}_e \qquad (\underline{\beta}_e = \beta_e \underline{B}/|\underline{B}|) \tag{1.1}$$

where $\underline{E}'$, the electric field in the rest frame of the flowing gas, is given in terms of the electric field $\underline{E}$ in the laboratory frame by the equation

$$\underline{E}' = \underline{E} + \underline{u} \wedge \underline{B} \tag{1.2}$$

The quantities σ_e and β_e are the electron conductivity and electron Hall parameter, respectively (often referred to here as simply the conductivity and Hall parameter). As we shall see in chapter 2, eqn. (1.1) assumes a negligible ion Hall parameter and ion current, and that thermal diffusion effects can be neglected. The second term on the right-hand side of eqn. (1.1) represents the Hall effect, which is usually important, since, for typical generator operating conditions, $\beta_e \gtrsim 1$. Taking the magnetic field to be uniform and in the z-direction, the components of eqn. (1.1) are

$$J_x = \frac{\sigma_e}{(1+\beta_e^2)} \left(E_x' - \beta_e E_y' \right), \tag{1.3a}$$

$$J_y = \frac{\sigma_e}{(1+\beta_e^2)} \left(E_y' + \beta_e E_x' \right), \tag{1.3b}$$

and

$$J_z = \sigma_e E_z', \tag{1.3c}$$

it can be seen that this configuration leads to the build up of an electric field in the x-direction, the so-called Hall field

$$E_x = \beta_e E_y' \tag{1.6}$$

and eqn. (1.3b) gives

$$J_y = \sigma_e E_y' \tag{1.7}$$

which is identical to the y-component of eqn. (1.1) in the absence of the Hall effect. Also P_{max} has the value assumed in the absence of the Hall effect:

$$P_{max} = \frac{\sigma_e u_x^2 B^2}{4} \tag{1.8}$$

The generator configuration described above is called a segmented Faraday generator. However, the action of the Hall effect in building up an axial electric field (see eqn. (1.6)) makes possible another generator configuration, called a Hall generator, in which the axial field is used to drive a current through a load connected between the upstream and downstream electrodes. In this generator configuration opposed electrodes are shorted; i.e., $E_y = 0$, so that, as can be seen from eqn. (1.3a), the voltage developed across a given load is a maximum. The open circuit electric field for the Hall generator is obtained from eqn. (1.3a) as

$$E_x = -\beta_e u_x B$$

and the maximum power density is, in this case, given by

$$P_{max} = \frac{\sigma_e u_x^2 B^2}{4} \frac{\beta_e^2}{(1+\beta_e^2)}$$

which approaches that of a segmented Faraday generator for large Hall parameters.

Descriptions of other possible generator configurations can be found in reference (1). In this thesis attention will be confined to segmented Faraday generators.

1.3 SIMPLIFIED DESCRIPTION OF THE PLASMA STATE

In this thesis the working fluid of the MHD generator is assumed to consist of helium gas (buffer gas), slightly seeded with caesium. For conditions characteristic of MHD generators, the plasma can be assumed to consist of four components: electrons, singly charged seed ions, seed atoms and buffer gas atoms. A simplified model of the plasma is presented in this section; a more complete model will be formulated in chapter 2.

In the flowing plasma of a closed cycle MHD power generator, electrons are accelerated by an induced electric field, and the energy so gained dissipated in elastic collisions with monatomic heavy particles. However, because of the inefficiency of energy exchange in elastic collisions between particles of disparate mass, an appreciable elevation of the electron temperature T_e above the heavy particle temperature T is possible. This electron temperature elevation is described by the electron energy equation (see section 2.5), which, in its simplest form, expresses a balance between the volumetric rate of gain of energy by the electron gas from the electromagnetic field, the Ohmic dissipation $\underline{E}'.\underline{J}$, and the volumetric rate of loss of energy of electrons in elastic collisions with heavy particles, denoted by L_e. Thus we write

$$\underline{E}'.\underline{J} = L_e$$

or, using eqn. (1.1),

$$J^2/\sigma_e = L_e \qquad (1.9)$$

As will be shown in chapter 2 (see eqn. (2.31)), L_e is given by

$$L_e = 3 m_e k_B (T_e - T) \frac{m_e}{m_h} \nu_{eh} \tag{1.10}$$

where ν_{eh} is the electron-buffer gas atom momentum transfer collision frequency given by

$$\nu_{eh} = c_e Q_{eh} n_h \tag{1.11}$$

where c_e is the root mean square speed of electrons $(8 k_B T_e / \pi m_e)^{1/2}$, Q_{eh} is the electron-buffer gas atom momentum transfer cross-section, and n_h is the buffer gas atom number density. The electron conductivity σ_e and electron Hall parameter β_e are shown in chapter 2 (see eqns. (2.209) and (2.111)) to be given by

$$\sigma_e = n_e e^2 / m_e \nu_{eh} \tag{1.12}$$

and

$$\beta_e = eB / m_e \nu_{eh} \tag{1.13}$$

In general, the electron energy equation in the form of eqn. (1.9) is valid only if the plasma is in a uniform and steady state. As will be seen in chapter 2, the free electron density is in this case given by the Saha equation; that is,

$$n_e^2 = (n_{n_0} - n_e) \left[\frac{2\pi m_e k_B T_e}{h^2} \right]^{3/2} \exp \left[- \frac{e V_I}{k_B T_e} \right] \tag{1.14}$$

the validity of which will be discussed further in chapter 2 (see section 2.5). In eqn. (1.14), the seed atom density n_n is written in the form

$$n_n = n_{n_0} - n_e$$

where n_{no} is the seed atom density of the unionized gas, it being assumed that the plasma is quasi-neutral. The density n_{no} is a free parameter, the value of which is specified by giving the seeding fraction χ , where

$$\chi = \frac{n_{no}}{n_h} = \frac{n_n + n_e}{n_h} \tag{1.15}$$

The seeding fraction is generally small for closed cycle MHD generators. The reason for this is the relatively large electron-seed atom cross-section for momentum transfer, which results in a decrease of σ_e with increasing χ for quite small values of χ , the electron-seed atom momentum transfer collision frequency being added to ν_{eh} in eqn. (1.12). This decrease of σ_e with increasing χ is due to the increase of total electron collision frequency dominating the increase of electron density in eqn. (1.12). For a given heavy particle temperature T and pressure p , and a given T_e , there exists a maximum in $\sigma_e(\chi)$ at a small value of χ . Typical seeding fractions used in experiments, and therefore used in this thesis, are small enough for the effects of electron-seed atom collisions to be completely negligible. However, there remains the possibility that electron-electron or electron-ion (Coulomb) collisions can be important. This will be considered in detail in chapter 2, where it will be shown that the assumption that electron-buffer gas atom collisions dominate Coulomb collisions, which is made here, is justified only for sufficiently low electron temperatures.

Using eqns. (1.10) - (1.15) one can calculate the parameters T_e, n_e, n_n, σ_e and β_e , so that the plasma state is fully defined for a given $|\underline{J}|$, p, T and χ . We consider as an example the current

density in a segmented electrode generator flowing under short circuit conditions:

$$J_y = -\sigma_e u_x B$$

which is obtained from eqn. (1.7) by setting $E_y = 0$. Eqn. (1.9) yields a quadratic for $(\bar{T}_e/T)$ whose physically significant root is given by

$$\frac{\bar{T}_e}{T} = \frac{1}{2}\left\{1 + \sqrt{1 + \frac{e^2 u_x^2 B^2 \pi m_h}{6p^2 m_e Q_{eh}^2}}\right\} \qquad (1.16)$$

Taking $B = 0.1\ T$, $u_x = 1200\ m.sec^{-1}$, $p = 8.32 \times 10^4\ N\,m^{-2}$, $\chi = 0.002$, and $T = 1500^\circ K$, eqn. (1.16) yields $T_e = 1783^\circ K$ and, from eqns. (1.12) and (1.14), we find that $n_e = 3.8 \times 10^{18}\ m^{-3}$ and $\sigma_e = 118\ mho.m^{-1}$. The equilibrium values of n_e and σ_e, obtained by setting $\bar{T}_e = T = 1500^\circ K$ in eqns. (1.12) and (1.14), are found to be $3.1 \times 10^{17}\ m^{-3}$ and $0.1\ mho\ m^{-1}$ respectively. It is clear that non-equilibrium ionization can result in ionization and conductivity levels considerably higher than those achieved if the plasma were in equilibrium.

1.4 EFFECTS IN CLOSED CYCLE MHD GENERATORS

In general, the ideal behaviour of a non-equilibrium MHD generator predicted by the simple theory presented in sections 1.2 and 1.3 is not in accord with experiment. In particular, the appreciable enhancement of conductivity as a result of non-equilibrium ionization is difficult to observe experimentally. In reality, the theoretical description is greatly complicated by the existence of a large number of interacting physical mechanisms, which have important effects on the plasma and electrical behaviour, and, consequently, the overall generator characteristics.

The extent of departure from the ideal generator behaviour as a result of these effects can be stated quantitatively in terms of the effective conductivity σ_{eff} and the effective Hall parameter β_{eff} defined as follows:

$$\sigma_{eff} = \frac{I}{(V_y + H\langle u_y \rangle B)} \frac{H}{WL}$$

and

$$\beta_{eff} = \frac{V_x}{(V_y + H\langle u_y \rangle B)} \left(\frac{H}{L}\right)$$

where $I = -WL\langle J_y \rangle$ is the load current, $V_y = -\int_0^H E_y dy$ is the Faraday voltage, $V_x = -\int_0^L E_x dx$ is the Hall voltage, and $\langle u_y \rangle = \int_0^H u_y dy$. The lengths W, H and L are the generator width, height and segmentation length respectively.

For a uniform plasma carrying a uniform current, it can be shown from eqns. (1.3) that $\sigma_{eff} = \sigma$ and $\beta_{eff} = \beta$. However, as a result of non-uniformities in plasma properties and the current distribution the ratios $\sigma_{eff}/\langle\sigma\rangle$ and $\beta_{eff}/\langle\beta\rangle$ are not equal to unity.

The physical mechanisms that will be considered in this thesis are discussed in the following subsections. Descriptions of other effects, not considered here, can be found in reference (24), for example.

(a) Non-uniform Current Distribution

The simple theory of segmented electrode generators, formulated in sections 1.2 and 1.3, in which $\bar{J}_y =$ constant and $\bar{J}_x = 0$ assumes the ideal case of infinitely segmented electrodes and a uniform plasma. In practice, the electrodes have finite dimensions and the Hall effect leads to a non-uniform current distribution.

In an open cycle generator the effect of this non-uniformity on the plasma parameters is small and the current distribution can often be taken to be governed by the equation for a uniform plasma; that is, Laplace's equation. This problem can be solved analytically[6]. The main feature of the obtained solutions is the prediction of large current concentrations occurring on the downstream edge of the cathode, and the upstream edge of the anode of a given electrode pair. This

non-uniformity of current distribution results in an increased internal impedance compared with the ideal theory; i.e., $\sigma_{eff}/\langle\sigma\rangle < 1$.

In a closed cycle generator the non-uniform current flow causes non-uniformities in the plasma parameters, and the equations governing the current distribution and the plasma parameters are strongly coupled. In this case, the current distribution and the distributions of plasma parameters must be obtained simultaneously, and, because of the non-linearity and complexity of the problems, numerical methods of solution must be employed. Further complication is introduced by the existence of the electrothermal instability, discussed in the next subsection, which makes the problem time dependent in the unstable regime.

(b) The Electrothermal Instability

Fluctuations of the electron density and electron temperature about the uniform steady plasma state considered in section 1.3 propagate as waves called electrothermal waves. These waves consist of two modes: the fast thermal mode, which is always heavily damped, and is of little physical interest; and the ionization mode, which is unstable under certain conditions. A detailed linear analysis of these waves has been carried out by Nelson and Haines[7]. It is found that the ionization mode is unstable for β_e greater than about 2, and that the growth rate depends on the orientation of the wave vector $\underline{k}$, defined by the angle

$$\alpha = \tan^{-1} \frac{\underline{J}_\perp \underline{k}.\underline{B}}{\underline{J}.\underline{k}\,|\underline{B}|}$$

having a maximum at $\alpha \pm \pi/4$. This instability is referred to as the electrothermal instability.

In a closed cycle MHD generator, non-uniformities in the current distribution and ohmic heating, described in the previous subsection, cause non-uniformities in the plasma parameters. As a result, the electrothermal instability can occur if the Hall parameter exceeds the critical value. With a growth time of 10^{-6} sec, which is typically much less than the time spent by the gas in an electrode segment, the instability can grow into the non-linear phase. This means that the full equations governing the plasma and current distributions in a segmented electrode channel must be solved in order to determine accurately the effects of the instability on generator performance. As mentioned in the preceding subsection, the complexity of this problem necessitates the employment of numerical methods of solution. A number of authors have considered this problem, but the most complete work to date is the two-dimensional time dependent numerical model by Uncles[8]. The most important result of the latter work is the prediction of current flow along high conductivity streamers transverse to the gas flow at times long enough for the non-linear phase of the instability to become fully developed. In the presence of these streamers the effective conductivity is increased by a factor of two over a uniform plasma case ofthe same geometry with conductivity and Hall parameter equal to the average values for the non-uniform case.

By virtue of the collisional coupling between the electron properties and heavy particle properties, fluctuations in the electron properties are coupled to fluctuations in the heavy particle properties.

The latter fluctuations, called magnetosonic waves[9], are sonic waves distorted by the fluctuating $\underline{J} \wedge \underline{B}$ force and Ohmic heating and can be unstable under certain conditions. However, the characteristic time for this instability is about 10^{-3} sec, which is typically much larger than the time spent by the gas in an electrode segment, so that the magnetosonic instability is of no importance in the case of non-equilibrium generators.

When the energy coupling between electrons and heavy particles is strong, so that $T_e = T$ (over much of the gas flow), only magnetosonic waves exist. This means that the operation of equilibrium (open cycle) generators is usually stable, magnetosonic waves causing relatively insignificant fluctuations in the fields and plasma properties. Consequently, the local behaviour in such devices can usually be considered as independent of time.

(c) Turbulent Boundary Layers and Turbulent Transport Processes

For flow conditions characteristic of MHD power generators, the gas flow in an MHD channel is of a compressible turbulent boundary layer character over much of the channel length[21],[22],[23],[24]. In other words, the overall properties of the gas; namely, the total mass density ρ, the total pressure p, the flow velocity $\underline{u}$ and the heavy particle temperature T, are governed by equations describing the development of turbulent boundary layers on the electrode walls and insulator side walls of an MHD channel. These equations are derived from the overall conservation equations for the partially ionized plasma by making the well known boundary layer assumptions[21],[22],[24], allowing for turbulent transport processes. The latter assumptions are not usually invalidated by the presence of a highly non-uniform current distribution, because

the $\underline{J} \wedge \underline{B}$ force and Ohmic heating can cause only slight streamwise variations of the overall plasma parameters in one segment of the generator. In other words, interaction lengths are typically much larger than the segmentation length. An exception to this is boundary layer separation caused by a strongly retarding $\underline{J} \wedge \underline{B}$ force[23,39].

In the wall boundary layer regions, significant elevation of the electron temperature and the electron number density above the gas temperature and corresponding equilibrium number density is nearly always present, even in the case of equilibrium generators. This is due to the fact that, for a given current density, the electron temperature elevation is inversely proportional to the square of the electron density, which is relatively small in the cold boundary layers close to the walls. Therefore, even in the case of equilibrium generators, the boundary layer equations must be supplemented by an electron continuity equation and an electron energy equation, as well as any other species continuity equations required to define the composition of the plasma. These equations, like the overall conservation equations, are time averaged over turbulent fluctuations. Terms then appear which depend on correlations between velocity fluctuations and species number densities in the case of the species continuity equations, and correlations between velocity fluctuations and electron enthalpy fluctuations in the case of the electron energy equation (see references (25), (26) and (17)). These terms represent transport of particles and electron enthalpy by turbulent fluctuations and are subjected to the boundary layer approximations. As in the case of the overall conservation equations, a method of relating turbulent correlations to mean flow quantities must be specified.

In the case of open cycle MHD generators, a sufficiently high degree of accuracy can usually be achieved by taking as the equations governing the local plasma behaviour in the channel the steady state forms of the turbulent boundary layer equations, and the continuity and electron energy equations, the latter being similarly subjected to the boundary layer approximations[25],[26],[17]. Also, as shown in reference (40), sufficiently accurate results can in many cases be obtained by employing some simplifications when solving for the electric and current fields; for example, the assumption of infinitely fine segmentation or the use of Laplace's equation for the current field, as mentioned in subsection (a).

However, as indicated in the preceding subsection, the full time dependent equations governing the current and plasma property distributions must be considered in the case of closed cycle MHD generators. The problem is further complicated by the necessity of having to consider a time dependent system of turbulent boundary layer equations. The complete problem in this case has not been considered. In particular, turbulent boundary layers are not considered in the work of Uncles[8].

(d) Plasma-Wall Interactions, Electron Emission, Seed Deposition and Sheath Effects

The accuracy with which the behaviour of the plasma and electrical fields in an MHD generator can be described, and overall generator characteristics thereby predicted, can depend to a large extent on the accuracy with which the interactions between the plasma and the containing walls can be modelled. At the present time there exists no exact theory of these interactions applicable to either open or closed cycle MHD generators.

Simplified theoretical models of plasma-wall interactions have been developed and the derived wall boundary conditions used for the numerical modeling of MHD generators by a number of authors (see references (16), (17) and (25), for example). Most of these studies assume the existence of collisionless sheaths in contact with non-emitting electrode surfaces. The effects of electron emission are considered in reference (25). Also considered in reference (25) are the effects of finite ion diffusion currents, which can be significant in the boundary layer regions where temperature gradients are large.

In the case of closed cycle MHD generators an important effect is the interaction between an electrode surface and seed particles. The essential feature of these interactions is the large affinity between the alkali metal and the surface. Practically all incident seed particles (ions and neutrals) are adsorbed to the surface and desorption takes place after a certain residence time. The adsorbed atoms strongly influence the rate at which electrons are emitted from the surface as well as the rate at which ions or atoms are desorbed.

Boundary conditions for the continuity equations, incorporating electrode-seed interaction effects, were first formulated by Sajben[29], assuming a collision dominated sheath. These were later used by Koester et al.[30] to solve numerically the continuity equations, restricting application to a tungsten cathode in a laminar stagnation flow geometry. An important result of this work is that, as a result of the plasma-surface interaction, electrode currents can be passed, at moderate voltage drops, which are greatly in excess of the electron current emitted from the surface under conditions of thermal equilibrium.

In all the above studies, the plasma is assumed to be in a steady-state, and plasma-wall interactions have not so far been considered in time dependent numerical models of closed cycle MHD generators.

1.5 DESCRIPTION OF PRESENT WORK

Theoretical and numerical models of open cycle MHD generators have reached the degree of sophistication needed for quite accurate quantitative agreement between theory and experiment to be obtained[24,26]. However, the modelling of closed cycle MHD generators is a considerably more difficult problem, and studies in the past have neglected a number of important physical effects. Much work remains to be done before accurate numerical predictions of the performance characteristics of closed cycle MHD generators can be made. At the time of writing this thesis, the most advanced work appeared to be that of Uncles[8,5], mentioned in subsection (b) (see section 1.4). In this work, effects of turbulent boundary layers, finite ion and neutral diffusion, and plasma-wall interactions are neglected.

In this thesis a time dependent theoretical and numerical model of a closed cycle MHD generator is developed incorporating physical effects previously considered only in steady-state theories of open cycle MHD generators. The present theory is an initial step towards the development of a theory having the ability to give accurate predictions of the performance characteristics of closed cycle MHD generators. It may also be regarded as an extension of the work of Uncles[8] to include the effects of turbulent boundary layers and turbulent transport processes, finite seed ion and seed atom diffusion, and plasma-wall interactions.

The basic theoretical model is developed in chapter 2 in which a number of assumptions are made that allow the governing equations to be decoupled into two independent systems of equations: the turbulent boundary layer equations; and the equations governing the plasma and current distributions. A simplified description of the flow in a MHD generator channel of rectangular cross-section is then developed by assuming a steady-state two-dimensional flow on each of the side walls of the channel. This is followed by the development of a two-dimensional time-dependent description of the behaviour of the plasma and current fields in a single segment of a linear segmented electrode MHD generator operated in the Faraday mode. Inlet relaxation effects are neglected and, in the derivation of the relevant wall boundary conditions, the existence of collisionless sheaths on the electrodes is assumed. This sheath analysis incorporates seed-electrode interaction effects.

In chapter 3 the numerical method of solution of the turbulent boundary layer equations is developed and applied to a real experimental MHD generator system, the IRD test facility. Comparison between a computed and an experimentally measured pressure distribution is attempted.

In chapter 4, the numerical method of solution of the two-dimensional, time-dependent model of the plasma and current behaviour in a single segment of an MHD generator is developed. Numerical solutions of this problem are finally presented and analyzed in chapter 5.

Emphasis in the present work is placed more on the formulation of the physical model and the development and testing of appropriate numerical methods of solution, rather than the analysis of results

obtained for various generator operating conditions in terms of the various acting physical processes, which is left for future studies. Thus, the boundary layer solutions presented and discussed in chapter 3, and the solution of the plasma and electrical problem in chapter 5 are for only one set of generator operating conditions.

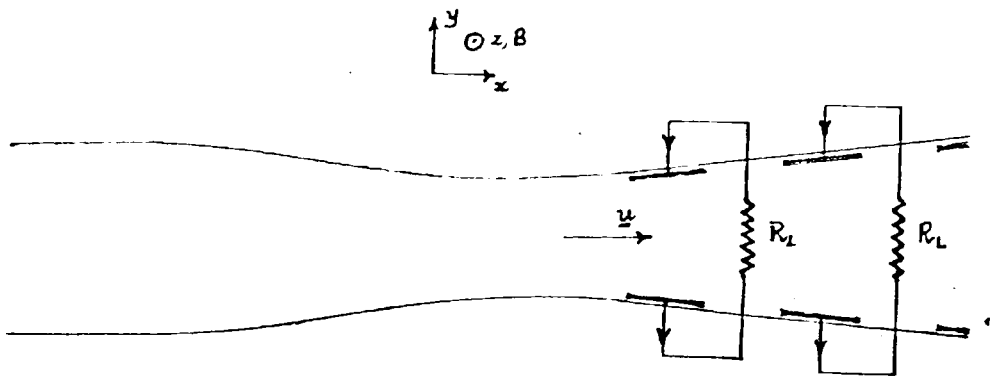

Fig. 1.1: Segmented Electrode Faraday Generator

CHAPTER 2

TWO-TEMPERATURE FLUID MODEL OF A PARTIALLY IONIZED PLASMA IN AN ELECTROMAGNETIC FIELD

2.1 INTRODUCTION

In this chapter a two-temperature fluid model of a partially ionized plasma in an electromagnetic field is formulated in order to describe the local behaviour in a closed cycle MHD generator, which utilizes as a working gas an inert gas (helium) slightly seeded with an alkali metal (caesium). The governing equations of this model can be obtained by multiplying the Boltzmann equation for each component particle species of the plasma (seed ions, seed atoms, buffer gas atoms and electrons) by the particle mass, momentum and energy, and then integrating over velocity space. The equations so obtained are the species conservation equations for mass, momentum and energy, and in a fluid description they are assumed to be sufficient to describe the evolution of the instantaneous local macroscopic state of the plasma; the state of the plasma is then defined by specifying the number density of each species and its characteristic temperature, and the mean mass velocity of the plasma. For a fluid description of the plasma each species is thus regarded as a separate fluid coexisting with and interacting with the fluids of the other species. A necessary condition for the applicability of such a description is that the plasma be collision dominated; that is, the mean free path for particle collisions for all species be much smaller than the characteristic length scale for macroscopic change, and that the particle collision intervals be much smaller than the characteristic time scale for macroscopic change. When these criteria are satisfied the distribution function of each heavy particle component of the plasma differs little from a Maxwellian distribution at a temperature T. For the electron distribution function to differ little from a Maxwellian distribution at a

temperature T_e it is necessary, in addition, that the electron density be large enough for electron-electron collisions to be sufficiently frequent for the electron energy distribution to be little affected by collisions of electrons with heavy particles, and that the energy gained by an electron from any external electric field be typically smaller than the mean electron thermal energy. Because of the inefficiency of energy exchange in elastic collisions between particles of disparate mass (when the heavy particles are monatomic), T_e may differ appreciably from T (heavy monatomic particles of different species have comparable masses so that energy exchange in elastic collisions between them is efficient and they may all be taken to be at the same temperature T). The aforementioned conditions are satisfied for conditions characteristic of closed cycle MHD power generators.

The species conservation equations contain terms depending on the particle diffusion velocities $\underline{U}_s$, the viscous stress tensors $\underline{\underline{\tau}}_s$ and the heat flux vectors $\underline{q}_s$, which relate to the transport of particles, momentum and energy, respectively, in the local frame of reference moving with the mean mass velocity of the plasma. In addition, these equations contain velocity moments of collision integrals, representing rates of change due to elastic collisions; terms representing rates of change due to inelastic collisions, and terms representing rates of change due to interactions between particles and the external electromagnetic field. All these terms can be calculated using approximations for the distribution functions which enable the transport quantities $\underline{U}_s$, $\underline{\underline{\tau}}_s$ and $\underline{q}_s$ to be calculated in terms of transport coefficients. The conservation equations then form a closed system when taken together with Maxwell's equations for the electromagnetic field.

A considerable amount of work has been devoted to the development of methods of approximation of the particle distribution functions and the calculation of transport coefficients[1], [10]. Two methods have been

developed for two-temperature ($T_e \neq T$) partially ionized plasmas. One method, described in reference (1), utilizes the classical chapman-Enskog method of approximation to calculate the transport coefficients appearing in the expressions for $\underline{V}_s$, q_s and $\underline{\tau}_s$ to arbitrary levels of approximation by expansions in terms of Sonine polynomials; the order of the approximation is equal to the number of terms used in the Sonine polynomial expansion. Whilst this method allows transport coefficients to be calculated to any order of approximation, expressions of general validity are not obtained for orders of approximation higher than the first in the case of partially ionized plasmas.

The second method is based on the application of Grad's 13-moment approximation and is discussed in reference (10) and the references cited therein. It has been shown to result in closed forms of the distribution functions, which include explicitly the transport quantities $\underline{V}_s$, q_s and $\underline{\tau}_s$. The expressions obtained for the transport coefficients are consistent with the results obtained in the second approximation of the first method. Unlike the first method, however, these expressions can be obtained in general forms applicable to partially ionized plasmas of arbitrary composition.

The second method will be used in this chapter to derive general expressions for the transport properties of a partially ionized plasma consisting of four components: buffer gas atoms, seed atoms, seed ions and electrons, seeding being assumed slight. When seeding is slight, the transport properties of interest are the species diffusion velocities, the electron heat flux vector and the transport properties of the neutral buffer gas. The expressions for the diffusion velocities so derived should be sufficiently accurate for many engineering applications; in particular, closed cycle MHD power generation, the application of interest in this thesis.

Although the assumption of slight seeding results in considerable simplification of the transport properties and the governing fluid equations, further simplifications have been found to be necessary because of the large demands made on computer resources (storage and

time) by the numerical models of chapters 3 and 4. Thus, electron-buffer gas atom collisions are assumed to dominate coulomb collisions, and approximate expressions for the transport properties, which are consistent with the lowest order approximations of the Chapman-Enskog approach are used. In addition, thermal diffusion is neglected, and the ion Hall parameter is assumed to be much less than unity.

Finally, the overall conservation equations are decoupled from the equations governing the other species by neglecting the Lorentz force terms in the overall momentum equation and the term representing energy loss of heavy particles due to elastic collisions with electrons in the overall heavy particle energy conservation equation. Because of the assumption of slight seeding, the overall momentum and heavy particle energy conservation equations are then approximately the same as for a gas consisting of buffer gas atoms only; these equations are referred to here as the 'gas dynamic' equations. The plasma equations consist of the electron and seed atom continuity equations and the electron energy equation.

It is well known that the flow behaviour in an MHD generator channel is typically of a turbulent boundary layer character. The gas dynamic equations are thus considered in simplified form in accordance with the boundary layer approximation, and steady state flow equations are obtained by averaging over turbulent fluctuations, assuming that the flow is steady on the average. Terms representing the transport of mean flow momentum and energy by turbulent fluctuations appear in the time averaged equations, and these are related to mean flow quantities and their gradients by means of eddy transport coefficients as in reference (11). A two-dimensional description of the flow in an MHD generator is then formulated by considering the flow in terms of two-dimensional boundary layers on each of the channel side walls.

The aforementioned plasma and gas-dynamic equations must be supplemented by equations for the electromagnetic field. These are obtained in this chapter from Maxwell's equations assuming that the plasma is quasi-neutral, and that any induced magnetic field can be neglected in comparision with the applied magnetic field, which is assumed to be uniform and constant. Taken together with the generalized Ohm's law, these equations are referred to here as the 'electrical' equations .

A description of the behaviour of the plasma and current fields in a single segment of a linear segmented electrode MHD channel, using the derived plasma and electrical equations is finally considered. Current flow along the magnetic field is neglected and all quantities are assumed to vary only in a plane perpendicular to the magnetic field. In addition, the gas dynamic parameters, which are obtained by solution of the boundary layer equations are assumed to be functions only of the cross-stream coordinate, variations along the flow being neglected.

Finally, the boundary conditions for the plasma and electrical equations are derived, assuming the existence of collisionless sheaths on the electrodes. This sheath analysis incorporates seed-electrode interactions.

Whilst the governing equations obtained by making the aforementioned simplifications are limited in accuracy, they should never-the-less form the basis of a fairly accurate description of the main features of many physical phenomena occuring in closed cycle MHD power generators operated under certain conditions. Moreover, comparision with the work of other authors can be more easily made and the numerical techniques used to solve the equations more easily developed and tested.

2.2 CONSERVATION EQUATIONS

The plasma formed by addition of a small amount of alkali metal to an inert gas, is assumed to consist of four components: electrons, singly charged seed ions, neutral seed atoms, and neutral buffer gas atoms.

The species conservation equations for mass, momentum and energy are obtained by multiplying the Boltzmann equation for each of the components of the plasma by the particle mass, momentum and energy, and then integrating over velocity space. The resulting equations are (see reference (1)), for species α particles $(\alpha = e, i, n, h)$,

$$\frac{\partial \rho_\alpha}{\partial t} + \nabla \cdot \rho_\alpha (\underline{u} + \underline{U}_\alpha) = \sum_\beta \Delta_{\alpha\beta} [\dot{m}_\alpha] + \dot{\rho}_\alpha = \dot{\rho}_\alpha \tag{2.1}$$

$$\frac{D(\rho_\alpha \underline{U}_\alpha)}{Dt} + \nabla \cdot \underline{\underline{p}}_\alpha - n_\alpha e_\alpha (\underline{E}' + \underline{U}_\alpha \wedge \underline{B}) + \rho_\alpha \frac{D\underline{u}}{Dt} + \rho_\alpha [\underline{U}_\alpha \nabla \cdot \underline{u} + (\underline{U}_\alpha \cdot \nabla)\underline{u}] = \sum_{\beta \neq \alpha} \Delta_{\alpha\beta} [m_\alpha \underline{C}] + \underline{\dot{M}}_\alpha \tag{2.2}$$

and

$$\frac{D}{Dt}(\rho_\alpha \mathcal{E}_\alpha) + \nabla \cdot \underline{q}_\alpha - n_\alpha e_\alpha \underline{U}_\alpha \cdot \underline{E}' + \rho_\alpha \underline{U}_\alpha \cdot \frac{D\underline{u}}{Dt} + \rho_\alpha \mathcal{E}_\alpha \nabla \cdot \underline{u} + \underline{\underline{p}}_\alpha : \nabla \underline{u}_\alpha = \sum_{\beta \neq \alpha} \Delta_{\alpha\beta} [\tfrac{1}{2} m_\alpha C^2] + \dot{N}_\alpha \tag{2.3}$$

where

$$\frac{D}{Dt} = \frac{\partial}{\partial t} + (\underline{u} \cdot \nabla) \tag{2.4}$$

and

$$\underline{E}' = \underline{E} + \underline{u} \wedge \underline{B} \tag{2.5}$$

are the time rate of change and electric field, respectively, in the frame of reference moving with mean mass velocity $\underline{u}$ of the plasma.

In equations (2.1) - (2.3), $\rho_\alpha = m_\alpha n_\alpha$, n_α, $\underline{U}_\alpha$ and $\mathcal{E}_\alpha$ are the average species α mass density, number density, diffusion velocity and kinetic energy per unit mass respectively. In general, the average of any velocity dependent function $\Phi_\alpha(\underline{C})$ for species α is given by

$$\overline{\Phi_\alpha} = \int \Phi_\alpha(\underline{C}) f_\alpha(\underline{C}) \, d^3\underline{C} \tag{2.6}$$

where the integration is over the whole of velocity space and $f_\alpha(\underline{C})$ is the species α velocity distribution function, which is assumed to satisfy the normalization condition

$$\int f_\alpha(\underline{C}) d^3\underline{C} = 1 \tag{2.7}$$

The quantities ρ_α, n_α, $\underline{U}_\alpha$ and $\mathcal{E}_\alpha$ are obtained from equation (2.6) when Φ_α is set equal to $m_\alpha n_\alpha$, n_α, $\underline{C}$ and $\frac{1}{2}C^2$ respectively. The average species α kinetic energy per unit mass can be written in terms of the species α temperature:

$$\mathcal{E}_\alpha = \tfrac{1}{2}\overline{(\underline{C}^2)}_\alpha \equiv \frac{3}{2}\frac{k_B}{m_\alpha}T_\alpha \tag{2.8}$$

The average energy per unit mass $\mathcal{E}_\alpha$ should include a contribution due to particles being in various internal energy states. In the case of interest here this contribution should be included for the neutral seed atoms. However, it can be shown (see section 2.5) that the population densities of the various excited energy levels can be neglected relative to the population density of the ground state, which can therefore be taken to be equal to the total neutral seed atom density, and the internal energy of a neutral seed atom taken to be constant, this constant is set equal to zero in $\mathcal{E}_n$.

In equation (2.6), the velocity $\underline{C}$ is the so called peculiar particle velocity; it is the velocity of a particle with respect to the frame of reference moving with the mean mass velocity of the plasma; that is,

$$\underline{C} = \underline{c} - \underline{u}(\underline{r}, t) \tag{2.9}$$

where $\underline{c}$ is the particle velocity in the laboratory frame of reference, and $\underline{u}$ is the mean mass velocity of the plasma, given by

$$\underline{u} = \frac{\sum \rho_\alpha \underline{u}_\alpha}{\sum \rho_\alpha}, \tag{2.10}$$

where $\underline{u}_\alpha$ is the average velocity of species α particles obtained from

equation (2.6) by setting $\Phi_\alpha = \underline{c}$, noting that $d^3\underline{C} = d^3\underline{c}$.

By definition of $\underline{U}_\alpha$,

$$\underline{U}_\alpha = \underline{u}_\alpha - \underline{u}(\underline{r},t) \tag{2.11}$$

and it follows from (2.10) that

$$\sum_\alpha \rho_\alpha \underline{U}_\alpha = 0 \tag{2.12}$$

The species α heat flux vector $\underline{q}_\alpha$ and momentum flux or pressure tensor $\underline{\underline{P}}_\alpha$, which appear in equations (2.2) and (2.3), and give the fluxes of translational energy and momentum transported by species α particles in the frame of reference moving with the plasma are defined by the following integrals over velocity space:

$$\underline{q}_\alpha = \tfrac{1}{2}\rho_\alpha \left(\overline{\underline{C}\,\underline{C}^2}\right)_\alpha \tag{2.13}$$

and

$$\underline{\underline{P}}_\alpha = \rho_\alpha \left(\overline{\underline{C}\,\underline{C}}\right)_\alpha \tag{2.14}$$

The scalar partial pressure p_α is defined as

$$p_\alpha \equiv \tfrac{1}{3} Tr\left(\underline{\underline{P}}_\alpha\right) = \tfrac{1}{3}\rho_\alpha \left(\overline{\underline{C}^2}\right)_\alpha \tag{2.15}$$

and, using (2.8), can be written in terms of T_α as follows:

$$p_\alpha = n_\alpha k_B T_\alpha \tag{2.16}$$

which is the equation of state for the species α component. The species viscous-stress tensor $\underline{\underline{\tau}}_\alpha$ is defined as

$$\underline{\underline{\tau}}_\alpha \equiv -\left(\underline{\underline{P}}_\alpha - p_\alpha \underline{\underline{1}}\right) \tag{2.17}$$

where $\underline{\underline{1}}$ is the unit tensor.

In equations (2.2) and (2.3), $\sum_{\beta\neq\alpha} \Delta_{\alpha\beta}\left[m_\alpha \underline{C}\right]$ and $\sum_{\beta\neq\alpha} \Delta_{\alpha\beta}\left[\tfrac{1}{2} m_\alpha C^2\right]$ are the mean rates of change per unit volume of momentum and translational energy of species α particles due to exchange of momentum and energy in elastic collisions with particles of different species. These quantities are given by the equations

$$\sum_{\beta\neq\alpha}\Delta_{\alpha\beta}[m_\alpha \underline{C}] = \sum_{\beta\neq\alpha} n_\alpha n_\beta \int_{-\infty}^{\infty}\int_{-\infty}^{\infty} m_\alpha (\underline{C}' - \underline{C}) f_\alpha(\underline{C}) f_\beta(\underline{W}) g b db d\epsilon d^3C d^3W \qquad (2.18)$$

and

$$\sum_{\beta\neq\alpha}\Delta_{\alpha\beta}\left[\tfrac{1}{2} m_\alpha C^2\right] = \sum_{\beta\neq\alpha} n_\alpha n_\beta \int_{-\infty}^{\infty}\int_{-\infty}^{\infty} \tfrac{1}{2} m_\alpha (\underline{C}'^2 - \underline{C}^2) f_\alpha(\underline{C}) f_\beta(\underline{W}) g b db d\epsilon d^3C d^3W, \qquad (2.19)$$

where $\underline{C}$ and $\underline{C}'$ are the velocities of a species α particle before and after a collision with a species β particle which is initially moving with a velocity $\underline{W}$; g is the relative speed $|\underline{C} - \underline{W}|$ of the particles; b is the impact parameter for collisions between species α and species β particles, and ϵ is the angle of scatter of species α particles; that is, the angle between the relative velocities of the particles before and after a collision.

The quantities $\dot{\rho}_\alpha$, $\dot{M}_\alpha$ and $\dot{N}_\alpha$, are the net rates of increase per unit volume of the mass, momentum and energy, respectively, of species α particles as a result of inelastic collisions. For the particular plasma conditions of interest here, excited states of ions and buffer gas atoms can be neglected and the relevant inelastic collisions are between electrons and seed atoms in various levels of electronic excitation that communicate energetically only with the free electrons and by emission and absorption of radiation. Of the quantities $\dot{\rho}_\alpha$, $\dot{M}_\alpha$ and $\dot{N}_\alpha$, only $\dot{\rho}_\alpha\,(\alpha = e, i, n)$ and $\dot{N}_\varepsilon$ are significant, the other quantities being negligible. Expressions for the significant inelastic collision terms will be presented in section 2.5.

The overall conservation equations for the plasma as a whole can be obtained by summation of equations (2.1) - (2.3) over all species in the plasma. The overall conservation equations for mass and momentum are obtained in this way, but the overall heavy species energy conservation equation, obtained by summation of equations (2.3) over the heavy species in the plasma is of greater interest here. The

resulting conservation equations are

$$\frac{\partial \rho}{\partial t} + \nabla \cdot \rho \underline{u} = 0 \tag{2.20}$$

$$\rho \frac{D\underline{u}}{Dt} = -\nabla p + \nabla \cdot \underline{\underline{\tau}} + \rho^c \underline{E}' + \underline{J} \wedge \underline{B} \tag{2.21}$$

$$\frac{D}{Dt}\left(\sum_{\alpha \neq e} \rho_\alpha \varepsilon_\alpha\right) + \left(\sum_{\alpha \neq e} \rho_\alpha \varepsilon_\alpha + \sum_{\alpha \neq e} p_\alpha\right) \nabla \cdot \underline{u} - \rho_e \underline{U}_e \cdot \frac{D\underline{u}}{Dt}$$

$$= -\nabla \cdot \left(\sum_{\alpha \neq e} \underline{q}_\alpha\right) + \sum_{\alpha \neq e} \underline{\underline{\tau}}_\alpha : \nabla \underline{u} + \underline{J}_i \cdot \underline{E}' - \sum_{\beta \neq e} \Delta_{e\beta}\left[\tfrac{1}{2} m_e C^2\right] \tag{2.22}$$

where $\rho = \sum_\alpha \rho_\alpha$ is the total mass density; and $\rho^c = \sum_\alpha e_\alpha n_\alpha = e(n_i - n_e)$ and $\underline{J} = \sum_\alpha n_\alpha e_\alpha \underline{U}_\alpha = \underline{J}_i + \underline{J}_e = e(n_i \underline{U}_i - n_e \underline{U}_e)$, where e is the magnitude of the electronic charge, are the total charge and conduction current densities respectively. In equation (2.21) use has been made of the definitions

$$\underline{\underline{\tau}} = \sum_\alpha \underline{\underline{\tau}}_\alpha \tag{2.23}$$

and

$$p = \sum_\alpha p_\alpha \tag{2.24}$$

of the viscous stress tensor and scalar pressure for the plasma as a whole. In deriving equations (2.20) - (2.22), use has also been made of the relations $\sum_\alpha \rho_\alpha \underline{U}_\alpha = 0$ and

$$\sum_\alpha \sum_{\beta \neq \alpha} \Delta_{\alpha\beta}\left[\tfrac{1}{2} m_\alpha \underline{C}^2\right] = 0,$$

the latter allowing us to write

$$\sum_{\alpha \neq e} \sum_{\beta \neq \alpha} \Delta_{\alpha\beta}\left[\tfrac{1}{2} m_\alpha \underline{C}^2\right] = -\sum_{\beta \neq e} \Delta_{e\beta}\left[\tfrac{1}{2} m_e \underline{C}^2\right]$$

in equation (2.22)

The absence of terms in equations (2.20) and (2.21) representing the effects of inelastic collisions results from the conservation of particle mass and, as mentioned above, the smallness of the inelastic

collision terms in equations (2.21).

It is assumed here that the conditions for applicability of a two-temperature collision dominated description of the partially ionized plasma, discussed in section 2.1, are satisfied so that the distribution functions are close to Maxwellians at a temperature T for the heavy particles and at a temperature T_e for the electrons. This allows us to write, using equations (2.8 and 2.16),

$$p = k_B T n_H + k_B T_e n_e \tag{2.25}$$

where use has been made of the definition (2.24) of p, and n_H is the total heavy species number density; and

$$\sum_{\alpha \neq e} \rho_\alpha \mathcal{E}_\alpha = \frac{3}{2} k_B T n_H \tag{2.26}$$

In the next section, expressions for $\underline{V}_\alpha$ $(\alpha = e, i, n)$, $\underline{q}_e$ and the elastic collision terms in equations (2.2) and (2.22) as functions of the variables ρ_α $(\alpha = e, i, n)$, T, T_e and their gradients, and the fields $\underline{E}'$ and $\underline{B}$, are determined by making use of the closed forms of distribution functions that result from the application of Grad's 13-moment approximation, which enables algebraic systems of transport equations for $\underline{V}_\alpha$ and $\underline{q}_\alpha$ to be obtained.

2.3 EXPRESSIONS FOR DIFFUSION VELOCITIES, ELECTRON HEAT FLUX VECTOR AND ELASTIC COLLISION TERMS IN MOMENTUM AND ENERGY EQUATIONS

In order to clarify the method used to derive the expressions for $\underline{U}_\alpha (\alpha = e, i, n)$, $\underline{q}_e$ and the elastic collision terms in the momentum and energy equations, the basic theory of reference (10) will be first described below.

Using Grad's 13-moment approximation, the distribution function f_α for each component of the partially ionized plasma can be derived in the closed form (see reference (10)).

$$f_\alpha = f_\alpha^{(0)} \left[1 + \gamma_\alpha \underline{U}_\alpha \cdot \underline{C} - (\gamma_\alpha / 2\rho_\alpha) \underline{\tau}_\alpha : \underline{C}\underline{C} + (\gamma_\alpha / 5\rho_\alpha)(\gamma_\alpha C^2 - 5) \underline{h}_\alpha \cdot \underline{C} \right] \tag{2.27}$$

where $f_\alpha^{(0)}$ the Maxwellian distribution given by

$$f_\alpha^{(0)} = (\gamma_\alpha / 2\pi)^{3/2} \exp\left(-\tfrac{1}{2}\gamma_\alpha C^2\right) \tag{2.28}$$

In these expressions, $\gamma_\alpha = m_\alpha / k_B T_\alpha$, where $T_{\alpha \neq e} = T$, and $\underline{h}_\alpha$ is the relative thermal flux vector of component α, defined by

$$\underline{h}_\alpha = \underline{q}_\alpha - \frac{5}{2} p_\alpha \underline{U}_\alpha \tag{2.29}$$

If the above closed forms for the distribution functions are used in equations (2.18) and (2.19), and quadratic terms in $\underline{U}_\alpha$, $\underline{\tau}_\alpha$ and $\underline{h}_\alpha$ are neglected, the following expressions are found for the collisional rates of change of momentum and energy:

$$\sum_{\beta \neq \alpha} \Delta_{\alpha\beta} [m_\alpha \underline{C}] = \sum_\beta a_{\alpha\beta} \left[\underline{U}_\beta - \underline{U}_\alpha + \gamma_{\alpha\beta} A_{\alpha\beta}^{(2)} \left(\frac{\underline{h}_\beta}{\gamma_\beta \rho_\beta} - \frac{\underline{h}_\alpha}{\gamma_\alpha \rho_\alpha} \right) \right] \tag{2.30}$$

and

$$\sum_{\beta \neq e} \Delta_{e\beta} \left[\tfrac{1}{2} m_e C^2 \right] = - n_e \sum_{\beta \neq e} \frac{3}{2} k_B (T_e - T) \frac{2 m_e}{m_\beta} \nu_{e\beta} \tag{2.31}$$

where

$$\gamma_{\alpha\beta} = \frac{\gamma_\alpha \gamma_\beta}{(\gamma_\alpha + \gamma_\beta)} = k_B \left[\frac{T_\alpha}{m_\alpha} + \frac{T_\beta}{m_\beta} \right]^{-1} \tag{2.32}$$

and $\nu_{e\beta}$ is defined below (see equations (2.40) and (2.41))

The coefficients $a_{\alpha\beta}$ and $A^{(2)}_{\alpha\beta}$ appearing in the expressions (2.30) are defined by

$$a_{\alpha\beta} = \frac{16}{3} n_\alpha n_\beta m_{\alpha\beta} \Omega^{(1)}_{\alpha\beta}(1) \tag{2.33}$$

and

$$A^{(2)}_{\alpha\beta} = \frac{2}{5}\left[\frac{\Omega^{(1)}_{\alpha\beta}(2)}{\Omega^{(1)}_{\alpha\beta}(1)}\right] - 1 \ , \tag{2.34}$$

where

$$m_{\alpha\beta} = \frac{m_\alpha m_\beta}{m_\alpha + m_\beta} \ , \tag{2.35}$$

and the collision parameters $\Omega^{(l)}_{\alpha\beta}(r)$ are defined by

$$\Omega^{(l)}_{\alpha\beta}(r) = \pi^{1/2} \int_0^\infty \int_0^\infty \zeta^{2r+2} \exp(-\zeta^2) g_{\alpha\beta} \left(1 - \cos^l \chi_{\alpha\beta}\right) b\, db\, d\zeta \ , \tag{2.36}$$

where $\zeta = g_{\alpha\beta}\left(\frac{1}{2} \gamma_{\alpha\beta}\right)^{1/2}$ and $\chi_{\alpha\beta}$ is the angle of scattering in the centre of mass system of the colliding particles.

The coefficient $a_{\alpha\beta}$ can be written in a form which more clearly shows its physical meaning by introducing the momentum transfer collision cross-section defined by

$$Q^{(1)}_{\alpha\beta} \equiv 2\pi \int_0^\infty (1 - \cos\chi_{\alpha\beta})\, b\, db \tag{2.37}$$

and the energy weighted average of the momentum transfer collision frequency $\nu^{(1)}_{\alpha\beta} = n_\beta g_{\alpha\beta} Q^{(1)}_{\alpha\beta}$ defined by

$$\nu_{\alpha\beta} = \int_0^\infty \left(\frac{m_{\alpha\beta} g^2_{\alpha\beta}/2}{3k_B T/2} \right) \nu^{(1)}_{\alpha\beta} f^{(0)}_{\alpha\beta}(g_{\alpha\beta}) 4\pi g^2_{\alpha\beta}\, dg_{\alpha\beta} \ , \tag{2.38}$$

where T must be taken to be T_e if either species α or species β particles are electrons. In equation (2.38), $f^{(0)}_{\alpha\beta}$ denotes a Maxwellian distribution for a hypothetical particle having the reduced mass $m_{\alpha\beta}$; i,e,,

$$f^{(0)}_{\alpha\beta} = \left(\frac{m_{\alpha\beta}}{2\pi k_B T}\right)^{3/2} e^{-m_{\alpha\beta} g^2_{\alpha\beta}/(2k_B T)} \tag{2.39}$$

It may be readily shown that equation (2.38) can be written in the form

$$\nu_{\alpha\beta} = n_\beta \bar{g}_{\alpha\beta} Q_{\alpha\beta} \tag{2.40}$$

where

$$\bar{g}_{\alpha\beta} = \left(\frac{8k_B T}{\pi m_{\alpha\beta}}\right)^{1/2} ,$$

and the average momentum transfer cross-section $Q_{\alpha\beta}$ is defined as

$$Q_{\alpha\beta} \equiv \frac{4}{3}\int_0^\infty \zeta^5 e^{-\zeta^2} Q_{\alpha\beta}^{(1)}\, d\zeta$$
$$= \frac{8\pi}{3}\int_0^\infty\int_0^\infty \zeta^5 e^{-\zeta^2}(1-\cos\chi_{\alpha\beta})\, b\, db\, d\zeta. \qquad (2.41)$$

It follows from the defining equations (2.32), (2.33), (2.35), (2.36), (2.40) and (2.41), that

$$\Omega_{\alpha\beta}^{(1)}(1) = \frac{3}{16}\bar{g}_{\alpha\beta} Q_{\alpha\beta} \qquad (2.42)$$

and

$$a_{\alpha\beta} = n_\alpha m_{\alpha\beta} \nu_{\alpha\beta} \qquad (2.43)$$

It should be noted that the relations (2.42) and (2.43) hold true only when, as is assumed in the present work, all heavy particle species are at the same common temperature T, which may differ from the electron temperature T_e; then

$$\gamma_{\alpha\beta} = \frac{m_{\alpha\beta}}{k_B T} = \frac{8}{\pi \bar{g}_{\alpha\beta}^2} \qquad (2.44)$$

where, if $\alpha = e$ or $\beta = e$, $m_{\alpha\beta} = m_e$ and T must be replaced by T_e.

When equations (2.30) are used to eliminate the terms $\sum_{\beta \neq e} \Delta_{\alpha\beta}[m_\alpha \underline{C}]$ in the species conservation equations of momentum, and a number of simplifying assumptions, to be described below, are made, an algebraic system of equations for the diffusion velocities $\underline{U}_\alpha$ is obtained. It is first necessary, however, to obtain a system of transport equations for the relative heat flux vectors $\underline{h}_\alpha$. The latter equations are obtained by multiplying the Boltzmann equation for each component α by the quantity $\left(\frac{1}{2} m_\alpha C^2 - \frac{5}{2} k_B T_\alpha\right)\underline{C}$ and integrating over velocity space. The resulting transport equations can then be reduced to algebraic equations by use of the aforementioned simplifying assumptions. The algebraic equations for the $\underline{h}_\alpha$ are found to have the form

$$\frac{1}{\gamma_\alpha}\nabla\cdot\underline{\underline{T}}_\alpha + \frac{5}{2}\frac{1}{\gamma_\alpha}\frac{p_\alpha}{T_\alpha}\nabla T_\alpha - \frac{e_\alpha}{m_\alpha}\underline{\underline{E}}'\cdot\underline{\underline{T}}_\alpha - \frac{e_\alpha}{m_\alpha}\underline{h}_\alpha \times \underline{B} = \sum_\beta \Delta_{\alpha\beta}\left[\left(\frac{1}{2} m_\alpha \underline{C}^2 - \frac{5}{2} k_B T_\alpha\right)\underline{C}\right] \qquad (2.45)$$

Using the closed form for the distribution function, equations (2.27), the collision term on the right hand side of (2.45) can be determined in the following form:

$$\sum_{\beta} \Delta_{\alpha\beta}\left[\left(\tfrac{1}{2} m_\alpha \underline{C}^2 - \tfrac{5}{2} k_B T_\alpha\right)\underline{C}\right] = -\frac{1}{\gamma_\alpha}\sum_{\beta} a_{\alpha\beta}\left[A^{(5)}_{\alpha\beta}\frac{\underline{h}_\alpha}{p_\alpha} + A^{(6)}_{\alpha\beta}\frac{\underline{h}_\beta}{p_\beta} + \frac{5}{2}\frac{\gamma_\beta}{(\gamma_\alpha+\gamma_\beta)} A^{(7)}_{\alpha\beta}(\underline{U}_\alpha - \underline{U}_\beta) + 5\xi_{\alpha\beta}\underline{U}_\alpha\right] \tag{2.46}$$

In this expression, use has been made of the definitions

$$\xi_{\alpha\beta} \equiv \left[1 - (T_\beta/T_\alpha)\right]\left[1 + (m_\beta/m_\alpha)\right]^{-1} \tag{2.47}$$

$$A^{(n)}_{\alpha\beta} \equiv - G^{(n)}_{\alpha\beta} / a_{\alpha\beta} \tag{2.48}$$

The coefficients $G^{(n)}_{\alpha\beta}$ are given in reference (10); they are all linearly dependent on $n_\alpha n_\beta$.

Eliminating the collision term in equation (2.45), using equation (2.46), the following algebraic system of equations for $\underline{h}_\alpha$ is obtained:

$$\underline{h}_\alpha + \sum_{\beta\neq\alpha} b_{\alpha\beta}\underline{h}_\beta = - \lambda_\alpha \underline{P}_\alpha + \underline{h}_\alpha \wedge \underline{\omega}_\alpha \tau_\alpha^* \tag{2.49}$$

where

$$\underline{P}_\alpha = \nabla T_\alpha + \frac{2T_\alpha}{5p_\alpha}\nabla\cdot\underline{\underline{I}}_\alpha - \frac{2}{5}\frac{e_\alpha}{k_B p_\alpha}\underline{\underline{E}}'\cdot\underline{\underline{I}}_\alpha + \frac{1}{k_B n_\alpha}\sum_{\beta} a_{\alpha\beta}\left[\frac{\gamma_\beta}{(\gamma_\alpha+\gamma_\beta)} A^{(7)}_{\alpha\beta}(\underline{U}_\alpha - \underline{U}_\beta) + 2\xi_{\alpha\beta}\underline{U}_\alpha\right] \tag{2.50}$$

$$(\tau_\alpha^*)^{-1} \equiv \tfrac{1}{2}\left(A^{(5)}_{\alpha\alpha} + A^{(6)}_{\alpha\alpha}\right)\nu_{\alpha\alpha} + \sum_{\beta\neq\alpha}\left(\frac{m_\beta}{m_\alpha+m_\beta}\right) A^{(5)}_{\alpha\beta}\,\nu_{\alpha\beta} \tag{2.51}$$

$$\lambda_\alpha \equiv \frac{5}{2}\frac{k_B p_\alpha}{m_\alpha}\tau_\alpha^* \,, \quad \underline{\omega}_\alpha = \frac{e_\alpha \underline{B}}{m_\alpha} \tag{2.52}$$

$$b_{\alpha\beta} \equiv \frac{m_\beta}{m_\alpha+m_\beta} A^{(6)}_{\alpha\beta}\frac{p_\alpha}{p_\beta}\nu_{\alpha\beta}\tau_\alpha^* \tag{2.53}$$

The relative thermal flux vectors $\underline{h}_\alpha$ $(\alpha = e, i, n, h)$ can be determined from the closed algebraic system of equations (2.49).

However, the equation for the electronic flux vector $\underline{h}_e$ becomes uncoupled from the heavy particle species thermal fluxes h_k $(k \neq e)$ after neglecting terms of order m_e/m_k, the coefficients b_{ek} being less than or of order $n_e m_e / n_k m_k \ll 1$. Thus, the equation for $\underline{h}_e$ takes the form

$$\underline{h}_e = -\lambda_e \underline{p}_e + \underline{h}_e \wedge \underline{\omega}_e \tau_e' \tag{2.54}$$

In addition to this uncoupling, further simplification in the equation for $\underline{h}_e$ is possible because $|\xi_{ek}| \ll 1$. Thus equations (2.50) for $\alpha = e$ reduces to

$$\underline{p}_e = \nabla T_e + \frac{2}{5}\frac{T_e}{p_e}\nabla \cdot \underline{\underline{\tau}}_e + \frac{2e}{5k_B p_e}\underline{\underline{\tau}}_e \cdot \underline{E}' + \frac{1}{k_B n_e}\sum_{k \neq e} a_{ek} A_{ek}^{(7)} (\underline{U}_e - \underline{U}_k), \tag{2.55}$$

while from the equations for the quantities $G_{\alpha\beta}^{(n)}$ it is shown in reference (10) that:

$$A_{ek}^{(5)} \approx \frac{5}{2} - \frac{2}{5}\frac{\left[5\Omega_{ek}^{(1)}(2) - \Omega_{ek}^{(1)}(3)\right]}{\Omega_{ek}^{(1)}(1)} \tag{2.56}$$

and

$$A_{ek}^{(7)} \approx A_{ek}^{(2)} \tag{2.57}$$

It can be shown that

$$\frac{1}{2}\left(A_{\alpha\alpha}^{(5)} + A_{\alpha\alpha}^{(6)}\right) = \frac{1}{5}\frac{\Omega_{\alpha\alpha}^{(2)}(2)}{\Omega_{\alpha\alpha}^{(1)}(1)} \tag{2.58}$$

It also follows from the smallness of the electron mass that the largest contribution to equation (2.30) is made by the electronic flux vector $\underline{h}_e$. It follows that equations (2.30) have the form

$$\sum_{k \neq e} \Delta_{ek}[m_e \underline{C}] = \sum_k a_{ek}(\underline{U}_k - \underline{U}_e) - \frac{\underline{h}_e}{p_e}\sum_k a_{ek} A_{ek}^{(2)} \tag{2.59a}$$

and

$$\sum_\beta \Delta_{k\beta}[m_k \underline{C}] = \sum_\beta a_{k\beta}(\underline{U}_\beta - \underline{U}_k) + a_{ek} A_{ek}^{(2)} \frac{\underline{h}_e}{p_e}, \quad k \neq e \tag{2.59b}$$

The flux vector $\underline{h}_e$ is given by equation (2.54), which can be solved

for $\underline{h}_e$ to give

$$\underline{h}_e = -\lambda_e \left[\underline{P}_e - \frac{\beta_e^*}{(1+\beta_e^{*2})} \underline{P}_e \wedge \underline{b} + \frac{\beta_e^{*2}}{(1+\beta_e^{*2})} (\underline{P}_e \wedge \underline{b}) \wedge \underline{b} \right] \qquad (2.60)$$

where

$$\beta_e^* = \frac{eB\tau_e^*}{m_e}$$

Substituting equation (2.60) in equation (2.59) it is such that the quantities $\sum_\beta \Delta_{\alpha\beta} [m_\alpha \underline{C}]$ can be expressed in the form

$$\sum_\beta \Delta_{\alpha\beta} [m_\alpha \underline{C}] = \sum_\beta a_{\alpha\beta} (\underline{v}_\beta - \underline{v}_\alpha) - \underline{\underline{b}}_\alpha \cdot \underline{P}_e \qquad (2.61)$$

where the operator $\underline{\underline{b}}_\alpha$ is defined through the relation

$$\underline{\underline{b}}_\alpha \cdot \underline{P}_e = b_\alpha^{(1)} \underline{P}_e + b_\alpha^{(2)} \underline{P}_e \wedge \underline{B} + b_\alpha^{(3)} (\underline{P}_e \wedge \underline{B}) \wedge \underline{B} \qquad (2.62)$$

and the scalars $b_\alpha^{(1)}$, $b_\alpha^{(2)}$, $b_\alpha^{(3)}$, are given by the following expressions:

for electrons,

$$\begin{bmatrix} b_e^{(1)} \\ b_e^{(2)} \\ b_e^{(3)} \end{bmatrix} = -\frac{5}{2} \frac{k_B}{m_e} \tau_e^* \sum_{k \neq e} a_{ek} A_{ek}^{(2)} \begin{bmatrix} 1 \\ -\beta_e^*/(1+\beta_e^{*2}) \\ \beta_e^{*2}/(1+\beta_e^{*2}) \end{bmatrix} \qquad (2.63a)$$

while, for a heavy component k,

$$\begin{bmatrix} b_k^{(1)} \\ b_k^{(2)} \\ b_k^{(3)} \end{bmatrix} = \frac{5}{2} \frac{k_B}{m_e} \tau_e^* a_{ek} A_{ek}^{(2)} \begin{bmatrix} 1 \\ -\beta_e^*/(1+\beta_e^{*2}) \\ \beta_e^{*2}/(1+\beta_e^{*2}) \end{bmatrix} \qquad (2.63b)$$

The system of differential equations for the diffusion velocities, obtained by using the expression (2.61) for the collisional momentum transfer in the species conservation of momentum equations, can be considerably simplified by assuming that, first, the viscous parts of the species pressure tensors can be neglected; and, second, the macroscopic parameters of the plasma change only slightly within distances of the order of the mean free path and during times of the order of

the collision times in the plasma. The first assumption can be shown to be generally valid (see reference (10)). The second assumption is satisfied in all but cases of extreme nonuniformities such as the case of a gasdynamic shock in the plasma or a very strong electric field. When the second assumption is satisfied, it is possible to neglect the derivatives of $\underline{U}_\alpha$, replacing derivatives of $\underline{u}_\alpha$ with derivatives of $\underline{u}$ (see reference (10)). This assumption is used to derive the equations (2.49) for the relative thermal fluxes $\underline{h}_\alpha$.

The above assumptions lead to species conservation of momentum equations

$$\rho_\alpha \frac{D\underline{u}}{Dt} + \nabla p_\alpha = q_\alpha \left(\underline{E}' + \underline{U}_\alpha \wedge \underline{B}\right) + \sum_{\beta \neq \alpha} \Delta_{\alpha\beta}\left[m_\alpha \underline{C}\right] \qquad (2.64)$$

where $D/Dt \equiv \partial/\partial t + \underline{u}\cdot\nabla$. The inelastic collision terms in equation (2.64) have been neglected just as the effects of inelastic collisions are neglected in the derivation of the transport equations for the quantities $\underline{h}_\alpha$. This follows from the fact that for the calculation of transport quantities, terms representing inelastic collisions in the Boltzmann equations can be neglected because the excitation and ionization cross-sections for most particles are much smaller than the cross-sections for elastic collisions and effects of inelastic collisions on the distribution functions are consequently small [1],[12].

Using the overall momentum equation, as obtained by summation of equations (2.64) over all components, namely

$$\rho \frac{D\underline{u}}{Dt} + \nabla p = \rho^c \underline{E}' + \underline{J} \wedge \underline{B} \qquad (2.65)$$

to eliminate $D\underline{u}/Dt$ from equations (2.64), we obtain the following algebraic system for the diffusion velocities:

$$\sum_\beta a_{\alpha\beta}\left(\underline{U}_\beta - \underline{U}_\alpha\right) + q_\alpha \underline{U}_\alpha \wedge \underline{B} = \frac{\rho_\alpha}{\rho}\underline{J} \wedge \underline{B} + \frac{\rho_\alpha}{\rho}\rho^c \underline{E}' + \nabla p_\alpha - \frac{\rho_\alpha}{\rho}\nabla p \qquad (2.66)$$
$$- q_\alpha \underline{E}' + \underline{b}_\alpha \cdot \underline{P}_e$$

where use has been made of equation (2.61).

Comparing terms arising from $\underline{\underline{b}}_\alpha \cdot \underline{p}_e$ with the other terms of equation (2.66), it is apparent that only the first and last terms of $\underline{p}_e$, which is given by equation (2.55), can make significant contributions. Retaining only these terms, we have

$$\underline{p}_e \simeq \nabla T_e + \frac{1}{k_B n_e} \sum_{k \neq e} a_{ek} A_{ek}^{(1)} (\underline{V}_e - \underline{V}_k) \tag{2.67}$$

So far, in this section, the work presented has been little more than a summary of the work of reference (10), and no use has been made of the fact that the plasma is an inert noble gas, slightly seeded with alkali metal; that is, the particle species are neutral noble gas atoms ($\alpha = h$), neutral seed atoms ($\alpha = n$), singly charged seed ions ($\alpha = i$), and electrons ($\alpha = e$). It is assumed that seeding is sufficiently slight that

$$\frac{\rho_e}{\rho} \ll 1 \,, \quad \frac{\rho_i}{\rho} \ll 1 \,, \quad \frac{\rho_n}{\rho} \ll 1 \tag{2.68}$$

This assumption of slight seeding makes possible great simplifications of the expressions for the diffusion velocities $\underline{V}_\alpha$ and the electron heat flux vector $\underline{h}_e$, as will be shown in the remainder of this section. Simplificiations can immediately be made if those terms of equation (2.66) which contain ρ_α/ρ $(\alpha \neq h)$ as a multiplicative factor are compared with appropriate other terms. Thus, for $\alpha = e$ or i, if we assume that $|q_\alpha \underline{V}_\alpha| \sim |\underline{J}|$, $|q_\alpha| \sim |\rho^c|$ and $|\nabla p_\alpha| \gg \left|\frac{\rho_\alpha}{\rho} \nabla p\right|$, the terms $\frac{\rho_\alpha}{\rho} \underline{J} \times \underline{B}$, $\frac{\rho_\alpha}{\rho} \rho^c \underline{E}'$ and $\frac{\rho_\alpha}{\rho} \nabla p$ can be neglected in equations (2.66). The same terms can be neglected in equation (2.66) for $\alpha = n$ if we assume, that, in addition to $|\nabla p_n| \gg \left|\frac{\rho_n}{\rho} \nabla p\right|$, equation (2.65) implies that $\nabla p \sim \rho^c \underline{E} + \underline{J} \times \underline{B}$. The simplified forms of equations (2.66) are, for $\alpha \neq h$,

$$\sum_\beta a_{\alpha\beta} (\underline{V}_\beta - \underline{V}_\alpha) + q_\alpha \underline{V}_\alpha \times \underline{B} = \nabla p_\alpha - q_\alpha \underline{E}' + \underline{\underline{b}}_\alpha \cdot \underline{p}_e \,, \tag{2.69}$$

where $q_e = -n_e e$, and $q_i = n_i e$

It is sufficient to consider the three $(\alpha = e, i, n)$ equations (2.69), since $\underline{U}_h$ can be eliminated using the relation (2.12) in the form

$$\underline{U}_h = -\left(\sum_{\gamma \neq h} \rho_\gamma \underline{U}_\gamma\right)/\rho_h \tag{2.70}$$

Equations (2.69) then constitute three algebraic equations for the three unknowns $\underline{U}_e$, $\underline{U}_i$ and $\underline{U}_n$. Further simplifications following from the slight seeding assumption (2.68) greatly simplify the solution of equations (2.69).

The three equations (2.69) with $\underline{U}_h$ eliminated using equation (2.70) can be written in the forms

$$C_{ei}\underline{U}_i + C_{en}\underline{U}_n - C_{ee}\underline{U}_e + q_e \underline{U}_e \wedge \underline{B} = \nabla p_e - q_e \underline{E}' + \underline{b}_e \cdot \underline{P}_e \tag{2.71a}$$

$$C_{ie}\underline{U}_e + C_{in}\underline{U}_n - C_{ii}\underline{U}_i + q_i \underline{U}_i \wedge \underline{B} = \nabla p_i - q_i \underline{E}' + \underline{b}_i \cdot \underline{P}_e \tag{2.71b}$$

$$C_{ne}\underline{U}_e + C_{ni}\underline{U}_i - C_{nn}\underline{U}_n = \nabla p_n + \underline{b}_n \cdot \underline{P}_e \tag{2.71c}$$

where

$$C_{ei} = a_{ei} - \frac{\rho_i}{\rho_h} a_{eh}, \quad C_{en} = a_{en} - \frac{\rho_n}{\rho_h} a_{eh}, \quad C_{ee} = \sum_{\gamma \neq e} a_{e\gamma} \simeq a_{ei} + a_{eh} \tag{2.72a}$$

$$C_{ie} = a_{ie} - \frac{\rho_e}{\rho_h} a_{ih} \simeq a_{ie}, \quad C_{in} = a_{in} - \frac{\rho_n}{\rho_h} a_{ih}, \quad C_{ii} = \sum_{\gamma \neq i} a_{i\gamma} \simeq a_{ih} \tag{2.72b}$$

$$C_{ne} = a_{ne} - \frac{\rho_e}{\rho_h} a_{nh} \simeq a_{ne}, \quad C_{ni} = a_{ni} - \frac{\rho_i}{\rho_h} a_{nh}, \quad C_{nn} = \sum_{\gamma \neq n} a_{n\gamma} \simeq a_{nh} \tag{2.72c}$$

The approximations made in equations (2.72) follow from the assumption of slight seeding and the smallness of the electron mass. It should be noted that a_{ei} is not neglected in C_{ee} so as to allow for the possibility that electron-ion collisions dominate electron-buffer gas atom collisions; i.e., $a_{ei} > a_{eh}$. The assumption of slight seeding and the smallness of electron mass allow further approximations to be made in equations (2.71), which finally reduce to the following system:

$$-C_{ee}\underline{U}_e + q_e \underline{U}_e \wedge \underline{B} = \nabla p_e - q_e \underline{E}' + \underline{b}_e \cdot \nabla T_e + \underline{b}_e \cdot \left\{\frac{1}{k_B n_e} \underline{U}_e \sum_{\alpha \neq e} a_{e\alpha} A_{e\alpha}^{(7)}\right\} \tag{2.73a}$$

$$-C_{ii}\underline{U}_i + q_i \underline{U}_i \wedge \underline{B} = \nabla p_i - q_i \underline{E}' + \underline{b}_i \cdot \nabla T_e \qquad (2.73b)$$

$$-C_{nn}\underline{U}_n = \nabla p_n \qquad (2.73c)$$

where

$$\sum_{\alpha \neq e} a_{e\alpha} A_{e\alpha}^{(7)} \simeq a_{ei} A_{ei}^{(7)} + a_{eh} A_{eh}^{(7)}$$

It should be noted that the disappearance of the term $\underline{b}_n \cdot \nabla T_e$ from the right handside of (2.73c) follows from its smallness compared to the term ∇p_n when slight seeding is assumed.

From equation (2.73c) we immediately have an expression for $\underline{U}_n$:

$$\underline{U}_n = -\frac{1}{C_{nn}} \nabla p_n$$
$$\simeq -\frac{1}{a_{nh}} \nabla p_n$$

or

$$\underline{U}_n = -\frac{1}{m_{nh} n_n \nu_{nh}} \nabla p_n \qquad (2.74)$$

From equation (2.73b) an expression for $\underline{U}_i$ can be found in the form

$$\underline{U}_i = -\frac{\sigma_i}{q_i^2}\left(\nabla p_i - q_i \underline{E}' + \underline{b}_i \cdot \nabla T_e\right) - \frac{\sigma_i}{q_i^2}\frac{\beta_i}{(1+\beta_i^2)}\left(\nabla p_i - q_i \underline{E}' + \underline{b}_i \cdot \nabla T_e\right) \wedge \underline{b}$$
$$-\frac{\sigma_i}{q_i^2}\frac{\beta_i^2}{(1+\beta_i^2)}\left\{\left(\nabla p_i - q_i \underline{E}' + \underline{b}_i \cdot \nabla T_e\right) \wedge \underline{b}\right\} \wedge \underline{b}, \qquad (2.75)$$

where

$$\underline{b} = \underline{B}/|\underline{B}|,$$

β_i is the ion Hall parameter defined as

$$\beta_i \equiv \frac{q_i B}{C_{ii}} = \frac{e n_i B}{C_{ii}} \simeq \frac{e n_i B}{a_{ih}} = \frac{eB}{m_{ih}\nu_{ih}}; \qquad (2.76)$$

and σ_i is the ion conductivity defined as

$$\sigma_i \equiv \frac{q_i^2}{C_{ii}} = \frac{n_i^2 e^2}{C_{ii}} \simeq \frac{n_i^2 e^2}{a_{ih}} = \frac{n_i e^2}{m_{ih}\nu_{ih}} \qquad (2.77)$$

Equation (2.73a) can be written in the form

$$-\left[C_{ee} + \frac{b_e^{(1)}}{k_B n_e}\sum_{\alpha \neq e} a_{e\alpha} A_{e\alpha}^{(7)}\right]\underline{U}_e + \left[q_e B + \frac{\beta_e^*}{(1+\beta_e^{*2})}\frac{b_e^{(1)}}{k_B n_e}\sum_{\alpha \neq e} a_{e\alpha} A_{e\alpha}^{(7)}\right]\underline{U}_e \wedge \underline{b}$$
$$-\frac{\beta_e^{*2}}{(1+\beta_e^{*2})}\frac{b_e^{(1)}}{k_B n_e}\left(\sum_{\alpha \neq e} a_{e\alpha} A_{e\alpha}^{(7)}\right)(\underline{U}_e \wedge \underline{b}) \wedge \underline{b} = \nabla p_e - q_e \underline{E}' + \underline{b}_e \cdot \nabla T_e \qquad (2.73)$$

from which

$$\underline{U}_e = -\frac{\sigma_e}{q_e^2}\left(\nabla p_e - q_e\underline{E}' + \underline{\underline{b}}_e\cdot\nabla T_e\right) + \frac{\sigma_e^*}{q_e^2}\frac{\beta_e}{(1+\beta_e^2)}\left(\nabla p_e - q_e\underline{E}' + \underline{\underline{b}}_e\cdot\nabla T_e\right)\wedge\underline{b} - \frac{\sigma_e}{q_e^2}\left(1-\frac{1}{(1+\beta_e^2)}\frac{\sigma_e^*}{\sigma_e}\right)\left\{\left(\nabla p_e - q_e\underline{E}' + \underline{\underline{b}}_e\cdot\nabla T_e\right)\wedge\underline{b}\right\}\wedge\underline{b} \qquad (2.79)$$

where

$$\sigma_e \equiv q_e^2\Big/\left[C_{ee} + \frac{b_e^{(1)}}{k_B n_e}\sum_{\alpha\neq e} a_{e\alpha}A_{e\alpha}^{(1)}\right], \qquad (2.80)$$

$$\sigma_e^* \equiv q_e^2\Big/\left[C_{ee} + \frac{1}{(1+\beta_e^{*2})}\frac{b_e^{(1)}}{k_B n_e}\sum_{\alpha\neq e} a_{e\alpha}A_{e\alpha}^{(1)}\right] \qquad (2.81)$$

$$\beta_e \equiv -\left[q_eB + \frac{\beta_e^*}{(1+\beta_e^{*2})}\frac{b_e^{(1)}}{k_B n_e}\sum_{\alpha\neq e} a_{e\alpha}A_{e\alpha}^{(1)}\right]\Big/\left[C_{ee} + \frac{1}{(1+\beta_e^{*2})}\frac{b_e^{(1)}}{k_B n_e}\sum_{\alpha\neq e} a_{e\alpha}A_{e\alpha}^{(1)}\right] \qquad (2.82)$$

and

$$C_{ee} \simeq a_{ei} + a_{eh} \qquad (2.83)$$

The quantity σ_e defined by equation (2.80) is the electron conductivity.

Finally, an expression for q_e is obtained from equation (2.60), in the form

$$q_e = \frac{5}{2}p_e\underline{U}_e - \lambda_e\left[\underline{P}_e - \frac{\beta_e^*}{(1+\beta_e^{*2})}\underline{P}_e\wedge\underline{b} + \frac{\beta_e^{*2}}{(1+\beta_e^{*2})}\left(\underline{P}_e\wedge\underline{b}\right)\wedge\underline{b}\right] \qquad (2.84)$$

where

$$\lambda_e = \frac{5}{2}\frac{k_B p_e}{m_e}\tau_e^* \qquad (2.85)$$

$$\beta_e^* = \frac{eB}{m_e}\tau_e^* \qquad (2.86)$$

and P_e is given by equation (2.67), which, if seeding is slight, has the approximate form

$$\underline{p}_e \approx \nabla T_e + \frac{1}{k_B n_e}\left[a_{ei} A_{ei}^{(7)} (\underline{U}_e - \underline{U}_i) + a_{eh} A_{eh}^{(7)} \underline{U}_e \right] \quad (2.87)$$

The coefficients of equations (2.74), (2.75), (2.79) and (2.84) for the diffusion velocities $\underline{U}_n$, $\underline{U}_i$, $\underline{U}_e$ and electron heat flux vector $\underline{q}_e$ depend on certain collision parameters $\Omega_{\alpha\beta}^{(l)}(r)$ defined by equation (2.36), which in turn depend on the laws of interaction between the various particles. The interactions of interest here are electron-electron, electron-neutral buffer gas atom, electron-seed ion, neutral seed atom - buffer gas atom, and seed ion - buffer gas atom interactions. For all applications considered here, the alkali metal seed and inert buffer gas are caesium and helium respectively. For interactions between heavy particles, only the parameters $\Omega_{\alpha\beta}^{(1)}(1)$, or equivalently, the cross-section $Q_{\alpha\beta}$ need to be known. The caesium atom – helium atom cross-section Q_{nh} is assumed to be independent of the heavy particle temperature and its value is taken to be that given in reference (13) for a temperature of 1160°K:

$$Q_{nh} = 1.62 \times 10^{-18}\ m^2$$

A value for the ion-buffer gas atom cross-section Q_{ih} cannot be found; its value is assumed here to be equal to Q_{nh}, i.e.,

$$Q_{ih} = Q_{nh}$$

For interactions involving electrons, it is necessary to determine, in addition to $\Omega_{ek}^{(1)}(1)$, the collision parameters $\Omega_{ee}^{(1)}(1)$, $\Omega_{ek}^{(1)}(2)$, $\Omega_{ek}^{(1)}(3)$, and $\Omega_{ee}^{(2)}(2)$, where the subscript k refers to ions and buffer gas atoms; this can be seen from equations (2.34), (2.56) and (2.58). Two cases of interactions can be distinguished:

(a) For electron-buffer gas atom collisions, use is made of the fact that the momentum transfer cross-section for electron-helium atom collisions Q_{eh} varies very little over a wide range of electron temperatures, unlike, for example, electron-argon atom collisions, the cross-

section for which has a very strong dependence on electron temperature. Argyropoulos and Casteel [14] give values of the electron-helium atom cross-section in the range

$$8.37 \times 10^{-20} m^2 \leq Q_{eh} \leq 8.71 \times 10^{-20} m^2$$

for

$$1000°K \leq T_e \leq 3000°K$$

The cross-section is assumed here to be constant and equal to the value $8.69 \times 10^{-20} m^2$; i.e.,

$$Q_{eh} = 8.69 \times 10^{-20} m^2$$

The weak dependence of the cross-section Q_{eh} on electron temperature means that the electron-helium interactions may be regarded as interactions between rigid elastic spheres of diameters σ_1 and σ_2 . The collision parameter $\Omega_{eh}^{(l)}(r)$ for such interactions is found from equation (2.36) to have the form

$$\Omega_{eh}^{(l)}(r) = \frac{\pi^{1/2}}{8} \sigma_{12}^2 \left[2 - \frac{1}{(l+1)} \left\{ 1 + (-1)^l \right\} \right] \left(\frac{2 k_B T_e}{m_e} \right)^{1/2} (r+1)! \qquad (2.83)$$

where $\sigma_{12} = \sigma_1 + \sigma_2$. From equations (2.34), (2.56), (2.57) and (2.88) the coefficients $A_{eh}^{(2)}$, $A_{eh}^{(5)}$ and $A_{eh}^{(7)}$ can be determined:

$$A_{eh}^{(2)} = A_{eh}^{(7)} = \frac{1}{5} \qquad (2.89a)$$

and

$$A_{eh}^{(5)} = \frac{13}{10} \qquad (2.89b)$$

These values of the coefficients $A_{eh}^{(2)}$, $A_{eh}^{(5)}$ and $A_{eh}^{(7)}$ are in close agreement with the values tabulated in Argyropoulos and Casteel [14] for $1000°K \leq T_e \leq 3000°K$

(b) For electron-electron and electron-seed ion collisions, which are coulomb interactions, the collision parameters $\Omega_{e\alpha}^{(l)}(1)$ $(\alpha = e, i)$ and hence the cross-sections $Q_{e\alpha}$, can be evaluated by cutting off the integration in equation (2.36) with respect to the impact parameter b

at the Debye length λ_D, which is given by the relation [10]

$$\lambda_D^{-2} = \frac{e^2}{k_B \epsilon_0}\left(\frac{n_e}{T_e} + \frac{n_i}{T}\right) \tag{2.90}$$

The collision parameters $\Omega_{ee}^{(1)}(1)$ and $\Omega_{ei}^{(1)}(1)$ so obtained are given by

$$\Omega_{ee}^{(1)}(1) = \frac{1}{8}\pi\left[\frac{e^2}{4\pi\epsilon_0}\frac{1}{k_B T_e}\right]^2 \bar{g}_{ee} \ln \Lambda_{ee} \tag{2.91a}$$

and

$$\Omega_{ei}^{(1)}(1) = \frac{1}{8}\pi\left[\frac{e^2}{4\pi\epsilon_0 k_B T_e}\right]^2 \bar{g}_{ei} \ln \Lambda_{ei} \tag{2.91b}$$

where

$$\bar{g}_{ee} = \left(\frac{16 k_B T_e}{\pi m_e}\right)^{1/2} \tag{2.92a}$$

$$\bar{g}_{ei} = \left(\frac{8 k_B T_e}{\pi m_e}\right)^{1/2} \tag{2.92b}$$

and

$$\Lambda_{ee} = \Lambda_{ei} = \lambda_D \frac{12\pi\epsilon_0 k_B T_e}{e^2} \tag{2.92c}$$

From equations (2.91a) and (2.91b), the cross-sections Q_{ee} and Q_{ei} can be obtained using equation (2.42):

$$Q_{ee} = Q_{ei} = \frac{2}{3}\pi\left[\frac{e^2}{4\pi\epsilon_0 k_B T_e}\right]^2 \ln \Lambda_{ee} \tag{2.93}$$

Evaluating the parameters $\Omega_{ei}^{(1)}(2)$ and $\Omega_{ei}^{(1)}(3)$ in the same way, it is found that

$$\Omega_{ei}^{(1)}(2) = \Omega_{ei}^{(1)}(1) \tag{2.94a}$$

and

$$\Omega_{ei}^{(1)}(3) = 2\,\Omega_{ei}^{(1)}(1) \tag{2.94b}$$

Using equations (2.94a), the coefficients $A_{ei}^{(2)}$, $A_{ei}^{(5)}$ and $A_{ei}^{(7)}$ can be found from equations (2.34), (2.56) and (2.57):

$$A_{ei}^{(21)} = -\frac{3}{5} \tag{2.95a}$$

$$A_{ei}^{(51)} = \frac{13}{10} \tag{2.95b}$$

and

$$A_{ei}^{(71)} = A_{ei}^{(21)} \tag{2.95c}$$

Finally, the collision parameter $\Omega_{ee}^{(2)}(2)$ can be evaluated and used in equation (2.58) to obtain

$$\frac{1}{2}\left(A_{ee}^{(51)} + A_{ee}^{(61)}\right) = \frac{2}{5}\left[1 - (2\ln\Lambda_{ee})^{-1}\right] \tag{2.96}$$

The condition for validity of the Debye cut off method used to evaluate the above collision parameters, is that there be many charged particles in a sphere of radius λ_D (Debye sphere). This condition is generally satisfied for plasmas used as working fluids of MHD power generators and means that the quantity Λ_{ee} is large; that is, the quantity in brackets on the right hand side of equation (2.96) is close to unity.

Making use of equations (2.89), (2.95) and (2.96), one obtains, from the defining equations (2.51), (2.63), (2.80), (2.81), (2.82) and (2.87),

$$(\tau_e^*)^{-1} = \frac{2}{5}\left[1 - (2\ln\Lambda_{ee})^{-1}\right]\nu_{ee} + \frac{13}{10}\left(\nu_{ei} + \nu_{eh}\right) \tag{2.97}$$

$$\begin{bmatrix} b_i^{(1)} \\ b_i^{(2)} \\ b_i^{(3)} \end{bmatrix} = -\frac{3}{2} k_B n_e \tau_e^* \nu_{ei} \begin{bmatrix} 1 \\ -\beta_e^*/(1+\beta_e^{*2}) \\ \beta_e^{*2}/(1+\beta_e^{*2}) \end{bmatrix} \tag{2.98}$$

$$\begin{bmatrix} b_e^{(1)} \\ b_e^{(2)} \\ b_e^{(3)} \end{bmatrix} = -\frac{3}{2} k_B n_e \tau_e^* \left(-\nu_{ei} + \frac{1}{3}\nu_{eh}\right) \begin{bmatrix} 1 \\ -\beta_e^*/(1+\beta_e^{*2}) \\ \beta_e^{*2}/(1+\beta_e^{*2}) \end{bmatrix} \tag{2.99}$$

$$\sigma_e = \frac{n_e e^2}{m_e\left[\nu_{ei} + \nu_{eh} + \frac{b_e^{(1)}}{k_B n_e}\left(A_{ei}^{(7)} n_i + A_{eh}^{(7)} \nu_{eh}\right)\right]} \tag{2.100}$$

$$\sigma_e^* = \frac{n_e e^2}{m_e\left[\nu_{ei} + \nu_{eh} + \frac{1}{(1+\beta_e^{*2})}\frac{b_e^{(1)}}{k_B n_e}\left(A_{ei}^{(7)}\nu_{ei} + A_{eh}^{(7)}\nu_{eh}\right)\right]} \tag{2.101}$$

$$\beta_e = \frac{\left[\frac{eB}{m_e} - \frac{\beta_e^*}{(1+\beta_e^{*2})}\frac{b_e^{(1)}}{k_B n_e}\left(A_{ei}^{(7)}\nu_{ei} + A_{eh}^{(7)}\nu_{eh}\right)\right]}{\left[\nu_{ei} + \nu_{eh} + \frac{1}{(1+\beta_e^{*2})}\frac{b_e^{(1)}}{k_B n_e}\left(A_{ei}^{(7)}\nu_{ei} + A_{eh}^{(7)}\nu_{eh}\right)\right]} \tag{2.102}$$

$$\underline{P}_e = \nabla T_e + \frac{m_e}{k_B}\left[\nu_{ei} A_{ei}^{(7)}\left(\underline{U}_e - \underline{U}_i\right) + \nu_{eh} A_{eh}^{(7)}\underline{U}_e\right] \tag{2.103}$$

where, in equations (2.100), (2.101) and (2.102),

$$\frac{b_e^{(1)}}{k_B n_e}\left(A_{ei}^{(7)}\nu_{ei} + A_{eh}^{(7)}\nu_{eh}\right) = -\frac{5}{2}T_e^*\left(A_{ei}^{(2)}\nu_{ei} + A_{eh}^{(2)}\nu_{eh}\right)^2$$

$$= -\frac{9}{10}T_e^*\left(-\nu_{ei} + \frac{1}{3}\nu_{eh}\right)^2 \tag{2.104}$$

In the case where the magnetic field is zero, equation (2.79) can be written in the form

$$\underline{U}_e = \frac{\sigma_e}{q_e}\left(\underline{E} - \frac{\nabla p_e}{q_e}\right) + \frac{1}{q_e}\phi_e \nabla T_e$$

where the thermal diffusion coefficient ϕ_e is given by

$$\phi_e = -\left(\frac{\sigma_e}{q_e}\right) b_e^{(1)} \tag{2.105}$$

Some idea of the accuracy of equation (2.79), with the coefficients given by equations (2.100) - (2.102), can be gained by evaluating the electron conductivity σ_e and the thermal diffusion coefficient ϕ_e in the two limits where electron buffer gas atom and coulomb collisions are dominant. In the limit where electron-buffer gas atom collisions are dominant, equation (2.100) gives

$$\sigma_e = \frac{13}{12}\frac{n_e e^2}{m_e \nu_{eh}} \simeq 1.08 \frac{n_e e^2}{m_e \nu_{eh}} \qquad (2.106a)$$

and from equation (2.105) we have

$$\phi_e = -0.417 \frac{n_e e k_B}{m_e \nu_{eh}} \qquad (2.106b)$$

The exact values of σ_e and ϕ_e in this limit are calculated, for rigid sphere interactions, to be [1]

$$\sigma_e = \frac{32}{9\pi}\frac{n_e e^2}{m_e \nu_{eh}} \simeq 1.13 \frac{n_e e^2}{m_e \nu_{eh}}$$

and

$$\phi_e = -\frac{4}{3\pi}\frac{n_e e k_B}{m_e \nu_{eh}} \simeq -0.424 \frac{n_e e k_B}{m_e \nu_{eh}}$$

which differ from the values given by equations (2.106a) and (2.106b) by about 5% and 2% respectively.

In the opposite limit of coulomb collisions dominant, equations (2.100) and (2.105) give

$$\sigma_e = 1.97 \frac{n_e e^2}{m_e \nu_{ei}} \qquad (2.107a)$$

and

$$\phi_e = 1.588 \frac{n_e e k_B}{m_e \nu_{ei}} \qquad (2.107b)$$

respectively. Spitzer and Härm have computed the exact values of σ_e and ϕ_e in this limit by numerical integration [1]:

$$\sigma_e = 1.975 \frac{n_e e^2}{m_e \nu_{ei}}$$

and

$$\phi_e = 1.389 \frac{n_e e k_B}{m_e \nu_{ei}}$$

which differ from the values given by equations (2.107a) and (2.107b) by about 0.3% and 13% respectively. Whilst, in this limit, the electron conductivity is very accurately represented, the accuracy of the thermal diffusion terms in equation (2.79), though acceptable, is evidently not so good.

The above comparisons indicate that the accuracy of the conductivity σ_e and electron thermal diffusion coefficient ϕ_e, obtained by application of Grad's 13-moment method, should be adequate for practical purposes, at least in the case where the dependence of the electron-buffer gas atom momentum transfer cross-section on electron temperature is weak. In fact, as indicated in reference (10), the conductivity given by equation (2.100) is identical with the second approximation of the Chapman-Enskog approach when $T = T_e$ and comparisons show that successive Chapman-Enskog approximations for the electron conductivity converge very rapidly after the first term [10]. However, the expression (2.84) for q_e, with λ_e, β_e^* and $\underline{P}_e$ given by equations (2.85) - (2.86) and equation (2.103) corresponds to the second approximation of the Chapman-Enskog approach of reference (15), which yields the first non-vanishing, and therefore the lowest order approximation for h_e. The error incurred by the use of equations (2.84), (2.85), (2.86) and (2.103) is for this reason larger than in the case of diffusion velocities. This is clear if use is made of equation (2.85) to calculate λ_e in the coulomb collision dominated limit. From equation (2.97) the formula so obtained is

$$\lambda_e = \frac{5}{2}\frac{k_B p_e}{m_e}\left[\frac{2.5}{(\sqrt{2}+3.25)\nu_{ei}}\right]$$

which coincides exactly with the formula obtained from the second approximation of the Chapman-Enskog approach of reference (15) and yields

$$\lambda_e = 1.34\frac{k_B p_e}{m_e \nu_{ei}} \qquad (2.108)$$

The exact formula obtained numerically by Spitzer and Härm is [15]

$$\lambda_e = 3.2 \frac{k_B p_e}{m_e \nu_{ei}}$$

which differs from that given by equation (2.198) by a factor of more than 2. The expressions (2.84)' and (2.85) for q_e (with $\beta_e^* = 0$) have been used in references (16) and (17), which are representative of the more sophisticated numerical studies of steady state flowing partially ionized plasmas in MHD generator channels.

The above considerations concerning the accuracy of the electron conductivity, and the thermal diffusion terms in equation (2.79), support the conclusion that the expressions derived here for the diffusion velocities should be regarded as completely adequate for partially ionized plasmas when seeding is slight. Such plasmas are utilized as working fluids of closed cycle MHD generators, and the aforementioned expressions should enable accurate quantitative predictions of the performance characteristics of such generators to be made. The expression for the electron heat flux vector, however, should be replaced with one of greater accuracy. The author has been unable to find such an expression in the literature, and in the present work makes use of a simplified form of the expression derived here, which is consistent with simplifications of the expressions for the diffusion velocities discussed below.

The expressions for the diffusion velocities, whilst much simplified by the assumption of slight seeding are too complex to be employed in the numerical model developed here because of the great demands made on computer resources. This has necessitated the use of simplified forms of the expressions. Thus the present work is restricted to the limit where electron-buffer gas atom collisions are dominant. From equations (2.97) and (2.104) it is clear that we can then, without significant loss of accuracy, neglect quantities proportional to

$$\frac{b_e^{(1)}}{k_B n_e} \left(A_{ei}^{(7)} \nu_{ei} + A_{eh}^{(7)} \nu_{eh} \right)$$

in equations (2.100) - (2.102), which reduce to

$$\sigma_e = \frac{n_e e^2}{m_e \nu_{eh}} \tag{2.109}$$

$$\sigma_e^* = \sigma_e \tag{2.110}$$

and

$$\beta_e = \frac{eB}{m_e \nu_{eh}} \tag{2.111}$$

From equation (2.79) the simplified expression for $\underline{U}_e$ is

$$\underline{U}_e = -\frac{\sigma_e}{q_e^2}\left(\nabla p_e - q_e \underline{E}' + \underline{b}_e \cdot \nabla T_e\right) + \frac{\sigma_e \beta_e}{q_e^2 (1+\beta_e^2)}\left(\nabla p_e - q_e \underline{E}' + \underline{b}_e \cdot \nabla T_e\right) \wedge \underline{b} - \frac{\sigma_e}{q_e^2}\frac{\beta_e^2}{(1+\beta_e^2)}\left[\left(\nabla p_e - q_e \underline{E}' + \underline{b}_e \cdot \nabla T_e\right) \wedge \underline{b}\right] \wedge \underline{b} \tag{2.112}$$

where $q_e = -n_e e$. The expressions (2.109) - (2.111) are identical with those obtained form the first approximation of the Chapman-Enskog approach of reference (1).

Consistent with the above simplifications, we replace equations (2.103), (2.84) and (2.85) with

$$\underline{P}_e = \nabla T_e,$$

$$\underline{q}_e = \frac{5}{2} p_e \underline{U}_e - \lambda_e \left[\nabla T_e - \frac{\beta_e}{(1+\beta_e^2)} \nabla T_e \wedge \underline{b} + \frac{\beta_e^2}{(1+\beta_e^2)} \left(\nabla T_e \wedge \underline{b}\right) \wedge \underline{b}\right], \tag{2.113}$$

and

$$\lambda_e = \frac{5}{2} \frac{k_B p_e}{m_e \nu_{eh}} \tag{2.114}$$

since, from equations (2.86) and (2.111) we set

$$\beta_e^* = \beta_e = \frac{eB}{m_e \nu_{eh}} \tag{2.115}$$

Whilst the accuracy of equations (2.113) and (2.114) is difficult to assess, because of the initial inaccuracy of equation (2.84), these equations do have the advantage of being relatively simple. Also, these equations are consistent with those used in most previous analytical

and numerical studies [7],[8],[19], and therefore allow comparisons of the results of the present work with those obtained by other authors to be more easily made.

The neglection of coulomb collisions imposes restrictions on the ranges of plasma conditions that can be considered in applications of the present theory, as can be seen, for example, from figure (2.1), in which the ratio (ν_{eh}/ν_{ei}) is plotted as a function of T_e for a seeding fraction of 0.002 using equations (1.9) and (1.14); it is apparent from figure (2.1) that the present theory is inaccurate at high electron temperatures. As we shall see in chapter 5, high electron temperatures can be obtained in regions of current concentration near electrode corners in an MHD generator, and some inaccuracy may be introduced as a result.

Most previous analytical and numerical studies of closed cycle MHD power generators have used equations (2.109) - (2.114) even when coulomb collisions are important, these collisions being accounted for by simply replacing ν_{eh} with $(\nu_{eh} + \nu_{ei})$. It is clear from the earlier considerations of accuracy that conclusions made in these studies regarding the effects of coulomb collisions may be quite inaccurate.

The expressions for the electron and ion diffusion velocities have been further simplified in the present work by neglecting the thermal diffusion terms; that is, the terms dependent on $\underline{b}_e \cdot \nabla T_e$ and $\underline{b}_i \cdot \nabla T_e$. The importance of these terms can be determined by estimating the dimensionless quantities $(b_e^{(1)} T_e/p_e)$ and $(b_i^{(1)} T_e/p_i)$; from equations (2.97) - (2.99),

$$\frac{b_e^{(1)} T_e}{p_e} = \frac{b_e^{(1)}}{k_B n_e} = -\frac{3}{2} T_e^{\frac{1}{2}} \left(-\nu_{ei} + \frac{1}{3}\nu_{eh}\right) = \left\{\frac{2}{5}\left[1 - (2\ln\Lambda_{ee})^{-1}\right]\nu_{ee} + \frac{13}{10}\left(\nu_{ei} + \nu_{eh}\right)\right\} \quad (2.116)$$

and

$$\frac{b_i^{(1)}T_e}{p_i} = \frac{b_i^{(1)}T_e}{k_B n_i T} = -\frac{3}{2}\tau_e^* \nu_{ei}\left(\frac{n_e}{n_i}\right)\left(\frac{T_e}{T}\right) = \frac{-\frac{3}{2}\nu_{ei}\left(\frac{n_e}{n_i}\right)\left(\frac{T_e}{T}\right)}{\left\{\frac{2}{5}\left[1-(2\ln\Lambda_{ee})^{-1}\right]\nu_e + \frac{13}{10}\left(\nu_i+\nu_h\right)\right\}} \quad (2.117)$$

In the limit where electron-buffer gas atom collisions dominate coulomb collisions $\nu_{eh} \gg \nu_{ei}$ and from equations (2.116) and (2.117),

$$\frac{b_e^{(1)}T_e}{p_e} \to -\frac{5}{13} \quad (2.118)$$

and

$$\frac{b_i^{(1)}T_e}{p_i} \to -\frac{15}{13}\frac{\nu_{ei}}{\nu_{eh}}\left(\frac{n_e T_e}{n_i T}\right) \quad (2.119)$$

From the limiting values (2.118) and (2.119) it follows that, whilst the ion thermal diffusion is negligibly small, electron thermal diffusion can be significant unless

$$\left|\frac{\nabla T_e}{T_e}\right| \ll \left|\frac{\nabla p_e}{p_e}\right| \quad (2.120)$$

The inequality (2.120) is difficult to justify a priori unless the electron density is given by Saha's equation, equation (1.14), according to which it is satisfied. It is concluded that electron thermal diffusion cannot in general be neglected even when $\nu_{eh} \gg \nu_{ei}$, though its omission should not result in large errors since the magnitude of the quantity $\left(b_e^{(1)}T_e / p_e\right)$ is less than unity. Neglecting the thermal diffusion terms, equations(2.75) and (2.112) reduce to

$$\underline{U}_i = -\frac{\sigma_i}{q_i^2}\left(\nabla p_i - q_i\underline{E}'\right) - \frac{\sigma_i}{q_i^2}\frac{\beta_i}{(1+\beta_i^2)}\left(\nabla p_i - q_i\underline{E}'\right)\wedge\underline{b} - \frac{\sigma_i}{q_i^2}\frac{\beta_i^2}{(1+\beta_i^2)}\left\{\left(\nabla p_i - q_i\underline{E}'\right)\wedge\underline{b}\right\}\wedge\underline{b} \quad (2.121)$$

and

$$\underline{U}_e = -\frac{\sigma_e}{q_e^2}\left(\nabla p_e - q_e\underline{E}'\right) + \frac{\sigma_e}{q_e^2}\frac{\beta_e}{(1+\beta_e^2)}\left(\nabla p_e - q_e\underline{E}'\right)\wedge\underline{b} - \frac{\sigma_e}{q_e^2}\frac{\beta_e^2}{(1+\beta_e^2)}\left\{\left(\nabla p_e - q_e\underline{E}'\right)\wedge\underline{b}\right\}\wedge\underline{b} \quad (2.122)$$

respectively.

Finally, it is assumed in the present work that

$$\beta_i \ll 1 \tag{2.123}$$

which can be satisfied when $\beta_e > 1$ since

$$\frac{\beta_e}{\beta_i} \sim \left(\frac{m_i}{m_e}\right)^{1/2} \gg 1$$

The condition (2.123), which imposes a limitation on the magnetic field for given plasma conditions, allows us to neglect the second and third terms of the right hand side of equation (2.121), which thus reduces to

$$\underline{U}_i = \frac{-\sigma_i}{q_i^2}\left(\nabla p_i - q_i \underline{E}'\right) \tag{2.124}$$

From equations (2.122) and (2.124) the electron and ion current densities

$$\underline{J}_e = q_e \underline{U}_e = -e n_e \underline{U}_e$$

and

$$\underline{J}_i = q_i \underline{U}_i = e n_i \underline{U}_i$$

are given by

$$\underline{J}_e = \sigma_e\left(\underline{E}' + \frac{\nabla p_e}{e n_e}\right) - \frac{\sigma_e \beta_e}{(1+\beta_e^2)}\left(\underline{E}' + \frac{\nabla p_e}{e n_e}\right)\wedge \underline{b} + \frac{\sigma_e \beta_e^2}{(1+\beta_e^2)}\left[\left(\underline{E}' + \frac{\nabla p_e}{e n_e}\right)\wedge \underline{b}\right]\wedge \underline{b} \tag{2.125a}$$

or

$$\sigma_e\left(\underline{E}' + \frac{\nabla p_e}{e n_e}\right) = \underline{J}_e + \beta_e\left(\underline{J}_e \wedge \underline{b}\right) \tag{2.125b}$$

and

$$\underline{J}_i = \sigma_i\left(\underline{E}' - \frac{\nabla p_i}{e n_i}\right) \tag{2.126}$$

respectively. From equations (2.125b) and (2.126) a relation can be derived between $\underline{J}_e$ and $\underline{J}$:

$$\underline{J}_e + \frac{\sigma_i \beta_e}{(\sigma_e+\sigma_i)}\left(\underline{J}_e \wedge \underline{b}\right) = \frac{\sigma_e}{(\sigma_e+\sigma_i)}\underline{J} + \frac{\sigma_e \sigma_i}{(\sigma_e+\sigma_i)}\left[\frac{\nabla p_i}{e n_i} + \frac{\nabla p_e}{e n_e}\right] \tag{2.127}$$

Now

$$\frac{\sigma_e}{\sigma_i} \sim \frac{\beta_e}{\beta_i} \sim \left(\frac{m_{ih}}{m_e}\right)^{1/2} >> 1 \qquad (2.128)$$

and, in equation (2.127),

$$\frac{\sigma_i \beta_e}{(\sigma_e+\sigma_i)} \simeq \frac{\sigma_i}{\sigma_e}\beta_e = \frac{n_i}{n_e}\beta_i << 1 \quad . \qquad (2.129)$$

where use has been made of the assumption (2.123). Using the result (2.129), the second term in the left hand side of equation (2.127) can be neglected and the following relation obtained:

$$\underline{J}_e \simeq \frac{\sigma_e}{(\sigma_i+\sigma_e)}\underline{J} + \frac{\sigma_e \sigma_i}{(\sigma_e+\sigma_i)}\left[\frac{\nabla p_i}{e n_i} + \frac{\nabla p_e}{e n_e}\right] \qquad (2.130)$$

By making use of the inequality (2.128), further approximations can be made in equations (2.130), which can be thus reduced to

$$\underline{J}_e \simeq \underline{J} + \sigma_i \left[\frac{\nabla p_i}{e n_i} + \frac{\nabla p_e}{e n_e}\right] \qquad (2.131)$$

The relation (2.131) is of great importance in the formulation of the final form of the electron continuity equation in section 2.5 .

Using equations (2.125) and (2.126) a relation between $\underline{E}'$ and $\underline{J}$, called the generalized Ohm's law, can be derived. Because of the limited amount of computer resources that could be made available to the author for the computational work reported in this thesis, a simplified form of generalized Ohm's law had to be used. This results from the assumption that either $|\underline{J}_e| >> |\underline{J}_i|$ or, if $|\underline{J}_e| \lesssim |\underline{J}_i|$, both $|\underline{J}_e|$ and $|\underline{J}_i|$ are negligibly small. Then the generalized Ohm's law is obtained by simply replacing $\underline{J}_e$ with $\underline{J}$ in equation (2.125b):

$$\sigma_e\left(\underline{E}' + \frac{\nabla p_e}{e n_e}\right) = \underline{J} + \beta_e(\underline{J} \wedge \underline{b}) \qquad (2.132)$$

The condition for validity of equation (2.132) is restrictive. For example, situations where $\underline{E}' \sim -\nabla p_e / n_e e$ which implies from equations (2.125a) and (2.126) that $|\underline{J}_e| \sim 0$ and $|\underline{J}_i| \sim \sigma_i \left|\frac{\nabla p_e}{e n_e} + \frac{\nabla p_i}{e n_i}\right|$.

Equation (2.132) must be excluded from consideration if $|\underline{J}|$ is significantly large.

Another example of violation of the condition for validity of equation (2.133) is the phenomenon of ambipolar diffusion. In the absence of a magnetic field, if $\underline{J}=0$, equations (2.125) and (2.126) yield

$$\underline{E}' = \frac{\left(\sigma_i \frac{\nabla p_i}{e n_i} - \sigma_e \frac{\nabla p_e}{e n_e}\right)}{(\sigma_e + \sigma_i)}$$

and

$$\underline{J}_e = -\underline{J}_i = \frac{\sigma_e \sigma_i}{(\sigma_e + \sigma_i)} \left(\frac{\nabla p_i}{e n_i} + \frac{\nabla p_e}{e n_e}\right) \qquad (2.133)$$

This phenomenon, which might occur if an electrically isolated electrode were in contact with the plasma, can invalidate the present theory if $|J_e|$ is significantly large.

2.4 THE GAS-DYNAMIC EQUATIONS AND COMPRESSIBLE TURBULENT BOUNDARY LAYERS. BASIC GAS-DYNAMIC EQUATIONS

Consistent with the assumption of slight seeding, as expressed by the inequalities (2.68),

$$\rho \simeq \rho_h \,, \quad p \simeq p_h \,, \quad \text{and} \quad \sum_{\alpha \neq e} \rho_\alpha \mathcal{E}_\alpha \simeq \rho_h \mathcal{E}_h$$

and the overall conservation equations for mass, momentum and heavy species energy, equations (2.20) - (2.22) have the approximate forms

$$\frac{\partial \rho_h}{\partial t} + \nabla \cdot \rho_h \underline{u} = 0, \tag{2.134}$$

$$\rho_h \frac{D\underline{u}}{Dt} = -\nabla p_h + \nabla \cdot \underline{\underline{\tau}}_h + \rho^c \underline{E}' + \underline{J} \times \underline{B} \tag{2.135}$$

and

$$\frac{D}{Dt}(\rho_h \mathcal{E}_h) + (\rho_h \mathcal{E}_h + p_h) \nabla \cdot \underline{u} = -\nabla \cdot \underline{q}_h + \underline{\underline{\tau}}_h : \nabla \underline{u} + \underline{E}' \cdot \underline{J}_i + n_e \frac{3}{2} k_B (T_e - T) \frac{2m_e}{m_h} \nu_{eh}, \tag{2.136}$$

where use has been made of equation (2.31). The term $-\rho_e \underline{u}_e \cdot \frac{D\underline{u}}{Dt}$ on the left hand side of equation (2.136) has been neglected as small because of the smallness of electron mass and the assumption of slight seeding. Equations (2.134) - (2.136) must be supplemented by the equations of state

$$p_h = \rho_h R_h T \quad \text{and} \quad \mathcal{E}_h = C_V T \tag{2.137}$$

where R_h is the gas constant and C_V is the specific heat at constant volume $\left(C_V = \frac{3}{2} R_h \right)$.

By virtue of the assumption of small ion Hall parameter ($\beta_i \ll 1$) the magnetic field has little effect on the total heavy particle heat flux vector q_H and the total viscous stress $\underline{\underline{\tau}}$, the electron contribution to which is negligibly small. It can be shown, using the theory presented in reference (1) that, when seeding is slight, the heavy particle transport properties are then approximately the same as those

for a gas consisting of buffer gas atoms only; that is, $\underline{\underline{\tau}} \doteq \underline{\underline{\tau}}_h$ and $\underline{q}_H \doteq \underline{q}_h$. The classical Chapman-Enskog theory shows that, for such a gas $\underline{\underline{\tau}}_h$ and $\underline{q}_h$ are given by the expressions [1]

$$(\tau_h)_{\alpha\beta} = \eta_h \left[\frac{\partial u_\alpha}{\partial x_\beta} + \frac{\partial u_\beta}{\partial x_\alpha} - \frac{2}{3} (\nabla \cdot \underline{u}) \delta_{\alpha\beta} \right] \tag{2.138}$$

and

$$\underline{q}_h = -\lambda_h \nabla T, \tag{2.139}$$

where η_h and λ_h are the buffer gas viscosity coefficient and thermal conductivity coefficient respectively. These coefficients can be calculated with the use of the Chapman-Enskog approach of expansion in Sonine polynomials. As in the case of $\underline{h}_e$ in section 2.3 , the second approximation of the Chapman-Enskog method yields the first nonvanishing, and therefore the lowest order approximations to η_h and λ_h . It is found that the lowest order approximations to η_h and λ_h are proportional, [18]

so that the dimensionless Prandtl number

$$P_r = \frac{C_p \eta_h}{\lambda_h} \tag{2.140}$$

is equal to a constant in this approximation. This constant is independent of the law of interaction between the particles and has a value of 2/3. The observed Prandtl number for monatomic gases varies little with T and is close to the predicted value: the value derived from experimental data for helium presented in Sears [20] is close to 0.68. It is assumed here that the Prandtl number is constant and equal to the latter value.

The expression for η_h used in this work is [3]

$$\eta_h = 5.1 \times 10^{-7} T^{0.65} \tag{2.141}$$

which is consistent with the power law dependence of η_h on the temperature predicted in the second approximation of the Chapman-Enskog method [19].

The work presented in this thesis is concerned, in part, with the description of the flow behaviour of the buffer gas in a closed cycle MHD power generator channel using equations (2.134) - (2.136). Limitations on the computer resources available to the author necessitated the introduction of a number of simplifying assumptions, made below , which effectively result in a decoupling of equations (2.134) - (2.136) from the equations governing the plasma and electromagnetic field properties. Whilst these assumptions impose great restrictions on the range of generator conditions that can be studied, as well as suppression of some relevant physical processes, they do enable a clearer understanding of the remaining important physical processes to be obtained. In addition, the numerical techniques used to solve equations (2.134) - (2.136) are quite different from those used to solve the other equations (see chapters 3 and 4), and these assumptions therefore facilitate the development and understanding of the numerical techniques employed, most of which can probably be extended without basic change to situations where some of the assumptions are not satisfied. It should be noted that the restrictions imposed on the range of generator conditions that can be considered because of these assumptions are consistent with those imposed because of the assumptions of negligible coulomb collisions and small ion Hall parameter made in section 2.3 .

Denoting the characteristic value of any quantity by the subscript c one obtains from the generalized Ohm's law, equation (2.132), for $\beta_e \ll 1$

$$E_c = u_c B_c \tag{2.141}$$

and

$$\bar{J}_c = \sigma_{ec} E_c \tag{2.142}$$

for the characteristic values of the electric field and current density respectively. Equation (2.141) assumes the electric field to be produced primarily by fluid motion in the magnetic field as is usually

the case in the bulk of the flow in an MHD generator channel.

Poisson's equation

$$\nabla \cdot \underline{E} = \rho^c / \epsilon_0 \tag{2.143}$$

yields a characteristic value for the charge density ρ^c given by

$$\rho^c = \frac{\epsilon_0 E_c}{L_c} \tag{2.144}$$

where the characteristic length scale L_c is, for the MHD generator considered here, taken to be equal to the length of a single segment of the generator, i.e., the segmentation length.

It follows from the equations (2.141), (2.142) and (2.144) that

$$\frac{\rho^c |\underline{u}|}{|\underline{J}|} \sim \left(\frac{\epsilon_0 E_c}{L_c}\right)\left(\frac{u_c}{\sigma_{ec} E_c}\right) = \left(\frac{u_c}{L_c}\right)\left(\frac{\epsilon_0}{\sigma_{ec}}\right) \ll 1 \tag{2.145}$$

and

$$\frac{\rho^c |\underline{E}'|}{|\underline{J} \wedge \underline{B}|} \sim \left(\frac{\epsilon_0 E_c}{L_c}\right)\left(\frac{u_c B_c}{\sigma_{ec} E_c B_c}\right) = \left(\frac{u_c}{L_c}\right)\left(\frac{\epsilon_0}{\sigma_{ec}}\right) \ll 1, \tag{2.146}$$

where it is assumed that

$$\frac{L_c}{u_L} \gg \frac{\epsilon_0}{\sigma_{ec}},$$

that is, that the time scale ϵ_0/σ_{ec} is much smaller than the time taken for the fluid to flow a distance equal to the segmentation length. Taking as typical values, $L_c = 2.54 \times 10^{-2}$ m, $u_c = 1200$ m/sec, and $\sigma_{ec} = 3$ mho/m, we find that

$$\left(\frac{u_c}{L_c}\right)\left(\frac{\epsilon_0}{\sigma_{ec}}\right) \sim 10^{-7}$$

so that the inequalities (2.145) and (2.146) are satisfied for the conditions of interest here. The inequality (2.146) shows that we can neglect the force acting on the fluid because of its net charge compared to the force resulting from currents (see equation (2.135)).

Using equations (2.141) and (2.142) the ratio of the $\underline{J} \wedge \underline{B}$ force to the inertial force can be estimated:

$$\frac{|\underline{J} \wedge \underline{B}|}{|\rho_h (\underline{u} \cdot \nabla)\underline{u}|} \sim \frac{L_c \sigma_{ec} B_c^2}{\rho_{hc} u_c} \equiv S \tag{2.147}$$

The parameter S is called the magnetic interaction parameter and the present theory is restricted to generator conditions for which

$$S \ll 1 \tag{2.148}$$

This allows us to neglect the $\underline{J} \wedge \underline{B}$ force in equation (2.135). The characteristic length L_c in (2.147) is to be taken to be equal to the generator length. Taking as typical values, $L_c = 0.6\,m$, $u_c = 1200$ m/sec, $\sigma_{ec} = 3\ mho/m$, $\rho_{hc} = 0.026\ kgm/m^3$, and $B_c = 1.4\,T$, we find that $S \simeq 0.1$, so that the condition (2.148) is satisfied for the conditions of interest in this work.

From the electron energy equation, the form of which is considered in detail in section 2.5 (see equation (2.214)), the term in equation (2.136) representing the transfer of energy to buffer gas atoms in elastic collisions with electrons is estimated to be of order the electron ohmic heating; i.e., the energy gained by the electrons from the electromagnetic field:

$$n_e \frac{3}{2} k_B (T_e - T) \frac{2m_e}{m_h} \nu_{eh} \sim \underline{E}' \cdot \underline{J}_e ,$$

so that, in equation (2.136),

$$\underline{E}' \cdot \underline{J}_i + n_e \frac{3}{2} (T_e - T) \frac{2m_e}{m_h} \nu_{eh}$$

$$\sim \underline{E}' \cdot \underline{J}_i + \underline{E}' \cdot \underline{J}_e = \underline{E}' \cdot \underline{J}$$

The latter quantity, which is the total ohmic heating, is compared to the rate of change of buffer gas energy due to convection:

$$\frac{|\underline{E}' \cdot \underline{J}|}{|\underline{u} \cdot \nabla (\rho_h \varepsilon_h + p_h)|} \sim \frac{\sigma_{ec} u_c^2 B_c^2}{(\rho_h \varepsilon_h)_c} \left(\frac{L_c}{u_c} \right)$$

$$= \frac{1}{\tau_h} \left(\frac{L_c}{u_c} \right) \ll 1 ,$$

if

$$\frac{L_c}{u_c} \ll \tau_h \tag{2.149}$$

where

$$\tau_h = \frac{\sigma_{oc} u_c^2 B_c^2}{(\rho_h \varepsilon_h)_c} \qquad (2.150)$$

The time scale τ_h defined by equation (2.150) is a characteristic time for changes in heavy particle temperature due to collisional energy exchange between the buffer gas atoms and electrons, and the inequality (2.149) states that these temperature changes can be neglected if the time spent by the fluid in the region of interest is much less than τ_h. If the inequality (2.149) is valid for L_c equal to the length of the generator, the last two terms of the right handside of equation (2.136) can be neglected. Taking as representative values $\sigma_{ec} = 3\ mho/m$, $u_c = 1200\ m/sec$, $B_c = 1.0T$, $p = 8.32 \times 10^4 n/m^2$ and $L_c = 0.6m$, it is found that $(1/\tau_h)(L_c/u_c) \sim 10^{-2}$, so that the inequality (2.149) is satisfied for the conditions of interest in this work, and the aforementioned simplification of equation (2.136) can be made.

Whilst the inequality (2.146), which allows one to neglect the electrostatic force compared to the $\underline{J} \wedge \underline{B}$ force in equation (2.135), is valid for a wide range of plasma conditions, the assumptions that the $\underline{J} \wedge \underline{B}$ force in equation (2.135), and the ion Ohmic heating and elastic collisional energy exchange terms in equation (2.136) be neglected are much more restrictive, and are justified only for conditions characteristic of some experimental generator systems. For conditions characteristic of MHD power generators designed for appreciable production of electrical power, these assumptions are generally not valid; in particular, $S \gtrsim 1$ for such generators.

The equations obtained from equations (2.134) - (2.136) after making approximations consistent with the above assumptions, when taken together with equations (2.137) - (2.141), constitute a closed system of partial differential equations for what will be called the gas dynamic variables ρ, ρ, $\underline{u}$ and T, where the subscript h has been

dropped for convenience. These equations are completely decoupled from the equations governing the plasma and electromagnetic field variables; this allows one to consider a steady flow of the buffer gas in the MHD generator, described by the following equations:

$$\nabla \cdot \rho \underline{u} = 0 , \tag{2.151}$$

$$\rho (\underline{u} \cdot \nabla) \underline{u} + \nabla p = \nabla \cdot \underline{\underline{T}}_h \tag{2.152}$$

and

$$\rho (\underline{u} \cdot \nabla) h_h - (\underline{u} \cdot \nabla) p = - \nabla \cdot \underline{q}_h + \underline{\underline{T}}_h : \nabla \underline{u} \tag{2.153}$$

where equation (2.153) is derived from equation (2.136) using equation (2.134) and the definition of the enthalpy h_h :

$$h_h = \varepsilon_h + p_h / \rho_h \tag{2.154}$$

which can be written in the form $h_h = c_p T$, where c_p is the specific heat at constant pressure.

Boundary Layer Approximations

The complex problem of solving the system of equations (2.151) - (2.153) for the case of flow in an MHD generator channel is greatly simplified by making use of the well known fact that the flow is of a boundary layer character. That is, considering the velocity distribution in the channel, the retardingeffects of the viscous forces are confined to layers in contact with the channel walls, called boundary layers (see figure 2.2). Consideringone of the channel walls, the flow velocity increases rapidly from zero (in the absence of slip) at the wall to approximately the velocity along the channel centre-line at the boundary layer edge, which is at a distance δ , called the boundary layer thickness, from the wall in question. Whereas in the boundary layers velocity gradients are large and viscous forces predominate, in the region external to the boundary layers, called the core of the flow, velocity gradients are small and inertial forces predominate.

Similar remarks apply to the temperature distribution; within the boundary layers, temperature gradients are large and viscous heating and thermal conduction are important, whereas in the core of the flow these effects are negligible and the temperature is approximately uniform and equal to the value at the channel centre-line.

As shown in reference (21), for example, the equations governing the boundary layer flow, the boundary layer equations, can be obtained from the full equations (2.151) - (2.153), which are thereby greatly simplified, by making approximations consistent with the well known boundary layer assumption

$$\delta/L_c \ll 1, \tag{2.155}$$

which can be shown to imply that

$$R_L \gg 1,$$

where $R_L = u_{xc} L_c \rho_c / \eta_{hc}$ is the Reynolds' number of the flow, the subscript c denotes channel centre-line value (u_{xc} is the component of velocity along the centre-line), and L_c is the characteristic length scale of variations of the gas-dynamic parameters along the channel.

Whilst the boundary layer equations are much simpler in form than equations (2.151) - (2.153) they still constitute a system of nonlinear partial differential equations which must be solved numerically. If no further approximations are made, the numerical solution of these equations imposes great demands on computer time because of the three dimensions involved. In the present work, the problem has been considerably simplified by reducing it to the solution of two mathematically identical systems of equations, each system involving two rather than three coordinates. This simplification follows from the fact that, as can be seen in figure 2.2, the boundary layers on each of the side walls are approximately two-dimensional with the exception of the corner regions. It is clear that an accurate description of the flow behaviour is possible by considering two-dimensional boundary layers on each of the side walls, provided corner effects can be neglected, which is the case for sufficiently small boundary layer thicknesses. This simplified model of the flow has been used for the

numerical work reported in this thesis even though the latter condition tends to be violated for the flows and generator conditions of interest here (see chapter 3).

Considering, then, two-dimensional boundary layers on each of the channel side walls, the boundary layer equations for one of the channel side walls, obtained from equations (2.151) - (2.153) by application of the condition (2.155), are as follows:

$$\frac{\partial}{\partial x}(\rho u_x) + \frac{\partial}{\partial y}(\rho u_y) = 0, \tag{2.156}$$

$$\rho u_x \frac{\partial u_x}{\partial x} + \rho u_y \frac{\partial u_x}{\partial y} = -\frac{\partial p}{\partial x} + \frac{\partial}{\partial y}\left[(\eta+\varepsilon)\frac{\partial u_x}{\partial y}\right] \tag{2.157}$$

$$\frac{\partial p}{\partial y} = 0 \tag{2.158}$$

and

$$c_p \rho u_x \frac{\partial T}{\partial x} + c_p \rho u_y \frac{\partial T}{\partial y} - u_x \frac{\partial p}{\partial x} = \frac{\partial}{\partial y}\left[\left(\frac{c_p \eta}{P_r} + \frac{c_p \varepsilon}{P_{rt}}\right)\frac{\partial T}{\partial y}\right] + (\eta+\varepsilon)\left(\frac{\partial u_x}{\partial y}\right)^2 \tag{2.159}$$

where u_x and u_y are the x and y components of velocity (the x-axis is taken to be parallel to the channel centre-line and the y-axis is perpendicular to the wall with the origin at the midpoint of the wall), and use has been made of equations (2.140) and (2.154). Equations (2.156) - (2.159) are to be supplemented by the equation of state, equation (2.137). Equation (2.158), which is derived from the y-component of the momentum equation (2.152), shows that the pressure is uniform over the channel cross-section and can only vary with x. The quantities ε and P_{rt} appearing in equations (2.157) and (2.159) represent the effects of hydrodynamic turbulence, which is briefly discussed below.

The steady state form of equation (2.156) means that one can define a fluid stream function $\psi(x,y)$ such that

$$\frac{\partial \psi}{\partial x} = -\rho u_y \tag{2.160a}$$

and

$$\frac{\partial \psi}{\partial y} = \rho u_x \tag{2.160b}$$

Using equations (2.160) and (2.137), the variables u_y, u_x and ρ can be eliminated from equations (2.157) and (2.159), which then assume the forms

$$\frac{\partial}{\partial y}\left[(\eta+\varepsilon)\frac{\partial}{\partial y}\left(T\frac{\partial \psi}{\partial y}\right)\right] = \frac{p}{R_g}\frac{dp}{dx} + p\frac{\partial \psi}{\partial y}\frac{\partial}{\partial x}\left(\frac{T}{p}\frac{\partial \psi}{\partial y}\right) - \frac{\partial \psi}{\partial x}\frac{\partial}{\partial y}\left(T\frac{\partial \psi}{\partial y}\right) \tag{2.161}$$

and

$$\frac{\partial}{\partial y}\left[\left(\frac{\varepsilon}{P_{rt}}+\frac{\eta}{P_r}\right)\frac{\partial T}{\partial y}\right] + \frac{R_g^2}{p^2 c_p}(\eta+\varepsilon)\left[\frac{\partial}{\partial y}\left(T\frac{\partial \psi}{\partial y}\right)\right]^2 = \frac{\partial \psi}{\partial y}\frac{\partial T}{\partial x} - \frac{\partial \psi}{\partial x}\frac{\partial T}{\partial y} - \frac{R_g T}{p c_p}\frac{\partial \psi}{\partial y}\frac{dp}{dx} \tag{2.162}$$

It is clear from the symmetry of the problem that equations (2.156) - (2.159) or (2.161) and (2.162) need only be applied between each of two adjacent walls and the centre-line. For each wall, separate consideration of two different regions, one for the boundary layer and one for the inviscid core of the flow has been avoided, the boundary layer equations being applied in the whole region between the wall and centre-line.

One restriction the present theory is subject to is that the angle of divergence of the walls must be small. This is because in the employed cartesian coordinates the x-axis is parallel to the centre-line and not to the walls of the channel. In MHD channels, the angle of divergence is generally small.

Effects of Turbulence

The two dimensional boundary layer equations obtained from equations (2.151) - (2.153) by making approximations consistent with the boundary layer assumption (2.155) are equations (2.156) - (2.159) with $\varepsilon = 0$. These equations describe laminar boundary layers and apply only in an entrance region of the channel where R_L is everywhere less than a

certain critical value R_{crit} . Sufficiently downstream of the channel entrance R_L usually exceeds R_{crit} and the flow becomes turbulent due to hydrodynamic instability. The turbulent flow is characterized by small irregular fluctuations of the gas-dynamic parameters, superimposed on the mean flow parameters, where the mean is defined as a time average taken over a time interval long compared to the time scale of the fluctuations. It is shown in reference (22), for example, that the boundary layer equations (2.156) - (2.159) are satisfied by the mean flow parameters provided that an additional turbulent stress τ and a turbulent heat flux q are introduced into equations (2.157) and (2.159). Physically, these quantities represent transport of mean flow momentum and energy by the turbulent fluctuations. It can be shown [21],[22] that the turbulent stress and heat flux are given by

$$\tau = -\langle \bar{\rho} u_y' u_x' \rangle \tag{2.163}$$

and

$$q = -c_p \langle \bar{\rho} u_y' T' \rangle \equiv -\langle \bar{\rho} u_y' h' \rangle \tag{2.164}$$

respectively, where the time average of any fluctuating parameter ξ is denoted by $\langle \xi \rangle$ or $\bar{\xi}$, and the prime denotes fluctuations; for example,

$$u_x' = u_x - \langle u_x \rangle$$

In writing down equation (2.164), use has been made of the definition of enthalpy h given by equation (2.154). In addition to transport of momentum and energy, there is a transport of mass by the turbulent fluctuations, which can be represented by an additional turbulent diffusion term in the mass continuity equation for each species of the plasma. In section 2.5, these terms will be derived for electrons and neutral seed atoms.

The turbulent fluxes in the y direction, namely the stress $-\langle \bar{\rho} u_y' u_x' \rangle$, and the heat conduction component $c_p \langle \bar{\rho} u_y' T' \rangle$ (see equations (2.163) and (2.164)) are additional unknowns that need to be either expressed algebraically in terms of the mean flow fields, or solved for by

extending the system of equations (2.156) - (2.159) to include equations for these additional unknowns. The first approach is used in the present work, where the well known assumption is made that, in analogy to fluxes in laminar flow, the turbulent fluxes can be related to the gradients of the corresponding flow quantities in terms of eddy-viscosity and eddy-conductivity coefficients. As indicated in reference (23) there is no a priori physical justification for this assumption and one has to employ phenomenological theories, such as that formulated in reference (11), for expressing the dependence of the eddy transport coefficients on the flow field. In contrast, the second approach, which is formulated in reference (23), uses additional transport equations to actually calculate the turbulent fluxes and thus avoids any a priori need to endow the fluid with fictitious eddy transport properties. This approach must, in general, be used for an accurate description of the effects of turbulent fluctuations on the mean flow fields, particularly when the interaction between the flow and the electromagnetic field cannot be neglected. The equations for the turbulent fluxes derived in reference (23) account for electromagnetic effects and have been used by the authors to obtain very accurate numerical predictions of open cycle MHD power generator performance characteristics.[24] It is shown in reference (23) that the equations derived using the second approach reduce to the equations of the eddy transport coefficient approach used here when convection and diffusion of turbulent fluxes, as well as electromagnetic effects, are omitted from the equations.

Assuming then that the turbulent stress and heat flux can be related to the gradients of the corresponding flow quantities in terms of eddy-viscosity and eddy-conductivity coefficients, ε and ε_h, we can write

$$\tau = -\langle \bar{\rho} u_y' u_x' \rangle = \varepsilon \partial u_x / \partial y \qquad (2.165)$$

and

$$q = \langle \bar{\rho} u_y' h' \rangle = -\varepsilon_h \frac{\partial T}{\partial y} \tag{2.166}$$

where u_x and T on the right hand sides of (2.165) and (2.166) are mean values. Defining, in analogy to laminar flow, the turbulent Prandtl number P_{rt} by the equation

$$P_{rt} = \frac{\varepsilon C_p}{\varepsilon_h}, \tag{2.167}$$

equation (2.166) can be written in the form

$$q = -\frac{\varepsilon C_p}{P_{rt}} \frac{\partial T}{\partial y} \tag{2.168}$$

Equations (2.157) and (2.159) follow from averaging the laminar boundary layer equations and using equations (2.165) and (2.168) [22] to eliminate the averages $\langle \bar{\rho} u_y' u_x' \rangle$ and $\langle \bar{\rho} u_y' h' \rangle$, if it is assumed that all other statistical correlations, in particular $\langle \rho' u_y' \rangle$, are negligible.

The eddy transport coefficient theory employed in this work is that formulated by Cebeci [11], which is applicable to compressible flows with heat and mass transfer and is quite accurate for a wide range of flow conditions. Mass transfer is found to be an important factor in the applications considered here (see section 3.5). The formulas of reference (11) are presented and briefly discussed below.

In the theory of reference (11), the turbulent boundary layer is regarded as a composite layer characterized by inner and outer regions. The existence of these two regions is due to the different response of the fluid to shear stress and pressure gradient in each region. In the inner region, an eddy viscosity ε_i based on Prandtl's mixing length theory [22] is used:

$$\varepsilon_i = \rho (0.4y)^2 \left[1 - \exp(-y/A)\right]^2 \left|\partial u_x / \partial y\right|, \tag{2.169}$$

where the distance $0.4y$ is the mixing length, and the damping factor

$$\left[1 - \exp(-y/A)\right]^2$$

accounts for the fact that the vanishing of the turbulent stress at a wall causes damping of turbulence near the wall. In fact, in a thin layer next to the wall, called the laminar sublayer, the turbulent stress is negligible compared with the viscous stress and the flow is nearly laminar. The damping length A is derived in reference (11), where it is shown to be given by

$$A = \frac{26}{N}\frac{\eta}{(\rho\tau_\omega)^{1/2}}, \tag{2.170a}$$

where

$$\tau_\omega = \eta_\omega \left(\frac{\partial u_x}{\partial y}\right)_\omega, \tag{2.170b}$$

and N is given by

$$N = \left\{ -\frac{\eta}{(\rho_\omega \tau_\omega) u_{y\omega}} \frac{dp}{dx} \left[1 - \exp\left(11.8 \frac{\eta_\omega}{\eta} \left(\frac{\rho_\omega}{\tau_\omega}\right)^{1/2} u_{y\omega} \right) \right] + \exp\left(11.8 \frac{\eta_\omega}{\eta} \left(\frac{\rho_\omega}{\tau_\omega}\right)^{1/2} u_{y\omega} \right) \right\}^{1/2}, \tag{2.170c}$$

the subscript ω denoting a wall value.

The eddy viscosity in the outer region is given by

$$\varepsilon_o = 0.0168 \left| \int_o^\infty (u_{xe} - u_x)\, dy \right| \gamma, \tag{2.171a}$$

where the subscript e denotes the value of a quantity at the boundary layer edge, and γ is the Klebanoff intermittancy factor given by the formula

$$\gamma = \left[1 + 5.5 \left(\frac{y}{\delta}\right)^6 \right]^{-1} \tag{2.171b}$$

The boundary layer edge velocity u_{xe} in equation (2.171a) is here taken to be the value at the channel centre-line and the formula (2.171a) is applied up to the centre-line. From (2.171b), the eddy viscosity rapidly decreases with y for $y > \delta$.

The turbulent Prandtl number defined by equation (2.167) is taken to be constant and equal to 0.9.

With the eddy viscosity and turbulent Prandtl number specified, the formulation of the gas-dynamic problem is completed for a given pressure distribution by specifying the boundary conditions to be satisfied by the boundary layer equations, and the initial gas-dynamic profiles. The initial gas-dynamic profiles will be discussed in section 3.3 as part of the numerical procedure used to solve the boundary layer equations; the boundary conditions are discussed below.

Boundary Conditions

The boundary conditions consist of conditions to be satisfied at the walls and at the centre-line, since equations (2.156) - (2.159), (2.161) and (2.162), are to be applied in the region between a wall and the centre-line. For a given wall, the boundary conditions at the wall $(y=0)$ are

(a) No slip:

$$u_x(x,0) = \left(\frac{1}{\rho}\frac{\partial \psi}{\partial y}\right)(x,0) = 0 \tag{2.172}$$

(b) Specified mass transfer rate:

$$\rho(x,0)\,u_y(x,0) = -\left(\frac{\partial \psi}{\partial x}\right)(x,0) = (\rho u_y)_w \tag{2.173}$$

The quantity $(\rho u_y)_w$ could be a function of the pressure which is calculated simultaneously with the solution of the equations (see below). In such cases, the functional dependence of $(\rho u_y)_w$ on the pressure must be prescribed. This is discussed further below.

(c) Specified Wall temperature or heat flux rate:

$$T(x,0) = T_w \tag{2.174a}$$

or

$$q_y(x,0) = -\left[\lambda \frac{\partial T}{\partial y}\right](x,0) = q_{yw} \tag{2.174b}$$

the latter condition being of the mixed type, since $q_y = q_y\,(T, \partial T/\partial y)$. The boundary conditions at the centre-line $(y = y_c)$ are the symmetry conditions

$$\frac{\partial T}{\partial y}(x, y_c) = 0 , \tag{2.175a}$$

and

$$\frac{\partial u_x}{\partial y}(x, y_c) = 0 . \tag{2.175b}$$

Calculation of Pressure Distribution

Finally, we note that the boundary conditions expressed by equations (2.172) - (2.175), together with the initial gas-dynamic profiles, are sufficient to solve the boundary layer equations only if the pressure distribution $p(x)$ is prescribed. However, the pressure distribution within an MHD channel is strongly influenced by the way in which the boundary layers develop along the walls, so that it cannot be specified a priori. The pressure distribution can be determined from the requirement that mass be conserved. Neglecting three-dimensional corner effects, the mass flow rate in the channel is given by

$$\dot{m} = \left(\int_0^{w/2} \rho_A u_{xA} \, dy_A \right) \left(\int_0^{H/2} \rho_B u_{xB} \, dy_B \right) \left[\frac{4}{(\rho u_x)_c} \right]$$

$$= \left[\psi_A\left(x, \frac{W}{2}\right) - \psi_A(x, 0) \right] \left[\psi_B\left(x, \frac{H}{2}\right) - \psi_B(x, 0) \right] \left[\frac{4}{(\rho u_x)_c} \right] , \tag{2.176}$$

where the subscripts A and B refer to two adjacent walls of lengths H and W respectively, the integrations are taken along the lines connecting the midpoints of the walls and the centre-line (for a given cross-section), and the subscript c refers to the centre-line value. To express $\dot{m}$ in terms of the values of ψ at the extremities of the two intervals use has been made of equation (2.160b). As a result of the assumed mass flow through the walls, $\dot{m}$ is not constant, its rate of change being given by

$$\frac{d\dot{m}}{dx} = 2H (\rho_A u_{yA})_w + 2W (\rho_B u_{yB})_w . \tag{2.177}$$

If the mass transfer rates $(\rho_A u_{yA})_\omega$ and $(\rho_B u_{yB})_\omega$ were specified functions of x, equation (2.177) could be integrated and the value of $\dot{m}$ at each x determined, provided that the value of $\dot{m}$ at some initial x-station is prescribed. The pressure could then be obtained from equation (2.176). However, as mentioned above, the mass transfer rates are in some cases functions of the pressure and the mass flow rate $\dot{m}$ must be treated, like the pressure, as an unknown parameter governed by equation (2.177). In fact, this is the case for the application of the theory to the actual experimental MHD channel considered in chapter 3.

2.5 THE PLASMA AND ELECTRICAL FLUID EQUATIONS

To complete the formulation of the two-temperature fluid model of the partially ionized plasma in an electromagnetic field, equations governing the seed atom density, the electron density, the electron temperature and the electromagnetic fields must be specified, assuming the plasma to be quasi-neutral. These equations, which will be presented in this section, will later be solved numerically to obtain a description of the local plasma and electrical behaviour as a function of time in a single segment of a closed cycle MHD generator. A number of simplifying assumptions have been introduced in order to simplify the theoretical and numerical models. These assumptions include: (i) neglect of all variations parallel to a uniform constant magnetic field, which is applied in the z-direction, perpendicular to the insulator side walls of the MHD channel (the effects of boundary layers on the insulator side walls are neglected); (ii) neglect of variations of the gas-dynamic parameters in the stream-wise x-direction, and neglect of the cross-stream velocity component u_y . In other words, the gas-dynamic parameters are considered as given functions of y obtained from the solution of the boundary layer equations for the electrode side walls. These assumptions will be further discussed in section 2.6 .

(a) Electron and Neutral Seed Atom Continuity Equations

The electron, neutral seed atom and ion number densities are governed by the continuity equations

$$\partial n_e/\partial t + \nabla . n_e \underline{u} + \nabla . n_e \underline{V}_e = \dot{n}_e , \tag{2.178}$$

$$\partial n_n/\partial t + \nabla . n_n \underline{u} + \nabla . n_n \underline{V}_n = \dot{n}_n , \tag{2.179}$$

and

$$\partial n_i/\partial t + \nabla . n_i \underline{u} + \nabla . n_i \underline{V}_i = \dot{n}_i , \tag{2.180}$$

which follow from the general species mass conservation equation, equation (2.1). The quantities $\dot{n}_e$, $\dot{n}_n$ and $\dot{n}_i$ are the net volumetric rates of production of electrons, neutral seed atoms and ions respectively. Because charge is conserved

$$\dot{n}_e = \dot{n}_i \,, \tag{2.181}$$

and it follows from equations (2.178) and (2.180) that

$$\frac{\partial \rho^c}{\partial t} + \nabla.\rho^c \underline{u} + \nabla.\underline{J} = 0 \,. \tag{2.182}$$

It has been shown in section 2.4 that the convection current density $\rho^c \underline{u}$ can be neglected in comparison with the conduction current density $\underline{J}$ (see the inequality (2.145)), so that $\underline{J}$ may be identified with the total current density and equation (2.182) written in the form

$$\frac{\partial \rho^c}{\partial t} + \nabla.\underline{J} = 0 \,. \tag{2.183}$$

The charge density and the current density in the fluid act as sources for the electromagnetic field quantities $\underline{E}$ and $\underline{B}$, which are governed by the Ampere-Maxwell and Faraday relations

$$\nabla \wedge \underline{B} = \mu_0 \left(\underline{J} + \epsilon_0 \frac{\partial \underline{E}}{\partial t} \right) \tag{2.184}$$

and

$$\nabla \wedge \underline{E} = - \frac{\partial \underline{B}}{\partial t} \,. \tag{2.185}$$

Equation (2.183) can be derived by taking the divergence of equation (2.184) and using Poisson's

$$\nabla.\underline{E} = \rho^c / \epsilon_0 \,. \tag{2.186}$$

In equation (2.184),

$$\frac{\left| \epsilon_0 \frac{\partial \underline{E}}{\partial t} \right|}{|\underline{J}|} \sim \frac{\epsilon_0 E_c}{t_c \sigma_{ec} E_c} = \frac{\epsilon_0}{t_c \sigma_{ec}} \,, \tag{2.187}$$

where the subscript c denotes the characteristic value of a quantity, and use has been made of the simplified form of Ohm's law $\underline{J} = \sigma_e \underline{E}$.

If the restriction

$$t_c \gg \frac{\epsilon_0}{\sigma_{ec}} \tag{2.188}$$

is imposed on the time scale t_c, equation (2.187) shows that the displacement current $\epsilon_0 \partial \underline{E}/\partial t$ can be neglected compared with $\underline{J}$ and equation (2.184) reduces to

$$\nabla \wedge \underline{B} = \mu_0 \underline{J}, \tag{2.189}$$

from which

$$\nabla . \underline{J} = 0. \tag{2.190}$$

The condition (2.188) may be written as

$$t_c \gg \frac{\nu_{eh}}{\omega_p^2}, \tag{2.191}$$

where ω_p is the plasma frequency $(n_e e^2/\epsilon_0 m_e)^{1/2}$. If this is taken together with the restriction

$$t_c \gg \frac{1}{\nu_{eh}}, \tag{2.192}$$

required for validity of the generalized Ohm's law in the form of equation (2.132) [1] one has the requirement that

$$t_c \gg \omega_p^{-1}, \tag{2.193}$$

which is the well known condition that charge neutrality be maintained in the plasma at least for characteristic length scales of variation larger than the Debye length [1]. Typical values of t_c, ϵ_0/σ_{ec} and $1/\nu_{eh}$ are 3×10^{-4} sec, 3×10^{-12} sec and 10^{-11} sec respectively (the time scale t_c is taken to be the growth time of the electrothermal instability), so that the conditions (2.188), (2.192) and, therefore, (2.193) are well satisfied. It follows that equations (2.189) and (2.190) are valid and that the plasma may be assumed quasineutral; i.e., $n_i \simeq n_e$

Assuming, as is usually the case for partially ionized gases in MHD channels, that flow occurs in a constant uniform externally applied magnetic field, the derivative $\partial \underline{B}/\partial t$ can be finite only because of fluctuating plasma parameters which produce an induced magnetic field.

If the relevant time dependent phenomenon is the electrothermal instability estimates based on the linear theory of the instability show that the induced magnetic field can usually be neglected [7],[8]. Equation (2.185) then becomes

$$\nabla \times \underline{E} = 0. \tag{2.194}$$

Returning to the continuity equations (2.178)-(2.180), since the plasma is assumed quasineutral, the ion continuity equation (2.180) is not required. Using equations (2.74) and (2.131) the electron and neutral seed atom diffusion fluxes can be written as

$$n_e \underline{U}_e = -\frac{\underline{J}_e}{e} = -\frac{1}{e}\underline{J} - \frac{\gamma_i}{n_e e^2}\nabla(p_i + p_e) \tag{2.195}$$

and

$$n_n \underline{U}_n = -\frac{1}{m_{nh} \nu_{nh}} \nabla p_n, \tag{2.196}$$

since $n_e \simeq n_i$.

Eliminating the diffusion fluxes from equations (2.178) and (2.179) using equations (2.195) and (2.196), one obtains the equations

$$\frac{\partial n_e}{\partial t} + \nabla \cdot n_e \underline{u} - \nabla \cdot \frac{\gamma_i}{n_e e^2}\nabla(p_e + p_i) = \dot{n}_e, \tag{2.197}$$

and

$$\frac{\partial n_n}{\partial t} + \nabla \cdot n_n \underline{u} - \nabla \cdot \left(\frac{1}{m_{nh}\nu_{nh}}\right)\nabla p_n = \dot{n}_n, \tag{2.198}$$

where use has been made of equation (2.190).

As mentioned in section 2.4., one has, in addition to laminar diffusion represented by the quantities $n_e \underline{U}_e$ and $n_n \underline{U}_n$ given by equations (2.195) and (2.196), transport of particles of various species by the turbulent fluctuations which can be represented by an additional term in the continuity equation (averaged over turbulent fluctuations) for each species. To determine the turbulent diffusion terms in equations (2.197) and (2.198) the general species α conservation of mass equation is considered; that is, the equation

$$\frac{\partial \rho_\alpha}{\partial t} + \nabla \cdot \rho_\alpha \underline{u} + \nabla \cdot \rho_\alpha \underline{U}_\alpha = \dot{\rho}_\alpha \tag{2.199}$$

Averaging equation (2.199) over turbulent fluctuations and neglecting all correlations between fluctuating quantities with the exception of $\langle \rho_\alpha' u_y' \rangle$, an equation for $\bar{\rho}_\alpha$ of the form

$$\frac{\partial \bar{\rho}_\alpha}{\partial t} + \nabla \cdot \bar{\rho}_\alpha \bar{\underline{u}} + \frac{\partial}{\partial y} \langle \rho_\alpha' u_y' \rangle + \nabla \cdot \bar{\rho}_\alpha \bar{\underline{V}}_\alpha = \bar{\dot{\rho}}_\alpha \tag{2.200}$$

is obtained, where the laminar diffusion term $\nabla \cdot \bar{\rho}_\alpha \bar{\underline{V}}_\alpha$ and the source term $\bar{\dot{\rho}}_\alpha$ are to be evaluated with the mean values of fluctuating quantities. Transport of species α particles by turbulent fluctuations is represented by the term

$$\frac{\partial}{\partial y} \langle \rho_\alpha' u_y' \rangle \tag{2.201}$$

of equation (2.200), the quantity $\langle \rho_\alpha' u_y' \rangle$ being the turbulent diffusion flux of species α particles. Assuming that this flux can be related to the gradient of the average of the mass fraction ρ_α / ρ in terms of the eddy-diffusion coefficient ε_d, we can write

$$\langle \rho_\alpha' u_y' \rangle = -\varepsilon_d \frac{\partial}{\partial y} \left\langle \frac{\rho_\alpha}{\rho} \right\rangle \underline{\underline{\sim}} -\varepsilon_d \frac{\partial}{\partial y} \left(\frac{\bar{\rho}_\alpha}{\bar{\rho}} \right) \tag{2.202}$$

In addition, we assume that a constant turbulent Schmidt number S_T can be defined such that

$$\varepsilon_d = \frac{\varepsilon}{S_T} \tag{2.203}$$

where ε is the eddy viscosity. Using equations (2.202) and (2.203), equation (2.200) can be written in the form

$$\frac{\partial \rho_\alpha}{\partial t} + \nabla \cdot \rho_\alpha \underline{u} - \frac{\partial}{\partial y} \frac{\varepsilon}{S_T} \frac{\partial}{\partial y} \left(\frac{\rho_\alpha}{\rho} \right) + \nabla \cdot \rho_\alpha \underline{V}_\alpha = \dot{\rho}_\alpha \tag{2.204}$$

where bars denoting averages have been omitted for convenience.

Dividing equation (2.204) throughout by m_α, and noting that for the small seeding fractions considered here $\rho \simeq \rho_h$, the species α continuity equation is obtained in the form

$$\frac{\partial n_\alpha}{\partial t} + \nabla \cdot n_\alpha \underline{u} - \frac{\partial}{\partial y} \left[\left(\frac{\varepsilon k_B}{m_h \rho S_T} \right) \frac{\partial}{\partial y} (n_\alpha T) \right] + \nabla \cdot n_\alpha \underline{V}_\alpha = \dot{n}_\alpha \tag{2.206}$$

From equation (2.206), it follows that the electron and neutral seed atom continuity equations averaged over turbulent fluctuations can be written as

$$\frac{\partial n_e}{\partial t} + u_x \frac{\partial n_e}{\partial x} - \frac{\partial}{\partial y}\left[\left(\frac{\varepsilon}{m_h p S_T}\right)\frac{\partial p_i}{\partial y}\right] - \nabla\cdot\left(\frac{\sigma_i}{n_e e^2}\right)\nabla(p_e + p_i) = \dot{n}_e \quad (2.207)$$

and

$$\frac{\partial n_n}{\partial t} + u_x \frac{\partial n_n}{\partial x} - \frac{\partial}{\partial y}\left[\left(\frac{\varepsilon}{m_h p S_T}\right)\frac{\partial p_n}{\partial y}\right] - \nabla\cdot\left(\frac{1}{m_{nh} \nu_{nh}}\right)\nabla p_n = \dot{n}_n, \quad (2.208)$$

where in (207) the condition $n_e \simeq n_i$ has been used to write $k_B n_e T \simeq p_i$. The representation of turbulent diffusion defined by equations (2.202) and (2.203) is in agreement with that used in references (25), (17) and (26). The value of S_T is taken to be 0.9 as in the latter references.

The importance of turbulent diffusion in equations (2.207) and (2.208) is measured by the ratios

$$R_1 = \left(\frac{\varepsilon}{m_h p S_T}\right) \Big/ \left(\frac{\sigma_i}{n_e e^2}\right)$$

and

$$R_2 = \left(\frac{\varepsilon}{m_h p S_T}\right) \Big/ \left(\frac{1}{m_{nh} \nu_{nh}}\right) \simeq R_1$$

From the numerical solutions of the boundary layer equations chapter 3, the ratio R_1, which (for slight seeding) is a function only of the gas-dynamic variables, can be calculated as a function of distance from the electrode wall at any particular x-location along the channel. For the x-location considered in the numerical solution of the plasma and electrical equations in chapter 5, to be specified in chapter 3, it is found that, like the eddy viscosity, R_1 is close to zero near the wall and the electrode wall boundary layer edge, but has a maximum value of *188* due to the eddy viscosity having a maximum at a distance of about $\delta/3 \simeq 1.6mm$ from the wall. Clearly, turbulent diffusion is an important effect.

In equations (2.207) and (2.208), the convection terms have been approximated in accordance with the assumptions made at the beginning of this section, which mean that $u_x = u_x(y)$ and $u_y \simeq 0$.

The formulation of the electron and neutral seed atom continuity equations is completed once the rate terms $\dot{n}_e$ and $\dot{n}_n$ have been specified. It is clear that

$$\dot{n}_n = -\dot{n}_e$$

so that only the form of $\dot{n}_e$ need be considered. For the ranges of electron temperatures and electron densities considered here, the relevant atomic interaction processes in the partially ionized gas are the processes of ionization and excitation of bound electronic levels of seed atoms and their inverses, resulting from either nonelastic collisions of the seed atoms with free electrons or from the emission and absorption of radiation [1]. Furthermore, electron densities are sufficiently large for the collisional processes to dominate radiative processes and $\dot{n}_e$ can be written in the form [1]

$$\dot{n}_e = \alpha(T_e)\left[(n_e^*)^2 - n_e^2\right] \tag{2.209}$$

where

$$(n_e^*)^2 \equiv n_n \left(\frac{n_e n_i}{n_n}\right)_{equil} = n_n \left(\frac{n_e^2}{n_n}\right)_{equil} \tag{2.210}$$

and $\alpha(T_e)$ is the three-body recombination coefficient. The quantity $(n_e^2/n_n)_{equil}$ is the ratio n_e^2/n_n when local thermodynamic equilibrium prevails $(\dot{n}_e = 0)$ and is given by Saha's equation

$$\left(\frac{n_e^2}{n_n}\right)_{equil} = \left(\frac{2\pi m_e k_B T_e}{h^2}\right)^{3/2} e^{-eV_i/k_B T_e} \tag{2.211}$$

where V_i is the ionization potential of the ground state. For caesium atoms,

$$V_i = 3.89\,eV$$

Combining equations (2.209), (2.210) and (2.211) one obtains the expression

$$\dot{n}_e = \alpha(T_e)\left[n_n \left(\frac{2\pi m_e k_B T_e}{h^2}\right)^{3/2} e^{-eV_i/k_B T_e} - n_e^2\right] \tag{2.212}$$

An approximate formula for $\alpha(T_e)$ has been derived by Hinnov and Hirschberg. They found that $\alpha(T_e)$ is given by the well known approximate formula [1]

$$\alpha(T_e) \simeq 1.09 \times 10^{-20} n_e T_e^{-9/2} m^3/sec, \qquad (2.213)$$

which is valid for $T_e \lesssim 3000°K$.

(b) Electron Energy Equation

The electron temperature is governed by the electron energy equation, which is obtained from equation (2.3) in the form

$$\frac{D}{Dt}\left(n_e \frac{3}{2} k_B T_e\right) + n_e \frac{5}{2} k_B T_e \nabla.\underline{u} + \nabla.\underline{q}_e - \underline{J}_e.\underline{E}' = n_e \frac{3}{2} k_B (T - T_e) \frac{2m_e}{m_h} \nu_{eh} + \dot{N}_e \qquad (2.214)$$

where the term $-(\quad)\ \underline{J}_e.D\underline{u}/Dt$ in equation (2.214) has been neglected as small and the electron viscous stress $\underline{\underline{\tau}}_e$ has been neglected in comparison with p_e. In deriving equation (2.214) from equation (2.3) use has been made of the expression (2.31) in which only collisions between electrons and buffer gas atoms are considered, seeding being assumed to be slight.

As in the case of the continuity equations, when the electron energy equation is averaged over turbulent fluctuations, terms appear representing transport by turbulent fluctuations. To derive these terms equation (2.214) is written in the form

$$\frac{\partial}{\partial t}\left(n_e \frac{3}{2} k_B \overline{T_e}\right) + \frac{5}{2}\frac{k_B}{m_e} \nabla.\rho_e \underline{u} T_e - \underline{u}.\nabla p_e + \nabla.\underline{q}_e - \underline{J}_e.\underline{E}' \qquad (2.215)$$
$$= n_e \frac{3}{2} k_B (T - T_e) \frac{2m_e}{m_h} \bar{\nu}_{eh} + N_e$$

Time averaging equation (2.215) over turbulent fluctuations, the second term of the left hand side of the resulting equation can be written as

$$\frac{5k_B}{2m_e} \nabla.\langle \rho_e T_e \underline{u} \rangle = \frac{5k_B}{2m_e} \nabla.\langle (\bar{\rho}_e + \rho_e')(\bar{T}_e + T_e')(\bar{\underline{u}} + \underline{u}') \rangle$$
$$= \frac{5k_B}{2m_e} \nabla.\bar{\rho}_e \bar{\underline{u}} \bar{T}_e + \frac{5k_B}{2m_e} \frac{\partial}{\partial y}\left(\bar{\rho}_e \langle T_e' u_y' \rangle\right) + \frac{5k_B}{2m_e} \frac{\partial}{\partial y}\left(\bar{T}_e \langle \rho_e' u_y' \rangle\right) \qquad (2.216).$$

where all correlations between fluctuating quantities have been neglected with the exception of the correlations $\langle T_e' u_y' \rangle$ and $\langle \rho_e' u_y' \rangle$. Making use of the relations (2.166), (2.167), (2.202) and (2.203), these correlations can be written in the forms

$$\langle T_e' u_y' \rangle = - \frac{\varepsilon}{\bar{\rho} P_{rt}} \frac{\partial \bar{T}_e}{\partial y}$$

and

$$\langle \rho_e' u_y' \rangle = - \frac{\varepsilon}{S_T} \frac{\partial}{\partial y} \left(\frac{\bar{\rho}_e}{\bar{\rho}} \right)$$

and equation (2.216) can be written as

$$\frac{5k_B}{2m_e} \nabla . \langle \rho_e T_e \underline{u} \rangle \simeq \frac{5k_B}{2m_e} \nabla . \bar{\rho}_e \bar{\underline{u}} \bar{T}_e - \frac{5k_B}{2m_e} \frac{\partial}{\partial y} \left[\frac{\bar{\rho}_e}{\bar{\rho}} \frac{\varepsilon}{P_{rt}} \frac{\partial \bar{T}_e}{\partial y} \right]$$
$$- \frac{5k_B}{2m_e} \frac{\partial}{\partial y} \left[- \bar{T}_e \frac{\varepsilon}{S_T} \frac{\partial}{\partial y} \left(\frac{\bar{\rho}_e}{\bar{\rho}} \right) \right]$$

$$\simeq \frac{5k_B}{2m_e} \nabla . \bar{\rho}_e \bar{\underline{u}} \bar{T}_e - \frac{5k_B}{2} \frac{\partial}{\partial y} \left[\left(\frac{\rho_i}{\rho} \right) \frac{\varepsilon}{m_h P_{rt}} \frac{\partial \bar{T}_e}{\partial y} \right] - \frac{5k_B}{2} \frac{\partial}{\partial y} \left[\bar{T}_e \frac{\varepsilon}{m_h \rho S_T} \frac{\partial \rho_i}{\partial y} \right] \qquad (2.217)$$

where use has been made of the approximations $n_e \simeq n_i$ and $\rho \simeq \rho_h$. Using equation (2.217), the time average of equation (2.215) over turbulent fluctuations can be written as

$$\frac{D}{Dt} \left(n_e \frac{3}{2} k_B T_e \right) - \frac{5k_B}{2} \frac{\partial}{\partial y} \left[\frac{\rho_i \varepsilon}{m_h \rho P_{rt}} \frac{\partial \bar{T}_e}{\partial y} \right] - \frac{5k_B}{2} \frac{\partial}{\partial y} \left[\frac{T_e \varepsilon}{m_h \rho S_T} \frac{\partial \rho_i}{\partial y} \right]$$
$$+ \nabla . \underline{q}_e - \underline{J}_e . \underline{E}' = n_e \frac{3}{2} k_B (T - T_e) \frac{2m_e}{m_h} \nu_{eh} + N_e , \qquad (2.218)$$

where bars denoting averages have been omitted for convenience. The term $n_e \frac{5}{2} k_B T_e \nabla . \underline{u}$ has been neglected in equation (2.215) in accordance with the assumptions made at the beginning of this section, which imply that $u_x \simeq u_x(y)$ and that $u_y \simeq 0$. It also follows that

$$\frac{D}{Dt} \left(n_e \frac{3}{2} k_B T_e \right) \simeq \frac{\partial}{\partial t} \left(n_e \frac{3}{2} k_B T_e \right) + u_x \frac{\partial}{\partial x} \left(n_e \frac{3}{2} k_B T_e \right)$$

The second and third terms on the left hand side of equation

(2.218) represent turbulent electron thermal conduction (transport of electron enthalpy by turbulent fluctuations of T_e) and transport of electron enthalpy due to turbulent diffusion; i.e., due to transport of electrons by turbulent fluctuations of u_y . The forms of these terms are in agreement with those used in reference (17); the second term on the left hand side of equation (2.218) is omitted in references (25) and (26).

For the formulation of the present physical model the simplified expression (2.113) is used for the electron heat flux. This expression can be written in the form

$$\underline{q}_e = -\frac{5}{2}\frac{k_B T_e}{e}\underline{J}_e - \frac{\lambda_e}{(1+\beta_e^2)}\left[\nabla T_e - \beta_e \nabla T_e \wedge \underline{b}\right] \qquad (2.219)$$

Since, as stated at the beginning of this section, all variations parallel to the magnetic field are neglected so that ∇T_e is perpendicular to $\underline{b}$. Also,

$$\nabla T_e \wedge \underline{b} = \left(\frac{\partial T_e}{\partial y}, -\frac{\partial T_e}{\partial x}, 0\right)$$

so that, from equation (2.219), since $n_e \simeq n_i$

$$\nabla \cdot \underline{q}_e = -\nabla \cdot \left\{\frac{5 k_B T_e}{2e}\left[\underline{J} + \frac{\sigma_i}{e n_e}\nabla(p_e + p_i)\right]\right\} - \nabla \cdot \left\{\frac{\lambda_e}{(1+\beta_e^2)}\left[\nabla T_e - \beta_e \nabla T_e \wedge \underline{b}\right]\right\}$$

$$= -\nabla \cdot \left\{\frac{5 k_B T_e}{2e}\left[\underline{J} + \frac{\sigma_i}{e n_e}\nabla(p_e + p_i)\right]\right\} - \frac{\partial}{\partial x}\left\{\frac{\lambda_e}{(1+\beta_e^2)}\left[\frac{\partial T_e}{\partial x} - \beta_e \frac{\partial T_e}{\partial y}\right]\right\} \qquad (2.220)$$

$$- \frac{\partial}{\partial y}\left\{\frac{\lambda_e}{(1+\beta_e^2)}\left[\frac{\partial T_e}{\partial y} + \beta_e \frac{\partial T_e}{\partial x}\right]\right\},$$

where the relation between $\underline{J}_e$ and $\underline{J}$ given by equation (2.131) has been used to eliminate $\underline{J}_e$ from equation (2.219).

The ohmic heating term $\underline{J}_e \cdot \underline{E}'$ in equation (2.215) may, using the relation between $\underline{J}_e$ and $\underline{E}'$ expressed by equation (2.125b), be written in the form

$$\underline{E}' \cdot \underline{J}_e = \frac{J_e^2}{\sigma_e} - \underline{J}_e \cdot \frac{\nabla p_e}{e n_e} \qquad (2.221)$$

The assumptions made in order to derive the simplified generalized Ohm's law given by equation (2.132) allow $\underline{J}_e$ to be replaced by the total current density $\underline{J}$ in equation (2.221), which then reads

$$\underline{E}'.\underline{J}_e = \frac{J^2}{\sigma_e} - \underline{J}.\frac{\nabla p_e}{e n_e} \tag{2.224}$$

Finally, the term $\dot{N}_e$, giving the net volumetric rate of gain of energy by free electrons due to inelastic collisions must be specified. Assuming, that the relevant, inelastic collisions are with seed atoms in various levels of electronic excitation that communicate energetically only with the free electrons and by emission and absorption of radiation, $\dot{N}_e$ can be obtained by considering an energy balance for the excited atoms. It can be shown that [1]

$$\dot{N}_e = -\dot{R} - \dot{n}_e \epsilon_i \tag{2.225}$$

where $\dot{R}$ is the local net rate per unit volume of radiant energy loss from the plasma and ϵ_i is the ionization energy of the ground state of a seed atom. It can be shown in the same way that the total seed atom number density and average seed atom energy per unit mass are approximately equal to the contributions to these quantities from seed atoms in the ground state. This was assumed earlier in section 2.2 . Replacing the quantities $\nabla.\underline{q}_e$, $\underline{J}_e.\underline{E}'$ and $\dot{N}_e$ in equation (2.218) by their expressions given by equations (2.220), (2.224) and (2.225), the electron energy equation assumes the form

$$\begin{aligned}
&\frac{D}{Dt}\left(n_e \tfrac{3}{2} k_B T_e\right) - \frac{5k_B}{2}\frac{\partial}{\partial y}\left[\frac{\rho_i \mathcal{E}}{m_h \rho \beta_{rt}}\frac{\partial T_e}{\partial y}\right] - \frac{5k_B}{2}\frac{\partial}{\partial y}\left[\frac{T_e \mathcal{E}}{m_h \rho S_T}\frac{\partial p_i}{\partial y}\right] \\
&- \nabla\left\{\frac{5k_B T_e}{2e}\left[\underline{J} + \frac{\sigma_i}{e n_e}\nabla(p_e + p_i)\right]\right\} - \nabla.\left\{\frac{\lambda_e}{(1+\beta_e^2)}\left[\nabla T_e - \beta_e \nabla T_e \wedge \underline{b}\right]\right\} \\
&- \frac{J^2}{\sigma_e} + \underline{J}.\frac{\nabla p_e}{e n_e} = n_e \frac{3}{2} k_B (T - T_e)\frac{2m_e}{m_h}\nu_{eh} - \dot{R} - \dot{n}_e \epsilon_i .
\end{aligned} \tag{2.226}$$

Eliminating the derivative Dn_e/Dt from equation (2.226) with the help

of equation (2.207), the electron energy equation can be written as

$$\frac{3}{2}k_B T_e \frac{\partial}{\partial y}\left\{\left(\frac{\varepsilon}{m_h p S_T}\right)\frac{\partial p_i}{\partial y}\right\} - \frac{5k_B}{2}\frac{\partial}{\partial y}\left\{\left(\frac{p_i \varepsilon}{m_h p P_{rt}}\right)\frac{\partial T_e}{\partial y}\right\}$$
$$-\frac{5k_B}{2}\frac{\partial}{\partial y}\left\{\left(\frac{T_e \varepsilon}{m_h p S_T}\right)\frac{\partial p_i}{\partial y}\right\} + \frac{3}{2}k_B T_e \nabla\cdot\left(\frac{\theta_i}{n_e e^2}\right)\nabla(p_e+p_i)$$
$$-\nabla\cdot\left(\frac{5k_B T_e}{2n_e e^2}\sigma_i\right)\nabla(p_e+p_i) - \nabla\cdot\left\{\frac{\beta_e}{(1+\beta_e^2)}\left[\nabla T_e - \beta_e \nabla T_e \wedge \underline{b}\right]\right\} \qquad (2.227)$$
$$-\nabla\cdot\frac{5k_B T_e}{2e}\underline{J} + \underline{J}\cdot\frac{\nabla p_e}{e n_e} = \frac{J^2}{\sigma_e} + n_e \frac{3}{2}k_B(T-T_e)\frac{2m_e}{m_h}\nu_{eh} - \left(\frac{3}{2}k_B T_e + \varepsilon_i\right)\dot{n}_e$$
$$-\dot{R},$$

where the electron thermal conduction term expressed in terms of the given cartesian coordinates is given by equation (2.220). The term $\frac{3}{2}k_B n_e \partial T_e / \partial t$ on the left hand side of equation (2.227) has been neglected as small; it being assumed that T_e instantaneously relaxes to changes in the plasma and electrical field parameters. This is refered to as the "temperature relaxation approximation", and is made here in order to eliminate the heavily damped fast thermal mode of electrothermal waves [27], which is of little physical significance here and imposes severe restrictions on the choice of time step used in the explicit numerical integration of the continuity equations (see section 4.6 and appendix C). The fast thermal mode can also be eliminated if, instead of the temperature relaxation approximation, Saha equilibrium ($\dot{n}_e = 0$) is assumed [27]. This is the approach used by Uncles [8] and requires restriction of conditions to those for which the electron temperature is very large. In addition, the cross-stream diffusion terms in the electron and seed atom continuity equations must be assumed negligible so that the effects of the plasma wall interactions discussed in section 2.7 on the bulk behaviour of the plasma in an MHD generator cannot be considered. In addition to the inclusion of the effects of turbulent velocity and temperature boundary layers (velocity and temperature variations and turbulent transport phenomena),

finite ion and seed atom diffusion fluxes, and plasma-wall interactions (see section 2.7), it is in the use of the temperature relaxation approximation, rather than the assumption of Saha equilibrium, that the present work differs from that of Uncles [8].

As is shown in appendix D, the radiative loss term on the right hand side of equation (2.227) cannot in general be exactly expressed in terms of local plasma properties and their gradients. However, an approximate expression for the radiative loss is derived in appendix D, where, using this expression, it is shown to be negligible compared with electron thermal conduction. Therefore, radiative energy loss has been neglected in this work.

The importance of the first, second and third terms on the left hand side of equation (2.227), which represent turbulent transport processes can be estimated in the same way as in sub-section (a), in which the importance of turbulent diffusion processes in the continuity equations was estimated. Since the first term comes from the electron continuity equation, and the third term is of the same order as the first term, the first and third terms need not be considered here, their order of magnitude relative to the laminar diffusion term having already been estimated in sub-section (a). The second term represents turbulent thermal conduction and its importance relative to the laminar electron thermal conduction is measured by the ratio

$$\frac{5k_B}{2}\frac{p_i E}{m_4 p R_t} \Big/ \frac{\lambda_e}{(1+\beta_e^2)}$$

As in sub-section (a), the latter ratio is estimated by considering the gas-dynamic profiles used in the numerical solution of the plasma and electrical equations. Taking $T_e = 2000°K$ and $\beta = 0.7$ it is found that the maximum value of the ratio is 0.1, and that the ratio is close to zero near the wall and near the centre-line. Turbulent thermal conduction is therefore of much less importance

in the electron energy equation than is turbulent diffusion in the continuity equations.

(c) Electrical Field Equations

The equations governing the electrical fields, that is the current and electric fields, are the charge conservation equation and Faraday's law, which, for the plasma and electromagnetic field conditions considered in this work, have the approximate forms of equations (2.190) and (2.194). Since, in accordance with the assumptions made at the beginning of this section, the current flow is perpendicular to a uniform magnetic field, taken to be in the z-direction, equation (2.190) implies that a current stream function ψ can be introduced such that

$$\underline{J} = -\nabla_1(\psi \underline{b}), \tag{2.228}$$

from which the components of $\underline{J}$ can be written as

$$J_x = -\frac{\partial \psi}{\partial y}, \quad J_y = \frac{\partial \psi}{\partial x}$$

The generalized Ohms' law (2.132), Faraday's law (2.190) and equation (2.228) are cast into a single scalar differential equation for ψ:

$$\nabla^2\psi + P\frac{\partial \psi}{\partial x} + Q\frac{\partial \psi}{\partial y} = R \tag{2.229}$$

where the coefficients P, Q and R are given by

$$P = \sigma_e\left[\frac{\partial}{\partial x}\left(\frac{1}{\sigma_e}\right) - \frac{\partial}{\partial y}\left(\frac{\beta_e}{\sigma_e}\right)\right] \tag{2.230a}$$

$$Q = \sigma_e\left[\frac{\partial}{\partial y}\left(\frac{1}{\sigma_e}\right) + \frac{\partial}{\partial x}\left(\frac{\beta_e}{\sigma_e}\right)\right] \tag{2.230b}$$

and

$$R = \frac{\sigma_e k_B}{e n_e}\left(\frac{\partial n_e}{\partial y}\frac{\partial T_e}{\partial x} - \frac{\partial n_e}{\partial x}\frac{\partial T_e}{\partial y}\right) \tag{2.230c}$$

2.6 BOUNDARY CONDITIONS FOR THE PLASMA AND ELECTRICAL EQUATIONS

For given gas-dynamic fields, equations (2.207), (2.208), (2.227) and (2.229) constitute a closed system of equations for the unknown fields n_e, n_n, T_e and ψ. These equations are of mixed elliptic-parabolic type, requiring specification of initial conditions for n_e and n_n, together with boundary constraints for n_e, n_n, T_e and ψ. The initial conditions will be discussed later in section 4.5, attention in the present section being confined to the boundary constraints.

The present work is concerned with the study of plasma and electrical behaviour in the main part of a linear segmented electrode channel. The main part of the channel is the region where inlet relaxation effects have subsided so that the plasma and electrical fields are nearly periodic functions of the streamwise coordinate x, with period the length L of one electrode segment. When the main part of the channel is considered, the geometry of the problem is that of one electrode segment. Within this region, the gas-dynamic fields T, p and $\underline{u}$ do not vary appreciably in the x-direction and may be considered given functions of y determined from the solutions of the boundary layer equations of section 2.4.

An individual segment of the segmented electrode channel is shown in figure (2.3). The segment has height H, width W, and length L, and occupies the region $0 \leq x \leq L$, $0 \leq y \leq H$ and $0 \leq z \leq W$. It is assumed that each electrode pair is connected externally to a resistive load R_L. The boundary conditions for the electrical quantities are

(i) $E_x = -d\Delta\phi/dx$ on the electrodes BC, FG

(ii) $J_y = 0$ on the insulators AB, CD, EF, GH,

(iii) $V_F = R_L \iint_{BC} \bar{J}_y \, dz \, dx = I R_L$

(iv) Periodicity of $\underline{J}$; i.e., $\underline{J}(x, y) = \underline{J}(x+L, y)$

I is the total current through an electrode pair, and the voltage drop across the plasma between the electrodes, the Faraday voltage V_f, is given by

$$V_F = -\int_0^H E_y\,dy - \Delta\phi_c + \Delta\phi_a \qquad (2.231)$$

where $\Delta\phi_a$ and $\Delta\phi_c$ are the anode and cathode sheath voltage drops respectively (see section 2.7). Using the generalized Ohm's law (2.132) and equation (2.228), equation (2.231) and condition (i) can be written in the forms

$$V_F = -\int_0^H \frac{1}{\sigma_e}\left[\frac{\partial\psi}{\partial x} - \frac{\sigma_e}{en_e}\frac{\partial p_e}{\partial y} + \beta_e\frac{\partial\psi}{\partial y} + \sigma_e u_x B\right]dy - \Delta\phi_c + \Delta\phi_a \qquad (2.232)$$

and

$$\frac{\partial\psi}{\partial y} = \sigma_e\frac{d\Delta\phi}{dx} - \frac{\sigma_e}{en_e}\frac{\partial p_e}{\partial x} + \beta_e\frac{\partial\psi}{\partial x} \qquad (2.233)$$

respectively, where $\Delta\phi = \Delta\phi_a$ or $\Delta\phi_c$

For the insulator walls at $y=0$ and $y=H$, condition (ii) requires that $J_y = \partial\psi/\partial x = 0$, yielding ψ = constant. Assuming that the electrode pairs are electrically separate, there can be no net current flow in the x-direction. This is ensured by setting $\psi(AB)=\psi(EF)=\psi_0$, and $\psi(CD)=\psi(GH)=\psi_1$, where $\psi_0 = 0$ arbitrarily. From equation (2.228) and conditions (iii) and (iv), it follows that

$$\psi_1 = \psi_0 + I/W \qquad (2.234)$$

and

$$\psi(x,y) = \psi(x+L,y) + I/W \qquad (2.235)$$

In this work it is assumed that I is a fixed prescribed quantity; i.e., a constant current is considered to be applied to the plasma as might be the case in practice if the section of generator considered were a preionizer Finite interaction between the external load circuits and the plasma is included in the work of Uncles [8], but is neglected in the present work.

The periodicity condition (iv) is also imposed on the plasma fields. Thus,

$$n_e(x,y) = n_e(x+L,y) \tag{2.236a}$$

$$n_n(x,y) = n_n(x+L,y) \tag{2.236b}$$

and

$$T_e(x,y) = T_e(x+L,y) \tag{2.236c}$$

The boundary constraints on the plasma fields at the insulator and electrode walls are obtained from an analysis of the plasma sheaths near the walls and plasma-wall interactions. This analysis is presented in section 2.7 .

2.7 ELECTROSTATIC SHEATHS AND ELECTRODE-PLASMA INTERACTIONS

In order to obtain the wall boundary conditions to be satisfied by the continuity equations (2.207) and (2.208), and the electron energy equation (2.227), interactions between the walls and the plasma, and the description of plasma behaviour in regions adjacent to the walls, must be considered. Much of this section is concerned with the interactions between electrodes and the plasma which are dependent on the presence of electrostatic sheaths adjacent to the electrode surfaces, and on the processes of emission, desorption, and absorption of electrons and seed particles by these surfaces. Interactions between insulator surfaces and the plasma are much less complex and will be considered after a detailed model of the plasma-electrode interactions has been formulated.

Three regions are assumed to exist near an electrode surface. The region nearest the wall is a region of significant departure from charge neutrality; that is, the electrostatic sheath. The sheath is assumed to be collisionless; that is, ion and electron collision effects are assumed to be negligible in the sheath. The extent of this region is the sheath thickness λ_s, where, from Poisson's equation,

$$\lambda_s \sim \left(|\Delta\phi|\epsilon_0/en_e\right)^{1/2} \tag{2.237}$$

which can be written in terms of the Debye length $\lambda_d = \left(\epsilon_0 k_B T_e/n_e e^2\right)^{1/2}$ as

$$\lambda_s \sim \left(e\,|\Delta\phi|/k_B T_e\right)^{1/2}\lambda_d \tag{2.238}$$

For ion and electron collision effects to be negligible in the sheath it is necessary that the sheath thickness λ_s be smaller than the smallest mean free path, which, in the case of electron-buffer gas atom collisions dominant, is the ion mean free path. In general, the mean free path of species α particles, when collisions between species α particles and buffer gas atoms are dominant, is given by

$$l_\alpha = \frac{1}{n_h Q_{\alpha h}} \left(\frac{m_h}{m_\alpha + m_h} \right)^{1/2} \qquad (2.23)$$

where $Q_{\alpha h}$ is the momentum transfer cross-section for collisions between species α particles and buffer gas atoms. The condition for electron and ion collision effects to be negligible in the sheath can be written in the form

$$\lambda_s < l_i \qquad (2.240a)$$

Taking as typical values, $T_e = 2000^\circ K$, $n_e = 10^{19} m^{-3}$, $n_h = 4 \times 10^{24} m^{-3}$, and using equation (2.237), the condition (2.240a) can be satisfied only if

$$|\Delta\phi| < \frac{e n_e}{\epsilon_o} l_i^2 \simeq 0.1 mV \quad , \qquad (2.240b)$$

or

$$\left(\frac{e|\Delta\phi|}{k_B T_e} \right)^{1/2} < 0.03$$

The values of the lengths λ_d, l_i and l_e, for the above values of plasma parameters are

$$\lambda_d = 10^{-6} m \quad , \quad l_i = 2 \times 10^{-7} m \quad , \text{ and } \quad l_e = 3 \times 10^{-6} m. \qquad (2.241)$$

It is apparent from condition (2.240b) that (2.240a) can be satisfied only for small sheath voltage drops. For larger sheath voltage drops such as might occur in regions of the cathode surface as current saturation is approached, the condition will not be satisfied unless the electron density is larger in those regions. It should be noted, however, that the value of electron density used in making the above estimates is the Saha equilibrium value at the given electron temperature. In reality, depletion of electrons and reduction of electron density below the Saha value can be caused by diffusion in regions of large electron density gradients. As a result, the restriction on the size of $\Delta\phi$ may be more severe than condition (2.240b)

suggests. It is clear that, in order to obtain accurate results, application of the present theory must be restricted to cases in which the magnitudes of the sheath voltage drops are small.

The second region is the transition region, which acts as a buffer region between the collisionless sheath and the collision dominated region. This region extends from λ_s to a distance equal to several times the maximum mean free path. The maximum mean free path is the electron mean free path; a typical value of which was given as one of the estimates (2.241).

The third region is the continuum region; this is the outer collision dominated region where the particle distribution functions are close to Maxwellians and the behaviour of the plasma can be described by the continuum continuity and electron energy equations derived in section 2.6 .

The following assumptions are introduced to simplify the model:

(i) In the transition region the velocity distributions of particles moving towards an electrode wall are half Maxwellians at temperatures T_w (wall temperature) for the ions and neutrals, and T_{ew} for the electrons; the variations of these temperatures across the transition region are negligible.

(ii) Ionization, recombination and convection effects are negligible in the sheath and transition regions.

(iii) The sheath and transition regions are locally one-dimensional.

(iv) The magnetic field has no effect on the particle motion in the sheath.

(v) The electron heat flux, the electron density and the seed atom density are approximately constant across the transition region.

Since the continuum region is collision dominated for all particles, the particles entering the transition region have half Maxwellian velocity distributions, and it is assumed in (i) that the perturbations

of these distributions due to the relatively few collisions in the transition region can be neglected.

Assumption (ii) is taken to imply that, as in the case of a stationary collision dominated plasma in a steady state, particle fluxes are constant across the transition region. The continuity of fluxes follows from an assumed smallness of the characteristic diffusion time compared with the time scales of variation of the plasma properties in the regions of plasma far removed from the electrode surfaces. This allows one to formulate relaxation free boundary conditions for the continuity equations, without detailed consideration of the transition region.

For assumption (ii) to be valid it is necessary that the extent of the sheath-transition region, which is about equal to l_e, be smaller than the average distance l^R traversed by an ion before it recombines, convection effects being negligible because of the small flow velocity near the wall and the small sheath thickness. Statistical considerations based on the random walk concept suggest that l^R be written as [1]

$$l^R \simeq \left(\frac{\nu_{ih}}{\nu_i^R}\right)^{1/2} l_i \qquad (2.242)$$

where ν_i^R is the collision frequency for three body recombination, which is obtained from equations (2.209) and (2.213) in the form

$$\nu_i^R = \alpha(T_e) n_e = 1.09 \times 10^{-20} n_e^2 T_e^{-9/2}. \qquad (2.243)$$

Taking as typical values, $n_e = 10^{19} m^{-3}$, $T_e = 2000°K$, $\overline{T} = 1500°K$ and $n_h = 4 \times 10^{24} m^{-3}$, it is found from equations (2.242) and (2.243) that $l^R \simeq 4 \times 10^{-4} m$. Comparison with estimates (2.241) show that, since $l^R >> l_e$, the condition for validity of assumption (ii) is satisfied.

Assumption (iii) is justified by the fact that l_e is much less than

the electrode dimensions.

For assumption (iv) to be valid it is necessary that

$$\lambda_s \ll \lambda_{eL} \tag{2.244}$$

where λ_{eL} is the electron Larmor radius, given by

$$\lambda_{eL} = \frac{m_e}{eB}\bar{c}_e \tag{2.245}$$

where $\bar{c}_e$ is the root mean square speed of electrons, given by

$$\bar{c}_e = (8k_B\bar{T}_e/\pi m_e)^{1/2} \tag{2.246}$$

For the typical values of n_e and $\bar{T}_e$ given above, the condition (2.244) is satisfied for $B < 45T$, assuming that $\Delta\phi \simeq 0.1mV$, so that $\lambda_s \simeq L_i$.

Assumption (v) and, to a lesser extent, assumption (i), cannot be justified without attempting to extract more information from the Boltzmann equations for the particle distribution functions in the transition region where departures from equilibrium are large for electrons and ions. It is suspected that some error is involved in making assumption (v), but it is only by making this assumption that one can exclude details of the particle motion in the transition region which are difficult, if not impossible, to determine with accuracy from the Boltzmann equations of the particles. It should be noted that no such problem exists in the case of a collision dominated sheath ($\lambda_s \ll L_i$) for which a transition region is not defined.

Effects of Seed Deposit on Electrodes

The theoretical model of electrode-plasma interactions developed here incorporates electrode-seed interactions. The essential feature of these interactions is the large affinity between the alkali metal and the surface. Practically all incident seed particles (ions and neutrals) are adsorbed to the surface and desorption takes place only after a certain residence time. The most important parameter characterizing the coated surface is the degree of coverage (θ), defined as

the ratio of the number of adsorbed atoms per unit area to the number of adsorption sites available per unit area. The value of θ strongly influences the rate at which electrons are emitted from the surface as well as the rates at which ions or atoms are desorbed. Expressions for the rate of emission of electrons ν_e, the rate of desorption of ions ν_i and the rate of desorption of neutrals ν_n have been given by Levine and Gyftopoulos [28]. In general these have the forms, neglecting the Schottky effect,

$$\nu_e = 4\pi m_e (k_B T_w) h^{-3} \exp\left(-e\Phi_e / k_B T_w\right) \qquad (2.247)$$

$$\nu_i = \bar{\nu} \sigma_f g_i \psi(\theta) \exp\left(-e\Phi_i / k_B T_w\right), \qquad (2.248)$$

and

$$\nu_n = \bar{\nu} \sigma_f g_n \psi(\theta) \exp\left(-e\Phi_n / k_B T_w\right), \qquad (2.249)$$

where, by application of the formulae presented in reference (28) to a caesium-tantalum combination, the following expressions have been found for the quantities appearing in equations (2.247) - (2.249):

$$g_n = 2,\ g_i = 1,\ \sigma_f = 4.2 \times 10^{18}\ m^{-2},\ \bar{\nu} = 10^{12}\ sec^{-1}\ ; \qquad (2.250a)$$

$$\psi(\theta) = \theta\,(1-\theta)^{-1}\left(1-\theta^{1/2}\right)^{-1} \exp\left\{\left[\theta/(1-\theta) + \theta^{1/2}/(1-\theta^{1/2})\right]/2\right\}; \qquad (2.250b)$$

and

$$\Phi_e = 4.19 - 2.54\left[1 - (1 - 3\theta^2 + 2\theta^3)\left\{1 - \left[\frac{2.258\theta}{1 + 1.004\theta^{3/2}}\right]\right\}\right]$$

$$\Phi_i = 2.091 + 4.495\theta + 2.638\theta^2 - 14.431\theta^3 + 12.093\theta^4 - 2.969\theta^5$$

$$\Phi_n = 2.416 - 1.492\theta - 1.429\theta^2 + 8.415\theta^3 - 10.341\theta^4 + 4.132\theta^5, \qquad (2.250c)$$

where the expressions for Φ_i and Φ_n are least square polynomial

fits to the exact expressions, which are rather complex.

The expressions for ν_e, ν_i and ν_n, given by equations (2.247), (2.248) and (2.249), are based on the assumption that all particles are emitted and desorbed in half Maxwellian distributions at the wall temperature T_w.

The variations of ν_e, ν_i and ν_n with θ are shown in figure 2.4 for a wall temperature of 1316°K, which is the wall temperature at the particular x-location at which the gas-dynamic profiles used to obtain the numerical solutions of the plasma and electrical equations in chapter 5 are taken. It can be seen from figure 2.4 that seed deposition on electrode surfaces results in a considerable enhancement of electron emission due to the large reduction of electron work function $\Phi_E(\theta)$ below the value for $\theta = 0$, which is 4.19; the emission rate appears to saturate at a maximum value, which is of order 10^{10} times the value for $\theta = 0$. It can also be seen that the relative magnitudes of ν_e, ν_i and ν_n strongly depend on the value of θ; the desorption rates ν_i and ν_n are zero at $\theta = 0$, but tend to infinity as $\theta \to 1$. Also, $\nu_n > \nu_e$ over the entire range of θ; $\nu_n > \nu_i$ for all but small values of θ (< 0.05); and $\nu_i < \nu_e$ for $0.2 < \theta < 0.9$.

Before the general wall boundary conditions are presented, it is useful to consider the values of θ and the corresponding values of ν_e, ν_i and ν_n in the equilibrium case, where all plasma properties are constant and the net fluxes of all particles are zero. This case has been considered in detail in reference (29) for a caesium-tungsten system, but is reconsidered here for a caesium-tantalum system, in which case the formulae (2.250) are somewhat different. In the equilibrium case the seed atom continuity conditions derived below in (c) yield, since the net seed atom flux is zero everywhere (see equation (2.272)).

$$\Gamma_{ny} = 2\nu_n - \tfrac{1}{2} n_n c_n = 0$$

or

$$\nu_n(\theta) = n_n c_n / 4$$

where c_n is the root mean square speed of seed atoms. For a given gas temperature and seeding fraction, and assuming Saha equilibrium at the gas temperature, the latter equation yields the equilibrium value of θ, and the corresponding values of ν_e, ν_i and ν_n can be found from equations (2.250). It is found that for a gas temperature equal to the wall temperature given above, i.e., 1316°K, and a seeding fraction of 0.002, the equilibrium value of θ is 0.35. It can be seen in figure 2.4 that, for this value of θ, $\nu_i \ll \nu_e < \nu_n$ and $\nu_e \simeq 2 \times 10^{22} m^{-2} sec^{-1}$, yielding a current density of about 3×10^3 A/m^2. Under near equilibrium conditions, the maximum obtainable current density is about equal to the latter value (see sub-section (b)). However, the work of Koester et al [30] has shown that as a result of the complex interactions between a non-equilibrium plasma and a seed covered electrode the maximum attainable current density can be greatly increased. It is one of the aims of the present work to investigate the effects of this phenomenon on the behaviour of the plasma in a closed cycle MHD generator.

Electrode Wall Boundary Conditions

Boundary conditions incorporating electrode-seed interaction effects were first considered by Sajben [29] who formulated boundary conditions for the continuity equations, but not for the electron energy equation, assuming a collision dominated sheath, and steady state plasma. These boundary conditions were used by Koester et al [30] to solve numerically the continuity equations and Poisson's equation. Again, the electron energy equation was not considered, and only steady plasma states were considered. In addition, the theory of reference (30) was restricted in application to a laminar stagnation flow geometry. The

present formulation of boundary conditions is based instead on the assumption of a collisionless sheath and includes a boundary condition for the electron energy equation with an allowance for finite surface coverage relaxation rates. In addition, boundary conditions incorporating electrode-seed interaction effects are applied for the first time to a MHD generator. The boundary conditions are derived below for each of the two electrodes (separated by a distance H) of a single segment of a segmented electrode MHD generator. To be specific, an electrode at $y=0$ is first considered and the boundary conditions then presented in a form applicable to either electrode.

In formulating the wall boundary conditions, two cases must be considered, according to the sign of the sheath voltage drop $\Delta\phi$, which is defined as the voltage of the sheath edge relative to the electrode in question. The physical distinction between these cases is discussed in sub-section (b) below, in which the continuity of the component of current density normal to an electrode across the transition region is considered.

(a) Ion continuity conditions

The boundary conditions for the electron continuity equation can be obtained in a convenient form by considering the ion motion. The behaviour of the ions in the sheath depends on the sign of the sheath voltage drop $\Delta\phi$, so that the two cases $\Delta\phi \geq 0$ and $\Delta\phi \leq 0$ must be considered separately.

$\Delta\phi \geq 0$

In the case of a positive sheath voltage drop, one has in the sheath region an acceleration of ions moving towards the wall, and a deceleration of ions moving away from the wall. The velocity distribution function in the sheath as a function of the local potential ϕ (relative to the electrode) can be derived by utilizing assumption (i) and the fact that ions are desorbed in half Maxwellian distributions.

Integration over velocity space then yields the following expression for the local ion density in the sheath:

$$n_i(\phi) = \frac{2\nu_i}{c_{i\omega}}\left[1+\mathrm{erf}\left\{\frac{e(\Delta\phi-\phi)}{k_B T_\omega}\right\}^{1/2}\right] e^{-\frac{e\phi}{k_B T_\omega}} + \frac{2\mu_{is}^-}{c_{is}}\left[1-\mathrm{erf}\left\{\frac{e(\Delta\phi-\phi)}{k_B T_\omega}\right\}^{1/2}\right] e^{\frac{e(\Delta\phi-\phi)}{k_B T_\omega}} \quad (2.251)$$

where the subscript s denotes a value at the outer sheath edge, $c_i = (8k_B T/\pi m_i)^{1/2}$ is the root mean square speed of ions with a Maxwellian velocity distribution at temperature T and μ_{is}^- denotes the flux of ions moving towards the wall at the sheath edge. In equation (2.251), we have, in accordance with assumption (i),

$$c_{is} = c_{i\omega} = \left(\frac{8k_B T_\omega}{\pi m_i}\right)^{1/2}$$

From equation (2.251) the ion density at the outer edge of the sheath, where $\phi = \Delta\phi$, is obtained:

$$n_{is} = \frac{2\nu_i}{c_{i\omega}} h_i + \frac{2\mu_{is}^-}{c_{is}} = \frac{2}{c_{i\omega}}\left(\nu_i h_i + \mu_{is}^-\right) \quad (2.252)$$

where the retardation factor h_i is given by

$$h_i = e^{-\frac{e\Delta\phi}{k_B T_\omega}} \quad (2.253)$$

Since charge neutrality prevails at the outer edge of the sheath,

$$n_{e\omega} \equiv n_{es} = n_{is}$$

and equation (2.252) can be written in the form

$$n_{ew} = \frac{2}{c_{iw}} \left(v_i h_i + \mu_{is}^{-} \right), \tag{2.254}$$

Since ions are desorbed in a half Maxwellian velocity distribution at the temperature T_w , the net ion flux in the y-direction at the outer edge of the sheath can be written as

$$\Gamma_{iy} = v_i h_i - \mu_{is}^{-} \tag{2.255}$$

or

$$\Gamma_{iy} = 2 v_i h_i - \frac{1}{2} n_{ew} c_{iw}, \tag{2.256}$$

where μ_{is}^{-} has been eliminated from equation (2.255) using equation (2.254).

According to equation (2.131), the macroscopic ion flux in the y-direction at the outer edge of the transition region is given by

$$\frac{1}{e} \left(J_y - J_{ey} \right) = - \left\{ \frac{\sigma_i k_B}{e^2 n_e} \frac{\partial}{\partial y} n_e \left(T + T_e \right) \right\}_t$$

which is equated to the net microscopic flux given by equation (2.256), in accordance with assumption (ii), to obtain the required boundary condition for the electron continuity equation:

$$- \left\{ \frac{\sigma_i k_B}{e^2 n_e} \frac{\partial}{\partial y} n_e \left(T + T_e \right) \right\}_w = 2 v_i h_i - \frac{1}{2} n_{ew} c_{iw}, \tag{2.257}$$

where, in accordance with assumptions (i) and (v), we have set $T_{et} = T_{ew}$, $T_t = T_w$ and $n_{et} = n_{ew}$.

The corresponding boundary condition for the wall at y = H is given by equation (2.257) with the sign of the right hand side reversed. The boundary condition for either wall can be written in the form

$$- \left\{ \frac{\sigma_i k_B}{e^2 n_e} \frac{\partial}{\partial y} n_e \left(T + T_e \right) \right\}_w = \epsilon \left(2 v_i h_i - \frac{1}{2} n_{ew} c_{iw} \right), \tag{2.258}$$

where $\epsilon = +1$ for the electrode at $y = 0$, and $\epsilon = -1$ for the electrode at $y = H$.

$\Delta\phi \lesssim 0$.

In the case of a negative sheath voltage drop, one has in the sheath region a deceleration of ions moving towards the wall and an acceleration of ions moving away from the wall. Deriving the velocity distribution function in the sheath as a function of the local potential and integrating over velocity space, as in the case where $\Delta\phi \gtrsim 0$, the local ion density in the sheath is obtained in the form

$$n_i(\phi) = \frac{2\nu_i}{c_{i\omega}}\left[1 - \mathrm{erf}\left\{-\frac{e\phi}{k_B T_\omega}\right\}^{1/2}\right] e^{-\frac{e\phi}{k_B T_\omega}} + \frac{2\mu_{is}}{c_{is}}\left[1 + \mathrm{erf}\left\{-\frac{e\phi}{k_B T_\omega}\right\}^{1/2}\right] e^{\frac{e(\Delta\phi - \phi)}{k_B T_\omega}} \qquad (2.259)$$

where, in accordance with assumption (i),

$$c_{is} = c_{i\omega} = \left(\frac{8 k_B T_\omega}{\pi m_i}\right)^{1/2}$$

From equation (2.259) the ion density at the outer edge of the sheath, where $\phi = \Delta\phi$, is obtained:

$$n_{is} = \frac{2\nu_i}{c_{i\omega}}\left[1 - \mathrm{erf}\left\{-\frac{e\Delta\phi}{k_B T_\omega}\right\}^{1/2}\right] e^{-\frac{e\Delta\phi}{k_B T_\omega}} + \frac{2\mu_{is}}{c_{i\omega}}\left[1 + \mathrm{erf}\left\{-\frac{e\Delta\phi}{k_B T_\omega}\right\}^{1/2}\right], \qquad (2.260)$$

and, since charge neutrality prevails at the outer edge of the sheath,

$$n_{is} = n_{es} \equiv n_{e\omega} \qquad (2.261)$$

Since particles entering the sheath region from the transition region have a half Maxwellian velocity distribution at the wall temperature T_ω (assumption (i)), the net ion flux in the y-direction at the outer

edge of the sheath can be written as

$$\Gamma_{iy} = \nu_i - \mu_i \bar{s} h_i \tag{2.262}$$

where the retardation factor h_i is given by

$$h_i = \exp\left(e\Delta\phi / k_B T_\omega\right)$$

Eliminating $\mu_i \bar{s}$ from equation (2.262) using equations (2.260) and (2.261) we can write

$$\Gamma_{iy} = \nu_i - \frac{h_i \left\{ \frac{1}{2} n_{e\omega} c_{i\omega} - \nu_i \left[1 - erf\left(-\frac{e\Delta\phi}{k_B T_\omega} \right)^{1/2} \right] e^{-\frac{e\Delta\phi}{k_B T_\omega}} \right\}}{\left[1 + erf\left(-\frac{e\Delta\phi}{k_B T_\omega} \right)^{1/2} \right]} \tag{2.263}$$

Equating the macroscopic ion flux in the y-direction at the outer edge of the transition layer, which is obtained from equation (2.131), to the net microscopic ion flux given by equation (2.263), in accordance with assumption (ii) the required boundary condition for the electron continuity equation is obtained; this is written in the general form

$$-\left\{ \frac{\sigma_i k_B}{n_e e^2} \frac{\partial}{\partial y} n_e (T + T_e) \right\}_\omega = \epsilon \left[\nu_i - \frac{h_i \left\{ \frac{1}{2} n_{e\omega} c_{i\omega} - \nu_i \left[1 - erf\left(-\frac{e\Delta\phi}{k_B T_\omega} \right)^{1/2} \right] e^{-\frac{e\Delta\phi}{k_B T_\omega}} \right\}}{\left\{ 1 + erf\left(-\frac{e\Delta\phi}{k_B T_\omega} \right)^{1/2} \right\}} \right] \tag{2.264}$$

where $\epsilon = +1$ for the electrode at y = o, and $\epsilon = -1$ for the electrode at $y = H$.

(b) Total Current Continuity Conditions

The analysis of (a) can be carried out for electrons and expressions derived for the net microscopic fluxes of electrons in the y-direction. For $\Delta\phi \geq 0$,

$$\Gamma_{ey} = \epsilon \left[\nu_e - h_e \frac{\left\{ n_{ew} - \frac{2\nu_e}{c_{ew}} \left[1 - erf\left(\frac{e\Delta\phi}{k_B T_w} \right)^{1/2} \right] e^{\frac{e\Delta\phi}{k_B T_w}} \right\}}{\frac{2}{c_{es}} \left(1 + erf\left(\frac{e\Delta\phi}{k_B T_{ew}} \right)^{1/2} \right)} \right] \tag{2.265}$$

where

$$h_e = e^{-e\Delta\phi / k_B T_{ew}}, \quad c_{ew} = \left(\frac{8 k_B T_w}{\pi m_e} \right)^{1/2}, \quad c_{es} = \left(\frac{8 k_B T_{ew}}{\pi m_e} \right)^{1/2};$$

while, for $\Delta\phi < 0$,

$$\Gamma_{ey} = \epsilon \left[\left(1 + \frac{c_{es}}{c_{ew}} \right) \nu_e h_i - \frac{1}{2} n_{ew} c_{es} \right] \tag{2.266}$$

where

$$h_i = e^{e\Delta\phi / k_B T_w}$$

The factor ϵ is $+1$ for the electrode at $y=0$, and -1 for the electrode at $y = H$.

The sheath voltage drop $\Delta\phi$ is determined from the requirement that the y-component of the total current density be constant across the transition region, so that

$$J_y = J_{yt} = e\left[\Gamma_{iy} - \Gamma_{ey} \right] \tag{2.267}$$

where Γ_{iy} is given by equation (2.256) when $\Delta\phi \geq 0$, and equation (2.263) when $\Delta\phi < 0$ (the signs of the right hand sides of equations (2.256) and (2.263) must be changed when the electrode at $y = H$ is

considered). The electron flux Γ_{ey} is given by equation (2.265) when $\Delta\phi \geq 0$, and equation (2.266) when $\Delta\phi \leq 0$. For a given current J_y, equation (2.267) is to be considered an equation for $\Delta\phi$.

In order to determine how J_y varies with $\Delta\phi$, the values of J_y in the limits $\Delta\phi \to -\infty$ and $\Delta\phi \to +\infty$, and in the intermediate case, where $\Delta\phi = 0$, are considered. The value of θ is taken to be 0.35, which, as mentioned earlier, is the equilibrium value of θ for a seeding fraction of 0.002 and a wall temperature of 1316°K; the corresponding values of ν_e and ν_i are, from figure 2.4, $2.3^{\circ} \times 10^{22}\ m^{-2}\ sec^{-1}$ and $4.32 \times 10^{17}\ m^{-2}\ sec^{-1}$ respectively. The electron temperature at the sheath edge T_{es} is taken to be 2000°K.

Thus, we consider the following cases for an electrode at y =0:

(i) $\Delta\phi \to -\infty$.

Equations (2.263) and (2.266) yield, in the limit $\Delta\phi \to -\infty$

$$\Gamma_{iy} = \nu_i \tag{2.268a}$$

and

$$\Gamma_{ey} = -\tfrac{1}{2} n_{ew} c_{es} \tag{2.268b}$$

respectively, and, using equation (2.267),

$$J_y = e\left(\nu_i + \tfrac{1}{2} n_{ew} c_{es}\right) \tag{2.268c}$$

(ii) $\Delta\phi = 0$.

Setting $\Delta\phi = 0$ in equations (2.263) and (2.266) we obtain

$$\Gamma_{iy} = 2\nu_i - \tfrac{1}{2} n_{ew} c_{iw}, \tag{2.269a}$$

and

$$\Gamma_{ey} = \left(1 + \frac{c_{es}}{c_{ew}}\right)\nu_e - \tfrac{1}{2} n_{ew} c_{es}, \tag{2.269b}$$

so that

$$J_y = e\left[2\nu_i - \tfrac{1}{2} n_{ew} c_{iw} - \left(1 + \frac{c_{es}}{c_{ew}}\right)\nu_e + \tfrac{1}{2} n_{ew} c_{es}\right] \tag{2.269c}$$

(iii) $\Delta\phi \to +\infty$

Equations (2.256) and (2.265) yield, in the limit $\Delta\phi \to \infty$,

$$\Gamma_{iy} = -\frac{1}{2} n_{ew} c_{iw} , \tag{2.270a}$$

and

$$\Gamma_{ey} = \nu_e \tag{2.270b}$$

so that

$$J_y = -e \left(\nu_e + \frac{1}{2} n_{ew} c_{iw} \right) \tag{2.270c}$$

Since $\nu_i \ll \nu_e$ for $\theta = 0.35$, and $c_{iw} \ll c_{es}$, equation (2.269c) can be approximately written as

$$J_y \simeq e \left[- \left(1 + \frac{c_{es}}{c_{ew}} \right) \nu_e + \frac{1}{2} n_{ew} c_{es} \right]$$

from which is follows that the sign of J_y for $\Delta\phi = 0$ is dependent on the value of n_{ew}; $J_y > 0$ for $\Delta\phi = 0$ if

$$n_{ew} > \frac{2}{c_{es}} \left(1 + \frac{c_{es}}{c_{ew}} \right) \nu_e \simeq 3.83 \times 10^{17} \, m^{-3} , \tag{2.271}$$

where use has been made of the values of T_w, T_{es} and ν_e given above. If the latter value of n_{ew} is compared with the value $n_e^* \simeq 1.76 \times 10^{19} \, m^{-3}$ obtained by assuming Saha equilibrium at the electron temperature $T_{es} = 2000^\circ K$, we see that, near Saha equilibrium, the condition (2.271) is satisfied and $J_y < 0$ only for sufficiently large $\Delta\phi$; for $n_e = n_e^*$, equations (2.268c), (2.269c) and (2.270c) yield the values $3.91 \times 10^5 \, A \, m^{-2}$, $3.92 \times 10^5 \, A \, m^{-2}$ and $-4.46 \times 10^3 \, A \, m^{-2}$, respectively, for J_y. As $\Delta\phi$ is increased from $\Delta\phi = -\infty$, J_y remains practically constant, for $\Delta\phi < 0$, at a value about equal to $e n_{ew} c_{es}/2$ because of the relatively minor contribution of the emitted electrons to J_y. But, for $\Delta\phi > 0$, J_y rapidly decreases with increasing $\Delta\phi$ due to the increasing reduction of the flux of electrons reaching the electrode surface from the plasma. Finally,

for sufficiently large $\Delta\phi$, J_y approaches the emitted current density $-e\nu_e$

However, as a result of diffusion, the electron density can be considerably reduced below its Saha value; the numerical results presented in chapter 5 show that the electron density can be of the order of $10^{17} m^{-3}$ with $T_e \simeq 2000^\circ K$ and $\theta \simeq 0.35$. Taking, for example, $n_e = 10^{17} m^{-3}$, equations (2.268c), (2.269c) and (2.270c) yield the values $2.23 \times 10^3 Am^{-2}$, $-6.29 \times 10^3 Am^{-2}$, and $-3.92 \times 10^3 Am^{-2}$. In this case, J_y rapidly decreases from a value of order $en_{e\omega} c_{es}/2$ as $\Delta\phi$ is increased from $\Delta\phi = -\infty$, due mainly to the increasing

contribution of emitted electrons to J_y , and eventually remains relatively constant at a value of order the emitted current $e\nu_e$ in the interval $0 < \Delta\phi < \infty$

It must be remembered that, in the above examples, θ is taken to be close to its equilibrium value of 0.35, at which $\nu_i \ll \nu_e$. Figure 2.4 shows that ν_i can exceed ν_e for $\theta < 0.2$ or $\theta > 0.9$. In the case where $\nu_i > \frac{1}{2}\left(1 + \frac{c_{es}}{c_{e\omega}}\right)\nu_e$, equations (2.268c) and (2.269c) show that $J_y > 0$ in $-\infty < \Delta\phi \leq 0$ independent of $n_{e\omega}$, since $c_{i\omega} \ll c_{es}$; one then has $J_y < 0$ only for sufficiently large positive values of $\Delta\phi$.

(c) Seed Atom Continuity Conditions

In the case of the neutral seed atoms, the transition is considered as extending from the inner edge of the collision dominated region to the outer edge of an electrode adjacent layer of thickness about equal to l_n called the Knudsen layer, within which collisions of seed atoms with buffer gas atoms can be neglected. Since $l_n \simeq l_i$, the Knudsen layer must necessarily be thicker than the sheath if the sheath is collisionless. Considering again the electrode at y = 0, the net flux of neutral

seed atoms in the y-direction, which is constant across the transition region, in accordance with assumption (ii), is given by

$$\Gamma_{ny} = \mu_{n\delta}^{+} - \mu_{n\delta}^{-} = v_n - \mu_{n\delta}^{-} \tag{2.272}$$

where $\mu_{n\delta}^{+}$ and $\mu_{n\delta}^{-}$ are the fluxes of seed atoms moving away and towards the wall, respectively, and the subscript δ refers to the outer edge of the Knudsen layer. Equation (2.272) gives

$$\mu_{n\delta}^{+} = v_n \tag{2.273}$$

It follows from equation (2.273) and assumption (i) that the seed atom density at the outer edge of the Knudsen layer is given by

$$n_{nw} = \frac{2v_n}{c_{nw}} + \frac{2\mu_{n\delta}^{-}}{c_{nw}} \tag{2.274}$$

where $c_{nw} = \left(8k_B T_w/\pi m_n\right)^{1/2}$. In accordance with assumption (v) n_n is taken to be constant across the transition region and given by equation (2.274). From equation (2.274) we obtain

$$\mu_{n\delta}^{-} = \frac{1}{2} n_{nw} c_{nw} - v_n \tag{2.275}$$

Eliminating $\mu_{n\delta}^{-}$ from equation (2.272) using equation (2.275) an expression is obtained for the net flux at the outer edge of the Knudsen layer:

$$\Gamma_{ny} = 2v_n - \frac{1}{2} n_{nw} c_{nw} \tag{2.276}$$

The flux given by equation (2.276) is equated to the macroscopic flux in the y-direction, given by equation (2.196), at the outer edge of the transition layer in accordance with assumption (ii) and the required boundary condition is obtained; this is written in the general form

$$-\left\{ \frac{k_B}{m_{nh} v_{nh}} \frac{\partial}{\partial y} n_n T \right\}_w = \epsilon \left(2v_n - \frac{1}{2} n_{nw} c_{nw} \right) \tag{2.277}$$

where $\epsilon = +1$ for the electrode at $y = 0$, and $\epsilon = -1$ for the electrode at $y = H$.

(d) Electron Energy Continuity Conditions

The boundary condition for the electron energy equation is obtained by equating the microscopic electron energy flux at the outer edge of the sheath to the macroscopic electron energy flux, the electron heat flux, at the outer edge of the transition region in accordance with assumption (v). The forms of the boundary conditions depend on the sign of $\Delta\phi$, and two cases must therefore be considered.

$\Delta\phi \geq 0$

In the case of a positive sheath voltage drop the microscopic electron energy flux in the y-direction at the outer sheath edge is given by

$$\Gamma_{Eey} = \nu_e \left(2k_B T_w + e\Delta\phi\right) - \mu\bar{e}_s \left(2k_B T_{ew} + e\Delta\phi\right) h_e \qquad (2.273)$$

where

$$h_e = e^{-\frac{e\Delta\phi}{k_B T_{ew}}}$$

The net flux of electrons in the y-direction at the outer sheath edge can be written as

$$\Gamma_{ey} = \nu_e - \mu\bar{e}_s h_e \qquad (2.279)$$

Eliminating $\mu\bar{e}_s$ from (2.278) using equation (2.279) we can write equation (2.27[illegible]) in the form

$$\Gamma_{Eey} = \nu_e \left(2k_B T_w + e\Delta\phi\right) - \left(\nu_e - \Gamma_{ey}\right)\left(2k_B T_{ew} + e\Delta\phi\right) \qquad (2.280)$$

where Γ_{ey} is given by the expression for the macroscopic electron flux

$$\Gamma_{ey} = -\frac{1}{e} J_{ey} = -\frac{1}{e}\left\{ J_y + \frac{\sigma_i k_B}{e n_e}\left[\frac{\partial}{\partial y} n_e \left(T + T_e\right)\right]\right\} \qquad (2.281)$$

obtained from equation (2.131).

The macroscopic electron heat flux in the y-direction at the

outer edge of transition region is obtained from equation (2.219) in the form

$$(q_{ey})_t = -\frac{5k_B T_{et}}{2e}\left[J_y + \frac{\sigma_i k_B}{e n_e}\frac{\partial}{\partial y} n_e(T+T_e)\right]_t - \left[\frac{\lambda_e}{(1+\beta_e^2)}\frac{\partial T_e}{\partial y}\right]_t \quad (2.282)$$

where, consistent with assumptions (iv) and (v), the Hall component of the electron heat flux has been omitted from equation (2.282). In accordance with assumptions (i) and (v),

$$\overline{T}_{et} = \overline{T}_{ew}, \quad \overline{n}_{et} = \overline{n}_{ew}, \quad \overline{T}_t = \overline{T}_w$$

and the macroscopic energy flux given by equation (2.282) is equated to the microscopic energy flux given by equation (2.280) to give the required boundary condition for the electron energy equation; this is written in a form applicable to the electrode at y = H:

$$-\frac{5k_B \overline{T}_{ew}}{2e}\left[\overline{J}_y + \frac{\sigma_i k_B}{e n_e}\frac{\partial}{\partial y} n_e(T+T_e)\right]_w - \left[\frac{\lambda_e}{(1+\beta_e^2)}\frac{\partial \overline{T}_e}{\partial y}\right]_w$$
$$= \epsilon\left[\nu_e\left(2k_B T_w + e\Delta\phi\right) - \left(\nu_e - \epsilon\Gamma_{ey}\right)\left(2k_B \overline{T}_{ew} + e\Delta\phi\right)\right] \quad (2.283)$$

where $\epsilon = +1$ for the electrode at y = 0, and $\epsilon = -1$ for the electrode at y = H.

$\Delta\phi \leq 0$

In the case of a negative sheath voltage drop the microscopic electron energy flux in the y-direction at the outer sheath edge is given by

$$\Gamma_{Eey} = \nu_e\left(2k_B \overline{T}_{ew}\right)h_i - 2k_B \overline{T}_{ew}\mu_{es}, \quad (2.284)$$

where

$$h_i = \exp\left(e\Delta\phi / k_B T_w\right)$$

By determining, as in the case of the ions, the velocity distribution

function of the electrons in the sheath as a function of the local potential and integrating over velocity space, it can be shown that

$$n_{ew} = \frac{2\nu_e}{c_{ew}} h_i + \frac{2\mu_{es}^-}{c_{es}} \tag{2.285}$$

Eliminating μ_{es}^- from equation (2.284) using equation (2.285) and equating the resulting expression for Γ_{Eey} to the macroscopic electron heat flux, as was done for the case of a positive sheath voltage drop, the desired boundary condition for the electron energy equation is obtained; this is written in a form applicable to the electrode at y = H:

$$-\frac{5k_0 T_{ew}}{2e}\left[J_y + \frac{\sigma_i k_B}{e n_e}\frac{\partial}{\partial y} n_e (T+T_e)\right]_w - \left[\frac{\lambda_e}{(1+\beta_e^2)}\frac{\partial T_e}{\partial y}\right]_w$$
$$= \epsilon\left[\nu_e (2k_B T_w) h_i - 2k_B T_{ew}\left(\frac{1}{2} n_{ew} c_{es} - \frac{c_{es}}{c_{ew}} \nu_e h_i\right)\right] \tag{2.286}$$

where $\epsilon = +1$ for the electrode at y = 0, and $\epsilon = -1$ for the electrode at y = H.

(c) Surface Coverage Equations

Equations for the surface coverage θ are obtained by equating the rate of increase of the number of adsorbed atoms per unit surface area to the net flux of seed particles (ions and seed atoms) to the wall. Thus,

$$\sigma_f \frac{\partial \theta}{\partial t} = -\epsilon\left(\Gamma_{ny} + \Gamma_{iy}\right) \tag{2.287}$$

where $\epsilon = +1$ for the electrode at y = 0, and $\epsilon = -1$ for the electrode at y = H. In deriving equation (2.287) use has been made of the definition of σ_f as the number of adsorption sites available per unit surface area. The seed atom flux Γ_{ny} is given by equation (2.276) and Γ_{iy} is given by equation (2.256) for $\Delta\phi \geq 0$, and equation (2.263) for $\Delta\phi \leq 0$. Equations (2.272), (2.256) and (2.263) assume that the electrode is at y = 0; the expressions for the other

electrode wall at y = H are obtained by changing the signs of the right hand sides of equations (2.276), (2.256) and (2.263). However, since the factor ϵ is already present in equation (2.287), general equations for θ applicable to both electrode walls are obtained by omitting ϵ from equation (2.287) and from equations (2.276), (2.256) and (2.263).

Insulator Wall Boundary Conditions

Finally the boundary conditions for the continuity and electron energy equations are considered in the case of an insulator wall. These boundary conditions are obtained by assuming that the insulator wallsreflect all particles incident to them, the electrons being reflected elastically. The boundary condition at the insulator walls are then obtained by equating the macroscopic particle and electron energy fluxes to zero. We thus obtain the conditions

$$\left\{ \frac{\partial}{\partial y} n_e (T+T_e) \right\}_w = 0, \tag{2.288}$$

$$\left\{ \frac{\partial}{\partial y} n_n T \right\}_w = 0, \tag{2.289}$$

and

$$\left(\frac{\partial T_e}{\partial y} \right)_w = 0, \tag{2.290}$$

where equations (2.288) and (2.289), obtained from equations (2.131) and (2.196), express the conditions that the ion and seed atom fluxes to an insulator wall be equal to zero; and equation (2.290), obtained from equation (2.219), expresses the condition that the electron energy flux to an insulator wall be equal to zero. In expressing the latter condition in the form of equation (2.290), the Hall component of electron heat flux has been neglected as in the case of the electrode boundary conditions.

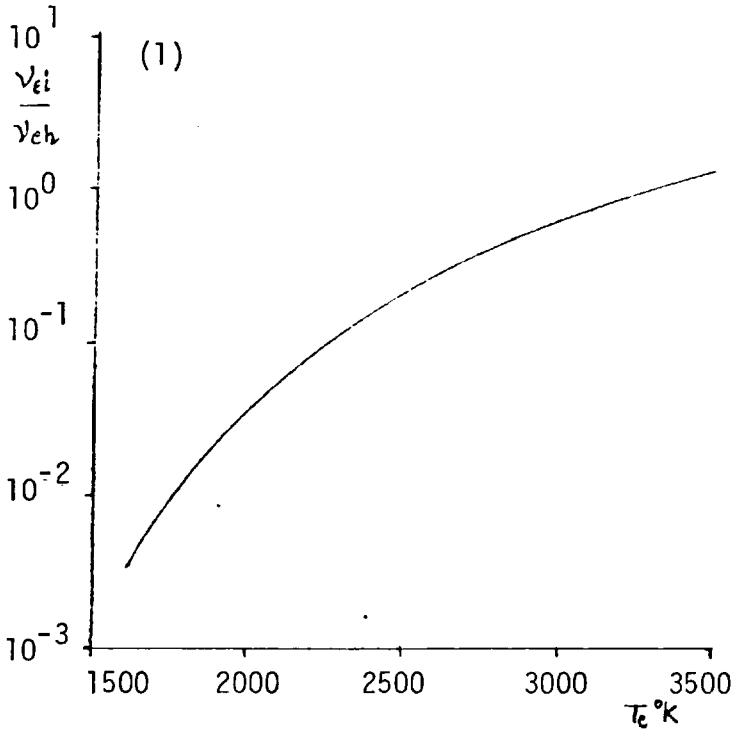

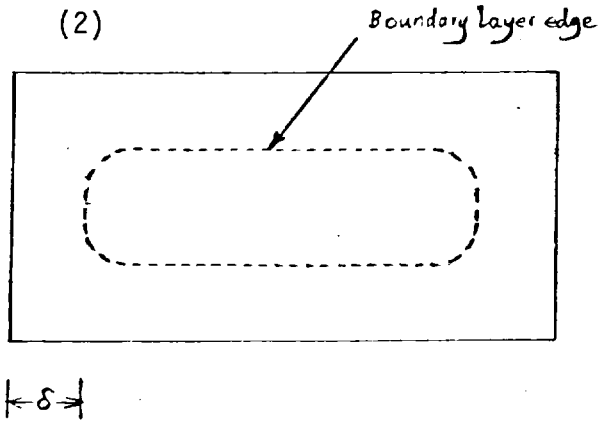

(1) Fig. 2.1: ν_{ei}/ν_{eh} against T_e for $x = 0.002$ and $T = 1519^{o}K$

(2) Fig. 2.2: A cross-section of the MHD channel showing approximately two-dimensional boundary layers on the side walls, with the exception of corner regions.

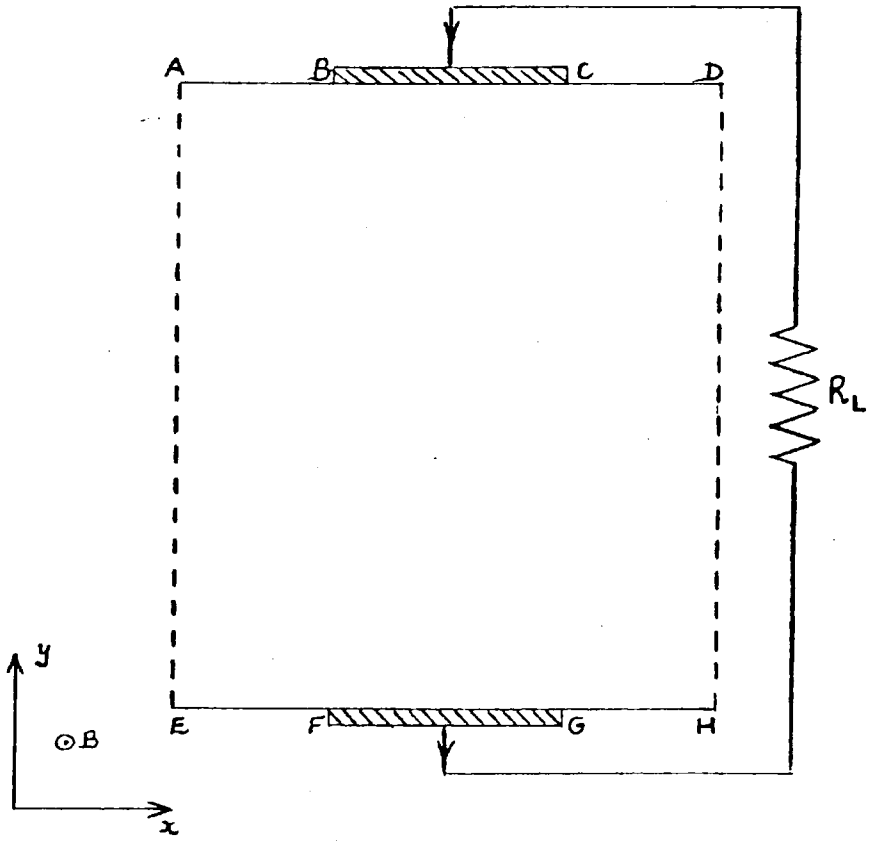

Fig. 2.3: One segment of a segmented electrode channel

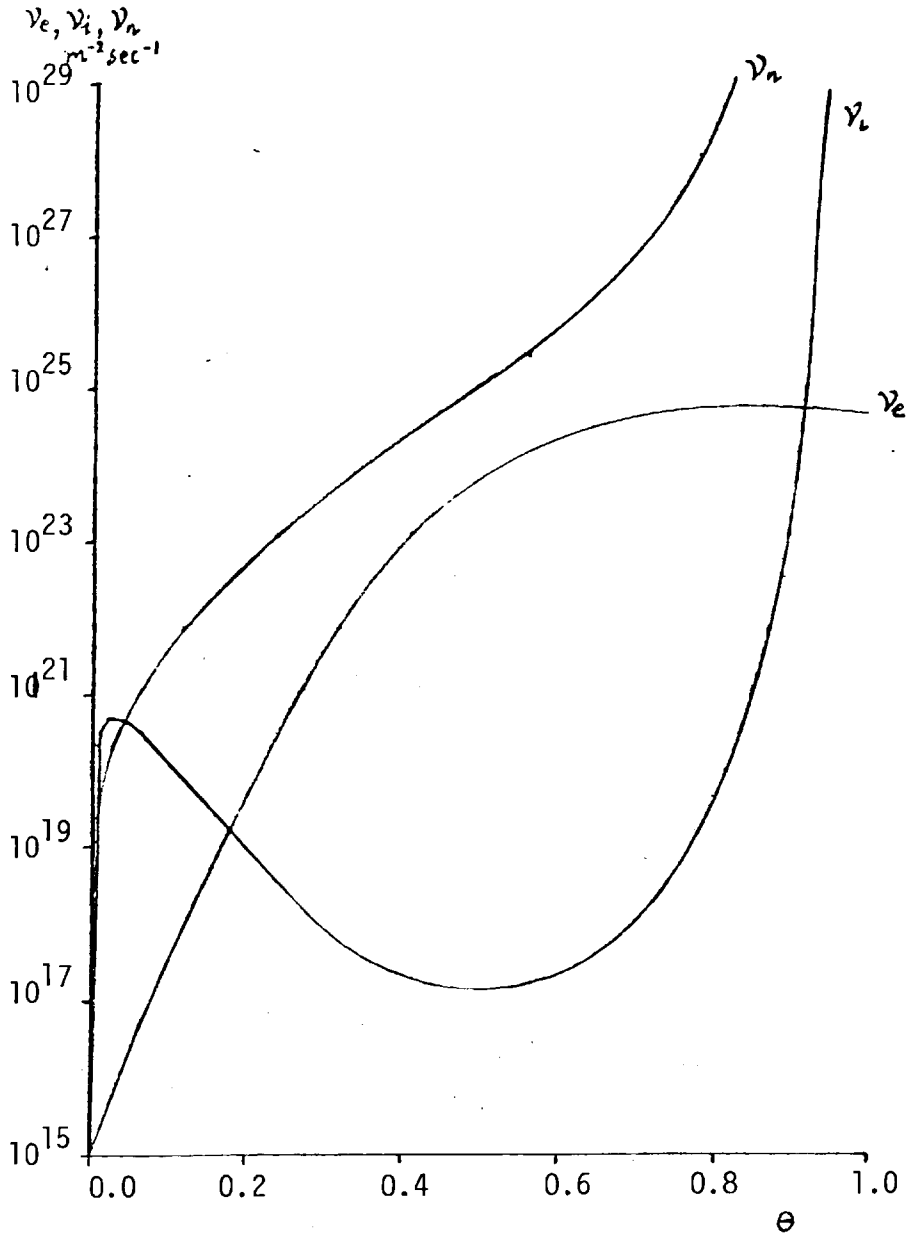

Fig. 2.4: The emission and desorption rates ν_e , ν_i and ν_n as functions of the surface coverage θ.

CHAPTER 3

NUMERICAL SOLUTION OF THE GAS-DYNAMIC EQUATIONS

3.1 Introduction

The assumptions made in section 2.4 led to a closed system of differential equations for the gas-dynamic variables p, ρ, $\underline{u}$ and T, completely decoupled from the equations for the plasma and electrical quantities presented in section 2.5. It was then indicated that the complex problem of solving the gas-dynamic equations for the flow in an MHD generator channel could be simplified by making approximations consistent with the boundary layer assumption expressed by the inequality (2.155). Further simplifications of the gas-dynamic problem were then made by neglecting three-dimensional corner effects so as to allow the flow behaviour in the channel to be described in terms of two-dimensional boundary layers on each of the four side walls of the channel. By symmetry, it is sufficient to determine the flow distributions between each of two adjacent side walls of the channel and the channel centre-line. Finally, it was mentioned that for flow conditions characteristic of most generator systems the boundary layer flows tend to be of a turbulent nature over much of the channel length. It was indicated that the flow could only be considered steady in the mean, the effects of turbulent fluctuations on the mean flow properties being described by effective eddy viscosity and eddy thermal conduction coefficients in the x-momentum and energy equations; the eddy viscosity formulation due to Cebeci [11] was used to relate the turbulent transport coefficients to mean flow parameters and their gradients.

In this chapter, the numerical procedure used to solve the boundary layer equations for the two-dimensional flow on each side wall of a MHD channel of rectangular cross-section is formulated. This numerical procedure is based on a finite difference scheme devised by Keller[31] for the solution of parabolic partial differential equations such as the turbulent boundary layer equations (2.156)-(2.159). It is an extension to compressible channel flow of the procedure used by Keller and Cebeci[32] to solve incompressible flow problems. Unlike the method of reference (32), cartesian coordinates with the y-axis normal to the wall and the x-axis parallel to the centre-line are used (the angle of divergence of the channel is assumed small, as is usually the case in MHD channels). Furthermore, instead of applying the outer boundary conditions at the boundary layer edge, as in reference (32), the boundary layer equations are applied to the whole domain from wall to centre-line along which the symmetry conditions expressed by equations (2.175a) and (2.175b) are taken as the outer boundary conditions. The need to introduce a separate system of inviscid equations for the core of the flow to be solved simultaneously with the boundary layer equations by iteration between solutions obtained in the two regions is thus avoided. The core of the flow is thus treated as two-dimensional in the present method. By introducing appropriate additional source terms in the boundary layer equations it should be possible to relax some of the assumptions made in section 2.4; that is, to allow, at least approximately, for finite energy exchange with the electron gas, and finite Lorentz forces, provided steady state conditions prevail. This is done in reference (26) using a different numerical scheme where it is shown that, as a result of the y-component of the Lorentz force, the pressure is a function of y as well as of x and important flow asymmetries can occur.

As stated earlier, this kind of problem is not considered here.

Having formulated the numerical procedure for the solution of the boundary layer equations, applications to a real experimental MHD generator system, the IRD test facility, will be considered, and a computed pressure distribution in the channel will be compared with that obtained experimentally.

3.2 Finite Difference Solution of Equations

The first step in the numerical procedure is to reformulate the problem in terms of a system of first order partial differential equations. The new independent variables u, v and f are introduced which are so defined that equations (2.161) and (2.162) can be written as the first order system

$$\psi' = u \tag{3.1a}$$

$$u' = v \tag{3.1b}$$

$$T' = f \tag{3.1c}$$

$$\left[e_1 (fu + Tv)\right]' = \frac{p}{R_g}\frac{dp}{dx} + pu\frac{\partial}{\partial x}\left(\frac{T}{p}\right) - \frac{\partial \psi}{\partial x}(fu + Tv) \tag{3.1d}$$

$$(e_2 f)' = u\frac{\partial T}{\partial x} - f\frac{\partial \psi}{\partial x} - \frac{R_g T}{p c_p} u\frac{dp}{dx} - \left(\frac{R_g}{p}\right)^2 \frac{e_1}{c_p}(fu + Tv)^2 \tag{3.1e}$$

where the prime denotes differentiation with respect to y, and the coefficients

$$e_1 = \eta + \varepsilon \tag{3.2a}$$

and

$$e_2 = \frac{\varepsilon}{P_{rt}} + \frac{\eta}{P_r} \tag{3.2b}$$

have been introduced in equations (3.1c) and (3.1d).

In terms of the new variables, the boundary conditions, given by equations (2.172) - (2.175), are

$$u(x,0)=0, \tag{3.3a}$$

$$\frac{\partial \psi}{\partial x}(x,0) = -\frac{\rho u_{y\omega}}{R_y \overline{T}_\omega}, \tag{3.3b}$$

$$\overline{T}(x,0)=\overline{T}_\omega, \tag{3.3c}$$

$$f(x,y_c)=0, \tag{3.3d}$$

$$v(x,y_c)=0, \tag{3.3e}$$

where equation (2.137) has been used to eliminate ρ_ω in equation (3.3b), and the wall temperature is assumed given. The wall and channel centre-line are taken to be at y = 0 and at y = y_c respectively.

The region between the wall and the centre-line is replaced with a two-dimensional mesh of points defined by the equations

$$x^n = x^{n-1} + \Delta x^{n-1}, \quad n=2,\ldots,N, \tag{3.4a}$$

$$y_1^n = 0, \tag{3.4b}$$

$$y_j^n = y_{j-1}^n + \Delta y_{j-1}^n, \tag{3.4c}$$

where mesh columns are labelled by the superscript n, and mesh rows are labelled by the subscript j.

The mesh spacings Δx^n and Δy_j^n in equations (3.4) are completely arbitrary and may have large variations. This is important for turbulent boundary layer calculations where steep gradients near a wall necessitate the use of small mesh spacing, whilst relatively large spacing can be used away from the wall. The definition of the mesh openings Δx^n and Δy_j^n is discussed in detail in appendix A.

The variables (ψ, u, T, f, σ) are approximated at points (x^n, y_j^n) of the mesh by mesh functions denoted by $(\psi_j^n, u_j^n, T_j^n, f_j^n, \sigma_j^n)$. The points and variables midway between mesh points are given by the following averages:

$$x^{n-1/2} = \frac{1}{2}(x^n + x^{n-1}), \quad y_{j-1/2}^n = \frac{1}{2}(y_j^n + y_{j-1}^n) \tag{3.5a}$$

$$g_j^{n-1/2} = \frac{1}{2}(g_j^n + g_j^{n-1}), \quad g_{j-1/2}^n = \frac{1}{2}(g_j^n + g_{j-1}^n) \tag{3.5b}$$

The averages given by equations (3.5b) are correct to second order accuracy in the x and y steps. The finite difference equations, which are to approximate equations (3.1), are formulated by considering one mesh cell, such as shown in figure 3.1. Equations (3.1a), (3.1b) and (3.1c) are approximated using centered difference quotients and averages about the midpoint $(x^n, y_{j-1/2}^n)$ of the segment P_1P_2 (see figure 3.1). Similarly, equations (3.1d) and (3.1e) are approximated by centering about the point $(x^{n-1/2}, y_{j-1/2}^{n-1/2})$. Thus, the finite difference approximations to equations (3.1) are:

$$\frac{\psi_j^n - \psi_{j-1}^n}{\Delta y_{j-1}^n} = \frac{1}{2}(u_j^n + u_{j-1}^n), \tag{3.6a}$$

$$\frac{u_j^n - u_{j-1}^n}{\Delta y_{j-1}^n} = \frac{1}{2}(\sigma_j^n + \sigma_{j-1}^n), \tag{3.6b}$$

$$\frac{T_j^n - T_{j-1}^n}{\Delta y_{j-1}^n} = \frac{1}{2}(f_j^n + f_{j-1}^n), \tag{3.6c}$$

$$\frac{1}{2\Delta y^n_{j-1}}\left\{\left[e_1(fu+Tv)\right]^n_j-\left[e_1(fu+Tv)\right]^n_{j-1}\right\}-\frac{1}{2\Delta x^{n-1}}(uT)^n_{j-1/2}\,u^n_{j-1/2}$$
$$+\frac{1}{2\Delta x^{n-1}}\,y^n_{j-1/2}\,(fu+Tv)^n_{j-1/2}=\frac{1}{2\Delta x^{n-1}}\left(\frac{p^{n-1}}{p^n}\right)(uT)^n_{j-1/2}\,u^{n-1}_{j-1/2}$$
$$-\frac{1}{2\Delta x^{n-1}}\left(\frac{p^n}{p^{n-1}}\right)u^n_{j-1/2}\,(uT)^{n-1}_{j-1/2}+\frac{1}{2\Delta x^{n-1}}\,y^{n-1}_{j-1/2}\,(fu+Tv)^n_{j-1/2}$$
$$-\frac{1}{2\Delta x^{n-1}}\,y^n_{j-1/2}\,(fu+Tv)^{n-1}_{j-1/2}+M^{n-1}_{j-1/2}, \qquad (3.6d)$$

where

$$M^{n-1}_{j-1/2}=\frac{1}{R_g}\,p^{n-1/2}\,\frac{(p^n-p^{n-1})}{\Delta x^{n-1}}-\frac{1}{2\Delta y^{n-1}_{j-1}}\left\{\left[e_1(fu+Tv)\right]^{n-1}_j-\left[e_1(fu+Tv)\right]^{n-1}_{j-1}\right\}$$
$$-\frac{1}{2\Delta x^{n-1}}(uT)^{n-1}_{j-1/2}\,u^{n-1}_{j-1/2}+\frac{1}{2\Delta x^{n-1}}\,y^{n-1}_{j-1/2}\,(fu+Tv)^{n-1}_{j-1/2},$$

and

$$\frac{1}{2\Delta y^n_{j-1}}\left\{(e_2f)^n_j-(e_2f)^n_{j-1}\right\}-\frac{1}{2\Delta x^{n-1}}\,u^n_{j-1/2}\,T^n_{j-1/2}+\frac{1}{2\Delta x^{n-1}}\,f^n_{j-1/2}\,y^n_{j-1/2}$$
$$+\frac{R_g}{2c_p\Delta x^{n-1}p^{n-1/2}}\,(p^n-p^{n-1})\,T^n_{j-1/2}\,u^n_{j-1/2}+\frac{R_g^2}{2c_p}\left(\frac{1}{p^{n-1/2}}\right)\left\{e_1(fu+Tv)^2\right\}^n_{j-1/2}$$
$$=\frac{1}{2\Delta x^{n-1}}\left(u^{n-1}_{j-1/2}\,T^n_{j-1/2}-u^n_{j-1/2}\,T^{n-1}_{j-1/2}\right)-\frac{1}{2\Delta x^{n-1}}\left(y^n_{j-\frac{1}{2}}\,f^{n-1}_{j-\frac{1}{2}}-y^{n-1}_{j-\frac{1}{2}}\,f^n_{j-\frac{1}{2}}\right)$$
$$+H^{n-1}_{j-1/2},$$

(3.6e)

where

$$H_{j-\frac{1}{2}}^{n-1} = \frac{1}{2\Delta x^{n-1}}\left(f_{j-\frac{1}{2}}^{n-1}\psi_{j-\frac{1}{2}}^{n-1} - T_{j-\frac{1}{2}}^{n-1}u_{j-\frac{1}{2}}^{n-1}\right) - \frac{1}{2\Delta y_{j-1}^{n-1}}\left\{(e_2 f)_j^{n-1} - (e_2 f)_{j-1}^{n-1}\right\}$$

$$- \frac{1}{2\Delta x^{n-1}}\frac{R_g}{c_p p^{n-\frac{1}{2}}}\left(p^n - p^{n-1}\right)T_{j-\frac{1}{2}}^{n-1}u_{j-\frac{1}{2}}^{n-1} - \frac{R_1^2}{2c_p}\frac{e_{1\,j-\frac{1}{2}}^{n-1}}{\left(p^{n-\frac{1}{2}}\right)^2}\left(fu + Tv\right)_{j-\frac{1}{2}}^{n-1}$$

Equations (3.6) are imposed for j = 2,3..., J. Consistent with the condition that the angle of divergence of the wall be small, we take $y_j^{n-1} = y_j^n$ and $\Delta y_j^{n-1} = \Delta y_j^n$ in equations (3.6).

The finite difference approximations to the boundary conditions, equations (3.3) are:

$$u_1^n = 0\,, \tag{3.7a}$$

$$\frac{1}{\Delta x^{n-1}}\left(\psi_1^n - \psi_1^{n-1}\right) = -\frac{1}{2R_g}\left\{\frac{(\rho u_y \omega)^n}{T_1^n} + \frac{(\rho u_y \omega)^{n-1}}{T_1^{n-1}}\right\}, \tag{3.7b}$$

$$T_1^n = T_\omega\,, \tag{3.7c}$$

$$f_J^n = 0\,, \tag{3.7d}$$

$$v_J^n = 0\,. \tag{3.7e}$$

Assuming $\left(\psi_j^{n-1}, u_j^{n-1}, T_j^{n-1}, f_j^{n-1}, v_j^{n-1}\right)$ for $1 \leq j \leq J$, and the pressure p^n to be known, equations (3.6) and (3.7) constitute a system of 5J non-linear equations for the 5J unknowns $\left(\psi_j^n, u_j^n, T_j^n, f_j^n, v_j^n\right)$, j = 1, 2, ..., J. This non-linear system is solved by means of Newton's method. The iterates $\left(\psi_j^{(i)}, u_j^{(i)}, T_j^{(i)}, f_j^{(i)}, v_j^{(i)}\right)$ are introduced, with the initial values

$$\rho_1^{(0)} = \rho_1^n = \rho_1^{n-1} - \frac{\Delta x^{n-1}}{2R_g}\left\{\frac{(\rho v_{y\omega})^n}{T_1^n} + \frac{(\rho v_{y\omega})^{n-1}}{T_1^{n-1}}\right\}.$$

$$u_1^{(0)} = 0,\quad T_1^{(0)} = T_1^n = T_\omega,\quad f_1^{(0)} = f_1^{n-1},\quad v_1^{(0)} = v_1^{n-1};$$

$$\rho_j^{(0)} = \rho_j^{n-1},\quad u_j^{(0)} = u_j^{n-1},\quad T_j^{(0)} = T_j^{n-1},\quad f_j^{(0)} = f_j^{n-1},\quad v_j^{(0)} = v_j^{n-1},\quad 2 \le j \le J-1;$$

$$\rho_J^{(0)} = \rho_J^{n-1},\quad u_J^{(0)} = u_J^{n-1},\quad T_J^{(0)} = T_J^{n-1},\quad f_J^{(0)} = 0,\quad v_J^{(0)} = 0 \tag{3.8}$$

For convenience, the new variables $(\delta\rho_j^{(i)}, \delta u_j^{(i)}, \delta T_j^{(i)}, \delta f_j^{(i)}, \delta v_j^{(i)})$ are defined by

$$\rho_j^{(i+1)} = \rho_j^{(i)} + \delta\rho_j^{(i)},\quad u_j^{(i+1)} = u_j^{(i)} + \delta u_j^{(i)},\quad T_j^{(i+1)} = T_j^{(i)} + \delta T_j^{(i)}$$

$$f_j^{(i+1)} = f_j^{(i)} + \delta f_j^{(i)},\quad v_j^{(i+1)} = v_j^{(i)} + \delta v_j^{(i)},\qquad 1 \le j \le J \tag{3.9}$$

These expressions are inserted into equations (3.6) in place of $(\rho_j^n, u_j^n, T_j^n, f_j^n, v_j^n)$ and only those terms linear in $(\delta\rho_j^{(i)}, \delta u_j^{(i)}, \delta T_j^{(i)}, \delta f_j^{(i)}, \delta v_j^{(i)})$ are retained. This procedure yields the following linear system:

$$\delta\rho_j - \delta\rho_{j-1} - \frac{\Delta y_{j-1}^n}{2}(\delta u_j + \delta u_{j-1}) = r_{3,j} \tag{3.10a}$$

$$\delta u_j - \delta u_{j-1} - \frac{\Delta y_{j-1}^n}{2}(\delta v_j + \delta v_{j-1}) = r_{4,j} \tag{3.10b}$$

$$\delta T_j - \delta T_{j-1} - \frac{\Delta y_{j-1}^n}{2}(\delta f_j + \delta f_{j-1}) = r_{5,j} \tag{3.10c}$$

$$\begin{aligned} &g_{1,j}\delta\rho_j + g_{2,j}\delta\rho_{j-1} + g_{3,j}\delta u_j + g_{4,j}\delta u_{j-1} + g_{5,j}\delta v_j \\ &+ g_{6,j}\delta v_{j-1} + g_{7,j}\delta T_j + g_{8,j}\delta T_{j-1} + g_{9,j}\delta f_j + g_{10,j}\delta f_{j-1} = r_{1,j} \end{aligned} \tag{3.10d}$$

$$\begin{aligned} &s_{1,j}\delta\rho_j + s_{2,j}\delta\rho_{j-1} + s_{3,j}\delta u_j + s_{4,j}\delta u_{j-1} + s_{5,j}\delta v_j \\ &s_{6,j}\delta v_{j-1} + s_{7,j}\delta T_j + s_{8,j}\delta T_{j-1} + s_{9,j}\delta f_j + s_{10,j}\delta f_{j-1} = r_{2,j} \end{aligned} \tag{3.10e}$$

for j = 2, 3, ..., J. For simplicity of notation, the superscripts i

have been dropped. The coefficients $r_{k,j}$ (k = 1, ...,5), $g_{k,j}$ (k = 1,...,10) and $S_{k,j}$ (k = 1, ...,10) are listed in appendix B.

The boundary conditions, equations (3.7), can be satisfied exactly with no iterations. The initial values $(\psi_1^{(0)}, u_1^{(0)}, T_1^{(0)}, f_J^{(0)}, v_J^{(0)})$ are set equal to the boundary values, as in equations (3.8), and to maintain these values in all iterations we take

$$\delta\psi_1^{(i)}=0,\ \delta u_1^{(i)}=0,\ \delta T_1^{(i)}=0,\ \delta v_J^{(i)}=0,\ \delta f_J^{(i)}=0 \quad . \tag{3.11}$$

The linear system , equations (3.10) and (3.11), has a block tri-diagonal structure and can be solved in an extremely efficient manner using a block elimination method. A detailed description of one such method can be found in reference (32).

Having solved the linear system, equations(3.10) and (3.11), the higher order iterates $(\psi_j^{(i+1)}, u_j^{(i+1)}, T_j^{(i+1)}, f_j^{(i+1)}, v_j^{(i+1)})$ are formed as in equations (3.9). The iterations are repeated until the following convergence condition is satisfied:

$$\left| \frac{\delta v_1^{(i)}}{\frac{1}{2}\left[v_1^{(i-1)} + v_1^{(i)}\right]} \right| < \varepsilon_I \tag{3.12}$$

where ε_I is a prescribed value, say 0.01.

3.3 Initial Conditions

The initial distributions $(\psi_j', u_j', T_j', f_j', v_j')$ for $1 \leq j \leq J$ at a given initial station $(x = x')$ must be specified to initiate the numerical solution. In fact, only u_j' and T_j' for $1 \leq j \leq J$ need be specified. Then ψ_j', f_j' and v_j' can be calculated by integration and differentiation from equations (3.1a) – (3.1c). All numerical results reported in this thesis were obtained by assuming that the flow was initially laminar $(\varepsilon = 0)$, transition to turbulent flow occurring at an x-station downstream of the initial x-station (see section 3.5).

Initial profiles which are approximations to the laminar boundary layer equations are therefore of interest here. A convenient rough approximation is obtained by representing the initial velocity profile in a boundary layer by a polynomial of the 4th degree[21]; that is,

$$\frac{u_x}{u_{xe}} = a\left(\frac{y}{\delta}\right) + b\left(\frac{y}{\delta}\right)^2 + c\left(\frac{y}{\delta}\right)^3 + d\left(\frac{y}{\delta}\right)^4 \tag{3.13}$$

where

$$a = 2 + \Lambda/6,\ b = -\Lambda/2,\ c = -2 + \Lambda/2,\ d = 1 - \Lambda/6 \tag{3.14}$$

and the subscript e denotes a boundary layer edge value. The so-called shape parameter Λ in equation (3.13) is given by

$$\Lambda = -\frac{\delta^2}{\mu_w u_{xe}}\frac{dp}{dx} \tag{3.15}$$

Since the pressure gradient at the initial station is not known a priori a value of Λ must be chosen such that the corresponding value of the pressure gradient is approximately equal to the computed value $(p^2 - p^1)/\Delta x^1$.

The velocity outside the boundary layer is assumed to be constant; that is,

$$u_x = u_{xe} = u_{xc},\ \delta \leq y \leq y_c \tag{3.16}$$

The temperature profile is formed by assuming a Crocco relationship[21] between the velocity and temperature profiles; that is:

$$T = T_w - \left(\frac{u_x}{u_{xe}}\right)\left(T_w - T_e - \frac{u_{xe}^2}{2C_p}\right) - \frac{u_{xe}^2}{2C_p} \tag{3.17}$$

for $0 \leq y \leq y_c$.

3.4 Calculation of Pressure Distribution

The pressure distribution in an MHD channel is determined from the requirement that mass be conserved; that is, the pressure distribution must be such that equation (2.176) is satisfied at every x-station, where the mass flow rate $\dot{m}$ is obtained by integration of equation (2.177), given the initial value of the mass flow rate. However, since the mass transfer rates $(\rho_A u_{yA})_\omega$ and $(\rho_B u_{yB})_\omega$ in equation (2.177) can be functions of the pressure, it is necessary, in general, to treat both the pressure and the mass flow rate as unknown functions of x governed by equations (2.176) and (2.177), respectively, both of which are to be solved simultaneously with the solution of the boundary layer equations. The numerical procedure used to calculate both the pressure and the mass flow rate distributions is described below.

The finite difference form of equation (2.177) at $x = x^{n-1/2}$ can be written as

$$\frac{\dot{m}^n - \dot{m}^{n-1}}{\Delta x^{n-1}} = \left[2H(\rho_A u_{yA})_\omega + 2W(\rho_B u_{yB})_\omega\right]^{n-1/2}$$

$$= \left[H(\rho_A u_{yA})_\omega + W(\rho_B u_{yB})_\omega\right]^n + \left[H(\rho_A u_{yA})_\omega + W(\rho_B u_{yB})_\omega\right]^{n-1},$$

which yields

$$\dot{m}^n = \dot{m}^{n-1} + \Delta x^{n-1}\left\{\left[H(\rho_A u_{yA})_\omega + W(\rho_B u_{yB})_\omega\right]^n + \left[H(\rho_A u_{yA})_\omega + W(\rho_B u_{yB})_\omega\right]^{n-1}\right\}, \quad (3.18)$$

from which the mass flow rate at every $x > x'$ could be found if the initial mass flow rate and the mass transfer rates $(\rho_A u_{yA})_\omega$ and $(\rho_B u_{yB})_\omega$ were given.

The value of the pressure at any x-station must be such that the mass flow rate given by equation (2.176), which is calculated using the solutions of the finite difference equations for the boundary layers, equals the mass flow rate obtained from equation (3.18). An iteration procedure devised by Doss et al.[26] for the case of a constant mass flow rate is used here to calculate the pressure.

The pressure at any x-station is first estimated by linear extrapolation of the values of the pressure at the two previous x-stations, and the finite difference equations are solved. The mass flow rate corresponding to the obtained solution is obtained from equation (2.176) and compared with the value obtained from equation (3.18). If the two mass flow rates so obtained happen to be sufficiently close, no adjustment of the estimated value of the pressure is needed. However, if the difference between the mass flow rates is large, the estimated value of the pressure is adjusted in proportion to the ratio of the two different mass flow rates, and the computation proceeds once more for a new iteration cycle. The iteration algorithm is of the form

$$p^{(i)} = p^{(i-1)} \left[\frac{\dot{M}\{p^{(i-1)}\}}{\dot{m}\{p^{(i-1)}\}} \right] \tag{3.19}$$

where $\dot{M}\{p^{(i-1)}\}$ is the mass flow rate calculated from equation (2.176), and $\dot{m}\{p^{(i-1)}\}$ is the mass flow rate calculated from equation (3.18).

Numerical experiments have shown that the rate of convergence of the above procedure is often considerably increased by replacing $p^{(i)}$ with the value $p^{(i)\prime}$ given by

$$p^{(i)\prime} = \frac{p^{(i)} + (2r-1)\, p^{(i-1)}}{2r} \tag{3.20}$$

where r = 1,2,3,... The value of r to be used in equation (3.20) has been found to depend on the flow conditions and the values of the mesh parameters. For any particular case there is an optimum value, or range of values, of r for which the convergence rate is a maximum. By applying the adjustment of $p^{(i)}$ defined by equation (3.20), it has been found possible to increase the convergence rate to such an extent that only one or two iterations are sufficient to obtain convergence to 0.01% at all x-stations, with the exception of those where transition from laminar to turbulent flow occurs and wall mass transfer is suddenly switched on or off. In some cases convergence can only be obtained if equation (3.20) is used, the use of the algorithm (3.19) alone giving iterates which oscillate about the correct value with increasing amplitude.

3.5 Application to IRD Experimental MHD Facility

The numerical method for computing the development of the gas-dynamic flow along MHD generator channels, described in the preceding sections, has been applied to the MHD closed cycle facility of the International Research and Development Co. Ltd. (IRD), Newcastle upon Tyne. By using flow conditions of actual experiments recently performed on the facility (October 1977), comparisons could be made between computed and experimental results.

Detailed description of the IRD closed loop facility is given elsewhere[3]; only details relevant to the computation of gas-dynamic flow in the MHD channel section are given here. In the facility, helium gas is circulated steadily around a closed loop at a mass flow rate of about 5 to 7 gm/sec, and heated in a three stage heater to about 1700^{o}K. The helium gas is slightly seeded with caesium vapour, accelerated through a nozzle to a velocity of about 900 to 1500 m/s, and allowed to interact with a magnetic field in a slightly diverging

channel of rectangular cross-section, which contains 15 tantalum electrode pairs at a constant pitch of 25.4 mm (1 inch). The channel has a length of 56.4 cms, an internal area of 195 mm^2 at the nozzle throat, and an aspect ratio of about 2:1; that is, the internal height is about twice the internal width. Each electrode has a circular cross-section of diameter 0.95 cm (3/8 ins) and is mounted flush with the inside wall on a tantalum stem whose point of fixture is some distance from the inside wall. Cavities thus exist behind all electrodes preventing direct contact of the electrode surfaces with the channel walls, there being small annular gaps of width 1.59mm (1/16 ins) between the electrode faces and the channel walls. A pair of electrodes of diameter 18 mm are mounted so as to enable a preionizing current to be passed parallel to the magnetic field; the upstream edge of each of these electrodes is at a distance of 57.6 mm from the nozzle throat, while the upstream edges of the electrodes of the first electrode pair are at a distance of 96.8 mm from the nozzle throat. Stagnation pressure in the nozzle inlet is determined from Pitot tube readings and static pressure readings, whilst the static pressure profile in the channel is measured at four tappings at electrode pair numbers 2, 5, 8 and 11. The static temperature is measured in the nozzle inlet and at electrode pair numbers 2, 5, 8, 11 and 14.

As mentioned earlier, the numerical method described in the preceding sections has been applied to the IRD facility for conditions of experiments performed on the facility in October 1977. Apart from a few exceptions the mass flow rates of these experimental runs of the facility were 5.37 gm/sec and 7.08 gm/sec. For the development of the numerical method, the experimental conditions of a representative run at the mass flow rate of 5.37 gm/sec were used. Run number 7 was selected as the representative run because the conditions of this run

appeared to be closest to the average flow conditions for runs at the common mass flow rate of 5.37 gm/sec. The numerical results presented are discussed below and for conditions of run number 7 unless otherwise stated; the conditions of this run are given in figure 3.2.

The gas-dynamic flow in the channel for conditions of run number 7 is determined by computing the two-dimensional boundary layer profiles on each wall simultaneously using the method of the preceding sections. In order that errors due to using approximate gas-dynamic profiles to initiate calculations of a confined flow be as small as possible, the initial station should be taken as close to the nozzle throat as possible without the number of cross-stream mesh points for each wall being too large. Results of numerical experiments show that a suitable initial distance from the nozzle throat in the present case is 0.0254 m.

The centre-line stagnation pressure and centre-line stagnation temperature at the initial station, which, for a given static pressure, define the initial centre-line values of the streamwise velocity component and static temperature, are taken to be the nozzle inlet values. The stagnation temperature is found from the formula

$$T_o = T(p_o/p)^{2/5},$$

which follows from the heavy particle energy and overall momentum equations in which viscous effects, thermal conduction and the cross-stream velocity component are neglected.

The wall temperatures at all points are determined by linearly interpolating and extrapolating the values measured at the locations of electrode pair numbers 2, 5, 8, 11 and 14. Insulator and electrode side walls are assumed to be at the same temperature at each x-station.

It can be seen from figure 3.3 that agreement between the computed and experimental pressure distributions is good at all points except the last, where the measured value is about 1% larger than the computed value. Of course agreement between theory and experiment is necessarily good for electrode pairs 2 and 5, because of the way in which the initial boundary layer thickness and mass transfer factor are chosen. It is thought that the slight discrepancy between theory and experiment at the last point in figure 3.3 is due to attempting to describe the flow with a quasi-three-dimensional model in a region of the channel where boundary layers are thick and three-dimensional effects, i.e., corner effects, are important. This is to some extent confirmed by the plots of figure 3.5, from which it can be seen that, whilst the electrode wall boundary layer continues to grow in thickness, the insulator side wall boundary layer thickness tends towards a constant value as the boundary layer edge approaches the channel centre-line.

Figures 3.3, 3.4 and 3.6 clearly show the effects of transition from laminar to turbulent flow. Due to the slight divergence of the channel walls and the subsonic character of the flow, the initially negative pressure gradient reverses sign at a point upstream of the large preionizer electrodes. The resultant adverse positive pressure gradient has a destabilizing effect on the flow[26] and allows one to assume that the initially laminar flow becomes turbulent at the upstream edges of the preionizer electrodes. At the transition station, the sudden decrease in the displacing effect of the boundary layers on the core flow causes a sudden increase of centre-line temperature and a decrease of centre-line velocity (see figures 3.4 and 3.6). However, a short distance downstream of the transition station, where the

turbulent flow is more fully established, the rate of growth of boundary layer thickness increases (see figure 3.5), causing a decrease of pressure and temperature gradient, and an increase of velocity gradient.

Although transition to turbulent flow causes a decrease of pressure gradient downstream of the transition station, the pressure gradient remains positive and the pressure would continue to increase steadily after the first electrode pair in the absence of wall mass transfer (see figure 3.3). However, the increase in mass flow rate due to wall mass transfer causes the flow to accelerate, the pressure and temperature gradients decreasing and the velocity gradient increasing (see figures 3.3, 3.4 and 3.6).

The calculated temperature and velocity boundary layer profiles on the electrode wall at the location of the center of one of the electrodes of electrode pair 2 are shown in figure 3.7. It can be seen that both the profiles exhibit small oscillations near the boundary layer edge, which are manifestations of numerical error. A method of removing these oscillations has not been found, but the amplitudes are so small that they may be safely neglected.

Attempts to compute the channel flow for conditions of an experimental run at the higher mass flow rate of 7.08 gm/sec have failed, because of the necessity of having to initiate the computation with a much smaller boundary layer thickness than for runs at a mass flow rate of 5.37 gm/sec. This means that, unless an unacceptably large number of mesh points in the cross-stream direction is employed, the mesh at large distances from a wall is too coarse to resolve the boundary layer profiles downstream of the initial station.

The initial laminar profiles of section 3.5 are used to initiate computations, the boundary layer thickness being treated as a parameter, so chosen as to obtain a pressure distribution in as close an agreement with experiment as possible. The initial pressure is determined iteratively using the method of section 3.4; that is, the iteration algorithm (3.19) is used with $\dot{m}$ equal to the prescribed mass flow rate of 5.37 gm/sec.

In order to obtain a pressure distribution in close agreement with experiment, it is necessary to allow for a slight transfer of gas through the electrode walls. It is thought that this transfer of gas occurred from a helium blanket between the channel and outer casing which was maintained at a pressure greater than that in the channel, and that gas could enter the channel through the annular spaces between the electrode surfaces and the channel walls. Further experimental evidence that transfer of gas occurred into the channel was the necessity to supply gas continuously to the helium blanket to keep the pressure at a fixed level. The analytical description of this mass transfer process is formulated below.

Denoting the measured pressure in the helium blanket by p_o, Bernoulli's equation gives for the y-component of velocity in the region between an electrode surface and the wall,

$$v_{yw} = \left[2(p_o - p)/\rho_w\right]^{1/2} \tag{3.21}$$

It is found that equation (3.21) gives an overestimate of the mass transfer flux $\rho_w v_{yw}$ through the wall and must be reduced by a factor f_o whose value is so chosen as to obtain results in as close an agreement with experiment as possible. Equation (2.176), and therefore equation (3.18), cannot be used to calculate the mass flow

rate at each x-station because the mass transfer flux is not uniform in a region of electrode wall defined by a step in the x-direction. Denoted by dA the element of area in this region through which gas flows, equation (2.177) must be replaced with

$$\frac{d\dot{m}}{dx} = 2\frac{dA}{dx}\rho_w u_{yw}, \tag{3.22}$$

where it is assumed that no mass transfer occurs through the insulator side wall. The derivative dA/dx depends on the annular geometry of the region between an electrode surface and channel wall; and it is non-zero only in this region. In the entrance region of the channel, before the first electrode pair, the mass flow rate is constant. In place of equation (3.18) for the mass flow rate at the x-location $x=x^n$ we have the finite difference form of equation (3.22):

$$\dot{m}^n = \dot{m}^{n-1} + \Delta x^{n-1}\left\{\left(\frac{dA}{dx}\right)^n \rho_w^n u_{yw}^n + \left(\frac{dA}{dx}\right)^{n-1} \rho_w^{n-1} u_{yw}^{n-1}\right\} \tag{3.23}$$

It should be noted that the variation of the local value of $\rho_w u_{yw}$ in the z-direction at each x-station necessarily requires a three-dimensional treatment of the flow if a detailed description of the effects of the mass transfer is to be obtained. This is avoided here by use of a two-dimensional treatment with the mass transfer flux at each x-station given by an average value $\langle \rho_w u_{yw} \rangle$, where

$$\langle \rho_w u_{yw} \rangle = \frac{1}{w}\frac{dA}{dx}\rho_w u_{yw} \tag{3.24}$$

the mass transfer flux on the right hand side being given by equation (3.21), multiplied by the factor f_c. Equation (3.24) is used in the boundary condition given by equation (2.173) or (3.3b).

The initial boundary layer thickness and the mass transfer factor f_c are chosen so that the best possible agreement between the computed and experimental pressure distributions is obtained. It is found that the best way of choosing these quantities is such that the computed values of pressure at the locations of the first two measurement stations (electrode pair numbers 2 and 5) are almost equal to the measured values. For the conditions of run number 7, these quantities are found to have the values

$$\delta = 1.97 mm \quad , \quad f_c = 1.47 \times 10^{-2}.$$

The flow in the channel is assumed to be initially laminar, with $\varepsilon = 0$ in equations (3.1d) and (3.1e), up to a certain x-station where transition to turbulent flow is allowed. The point of transition is taken to be at the upstream edge of the preionizer electrode pair mentioned above, where the flow is expected to become turbulent due to the destabilizing effects of a positive pressure gradient and finite projection of the electrodes into the flow (see reference (21)).

For a given wall, the non-uniform mesh in the cross-stream y-direction is determined, for a given number of steps, at the initial station by choosing the product $\alpha' y_c'$ in the equation for $\Delta y_1'$ (see appendix A) to be such that

$$\Delta y_1' < f_2 \delta \tag{3.25}$$

where f_2 is a specified fraction of the initial boundary layer thickness. In practice, the quantity α' is taken to be an integer which is increased until the condition (3.25) is satisfied. The choice of the factor f_2 is governed by the requirement that Δy_1 be, at every station downstream of the transition station, small compared with the thickness of the laminar sublayer (see section (2.4)) in which there are steep velocity and temperature gradients. At the same time the number of

mesh points in the y-direction must be large enough for the accurate description of the growth of a boundary layer, from its initially small thickness to a thickness of half the channel height. This requires that there be a large enough number of points outside the boundary layer region at the initial station. The numerical results presented here are obtained with a mesh of J=41 points in the y-direction. The value of the factor f_2 is taken to be 0.0025, which gives, for an electrode wall, $\alpha' = 322 m^{-1}$ and $\alpha' y_c' = 6.629$ where $y_c = 1.029 \times 10^{-2} m$ at the initial station. Using the latter value of $\alpha' y_c'$, the distribution of mesh points in the y-direction can be obtained at each x-station using the formula (see appendix A)

$$y_j^n = y_c^n \left[1 - \frac{\tanh \alpha^n y_c^n \left(\frac{J-j}{J-1} \right)}{\tanh \alpha^n y_c^n} \right], \qquad (3.26)$$

At $x = x'$ the mesh step $\Delta y_j'$ increases from $\Delta y_1' = 4.9 \times 10^{-6} m$ at the wall to $\Delta y_{J-1}' = 1.41 \times 10^{-3} m$ at the centre-line.

The step size in the x-direction is chosen to be a certain fraction f_1 of the local boundary layer thickness (see appendix A); that is,

$$\Delta x^n = f_1 \delta^n \qquad (3.27)$$

The value of f_1 is taken to be constant and equal to 0.1 at all x-stations except near the transition station and the edges of the intervals of x where mass transfer through the walls occurs, where, to resolve accurately the effects of sudden changes in the flow behaviour, smaller values of f_1 must be used. In practice, a check is made at

each x-station to determine whether the transition station or an edge of a mass transfer region has been passed. If it has, the calculation is taken from the station before using a smaller value of f_1 until the transition or edge of mass transfer region is passed; f_1 is then increased to its larger value. From numerical experiments it is found that a suitable factor for reducing f_1 in the present case is $1/4$ for both the transition station and an edge of a mass transfer region. The numerical results obtained for the conditions of run number 7 are now discussed.

The computed pressure distribution is shown in figure 3.3, in which experimentally measured values are shown for comparison; for convenience, pressure and distance are measured in psia and inches respectively. The computed distributions of centre-line temperature, electrode and insulator side wall boundary layer thicknesses and centre-line velocity are shown in figures 3.4, 3.5 and 3.6. The electrode wall temperature and velocity boundary layer profiles near the centre of electrode pair 2 are shown in figure 3.7; these are used as data for the numerical solution of the plasma and current equations (see chapter 5). It should be noted that the discontinuous decrease in boundary layer thickness from the assumed initial value after a single step in the x-direction is due to the method used to determine the boundary layer thickness. The initial boundary layer thickness is prescribed and the velocity and temperature are assumed constant between the boundary layer edge and the centre-line, but at all x-stations downstream of the initial station, the boundary layer thickness is taken to be the distance from the wall in question of the point at which the velocity is 0.99 of the centre-line value.

(1)

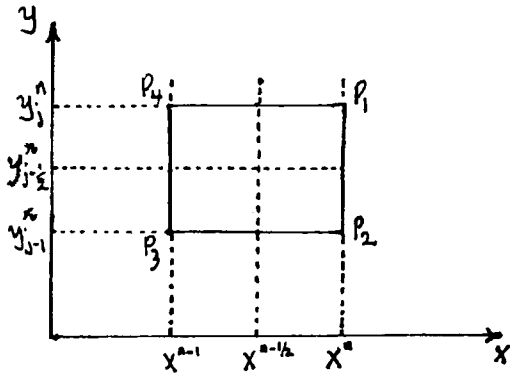

(2)

Gas-dynamic Conditions of Run 7	
Mass flow rate	= 5.37 gm/sec
Centre-line stagnation pressure in nozzle inlet	= 15.0 psia
Centre-line stagnation temperature in nozzle throat	= 1687^{o}K
Pressure in helium blanket	= 14.95 psia

Static Pressure and Wall Temperature in Channel

Electrode Pair Number	Pressure (psia)	Wall Temperature (^{o}K)
2	12.07	1295
5	12.04	1358
8	11.92	1391
11	11.87	1365
14		1362

(1) Fig. 3.1: Cell of two-dimensional mesh used for finite differencing of boundary layer equations

(2) Fig. 3.2: Table of gas-dynamic conditions of Run 7 of the October 1977 sequence of runs of the IRD facility

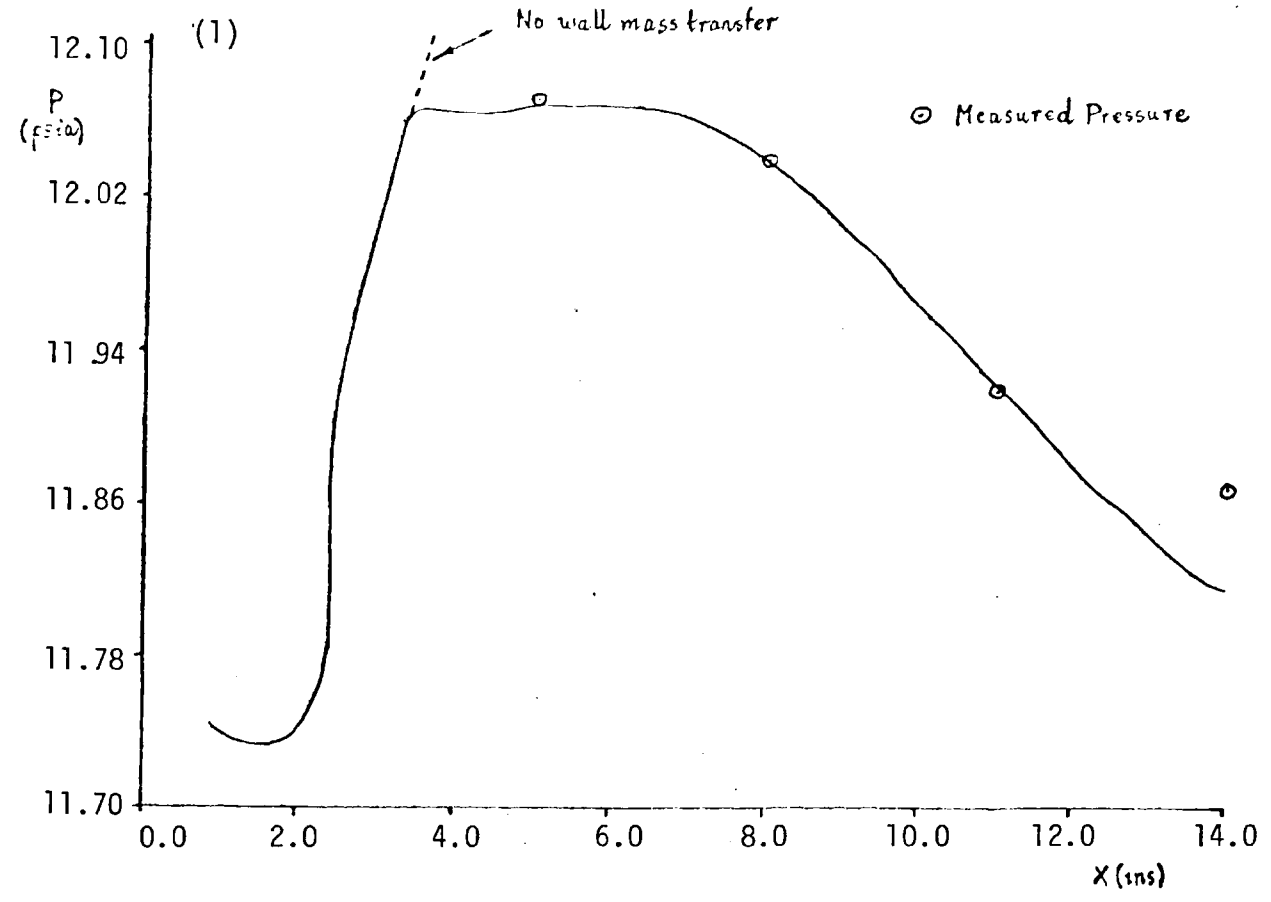

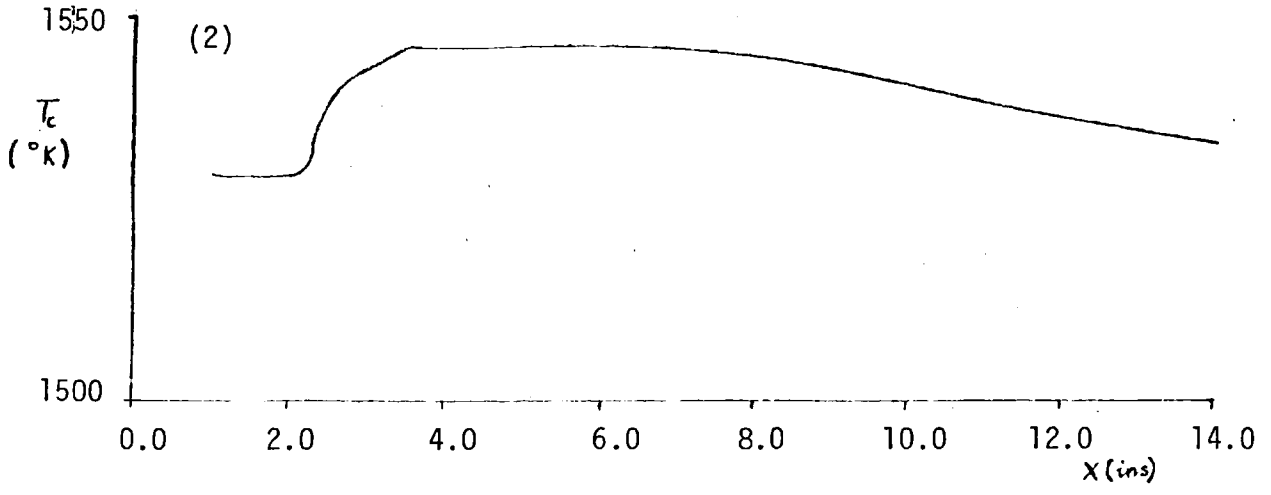

(1) Fig. 3.3: Computed pressure against distance from nozzle throat. Experimental values are shown for comparison.

(2) Fig. 3.4: Computed centreline temperature against distance from nozzle throat.

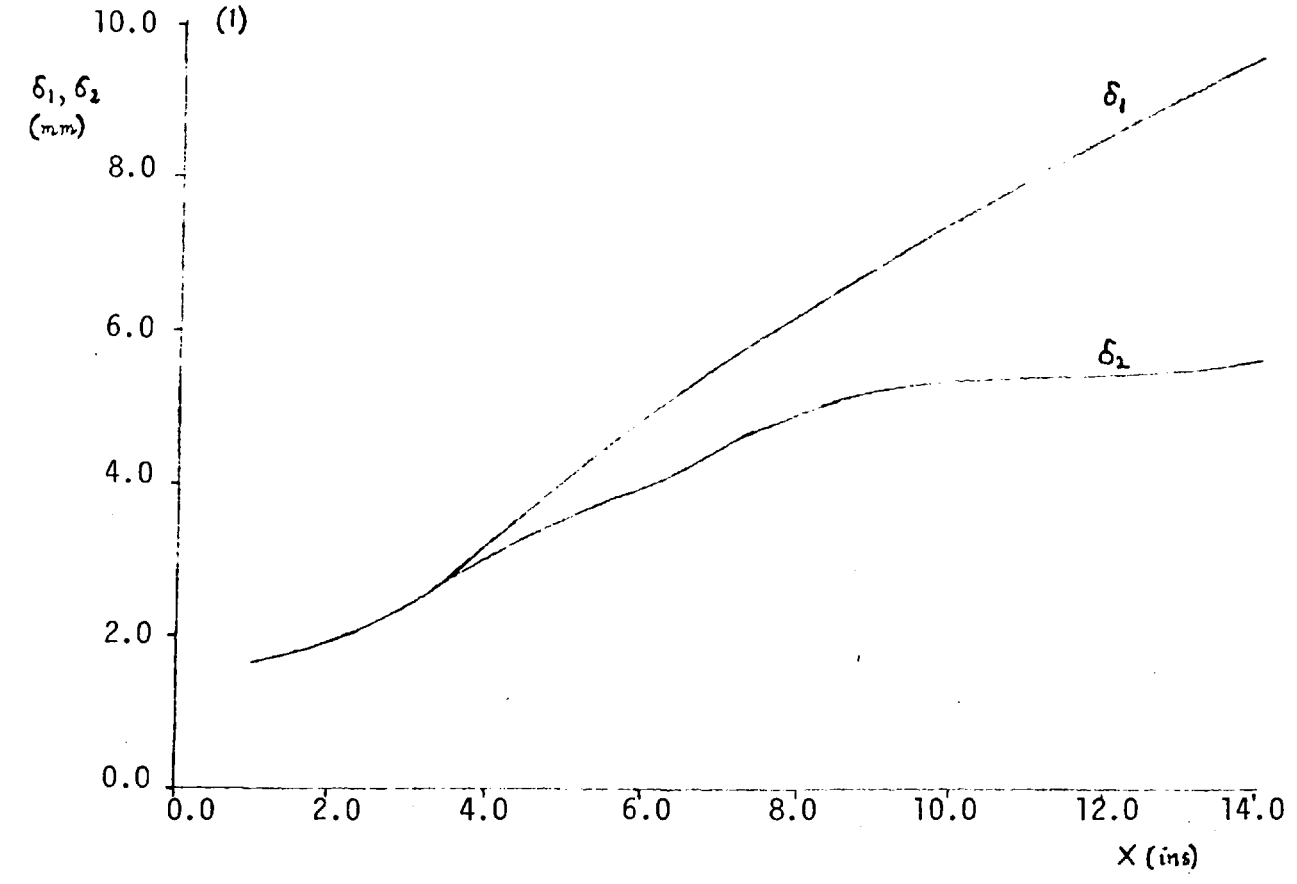

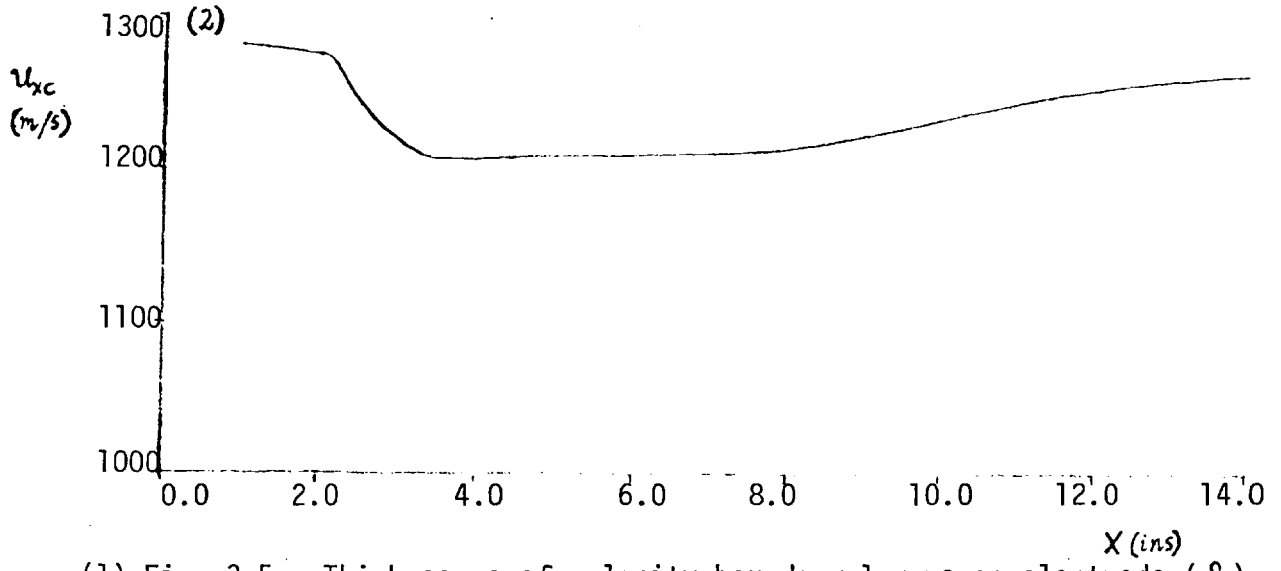

(1) Fig. 3.5: Thicknesses of velocity boundary layers on electrode (δ_1) and insulator (δ_2) side walls against distance from nozzle throat.

(2) Fig. 3.6: Computed centerline gas velocity against distance from nozzle throat.

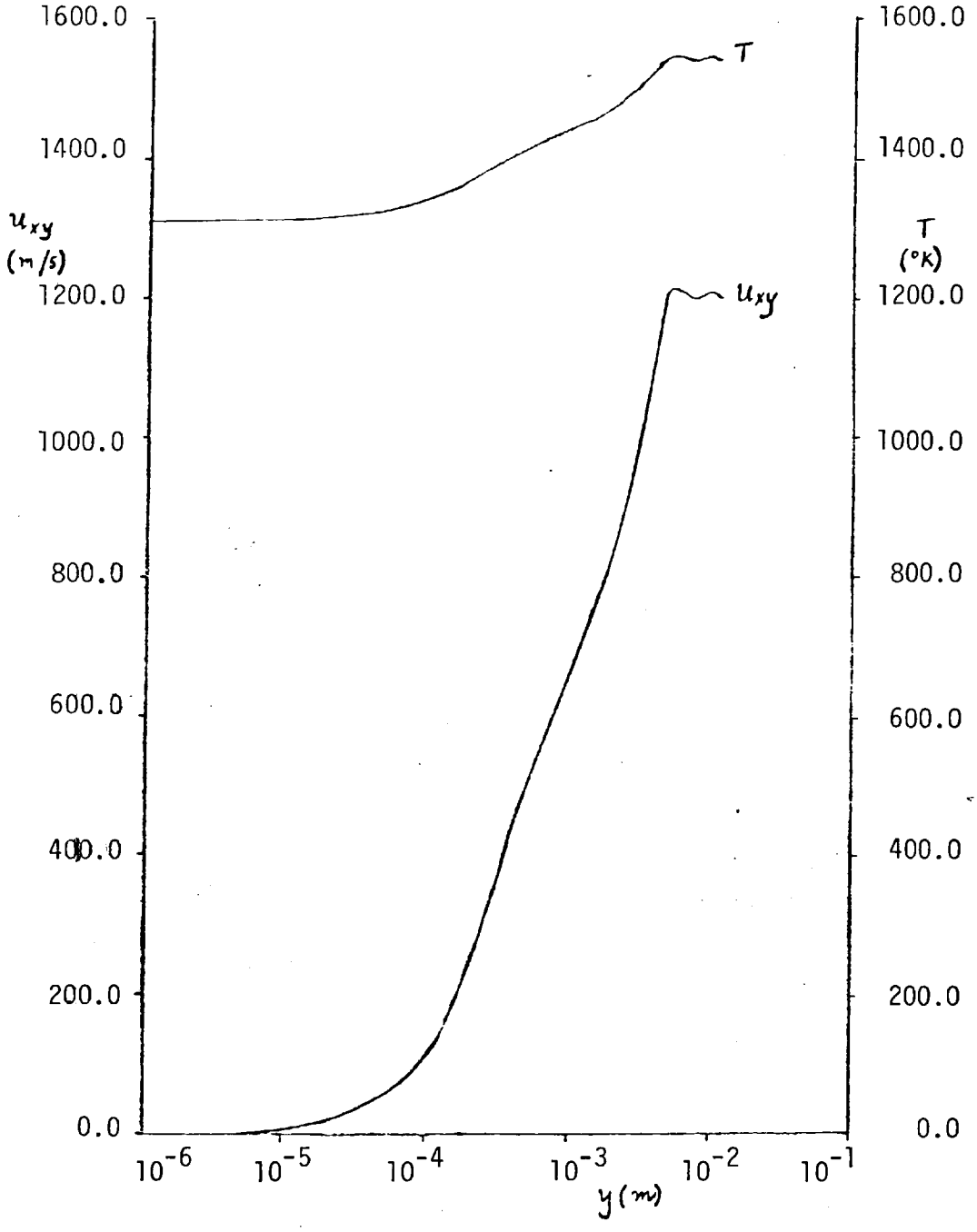

Fig. 3.7: Computed gas temperature and x-component of velocity electrode wall boundary layer profiles at the x-station nearest the centreline of electrode pair 2.

CHAPTER 4

NUMERICAL SOLUTION OF THE PLASMA AND ELECTRICAL FIELD EQUATIONS

4.1 Introduction

The equations governing the plasma and electrical fields, namely, the seed atom density, the electron density, the electron temperature, and the current stream function, and the appropriate boundary conditions for the case of a flowing partially ionized plasma in a linear segmented electrode MHD generator channel, were derived in sections 2.5, 2.6 and 2.7 on the basis of a number of simplifying assumptions. Thus the main part of the channel is considered so that the geometry of the problem is that of one electrode segment, and the gas-dynamic fields T, p and $\underline{u}$ are assumed given functions of y, the coordinate normal to the electrode side walls, determined from the solution of the boundary layer equations using the numerical procedure described in chapter 3. All variations in the z direction, which is the direction of application of a uniform constant magnetic field, and therefore the effects of insulator side wall boundary layers, are neglected.

In this chapter a numerical method of solution of the plasma and electrical equations, consistent with the aforementioned boundary conditions and simplifying assumptions, will be developed and used in chapter 5 to study some physical phenomena occurring in a closed cycle MHD general channel for conditions typical of those of a series of experiments recently performed on the IRD generator facility, thus allowing comparisons of theory and experiment to be made wherever possible.

Similar numerical studies have been reported by a number of authors in the past, who demonstrated some qualitative agreement between theory and experiment[8], but time dependent numerical models have so far not reached the degree of sophistication needed for accurate quantitative agreement between theory and experiment to be obtained. The present work may be regarded as an initial step towards achieving this degree of sophistication, by including a number of effects previously considered only in steady-state numerical models of open cycle MHD generators, which have the ability to give accurate predictions of generator characteristics[26],[24]. These effects include finite turbulent velocity and temperature boundary layers, finite ion and seed atom diffusion, collisionless sheaths, turbulent diffusion and turbulent energy transport. It should be noted that no model of electrode-plasma interactions, incorporating seed-electrode interactions, has ever been used for the formulation of boundary conditions for an MHD generator, despite the importance of seed-electrode interaction effects[29],[30].

The inclusion of the aforementioned effects, together with the assumption of instantaneous electron temperature relaxation, previously only considered by Kolb[18], meant that a complex numerical method, incorporating a number of novel features, had to be developed for the solution of the plasma and electrical equations consistent with the boundary conditions. This method will be described in detail in this chapter. It should be noted that, whilst the collisionless sheath model of section 2.7 is rather limited in applicability because of the restriction imposed by the condition (2.240b) the same basic numerical method should be applicable without much modification to the case of a collision dominated sheath, in which an ion continuity equation must be considered, Poisson's equation for the electrostatic potential then replacing the current stream function equation.

4.2 Space-Differencing

For the numerical solution of the plasma and electrical equations, both the space and time coordinates must be discretized so that the governing equations and their boundary conditions can be replaced by finite difference representations. Thus the domain of the calculation, shown in Fig.2.3, is replaced by a two-dimensional mesh. Whilst the step size in the x-direction can be taken to be constant, the large velocity and gas temperature gradients near the walls necessitate the use of a variable step size in the y-direction. A step size distribution in the y-direction, which is symmetric with respect to the centre-line, is obtained from equation (A.3) in appendix A. Thus,

$$y_j = \frac{H}{2}\left[1 - \frac{\tanh\frac{\alpha H}{2}\left(1-\frac{2\zeta}{H}\right)}{\tanh\frac{\alpha H}{2}}\right], \qquad (4.1)$$

where, with J-1 steps in the y-direction,

$$\zeta_j = H\left(\frac{j-1}{J-1}\right), \quad 1 \leq j \leq J. \qquad (4.2)$$

The quantity $\alpha H/2$ in equation (4.1) is treated as a constant determined, as shown in appendix A, from the velocity profile used to initiate the numerical solution of the boundary layer equations for the wall at y = 0.

Equation (4.1) defines the mesh to be symmetric with respect to the centre-line. This is in accordance with the assumed symmetry of the gas-dynamic fields, which allows us to define, for example, the gas temperature for $\frac{H}{2} < y < H$ by the symmetry condition

$$T_{J-j} = T_j, \quad 1 \leq j \leq J,$$

so that the profiles for $\frac{H}{2} < y \leq H$ are obtained from the solution of the boundary layer equations for $0 \leq y \leq H/2$.

Unlike the boundary layer equations, finite difference forms of the plasma and electrical equations, as well as of the wall boundary conditions, accurate to second order in the space step, cannot be derived when the step size is variable, as it is above. To obtain second order accurate finite difference forms it is necessary to transform the y-coordinate to the variable ζ defined by equation (4.1), the mesh then being transformed into a rectangular mesh. This transformation is effected by replacing the differential operator $\partial/\partial y$ with $\xi\,\partial/\partial\zeta$, where

$$\xi = \frac{d\zeta}{dy} = \frac{\tanh\left(\frac{\alpha H}{2}\right)}{(\alpha H/2)} \cosh^2 \frac{\alpha H}{2}\left(1 - \frac{2\zeta}{H}\right), \tag{4.3}$$

in the plasma and electrical equations, and the wall boundary conditions. All plasma and electrical quantities are then considered as functions of the coordinates (x, ζ).

The points of the finite difference mesh in (x, ζ) space are defined by the equations

$$\begin{aligned} &x_1 = 0\ ,\ x_{i+1} = x_i + \Delta x;\ i = 1, 2, \ldots, I \\ &\zeta_1 = 0\ ,\ \zeta_{j+1} = \zeta_j + \Delta\zeta,\ j = 1, 2, \ldots, J \end{aligned} \tag{4.4}$$

and the value of the function $\phi(x,y)$ at the mesh point (x_i, ζ_j) is denoted by $\phi_{i,j}$. Thus,

$$\phi_{i,j} = \phi\,(x_i, y_j) \tag{4.5}$$

The finite difference forms of the plasma and electrical equations, equations (2.207), (2.208), (2.227) and (2.229), at a mesh point (x_i, ζ_j) can be obtained by employing the following second order accurate finite difference representations of the spatial derivatives:

$$\left(\frac{\partial \phi}{\partial x}\right)_{i,j} = \frac{\phi_{i+1,j} - \phi_{i-1,j}}{2\Delta x} \tag{4.6a}$$

$$\left(\frac{\partial \phi}{\partial \zeta}\right)_{i,j} = \frac{\phi_{i,j+1} - \phi_{i,j-1}}{2\Delta \zeta} \tag{4.6b}$$

$$\left[\frac{\partial}{\partial x}\left(k\frac{\partial \phi}{\partial x}\right)\right]_{i,j} = \frac{(3k_{i+1,j} + k_{i-1,j})\phi_{i+1,j} - 4(k_{i+1,j} + k_{i-1,j})\phi_{i,j} + (k_{i+1,j} + 3k_{i-1,j})\phi_{i-1,j}}{4\Delta x^2} \tag{4.6c}$$

$$\left[\frac{\partial}{\partial \zeta}\left(k\frac{\partial \phi}{\partial \zeta}\right)\right]_{i,j} = \frac{(3k_{i,j+1} + k_{i,j-1})\phi_{i,j+1} - 4(k_{i,j+1} + k_{i,j-1})\phi_{i,j} + (k_{i,j+1} + 3k_{i,j-1})\phi_{i,j-1}}{4\Delta \zeta^2} \tag{4.6d}$$

where k and ϕ are any two functions. For the wall boundary conditions, the finite difference representations

$$\left(\frac{\partial \phi}{\partial \zeta}\right)_{i,1} = \frac{4\phi_{i,2} - 3\phi_{i,1} - \phi_{i,3}}{2\Delta \zeta} \tag{4.7a}$$

and

$$\left(\frac{\partial \phi}{\partial \zeta}\right)_{i,J} = \frac{3\phi_{i,J} + \phi_{i,J-2} - 4\phi_{i,J-1}}{2\Delta \zeta} \tag{4.7b}$$

must be used in place of equations (4.6b) at j = 1 and j = J respectively, so that values of ϕ at mesh points outside the physical domain are avoided. Since both the current stream function equation (2.229) and, assuming instantaneous electron temperature relaxation (see section 2.5), the electron energy equation (2.227) are steady-state equations their finite difference forms at any instant of time can be easily obtained by using the finite difference representations defined by equations (4.6) and (4.7). The resultant finite difference equations will be considered in detail in section 4.4.

4.3 Numerical Solution of Continuity Equations

The electron and seed atom continuity equations, equations (2.207) and (2.208), have the general form

$$\frac{\partial f}{\partial t} = -u_x \frac{\partial f}{\partial x} + D_x + D_y + S \tag{4.8}$$

where $f = n_e$ or n_n; D_x and D_y represent the terms describing diffusion in the x and y directions respectively, and S represents the source terms. The integration scheme for equation (4.8) is formulated by considering the Taylor expression

$$f^n = f^{n-1} + \Delta t \left(\frac{\partial f}{\partial t}\right)^{n-1} + \frac{1}{2}\Delta t^2 \left(\frac{\partial^2 f}{\partial t^2}\right)^{n-1} + O(\Delta t^2) \tag{4.9}$$

where n is the time level, and Δt is the time step. Equation (4.9) may be regarded as the sum of two equations:

$$f^{n*} - f^{n-1} = \Delta t \left(\frac{\partial f_1}{\partial t}\right)^{n-1} + \frac{1}{2}\Delta t^2 \left(\frac{\partial^2 f_1}{\partial t^2}\right)^{n-1} + O(\Delta t^3) \tag{4.10a}$$

and

$$f^{n} - f^{n*} = \Delta t \left(\frac{\partial f_2}{\partial t}\right)^{n-1} + \frac{1}{2}\Delta t^2 \left(\frac{\partial^2 f_2}{\partial t^2}\right)^{n-1} + O(\Delta t^3) \tag{4.10b}$$

where

$$\frac{\partial f_1}{\partial t} = -u_x \frac{\partial f}{\partial x} + D_x + S \tag{4.11a}$$

and

$$\frac{\partial f_2}{\partial t} = D_y \tag{4.11b}$$

The advancement of f in time can therefore be regarded as composed of two operations, a first, in which the convective, x-diffusion and source terms are advanced; and a second, in which the y-diffusion terms are advanced. An explicit second order accurate integration scheme for the convective,

x-diffusion and source terms can be formulated by replacing the second derivative in equation (4.10a) by the backward difference approximation

$$\left(\frac{\partial^2 f_1}{\partial t^2}\right)^{n-1} = \left[\left(\frac{\partial f_1}{\partial t}\right)^{n-1} - \left(\frac{\partial f_1}{\partial t}\right)^{n-2}\right] / \Delta t$$

so that, to second order accuracy,

$$f^{n*} - f^{n-1} = \frac{\Delta t}{2}\left[3\left(\frac{\partial f_1}{\partial t}\right)^{n-1} - \left(\frac{\partial f_1}{\partial t}\right)^{n-2}\right] \tag{4.12}$$

This is commonly called the Adams-Bashforth scheme. The finite difference forms of $\partial f_1/\partial t$ at a point (i,j) of the mesh are

$$\left(\frac{\partial f_1}{\partial t}\right)_{i,j} = -\frac{u_{xj}}{2\Delta x}\left(n_{ei+1,j} - n_{ei-1,j}\right) + \frac{1}{\Delta x^2}\left(\frac{\sigma_i k_B}{n_e e^2}\right)_j \left\{\left[n_e(T+T_e)\right]_{i+1,j} - 2\left[n_e(T+T_e)\right]_{i,j} + \left[n_e(T+T_e)\right]_{i-1,j}\right\} + \dot{n}_{ei,j} \quad (f = n_e) \tag{4.13}$$

and

$$\left(\frac{\partial f_1}{\partial t}\right)_{i,j} = -\frac{u_{xj}}{2\Delta x}\left(n_{ni+1,j} - n_{ni-1,j}\right) + \frac{1}{\Delta x^2}\left(\frac{k_B T}{m_{nh}\nu_{nh}}\right)\left(n_{ni+1,j} - 2n_{ni,j} + n_{ni-1,j}\right) - \dot{n}_{ei,j} \quad (f = n_n) \tag{4.14}$$

The updated densities n_e^{n*} and n_n^{n*} at each interior (non-boundary) mesh point are obtained from equations (4.12), (4.13) and (4.14). Owing to the periodicity boundary conditions (2.236a) and (2.236b), equations (4.12), (4.13) and (4.14) are also used for mesh points on the boundary AE (see Fig. 2.3), excluding the corner points. Updated values at mesh points on the boundary DH are obtained by equating with the values on the boundary AE.

The ξ-diffusion terms are advanced by application of the Crank-Nicholson method of differencing[33]. The second derivative in equation (4.10b) is replaced by the forward difference approximation

$$\left(\frac{\partial^2 f_2}{\partial t^2}\right)^{n-1} = \left[\left(\frac{\partial f_2}{\partial t}\right)^{n} - \left(\frac{\partial f_2}{\partial t}\right)^{n-1}\right] / \Delta t \qquad (4.15)$$

so that, to second order accuracy,

$$f^{n} - f^{n*} = \frac{\Delta t}{2}\left[\left(\frac{\partial f_2}{\partial t}\right)^{n} + \left(\frac{\partial f_2}{\partial t}\right)^{n-1}\right] \qquad (4.16)$$

The finite difference forms of $\partial f_2/\partial t$ at a point (i,j) of the mesh are

$$\begin{aligned}\left(\frac{\partial f_2}{\partial t}\right)_{i,j} = \frac{1}{4\Delta\xi^2}\Bigg\{&\left[3\left(\frac{\sigma_i k_B \xi}{n_e e^2}\right)_{j+1} + \left(\frac{\sigma_i k_B \xi}{n_e e^2}\right)_{j-1}\right]\left[n_e(T+T_e)\right]_{i,j+1} \\ &- 4\left[\left(\frac{\sigma_i k_B \xi}{n_e e^2}\right)_{j+1} + \left(\frac{\sigma_i k_B \xi}{n_e e^2}\right)_{j+1}\right]\left[n_e(T+T_e)\right]_{i,j} \\ &+ \left[\left(\frac{\sigma_i k_B \xi}{n_e e^2}\right)_{j+1} + 3\left(\frac{\sigma_i k_B \xi}{n_e e^2}\right)_{j-1}\right]\left[n_e(T+T_e)\right]_{i,j-1} \\ &+ \left(\frac{R_g}{S_{TP}}\right)\left[3(\varepsilon\xi)_{j+1} + (\varepsilon\xi)_{j-1}\right](n_e T)_{i,j+1} \\ &- 4\left(\frac{R_g}{S_{TP}}\right)\left[(\varepsilon\xi)_{j+1} + (\varepsilon\xi)_{j-1}\right](n_e T)_{i,j} \\ &+ \left(\frac{R_g}{S_{TP}}\right)\left[(\varepsilon\xi)_{j+1} + 3(\varepsilon\xi)_{j-1}\right](n_e T)_{i,j-1}\Bigg\} \quad (f = n_e)\end{aligned} \qquad (4.17)$$

and

$$\left(\frac{\partial f_2}{\partial t}\right)_{i,j} = \frac{1}{4\Delta\xi^2}\Bigg\{\left[3\left(\frac{k_B\xi}{m_{nk}v_{nk}}\right)_{j+1} + \left(\frac{k_B\xi}{m_{nk}v_{nk}}\right)_{j-1}\right](n_nT)_{i,j+1}$$
$$- 4\left[\left(\frac{k_B\xi}{m_{nk}v_{nk}}\right)_{j+1} + \left(\frac{k_B\xi}{m_{nk}v_{nk}}\right)_{j-1}\right](n_nT)_{i,j}$$
$$+ \left[\left(\frac{k_B\xi}{m_{nk}v_{nk}}\right)_{j+1} + 3\left(\frac{k_B\xi}{m_{nk}v_{nk}}\right)_{j-1}\right](n_nT)_{i,j-1}$$
$$+ \left(\frac{R_g}{S_{TP}}\right)\left[3(\varepsilon\xi)_{j+1} + (\varepsilon\xi)_{j-1}\right](n_nT)_{i,j+1}$$
$$- 4\left(\frac{R_g}{S_{TP}}\right)\left[(\varepsilon\xi)_{j+1} + (\varepsilon\xi)_{j-1}\right](n_nT)_{i,j}$$
$$+ \left(\frac{R_g}{S_{TP}}\right)\left[(\varepsilon\xi)_{j+1} + 3(\varepsilon\xi)_{j-1}\right](n_nT)_{i,j-1}\Bigg\}\quad (f=n_n)$$

(4.18)

Using equations (4.17) and (4.18) the finite difference forms of equation (4.16) can be written in the forms

$$A_{ei,j}\, n^n_{ei,j-1} + B_{ei,j}\, n^n_{ei,j} + C_{ei,j}\, n^n_{ei,j+1} = D_{ei,j}\quad (f=n_e) \tag{4.19}$$

and

$$A_{ni,j}\, n^n_{ni,j-1} + B_{ni,j}\, n^n_{ni,j} + C_{ni,j}\, n^n_{ni,j+1} = D_{ni,j}\quad (f=n_n) \tag{4.20}$$

where $2 \leq j \leq J-1$.

The coefficients A_e, B_e and C_e depend on the updated electron temperature $T_{e_{i,j}}^{n}$, and the wall values of n_e^n and n_n^n are obtained from the finite difference forms of the wall boundary conditions for the continuity equations, which are coupled to the other wall boundary conditions (see section 4.5). Therefore, equations (4.19) and (4.20) must be solved simultaneously with the solution of the electron energy and current stream function equations (see section 4.4), equations (2.227) and (2.229). For given $T_{e_{i,j}}^{n}$, and wall values of n_e^n and n_n^n, equations (4.19) and (4.20) are two linear tridiagonal systems of equations for the updated densities $n_{e_{i,j}}^{n}$ and $n_{n_{i,j}}^{n}$ $(2 \leq j \leq J-1)$, which can be solved for every mesh column excluding the boundary DH (Fig. 2.3), along which the updated densities can be obtained by application of the periodicity conditions, equations (2.236a) and (2.236b).

Application of equation (4.12) requires the use of a constant time step; to perform the first time advance, and to revise Δt where necessary, a form of second order accurate Runge-Kutta method is used. Omitting the second derivative in equation (4.10a), and eliminating the second derivative in equation (4.10b) using equation (4.15), equations (4.10a) and (4.10b) can be written in the approximate forms

$$f^{n*} - f^{n-1} = \Delta t \left(\frac{\partial f_1}{\partial t}\right)^{n-1} \tag{4.20a}$$

and

$$f^{\bar{n}} - f^{n*} = \frac{\Delta t}{2}\left[\left(\frac{\partial f_2}{\partial t}\right)^{\bar{n}} + \left(\frac{\partial f_2}{\partial t}\right)^{n-1}\right], \tag{4.20b}$$

respectively. Equations (4.20a) and (4.20b) determine the updated f, denoted by $f^{\bar{n}}$, to first order accuracy. Using $f^{\bar{n}}$ and f^{n-1} the second derivative in equation (4.10a) can be approximated. Thus,

$$\left(\frac{\partial^2 f_1}{\partial t^2}\right)^{n-1} \simeq \left[\left(\frac{\partial f_1}{\partial t}\right)^{\bar{n}} - \left(\frac{\partial f_1}{\partial t}\right)^{n-1}\right]/\Delta t. \qquad (4.21)$$

Inserting equation (4.21) into equation (4.10a) and eliminating the second derivative in equation (4.10b) using equation (4.15), equations (4.10a) and (4.10b) can be written in the approximate forms

$$f^{n*/} - f^{n-1} = \frac{\Delta t}{2}\left[\left(\frac{\partial f_1}{\partial t}\right)^{\bar{n}} + \left(\frac{\partial f_1}{\partial t}\right)^{n-1}\right] \qquad (4.22a)$$

and

$$f^{n} - f^{n*/} = \frac{\Delta t}{2}\left[\left(\frac{\partial f_2}{\partial t}\right)^{n} + \left(\frac{\partial f_2}{\partial t}\right)^{n-1}\right] \qquad (4.22b)$$

respectively. Equations (4.22a) and (4.22b) determine the updated f, denoted by f^{n}, to second order accuracy.

The procedure used to update the electron and seed atom densities, is defined by equations (4.12) and (4.16) for a constant time step, and equations (4.20a), (4.20b), (4.22a) and (4.22b) for variable time step. In this procedure the x-diffusion, source and convection terms are treated by an explicit second order accurate integration scheme, while the cross-stream diffusion terms are treated by the implicit second order accurate Crank-Nicholson scheme. A procedure of this kind appears to have been first used by Oliver[34], but in a form less accurate than that formulated here. The procedure used here reduces to that used by Uncles[8] in the absence of the ζ - diffusion terms in the continuity equations.

The accuracy of the one time step explicit integration scheme defined by equations (4.20a), (4.20b), (4.22a) and (4.22b) when ζ-diffusion is present has been checked by performing numerical experiments in which both this scheme and that defined by equations (4.12) and (4.16) were used to update quantities, keeping the time step fixed. The two sets of results so obtained were found to differ by negligible amounts.

The choice of the time step is governed by considerations of numerical stability, which is discussed in detail in section 4.6. The explicit part of the calculation is stable only if the time step is sufficiently smaller than the minimum characteristic time scale of the physical processes involved in the evolution of the densities (excluding ζ-diffusion). There remains, however, a weak instability due to convection which has necessitated the introduction of artificial diffusion (see section 4.6). On the other hand, the implicit part of the calculation is unconditionally stable, which is desirable since strong ζ-diffusion near the walls would impose severe restrictions on the size of time step used if an explicit integration scheme were used.

4.4 Numerical Solution of Electron Energy and Current Stream Function Equations

The current stream equation, equation (2.229), can be written in the form

$$\frac{\partial^2 \psi}{\partial x^2} + \xi^2 \frac{\partial^2 \psi}{\partial \zeta^2} + P \frac{\partial \psi}{\partial x} + \left[Q + \frac{d\xi}{d\zeta} \right] \xi \frac{\partial \psi}{\partial \zeta} = R, \qquad (4.23)$$

where the y-coordinate has been transformed to the coordinate ζ. The finite difference form of equation (4.23) at an interior (non-boundary)

point (i,j) can be written in the form

$$F_{1i,j} \equiv C_{1j}\left(\psi_{i+1,j}+\psi_{i-1,j}\right)+\frac{1}{2}C_{1j}\,\Delta x\,P_{i,j}\left(\psi_{i+1,j}-\psi_{i-1,j}\right)$$
$$+C_{2j}\psi_{i,j+1}+C_{3j}\psi_{i,j-1}+\frac{1}{2}C_{1j}\,\xi_j\left(\frac{\Delta x}{\Delta\xi}\right)^2\Delta\xi\,Q_{i,j}\left(\psi_{i,j+1}-\psi_{i,j-1}\right)$$
$$-\psi_{i,j}-C_{1j}\,\Delta x^2 R_{i,j}=0 \qquad (4.24a)$$

where

$$C_{1j}=\frac{1}{2\left[1+\left(\frac{\Delta x}{\Delta\xi}\right)^2\xi_j^2\right]} \qquad (4.24b)$$

$$C_{2j}=\xi_j^2\left(\frac{\Delta x}{\Delta\xi}\right)^2\left[1+\Delta\xi\,\frac{1}{2\xi_j}\left(\frac{d\xi}{d\xi}\right)_j\right]C_{1j} \qquad (4.24c)$$

$$C_{3j}=\xi_j^2\left(\frac{\Delta x}{\Delta\xi}\right)^2\left[1-\Delta\xi\,\frac{1}{2\xi_j}\left(\frac{d\xi}{d\xi}\right)_j\right]C_{1j} \qquad (4.24d)$$

and $P_{i,j}$, $Q_{i,j}$ and $R_{i,j}$ are the finite difference approximations to equations (2.230a)-(2.230c).

The finite difference form of the electron energy equation at an interior (non-boundary) mesh point (i,j) is written as

$$F_{2i,j}=0. \qquad (4.25)$$

For given $n^n_{ei,j}$, $n^n_{ni,j}$ and wall values of $\overline{T}^n_{ei,j}$ and $\psi^n_{i,j}$, equations (4.24) and (4.25) are two coupled systems of non-linear algebraic equations for the unknowns $\psi^n_{i,j}$ and $\overline{T}^n_{ei,j}$ at all mesh points excluding the walls. The system of equations is solved iteratively using an extension of the non-linear relaxation method originally developed by Lieberstein[35] for the solution of a system

of non-linear algebraic equations obtained by finite differencing a single non-linear elliptic equation.

Equations (4.24a) and (4.25) are linearized by introducing the iterates $\psi_{i,j}^{(k)}$ and $\overline{Te}_{i,j}^{(k)}$ (k is the iteration level) and replacing $F1_{i,j}$ and $F2_{i,j}$ by expansions of $F1_{i,j}^{(k+1)}$ and $F2_{i,j}^{(k+1)}$ about $\psi_{i,j}^{(k)}$ and $\overline{Te}_{i,j}^{(k)}$. The algorithm of the non-linear relaxation method is obtained by ignoring variations of Te and ψ at mesh points in the immediate neighbourhood of the point (i,j) in these expansions. Thus, we obtain the expansions

$$F1_{i,j}^{(k)} + \left(\frac{\partial F1_{i,j}}{\partial \overline{Te}_{i,j}}\right)^{(k)}\left(\overline{Te}_{i,j}^{(k+1)} - \overline{Te}_{i,j}^{(k)}\right) + \left(\frac{\partial F1_{i,j}}{\partial \psi_{i,j}}\right)\left(\psi_{i,j}^{(k+1)} - \psi_{i,j}^{(k)}\right) = 0 \qquad (4.26a)$$

and

$$F2_{i,j}^{(k)} + \left(\frac{\partial F2_{i,j}}{\partial \overline{Te}_{i,j}}\right)^{(k)}\left(\overline{Te}_{i,j}^{(k+1)} - \overline{Te}_{i,j}^{(k)}\right) = 0 , \qquad (4.26b)$$

the latter equation following from the fact that $F2_{i,j}^{(k)}$ is not explicitly dependent on $\psi_{i,j}^{(k)}$.

Introducing a relaxation parameter ω and setting $\left(\partial F1_{i,j}/\partial \psi_{i,j}\right)^{(k)} = -1$ (see equation (4.24a)), the following equations are obtained from equations (4.26a) and (4.26b):

$$\overline{Te}_{i,j}^{(k+1)} = \overline{Te}_{i,j}^{(k)} - \omega \frac{F2_{i,j}^{(k)}}{\left(\frac{\partial F2_{i,j}}{\partial \overline{Te}_{i,j}}\right)^{(k)}} , \qquad (4.27a)$$

$$\psi_{i,j}^{(k+1)} = \psi_{i,j}^{(k)} + \omega\left[F1_{i,j}^{(k)} + \left(\frac{\partial F1_{i,j}}{\partial \overline{Te}_{i,j}}\right)^{(k)}\left(\overline{Te}_{i,j}^{(k+1)} - \overline{Te}_{i,j}^{(k)}\right)\right] \qquad (4.27b)$$

A single iteration is performed by scanning the mesh replacing the values of $\overline{Te}_{i,j}^{(k)}$ and $\psi_{i,j}^{(k)}$ at each point by the right-hand sides of equations (4.27a) and (4.27b) respectively, where $F1_{i,j}$, $F2_{i,j}$ $\partial F1_{i,j}/\partial \overline{Te}_{i,j}$ and $\partial F2_{i,j}/\partial \overline{Te}_{i,j}$ are evaluated using

corrected results immediately upon becoming available. The iterations are stopped when a convergent solution is obtained satisfying $|T_{e_{i,j}}^{(k+1)} - T_{e_{i,j}}^{(k)}| < \varepsilon\omega$ for all mesh points (i,j), where ε is a prescribed value, say 1^{0}K.

Owing to the periodicity assumption, equations (4.27a) and (4.27b) also apply at mesh points on the boundary AE of the domain (see Fig. 2.3). The values of $T_{e_{i,j}}^{(k+1)}$ and $\psi_{i,j}^{(k+1)}$ along the boundary DH are obtained by application of the periodicity condition (2.236c) and equation (2.235).

For mesh points lying on the insulators CD and GH of Fig. 2.3, equation (2.234) gives

$$\psi_{i,j}^{(k+1)} = \psi_0 + I^{(k)}/W,$$

where

$$I^{(k)} = V^{(k)}/R_L,$$

the voltage drop $V^{(k)}$ being obtained from equation (2.232) using Simpson's rule and the T_e and ψ distributions at the kth iteration level. For applications considered here this is not necessary since fixed applied currents are assumed so that I^k is constant and the insulator wall values of $\psi_{i,j}$ are fixed.

The values of $\psi_{i,j}^{(k+1)}$ at mesh points lying on the electrodes BC and FG of Fig. 2.3 are obtained from the finite difference forms of equation (2.233), the values of ψ outside the physical domain being eliminated using equation (4.24a). To ensure that the boundary condition $J_y = 0$ is satisfied at all insulator wall points, the values of $\psi_{i,j}^{(k+1)}$ at electrode corner points are set equal to the values on the adjacent insulator walls.

For stability of the non-linear relaxation method the parameter ω must lie in the range $0<\omega<2$ (see reference (33), the method being one of over-relaxation if $1<\omega<2$, and under-relaxation if $0<\omega<1$. For given values of $n_{e_{i,j}}^{n}$, $n_{n_{i,j}}^{n}$ and boundary values of $Te_{i,j}^{n}$ one can optimize the convergence rate by suitably adjusting the relaxation parameter ω at every iteration. However, as indicated in reference (33), the amount of computational work involved in doing this is too great for there to be any useful gains in computational efficiency. Instead, an optimum value of ω can be found for a sequence of iterations defined by equations (4.27), by testing a number of values of ω and comparing the numbers of iterations required for convergence. The optimum value of ω so obtained could be adjusted occasionally in the course of advancement of the solution in time. This approach, used by Uncles[8], has not been followed in the present work because of the large number of calculations performed in advancing the solution a single time step. Instead, an optimum value of ω is found by computing the initial state using several values of ω and finding the value of ω for which the number of iterations required for convergence is a minimum. For an applied current of 0.5A, a seeding fraction of 10^{-3}, a magnetic field of 0.5T, and a mesh of 15 columns and 49 rows, the optimum value of ω is found to be 1.5. This value of ω has been used for all computations reported in chapter 5. Numerical experiments have shown that instability can occur if the difference between the value of ω used and the optimum value is large. In particular, the scheme can be unstable if the relaxation parameter is taken to be equal to the optimum value for solution of Laplace's equation on a mesh of constant step size in the x- and y-directions, which is given by[33]

$$\omega_{opt} \simeq 2\left[1+\pi\left\{\frac{1}{2J^2}+\frac{1}{2I^2}\right\}\right]^{-1} \quad I, J \gg 1.$$

This formula yields an optimum value of 1.98 for ω, where I = 15 and J = 49.

Numerical calculations based on the assumption of instantaneous electron temperature relaxation, have been reported by Kolb[18], who applied the non-linear relaxation method of solution to the electron energy equation alone, following the original method due to Lieberstein[35]. This meant that a sequence of iterations had to be performed between the solution of the elliptic equation for the electrostatic potential, obtained by means of the method of linear relaxation and the solution of the electron energy equation. This has been avoided here by extension of the method of non-linear relaxation.

4.5 Numerical Solution Consistent with Wall Boundary Conditions

The wall boundary conditions for the continuity and electron energy equations were derived in section 2.7 from a study of interactions between the plasma and electrode walls. The spatial finite difference forms of these boundary conditions are obtained by replacing the derivatives with respect to ζ by the finite difference representations given by equations (4.7). For given $\psi^n_{i,j}$ (including electrode wall values) and interior values of $T^n_{ei,j}$, $n^n_{ei,j}$ and $n^n_{ni,j}$, one then has a system of equations at each wall mesh point for the unknown wall values of $T^n_{ei,j}$, $n^n_{ei,j}$ and $n^n_{ni,j}$.

Considering an electrode wall, the ion and seed atom continuity conditions can be used to eliminate the wall values of $n^n_{ei,j}$ and $n^n_{ni,j}$ from the electron energy, total current continuity and surface coverage equations; these equations can then be written in the forms

$$G_{1i,j}^{n}\left(T_e, \Delta\phi, \theta\right) = 0 , \tag{4.28}$$

$$G_{2i,j}^{n}\left(T_e, \Delta\phi, \theta\right) = 0 , \tag{4.29}$$

$$\left(\frac{\partial\theta}{\partial t}\right)_{i,j}^{n} = G_{3i,j}^{n}\left(T_e, \Delta\phi, \theta\right) \tag{4.30}$$

where $j = 1$ or J and the forms of G_1, G_2 and G_3 depend on the sign of $\Delta\phi$. The equation for the surface coverage, equation (4.30), is time differenced by replacing $\left(\partial\theta/\partial t\right)_{i,j}^{n-1/2}$ with $\left(\theta^{n}-\theta^{n-1}\right)/\Delta t$, and $G_{3i,j}^{n-1/2}$ with the average $\left(G_{3i,j}^{n}+G_{3i,j}^{n-1}\right)/2$. Thus, to second order accuracy, equation (4.30) can be written in the form

$$G_{4i,j}^{n}\left(T_e, \Delta\phi, \theta\right) \equiv \theta_{i,j}^{n}-\theta_{i,j}^{n-1}-\frac{\Delta t}{2}\left(G_{3i,j}^{n}+G_{3i,j}^{n-1}\right)=0 \tag{4.31}$$

Equations (4.28), (4.29) and (4.31) constitute a non-linear system of equations for the unknowns $T_{ei,j}^{n}$, $\Delta\phi_{i,j}^{n}$ and $\theta_{i,j}^{n}$. These equations can be solved iteratively by means of Newton's method. The equations are linearized by introducing the iterates $\left(T_{ei,j}^{(k)}, \Delta\phi_{i,j}^{(k)}, \theta_{i,j}^{(k)}\right)$, where k is the iteration level, and replacing $G_{1i,j}^{n}$, $G_{2i,j}^{n}$ and $G_{4i,j}^{n}$ by expansions of $G_{1i,j}^{(k+1)}$, $G_{2i,j}^{(k+1)}$ and $G_{4i,j}^{(k+1)}$ about $\left(T_{ei,j}^{(k)}, \Delta\phi_{i,j}^{(k)}, \theta_{i,j}^{(k)}\right)$, retaining only those terms linear in $\left(T_{ei,j}^{(k+1)}-T_{ei,j}^{(k)}\right)$ etc. Thus, equations (4.28), (4.29) and (4.31) become

$$G_{1i,j}^{(k)}+\left(\frac{\partial G_1}{\partial T_e}\right)_{i,j}^{(k)}\delta T_{ei,j}^{(k)}+\left(\frac{\partial G_1}{\partial\Delta\phi}\right)_{i,j}^{(k)}\delta\Delta\phi_{i,j}^{(k)}+\left(\frac{\partial G_1}{\partial\theta}\right)_{i,j}^{(k)}\delta\theta_{i,j}^{(k)}=0 \tag{4.32a}$$

$$G_{2i,j}^{(k)}+\left(\frac{\partial G_2}{\partial T_e}\right)_{i,j}^{(k)}\delta T_{ei,j}^{(k)}+\left(\frac{\partial G_2}{\partial\Delta\phi}\right)_{i,j}^{(k)}\delta\Delta\phi_{i,j}^{(k)}+\left(\frac{\partial G_2}{\partial\theta}\right)_{i,j}^{(k)}\delta\theta_{i,j}^{(k)}=0 \tag{4.32b}$$

and

$$G_{4i,j}^{(k)}+\left(\frac{\partial G_4}{\partial T_e}\right)_{i,j}^{(k)}\delta T_{ei,j}^{(k)}+\left(\frac{\partial G_4}{\partial\Delta\phi}\right)_{i,j}^{(k)}\delta\Delta\phi_{i,j}^{(k)}+\left(\frac{\partial G_4}{\partial\theta}\right)_{i,j}^{(k)}\delta\theta_{i,j}^{(k)}=0 \tag{4.32c}$$

where

$$\delta \overline{Te}_{i,j}^{(k)} = \overline{Te}_{i,j}^{(k+1)} - \overline{Te}_{i,j}^{(k)}, \quad \delta \Delta\phi_{i,j}^{(k)} = \Delta\phi_{i,j}^{(k+1)} - \Delta\phi_{i,j}^{(k)}, \quad \text{and} \quad \delta\theta_{i,j}^{(k)} = \theta_{i,j}^{(k+1)} - \theta_{i,j}^{(k)} \tag{4.33}$$

Having solved equations (4.32), the higher order iterates are obtained from equations (4.33). The iterations are repeated until $|\delta \overline{Te}_{i,j}^{(k)} / \overline{Te}_{i,j}^{(k+1)}| < \varepsilon$ where ε is, say, 10^{-4}. It should be noted that the forms of $G_{1i,j}^{(k)}$, $G_{2i,j}^{(k)}$ and $G_{4i,j}^{(k)}$, and their derivatives, must be changed whenever the sign of $\Delta\phi_{i,j}^{(k)}$ changes during the iterations.

Having determined $\overline{Te}_{i,j}^{n}$, $\Delta\phi_{i,j}^{n}$ and $\theta_{i,j}^{n}$, the electrode wall values of $n_{ei,j}^{n}$ and $n_{ni,j}^{n}$ are obtained from the ion and seed atom continuity conditions.

The insulator wall values of $n_{ei,j}^{n}$, $n_{ni,j}^{n}$ and $\overline{Te}_{i,j}^{n}$ are much more easily obtained. For example, for an insulator wall segment at y = 0, one has

$$\overline{Te}_{i,j}^{n} = (4\,Te_{i,2}^{n} - Te_{i,3}^{n})/3 \tag{4.34a}$$

$$n_{ei,j}^{n} = \left\{4\left[n_e(T+Te)\right]_{i,2}^{n} - \left[n_e(T+Te)\right]_{i,3}^{n}\right\} \Big/ \left[3(T+Te)\right]_{i,j}^{n} \tag{4.34b}$$

$$n_{ni,j}^{n} = \left[4\left(n_n^{n}T\right)_{i,2} - \left(n_n^{n}T\right)_{i,3}\right] / (3T_i) \tag{4.34c}$$

Numerical solutions of the continuity, electron energy and current stream function equations consistent with the wall boundary conditions may be obtained in a number of ways. One procedure, which has been tested, is outlined in block form in figure 4.1, assuming a constant time step.

A suitable alternative to the procedure outlined in figure 4.1 might seem to be one in which the wall boundary values are obtained from equations (4.28), (4.29), (4.31) and (4.34) at every iteration of

$\psi^n_{i,j}$ and the interior value of $T^n_{ei,j}$; that is, at every iteration of the non-linear relaxation method. As indicated in reference (36), such a procedure suffers from a slow instability; that is, a slow drifting away from the true solution as the iterations are performed. With a sufficiently stringent convergence criterion, a convergent solution is never obtained and any result obtained by terminating the iterations at some point bears little resemblance to the true solution. This instability has been observed by the present author in numerical experiments employing the aforementioned procedure.

To initiate calculations, the initial distributions $n^o_{ei,j}$, $n^o_{ni,j}$ and $\theta^o_{i,j}$ must be specified, together with guesses for $T^o_{ei,j}$ and $\psi^o_{i,j}$. These are obtained by making the following assumptions:

(i) The current stream function satisfied Laplace's equation

$$\nabla^2 \psi = 0,$$

subject to the boundary conditions given by equations (2.233), (2.234) and (2.235); equation (2.233) is used in the form

$$\frac{\partial \psi}{\partial y} = \beta_e \frac{\partial \psi}{\partial x},$$

and the current I is given.

(ii) The seeding fraction $\chi = (n_n^o + n_e^o)/n_h$ is a specified constant.

(iii) The electron density is given by Saha's equation:

$$\dot{n}_e = 0$$

(iv) The electron energy equation has the simplified form

$$J^2/\sigma_e = 3 n_e k_B (T_e - T) \frac{m_e}{m_h} \nu_{eh}$$

(v) The surface coverage is equal to its thermal equilibrium value (see section 2.7).

The $u^o_{i,j}$ and $T_{ei,j}^o$ distributions, and the wall values of $n_{ei,j}^o$ and $n_{ni,j}^o$, are found by solving the full electron energy and current stream function equations consistent with the wall boundary conditions for fixed surface coverage.

4.6 Stability Considerations

For the explicit part of the integration scheme for the continuity equations, formulated in section 4.3, to be numerically stable and accurate the time step must be sufficiently smaller than the characteristic time scales of the physical processes described. The implicit treatment of the ζ-diffusion terms requires only that the time step be sufficiently small for accuracy, since the Crank Nicholson scheme is unconditionally stable[33]. This is also true of the implicit treatment of the surface coverage equation (see equation (4.31)).

The explicit integration scheme is applied to the convection, x-diffusion and source terms of the continuity equations. The stability of the scheme is examined by use of the approximate approach of reference (8), in which the stability of the scheme to source terms, convection terms and x-diffusion terms is considered separately.

(a) Stability to source terms

In order to investigate the stability of the explicit integration scheme to source terms, small perturbations of n_e and n_n are considered, and the linear theory of appendix C is applied. Consistent with the temperature relaxation approximation, the evolution of the perturbations n_e' and n_n' is described by the equation

$$\partial u / \partial t = u/\tau , \tag{4.35}$$

where $u = n_e'$ or n_n' and τ is the growth/decay time of the ionization instability; i.e., g_+^{-1} . The explicit integration scheme defined by equation (4.12) yields for u at time level n,

$$u^n = u^{n-1} + \frac{\Delta t}{2\tau}\left[3u^{n-1} - u^{n-2}\right] \tag{4.36}$$

By solving equations (4.35) and (4.36) and comparing the solutions, it is shown in reference (18) that, for $\tau > 0$, the numerical scheme approximates the exact solution to second order accuracy in $(\Delta t/\tau)$ if

$$\Delta t < 0.48\,\tau \tag{4.37}$$

For an exponentially decreasing solution, the stability condition is

$$\Delta t < 0.5|\tau| \quad , \quad (\tau < 0), \tag{4.38}$$

which is slightly less restrictive than condition (4.37).

The numerical results presented in chapter 5 are obtained by considering the characteristic time scale for ionization (see equation (2.212))

$$\tau_I = 1/\left[A_1 (n_n - n_e)\right],$$

where

$$A_1 = \alpha(T_e)\left(\frac{2\pi m_e k_B T_e}{h^2}\right)^{3/2} e^{-\frac{eV_I}{k_B T_e}}$$

in place of the growth/decay time of the ionization instability in equation (4.35). This is due to the fact that the linear theory of appendix C is not applicable to small departures from highly non-uniform plasma states; application of the expression for the growth rate of the ionization instability in the temperature relaxation approximation derived in appendix C is found to lead to unnecessarily short time steps.

(b) Stability to convective terms

The simple convection equation

$$\frac{\partial u}{\partial t} = -u_x \frac{\partial u}{\partial x} , \tag{4.39}$$

where u_x = constant, is considered. The explicit integration scheme defined by equation (4.12) when applied to equation (4.39) yields

$$u_i^n = u_i^{n-1} - \frac{\Delta t u_x}{4\Delta x}\left[3\left(u_{i+1}^{n-1} - u_{i-1}^{n-1}\right) - \left(u_{i+1}^{n-2} - u_{i-1}^{n-2}\right)\right] \tag{4.40}$$

By considering a Fourier mode of solution of equation (4.40) it is shown in reference (8) that, for

$$\frac{u_x \Delta t}{2\Delta x} \leq 0.5 \tag{4.41}$$

the numerical scheme approximates the exact solution to second order accuracy in $u_x\Delta t/\Delta x$, but possesses a weak instability in fourth order; that is,

$$|g| = 1 + O(\Delta t^4) \geq 1$$

where $g = u_i^n / u_i^{n-1}$. It is shown in reference (27) that this instability is removed if after every time step new values of the variables are defined according to

$$u_i^{n+} = u_i^n + \frac{\epsilon}{16}\left(\frac{u_x \Delta t}{\Delta x}\right)^4 \left[u_{i+1}^{n-1} - 2u_i^{n-1} + u_{i-1}^{n-1}\right] \tag{4.42}$$

where $\epsilon > 64/27$. The accuracy of the solution is little affected by the introduction of this artificial diffusion.

Uncles[8] found that stabilization was not required in his work because the time scale for convection $\frac{\Delta x}{u_x}$ was much larger than the electrothermal time scales so that the factor $(u_x \Delta t/\Delta x)^4$ was

very small. In the present work, however, conditions are such that the time scale for convection is comparable to the electrothermal and ionization/recombination time scales and stabilization is necessary.

Artificial diffusion is applied to the integration scheme of section 4.3 as follows. Assuming a constant time step, application of the explicit integration scheme defined by equation (4.12) is followed by an evaluation of the variable f according to equation (4.42):

$$\overline{f_{i,j}^{n*}} = f_{i,j}^{n*} + \frac{\epsilon}{16}\left(\frac{u_x \Delta t}{\Delta x}\right)^4 \left[f_{i+1,j}^{n-1} - 2f_{i,j}^{n-1} + f_{i-1,j}^{n-1}\right]$$

The value f^{n*} in equation (4.16) is then replaced with the value $\overline{f^{n*}}$.

The artificial diffusion scheme, defined by equation (4.42), is applied to the ~~explicit~~ one step integration scheme, defined by equations (4.20) and (4.22), by replacing f^{n*} and $f^{n*\prime}$ in equations (4.20b) and (4.22b) with $\overline{f^{n*}}$ and $\overline{f^{n*\prime}}$, respectively, where

$$\overline{f_{i,j}^{n*}} = f_{i,j}^{n*} + \frac{\epsilon}{16}\left(\frac{u_x \Delta t}{\Delta x}\right)^4 \left[f_{i+1,j}^{n-1} - 2f_{i,j}^{n-1} + f_{i-1,j}^{n-1}\right],$$

$$\overline{f_{i,j}^{n*\prime}} = f_{i,j}^{n*\prime} + \frac{\epsilon}{16}\left(\frac{u_x \Delta t}{\Delta x}\right)^4 \left[f_{i+1,j}^{n-1} - 2f_{i,j}^{n-1} + f_{i-1,j}^{n-1}\right],$$

the quantities $f_{i,j}^{n*}$ and $f_{i,j}^{n*\prime}$ being given by equations (4.20a) and (4.22a).

(c) Stability to diffusive terms

Application of the explicit integration scheme defined by equation (4.12) to the simple diffusion equation

$$\frac{\partial u}{\partial t} = k_D \frac{\partial^2 u}{\partial x^2} \tag{4.43}$$

yields

$$u_i^n = u_i^{n-1} + \frac{\Delta t k_D}{2\Delta x^2}\left[3\left(u_{i+1}^{n-1} - 2u_i^{n-1} + u_{i-1}^{n-1}\right) - \left(u_{i+1}^{n-2} - 2u_i^{n-2} + u_{i-1}^{n-2}\right)\right] \tag{4.44}$$

By considering a Fourier mode of solution of equation (4.44), it can be shown that the condition for stability is that

$$\Delta t < \frac{0.5\,\Delta x^2}{k_D} \tag{4.45}$$

The conditions (4.37) or (4.38), (4.41) and (4.45) impose restrictions on the size of time step used for the explicit integration scheme defined by equations (4.12) to be numerically stable and accurate. These conditions require that the time step be sufficiently smaller than the time scales of the physical processes concerned. Characteristic time scales are discussed in greater detail in appendix C.

Another form of numerical instability can occur as a result of large truncation error when a space step mesh size exceeds the characteristic length scale for electron thermal conduction. This instability has been reported by Kolb[18] and has been observed in the present work in numerical experiments where electron temperature gradients near the electrode corners are very large. In these cases it is found that when the step size in the x-direction is too large, large electron temperature peaks, which tend to increase with time, occur in the higher current density regions near the electrodes. These peaks disappear when a smaller step size is used. An expression is derived below for the characteristic length scale of electron thermal conduction, which is used to obtain upper limits on the choice of step size in the x-direction.

A uniform plasma state described by the simplified continuity and electron energy equations

$$\dot{n}_{e_0} = 0 \tag{4.46a}$$

and

$$J^2/\sigma_{eo} = L_{eo}. \tag{4.46b}$$

is considered, where the subscript o refers to steady-state quantities and L_{eo} is the volumetric rate of loss of energy of the electron gas as a result of elastic collisions with the heavy particles; this is given by (see equation (2.31))

$$L_{eo} = 3k_B n_e (T_e - T)\frac{m_e}{m_h}\nu_{eh}. \tag{4.47}$$

Spatial variations are introduced such that

$$n_e = n_{eo} + Re\{\tilde{n}_e e^{ikx}\} \equiv n_{eo} + n_e' \tag{4.48a}$$

and

$$T_e = T_{eo} + Re\{\tilde{T}_e e^{ikx}\} \equiv T_{eo} + T_e'. \tag{4.48b}$$

Linearization of the simplified system of equations, considered in appendix C, equations (C.1)-(C.6), with respect to the perturbations defined by equations (4.48) yields the equations

$$\frac{Dn_e'}{Dt} = a_0 n_e' + a_1 T_e' \tag{4.49a}$$

and

$$a_2\frac{Dn_e'}{Dt} + a_3\frac{DT_e'}{Dt} = a_4 n_e' + a_5 T_e' - \lambda_{eo}k^2 T_e', \tag{4.49b}$$

where the coefficients $a_0 - a_5$ are listed in appendix C. The additional term $\lambda_{eo}\frac{\partial^2 T_e'}{\partial x^2} = -\lambda_{eo}k^2 T_e'$ has been introduced on the right-hand side of equation (4.49b) to account for electron thermal conduction. Eliminating Dn_e'/Dt from equation (4.49b) using equation (4.49a), we obtain

$$a_3 \frac{DTe'}{Dt} + (a_2 a_0 - a_4) n_e' = -(a_1 a_2 - a_5 + \lambda_{eo} k^2) T_e',$$

from which it is clear that electron thermal conduction is important if the wavelengths of spatial variations are sufficiently small that

$$\lambda_{eo} k^2 \gtrsim (a_1 a_2 - a_5),$$

from which a characteristic length scale for electron thermal conduction can be defined as

$$L_{\lambda e} = 2\pi \left\{ \frac{\lambda_{eo}}{(a_1 a_2 - a_5)} \right\}^{1/2}. \qquad (4.50)$$

The angle θ in equation (C.9f) of appendix C is taken to be $\pi/2$, for which the magnitude of the coefficient a_5 is a maximum and $L_{\lambda e}$ therefore a minimum. Using equations (C.9b), (C.9c) and (C.9f) we can then write

$$a_1 a_2 - a_5 = 1.09 \times 10^{-20} T_{eo}^{-9/2} n_{eo}^3 k_B \left(\frac{\varepsilon_i}{k_B T_{eo}} + \frac{3}{2} \right)^2 + \frac{1}{T_{eo}} \frac{J_o^{-2}}{\sigma_{eo}} \frac{(3T_e - T)}{(T_e - T)}. \qquad (4.51)$$

From equation (2.114), λ_{eo} is given by

$$\lambda_{eo} = \frac{5 n_e k_B^2 T_e}{2 m_e \nu_{eh}}. \qquad (4.52)$$

Taking as a representative set of values, for a seeding fraction of 0.002, $T_e = 2000^0$K, $n_e = 1.637 \times 10^{19}/m^3$, $J = 4.319 \times 10^3$ A/m^2, and $\sigma_e = 4.365$ mhs/m, we obtain from equations (4.50)-(4.52), $L_{\lambda e} = 0.56$ mm. The smallness of $L_{\lambda e}$ compared with a segment length of 25.4 mm, used in all numerical experiments carried out by the author, necessitates the use of a large number of steps in the x-direction (> 45) in cases where electron temperature gradients are very large. In the work of Kolb[18], the numerical instability occurs with a coarse mesh in cases where the electron temperature at a wall point is set equal

to the gas temperature leading to large electron temperature gradients in the regions of current concentration near the electrode edges. In the present work, the numerical instability occurs when a coarse mesh is employed and the initial value of the surface coverage is taken to be much larger than the equilibrium value leading to large electron temperature gradients. The instability does not occur in the case considered in chapter 5, even though a coarse mesh of 17 points in the x-direction is employed.

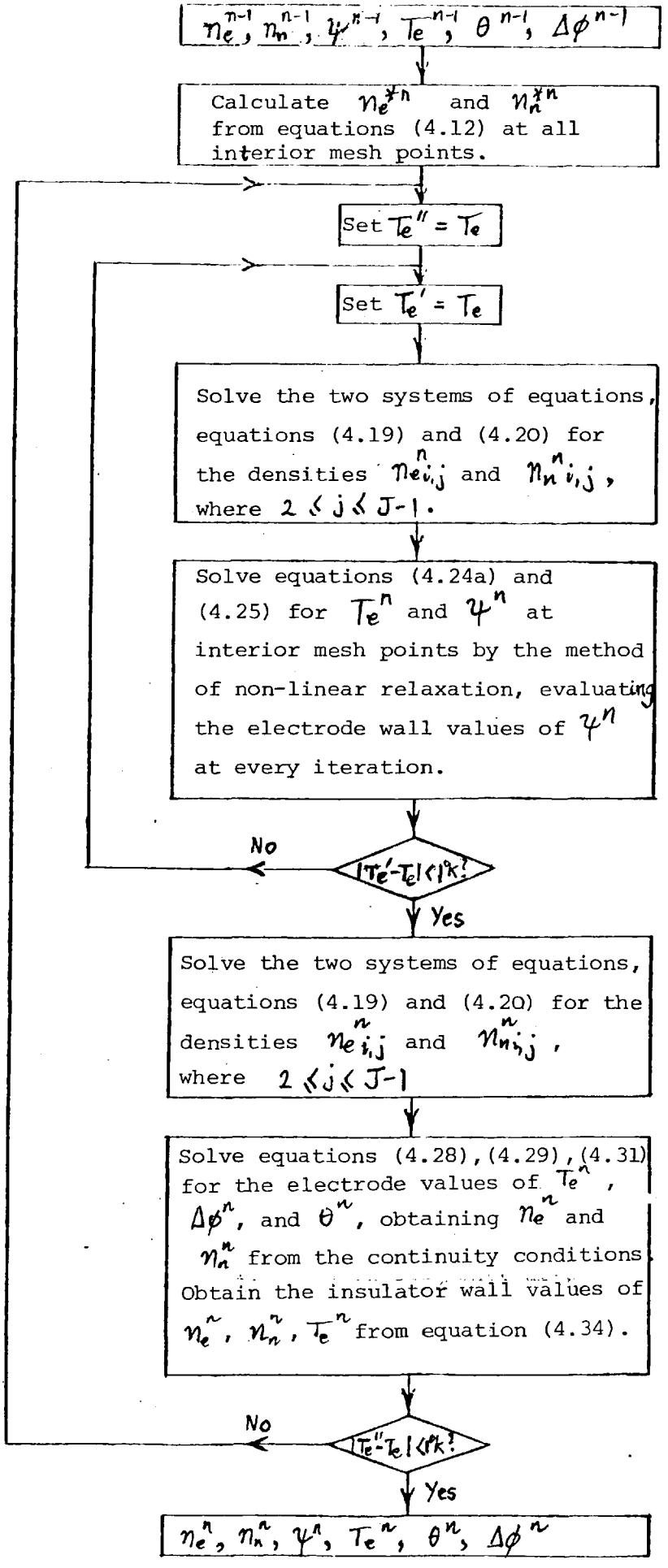

Fig. 4.1: Updating Procedure for Constant Time Step

CHAPTER 5

RESULTS OF COMPUTATIONS OF THE LOCAL BEHAVIOUR IN A CLOSED CYCLE MHD GENERATOR

5.1 Introduction

In this chapter some results of computations of the temporal development of the local plasma and electrical behaviour in a single segment of a closed cycle MHD generator, using the numerical method developed in the last chapter, are presented and discussed.

Similar computations have been reported by other authors, in particular, Kolb[18], Uncles[8] and Argyropoulos[24]. Of these studies that of Uncles appears to be the most advanced in that, as well as including physical processes not previously considered by other authors the temporal development of the plasma and electrical behaviour is followed up to times long enough for quasi-steady state conditions to be established. In addition, effects of varying the channel dimensions and applied magnetic field are considered in reference (8). In particular, generator operation in the regimes of stability and instability of the ionization mode of electrothermal waves (see appendix C) is investigated. An important result of the computations performed by Uncles is the possibility that non-uniformities introduced by the finite segmentation can grow into 'streamers', or high conductivity paths, transverse to the gas flow, along which the bulk of the current can flow. As a result, the effective electrical conductivity σ_{eff}, introduced in chapter 1, is increased by a factor of about two over the average conductivity $\langle\sigma\rangle$. This result is in contrast to the linear theory of the electrothermal instability, which predicts, for a weakly unstable plasma, the occurrence of plane-wave

like plasma non-uniformities at an angle of about 45^{o} to the channel axis, leading to reduction of the ratio $\sigma_{eff}/\langle\sigma\rangle$ [41].

However, as mentioned earlier, the work of Uncles excludes a number of important physical processes, which have previously been considered only in the case of open cycle MHD generators, in which steady-state plasma and electrical behaviour can be assumed. As mentioned in the introduction, emphasis in the present work is more on the development of a physical model incorporating some of these effects, together with some effects not previously considered, and the development of numerical methods of solution of the governing equations. Thus detailed analysis of computational results in terms of the acting physical mechanisms for various generator operating conditions and dimensions is not attempted here. Instead, some computational results obtained for one representative set of generator operating conditions are presented and discussed in this chapter.

The large demands made on computer time by the program that solves the plasma and electrical problem necessitates restriction to one set of generator operating conditions. For the same reason a rather coarse space mesh of 49 points in the cross-stream ζ (or y-) direction and 17 points in the x-direction is employed and the computation not performed for a long enough time for a quasi-steady final state to be reached. Fortunately, the numerical instability reported by Kolb[18], discussed in section 4.6 is not encountered in the computer run considered here even though the step size in the x-direction exceeds the characteristic length scale for electron thermal conduction. The reason for this has already been given in section 4.6.

The generator conditions considered in this chapter are representative of those of the experimental runs of the IRD closed loop

facility carried out in October 1977 (see section 3.5). Thus, as in section 3.5, the gas-dynamic conditions of run 7 are considered, and the channel dimensions at the location of electrode pair 2 are used; that is, $L = 2.54 \times 10^{-2}$ m, $H = 2.23 \times 10^{-2}$ m, $W = 1.08 \times 10^{-2}$ m. With a mesh of 17 points in the x-direction the number of mesh points allocated to each electrode is 7, yielding an effective electrode length of 9.5 mm , which is equal to the electrode diameter. Whilst the actual electrode cross-section is circular, application of the two-dimensional numerical model requires that an electrode of rectangular cross-section be considered. Thus, the electrode length in the x-direction is taken to be 9.5 mm , while the electrode length in the transverse z-direction is taken to be equal to the channel width; i.e., 1.08×10^{-2}m. This gives an effective electrode area of 10.29×10^{-5} m^2 compared with an actual electrode area of 7.13×10^{-5} m^2. This difference in electrode area must be allowed for in any attempt to compare numerical and experimental results.

The gas pressure and electrode wall gas velocity and gas temperature profiles are obtained from the solution of the boundary layer equations discussed in section 3.5, the appropriate x-location being taken to be that of the centre of electrode pair 2.

Experimentally it is found that, for a seeding fraction of 0.002, inlet ionization relaxation is completed well before electrode pair 2[4]. Therefore the latter value of seeding fraction is used to initialize the computation. The corresponding equilibrium value of the surface coverage (see section 2.7) is approximately 0.35; this is taken to be the initial value of the surface coverage at all electrode mesh points.

The applied magnetic field is taken to be 0.7 Tesla. At higher magnetic fields, convergence problems are encountered in the numerical solution of the coupled current stream function and electron energy equation using the method of section 4.4 due to concentrations of current at the downstream edge of the cathode and upstream edge of the anode. A satisfactory method of overcoming these convergence problems has not been found. Of course it is only at magnetic fields sufficiently large for the plasma to be locally unstable that the electrothermal instability can have any effect on the local plasma and electrical behaviour and derived generator characteristics.

It was shown in section 2.7 that, for a surface coverage of 0.35, $\nu_i \ll \nu_e$ and the emitted electron current density is 3813 A/m^2. Numerical experiments show that convergence problems arise in calculating the electrode wall values of $\Delta\phi$ and T_e for $\theta = 0.35$ using the method of section 4.5 when the applied current exceeds about 0.1A. The average electrode current density for an applied current of 0.1A is 972 A/m^2, which is much less than the emitted current density. However, due to the Hall effect, large concentrations of current occur at the downstream edge of the cathode where the current density is much larger than the average value. As a result, saturation can occur in the region of current concentration with the sheath voltage drop tending to infinity, even when an applied current much less than the emitted electron current is used. This problem becomes increasingly severe as the mesh step in the x-direction is reduced due to the enhancement of current concentration. The results presented in this chapter are obtained with a fixed current of 0.1A, applied in the direction of the $\underline{u} \wedge \underline{\beta}$ emf. Whilst finite interaction between the

plasma and external load circuits is allowed in the theory of Uncles[8], it is not considered in the present work.

The size of the time step used in the time integration of the equations is chosen in accordance with the considerations of section 4.6, in order to ensure the stability and accuracy of the obtained solutions. As mentioned in section 4.6, the characteristic time scale for ionization $\tau_I = |1/[A_1 (n_n - n_e)]|$ is considered in place of the growth/decay time of the electrothermal instability in obtaining the solutions reported in the next section. Denoting the characteristic time scales for convection and x-diffusion by τ_u and τ_{dx} (see appendix C), a minimum time scale $\tau^{(1)}_{min}$ is first obtained from the solutions at any given time level as follows:

$$\tau^{(1)}_{min} = \left((\tau_I)_{min}, (\tau_u)_{min}, (\tau_{dx})_{min} \right)_{min}$$

If the time step is chosen as $\Delta t = 0.1\, \tau^{(1)}_{min}$, the solutions obtained, whilst stable, are inaccurate. This is due to the smallness of the characteristic time scale for cross-stream diffusion, which can be defined as follows:

$$\tau_{dy} = \frac{m_{ih} V_{ih} \Delta\xi^2}{\xi^2 k_B T},$$

where, typically, $(\tau_{dy})_{min} \lesssim 0.1\, \tau^{(1)}_{min}$. In order to obtain accurate solutions the time step Δt is chosen as

$$\Delta t = 0.1 \sqrt{(\tau_{dy})_{min}\, \tau^{(1)}_{min}}$$

5.2 Analysis of Results and Conclusions

(a) State at t = 0

The initial plasma and current distributions are obtained by the method described in section 4.5. Thus, the n_e, n_n, ψ and $\overline{T_e}$ distributions are first computed using the simplified form of electron energy equation, equation (1.9); Saha's equation,

equation (1.14); and Laplace's equation $\nabla^2\psi = 0$, subject to the boundary conditions $\partial\psi/\partial y = \beta_c \partial\psi/\partial x$ on the electrodes and ψ = constant on the insulators. The seeding fraction is taken to be a specified constant (χ = 0.002). From the resultant n_e and n_n distributions, the initial values of n_e and n_n at all mesh points, except those lying on the electrodes and insulators, are obtained. The initial T_e and ψ distributions as well as the electrode values of $\Delta\phi$, ψ, n_e, n_n and $\overline{T_e}$, and insulator values of n_e , n_n and $\overline{T_e}$ are then obtained by solving the coupled electron energy and current stream function equations consistently with the wall boundary conditions for a fixed surface coverage (θ = 0.35).

Figure 5.1 shows the computed anode sheath voltage drop $\Delta\phi_a$ and cathode sheath voltage drop $\Delta\phi_c$ distributions at t = 0. Contour plots representing the initial T_e , ψ and n_e distributions in (x, ζ) space are shown in figures 5.4, 5.5 and 5.6; the relation between ζ - and y-coordinates is shown in figure 5.7, in which the distribution of Faraday voltage along the line through the electrode centres is also shown. The initial value of the average Hall parameter $\langle\beta_e\rangle$ is 1.39.

It can be seen from figure 5.1 that the sheath voltage drop is positive everywhere on the anode and cathode, the electron density on both electrodes satisfying the condition $n_{ew} > \frac{2}{C_{es}}\left(1 + \frac{C_{es}}{C_{ew}}\right) V_e$ (see (2.271)). The sheath voltage drop has a maximum value at the downstream edge of the cathode where the current density is maximum in magnitude.

The initial ψ distribution is represented by a contour plot in figure 5.5 in which the contour interval $\Delta\psi$ is taken to be $1\,A/m$ and the value of ψ on a contour numbered "p" is given by

$$\psi(p) = (p-1)\Delta\psi$$

The orientation and relative separation of the contours represents the direction of current flow and magnitude of current density respectively.

The tendency of the current to concentrate at the upstream edge of the anode and downstream edge of the cathode as a result of the Hall effect can clearly be seen in figure 5.5. It is also clear that there is an asymmetry between anode and cathode conduction; this is a result of the large asymmetries in the electron temperature distribution, and is further discussed below.

The initial electron temperature distribution is represented by a contour plot in figure 5.4 in which the contour interval ΔT_e is taken to be $150^{o}K$ and the value of electron temperature on a contour numbered "p" is given by

$$T_e(p) = (p + n_{min} - 1)\,\Delta T_e$$

where $p \geq 1$, and n_{min} is the minimum integer such that $T_e(1) = n_{min}\Delta T_e > T_{emin}$; the minimum electron temperature is T_{emin}.

In figure 5.4, a high electron temperature region can be seen to exist in the plasma near the downstream edge of the cathode, the electron temperature decreasing rapidly from its maximum value of $3192^{o}K$ at the downstream edge to values close to the wall temperature ($1316^{o}K$) towards the upstream edge. However, a region of relatively low electron temperature exists near the anode surface; the electron temperature decreases rapidly from $1570^{o}K$ at the upstream edge to values close to the wall temperature towards the

downstream edge. At some points on the anode the electron temperature is actually less than the wall temperature; the electron temperature has its minimum value of $1216^{o}K$ at the anode mesh point adjacent to the upstream edge. The temperature profile on the insulator segment upstream of the anode has a maximum about equal to the electron temperature at the corresponding point on the insulator segment downstream of the cathode. However, instead of a high electron temperature region similar to that near the downstream edge of the cathode, which extends some distance along the adjacent insulator segment, there is a region of high electron temperature gradient near the upstream edge of the anode, opposite which there is a small region of high electron temperature.

This large asymmetry in the electron temperature distribution is due to the asymmetrical effect of the electron pressure gradient on the Ohmic heating near the anode and cathode, together with the asymmetry of the anode and cathode wall boundary conditions on the electron energy equation derived in section 2.7.

As we shall see later in this section, application of the ion continuity conditions yields electron density gradients of very large magnitude near the upstream edge of the anode and downstream edge of the cathode (see figure 5.6). The electron pressure gradients are also large in magnitude at these points and, since the directions of these gradients are almost parallel or antiparallel to the current density, they have large effects on the Ohmic heating.

The effect of the electron pressure gradient on the Ohmic heating is neglected in the simplified form of the electron energy equation, equation (1.9), which is used to obtain the original electron temperature distribution. If the effect of the electron pressure gradient is included, the Ohmic heating term has the form (see equation (2.224))

$$\underline{E}' \cdot \underline{J} = J^2/\sigma_e - \underline{J} \cdot \nabla p_e/(en_e) \; . \qquad (5.1)$$

Near the downstream edge of the cathode, the term $\underline{J} \cdot \nabla p_e/(en_e)$ in equation (5.1) is negative and large in magnitude; this results in an increased Ohmic heating, leading to values of electron temperature larger than those obtained using the simplified form of electron energy equation. The region of plasma near the downstream edge of the cathode, in which the electron temperature is increased, coincides with the region of highest electron density nearest the cathode wall, as can be seen by comparing figures 5.4 and 5.6. The large electron density gradients in the downstream direction in a region near the downstream edge of the cathode (electrode side) yield values of $\underline{J} \cdot \nabla p_e/(en_e)$ that are small in magnitude; this, together with the rapid decrease of $|\underline{J}|$ in the upstream direction, leads to large electron temperature gradients in the downstream direction in the same region.

Near the upstream edge of the anode, the term $\underline{J} \cdot \nabla p_e/(en_e)$ in equation (5.1) is large and positive; this results in decreased Ohmic heating, leading to values of electron temperature smaller than those obtained using the simplified form of electron energy equation. This reduction of the electron temperature occurs to a lesser extent over much of the remainder of the region near the anode surface. With increasing distance from the anode surface, near the upstream edge, the electron pressure gradient rapidly decreases in magnitude and the Ohmic heating rapidly increases; this results in a region of high electron temperature gradient near the upstream edge of the anode.

The sheath voltage drop at every point on the anode and cathode surfaces is positive. The appropriate electrode wall boundary condition on the electron energy equation in this case can be written as an expression for the y-component of the electron heat flux at a wall mesh point (see equation (2.282)) of the form

$$(q_{ey})_w = \frac{5}{2} k_B T_{ew} \Gamma_{ey} - \frac{\lambda_{ew}}{(1+\beta_{ew}^2)} \left(\frac{\partial T_e}{\partial y}\right)_w$$

$$= \varepsilon \left[\nu_e \left(2k_B T_w + e\Delta\phi\right) - \left(\nu_e - \varepsilon \bar{\Gamma}_{ey}\right) \left[2k_B T_{ew} + e\Delta\phi\right] \right], \quad (5.2)$$

where $\varepsilon = +1$ for the cathode and $\varepsilon = -1$ for the anode. In equation (5.2), the net y-component of electron flux $\bar{\Gamma}_{ey}$ is given by

$$\bar{\Gamma}_{ey} = -\frac{1}{e} J_y + \bar{\Gamma}_{iy} . \quad (5.3)$$

Using the expression for $\bar{\Gamma}_{iy}$ given by equation (2.256) we can write equation (5.3) in the form

$$\bar{\Gamma}_{ey} = -\frac{1}{e} J_y + \varepsilon \left(2\nu_i h_i - \frac{1}{2} n_{ew} c_{iw}\right).$$

As in section 2.7 we have, for typical values of n_{ew}, $2\nu_i h_i \ll \frac{1}{2} n_{ew} c_{iw}$ so that

$$\bar{\Gamma}_{ey} \simeq -\frac{1}{e} J_y - \varepsilon \frac{1}{2} n_{ew} c_{iw} . \quad (5.4)$$

Making use of equation (5.4) we can write equation (5.2) in the form

$$(q_{ey})_w = \varepsilon \left[\nu_e \left(2k_B T_w - 2k_B T_{ew}\right) + \left(-\frac{1}{e} J_y \varepsilon - \frac{1}{2} n_{ew} c_{iw}\right)\left(2k_B T_{ew} + e\Delta\phi\right) \right] \quad (5.5)$$

From equation (5.5) the expressions for the y-component of electron heat flux at the cathode and anode walls are

Cathode Mesh Point	1	2	3	4	5	6	7
$2\nu_e k_B(T_w - T_{ew})$	-17	-32	-48	-21	-359	-1043	-921
$-\frac{1}{e} J_y$	4×10^{20}	7×10^{20}	10^{21}	7×10^{20}	-5×10^{21}	2×10^{22}	2×10^{22}
$\Gamma_{iy} \simeq -\frac{1}{2} n_{ew} c_{iw}$	-4×10^{19}	-4×10^{19}	-4×10^{19}	-4×10^{19}	-5×10^{19}	-7×10^{20}	-2×10^{21}
$\Gamma_{ey}(2k_B T_{ew} + e\Delta\phi)$	-6	16	23	15	-195	3169	5724
$(q_{ey})_w$	-23	-17	-26	-7	-554	2126	4802
$\frac{5/2 k_B T_{ew} \Gamma_{ey}}{(q_{ey})_w}$	-0.6	-2	-1.9	-4.8	0.6	0.8	0.4

$$(q_{ey})_w = \nu_e \left(2k_B T_w - 2k_B T_{ew}\right) + \left(-\frac{1}{e} J_y - \frac{1}{2} n_{ew} c_{iw}\right)\left(2k_B T_{ew} + e\Delta\phi\right) \quad (5.6)$$

and

$$(q_{ey})_w = -\nu_e \left(2k_B T_w - 2k_B T_{ew}\right) + \left(-\frac{1}{e} J_y + \frac{1}{2} n_{ew} c_{iw}\right)\left(2k_B T_{ew} + e\Delta\phi\right) \quad (5.7)$$

respectively.

Considering the cathode wall, the y-component of electron heat flux given by equation (5.6) decreases very rapidly from positive to negative values with increasing distance from the downstream edge. This rapid reduction is due to the rapid decrease of $|J_y|$, T_e and $\Delta\phi$, and is clearly shown in the table on the opposite page in which cathode mesh points are numbered from the upstream edge. The large value of $(q_{ey})_w$ near to the downstream edge, together with the heating effect of the electron pressure gradient leads to the existence of the region of high electron temperature described above. However, the rapid reduction of $(q_{ey})_w$ with increasing distance from the downstream edge allows the existence of the region of relatively low electron temperature in which the Ohmic heating is small.

The high Hall parameter in the low temperature region near the cathode results in a tendency for the current to be concentrated near the downstream edge of the cathode. This tendency is opposed by the high conductivity in the low temperature region.

The y-component of electron heat flux at the anode wall, as given by equation (5.6), is negative over much of the electrode surface and rapidly decreases in magnitude with increasing distance from the upstream edge, actually becoming positive at a point where the direction of the current reverses (see figure 5.5). The magnitude of $(q_{ey})_w$ at the upstream edge of the anode is much less than the value

of $(q_e j)_w$ at the downstream edge of the cathode, due to the smaller values of T_e and $\Delta\phi$ at the upstream edge of the anode. This, together with the reduction of the Ohmic heating due to the finite electron pressure gradient, results in the existence of the region of low electron temperature near the anode surface.

The low electron temperature in the region of the plasma near the upstream edge of the anode results in a higher conductivity and Hall parameter in this region compared with the conductivity and Hall parameter in the region of the plasma near the downstream edge of the cathode. As a result, the concentration of current is greater near the upstream edge of the anode, as can be seen in figure 5.5.

Figure 5.5 shows the existence of current stream lines that begin and end on the same electrode; some of these stream lines are located near the upstream edge of the anode, and some are located near the downstream edge of the cathode. The occurrence of these stream lines is due to the term dependent on the gradient of the electron pressure in Ohm's law. This term is important in the high electron density gradient regions near the upstream edge of the anode and near the downstream edge of the cathode (see figure 5.6).

The initial electron density distribution is represented by a contour plot in figure 5.6 in which the contour interval Δn_e is taken to be $0.5 \times 10^{18}\ m^{-3}$, and the value of electron density on a contour numbered "p" is given by

$$n_e(p) = p\,\Delta n_e$$

where $p \geq 1$.

Regions of large electron density gradients are seen to exist near the upstream edge of the anode and downstream edge of the cathode.

From Saha's equation, it follows that, $|\nabla n_e / n_e| >> |\nabla T_e / T_e|$; that is, the fractional electron density variations are much larger than the fractional variations of electron temperature determined from the simplified form of electron energy equation. The very large cross-stream variations of electron density at the anode and cathode surfaces follow from the application of the ion continuity condition (2.258) of section 2.7, which is the relevant condition since $\Delta\phi > 0$ everywhere. This results in an electron density at each point that is much less than the Saha value at the original electron temperature. This is due to the fact that electrons are lost to both electrodes, since $\nu_i h_i << \frac{1}{2} n_{ew} c_{iw}$ and $\Gamma_{iy} \simeq -\varepsilon \frac{1}{2} n_{ew} c_{iw}$; that is, $\Gamma_{iy} < 0$ on the cathode, and $\Gamma_{iy} > 0$ on the anode.

The seed atom density distribution, which is not given here, shows little variations in the x-direction because conditions are such that the degree of ionization is very small. However, the seed atom density at each point on the electrodes is slightly larger than the corresponding value obtained from a seeding fraction of 0.002. This is due to the fact that the value of θ in the equilibrium case is not exactly equal to 0.35. It is found that $\Gamma_{ny} > 0$ at the cathode and $\Gamma_{ny} < 0$ at the anode, and there is initially a flux of seed atoms from each point of either electrode into the plasma.

The Faraday voltage distribution at t = 0 is shown in figure 5.7. This is obtained by integrating the y-component of electric field along the electrode centre-line. Near y = 0, the voltage increases

rapidly with y due to the effect of the y-component of the electron pressure gradient, which is large and positive in magnitude in a narrow region near the cathode wall in which the electron density rapidly increases from small values at the wall. However, with increasing distance from the cathode, the y-component of electron pressure gradient and, therefore, the magnitude of the y-component of electric field rapidly decrease and the voltage gradient greatly decreases after a short distance from the wall. Similar behaviour occurs near the anode, where the existence of a narrow region in which the electron density decreases rapidly towards the wall and the electron pressure gradient is large in magnitude and negative leads to a rapid reduction of voltage gradient to negative values near the wall.

At most points on the electrode centre-line, the voltage gradient is positive due to the existence of an x-component of the current density, and the Faraday voltage across the channel is positive. Therefore, as a result of the Hall effect, the system acts as a resistive load rather than as a generator of electrical power.

(b) State at $t > 0$

The temporal development of the plasma and current distributions and derived generator characteristics is followed numerically up to a time $t = 8 \times 10^{-6}$ sec. This is to be compared with the minimum cross-stream diffusion and ionization time scales, which are 8×10^{-9} sec and 2.6×10^{-7} sec, respectively, at the initial time $t = 0$. While the cross-stream diffusion time scale remains constant, the ionization time scale increases slightly to 3.4×10^{-7} sec at the final time. The minimum convection time scale is constant and equal to 1.3×10^{-6} sec.

(i) Plasma and current distributions

Figure 5.3 shows the variation with time of the maximum, minimum and average values of the seeding fraction; these quantities are denoted by χ_{max}, χ_{min} and $\langle\chi\rangle$ respectively. While $\langle\chi\rangle$ remains constant and equal to the initial value of 0.002, χ_{max} increases to a maximum of 2.12, and χ_{min} decreases to a minimum of 1.7 in a time of about 1.5×10^{-7} sec. Both χ_{max} and χ_{min} then gradually approach steady values.

These variations of χ_{max} and χ_{min} are due to diffusion of electrons and neutrals and possibly also ionization; the time scale for recombination (initially about 3×10^{-5} sec) is too long for it to be of any importance in the initial variations of seeding fraction.

The seeding fraction is maximum near to the downstream edge of the cathode and minimum near to the downstream edge of the anode.

The anode and cathode distributions of surface coverage at the final time of the computation ($t = 8 \times 10^{-6}$ sec), shown in figure 5.2, have features similar to the distributions at times $t < 1.5 \times 10^{-7}$ sec. The increase of surface coverage above the equilibrium value near to the downstream edge of the cathode is an important result of the theory. A similar result is found in the work of Koester et al.[30]; it means that the possibility exists of passing currents greatly in excess of the equilibrium emitted electron current without onset of arcing.

The seeding fraction is maximum near the downstream edge of the cathode and minimum near the downstream edge of the anode.

The anode and cathode sheath voltage drop distributions at $t = 8 \times 10^{-6}$ sec are compared with the distributions at time $t = 0$ in figure 5.1. It can be seen that, as at $t = 0$, the cathode sheath voltage drop is positive near to the downstream edge, having a maximum value at the edge; this maximum is larger at the later time due to increased current concentration (see below). Farther upstream the sheath voltage drop has decreased to negative values due to the electron density having decreased to the extent that condition (2.271) is no longer valid; this condition remains valid at the downstream edge and the mesh point nearest this edge.

The sheath voltage drop over the entire anode surface can be seen to have decreased to negative values at $t = 8 \times 10^{-6}$ sec. This is due, in part, to the electron density having decreased to the extent that condition (2.271) is invalidated at all mesh points with the exceptions of the upstream edge and the adjacent mesh point.

Contour plots representing the electron temperature, current and electron density distributions in (α, ζ) space at time $t = 8 \times 10^{-6}$ sec are shown in figures 5.8, 5.9 and 5.10. Contour intervals are the same as for $t = 0$. The Faraday voltage distribution at $t = 8 \times 10^{-6}$ sec is shown in figure 5.11.

In figure 5.10 it can be seen that the high electron density gradient region adjacent to the anode wall (see figure 5.6) has spread out into a larger region, the electron density on and near the anode decreasing in value. This is probably due to ion diffusion and leads to an enhancement of conductivity in a region near the insulator segment upstream of the anode, resulting in a deviation of the current streamlines towards the insulator segment, together with a slight displacement of the current streamlines towards the upstream edge (see figure 5.9). This, in turn, results in an increased Ohmic

heating in the region of the plasma upstream of the anode, leading to an increase of electron temperature and, by ionization, to an increase of electron density in that region (see figures 5.8 and 5.10). These enhancements of electron temperature and density are allowed by the boundary conditions at the insulator walls (see section 2.7).

A similar spreading of the high electron density gradient region adjacent to the cathode can be seen to occur in figure 5.10, the electron density on and near to much of the cathode surface also decreasing in value. However, this leads to a slight deviation of the current lines towards the insulator segment downstream of the cathode compared to the deviation towards the insulator segment upstream of the anode (see figure 5.9). This is probably because of the region of high electron temperature near the downstream edge of the cathode, which includes part of the cathode itself; the electron density and conductivity at and opposite the downstream edge are actually enhanced. The extent of the region of high electron temperature and high electron density adjacent to the insulator segment downstream of the cathode is therefore less than that of the similar region adjacent to the insulator segment upstream of the anode (see figures 5.8 and 5.10). However, there is an increase in current concentration near the downstream edge of the cathode, probably due to the enhancement of conductivity at the edge itself.

The effect of convection on the electron density and current distributions is quite clearly shown in figures 5.9 and 5.10. The high electron density and electron conductivity regions upstream of the anode and near the downstream edge of the cathode can be seen to be displaced downstream. This results in a downstream displacement of the current lines. However, near the wall the flow velocity is low and the effects of convection are negligible. In particular, the region of high electron density upstream of the anode is not displaced

by convection into the anode itself, on and near the surface of which the electron density can attain relatively low values.

Figure 5.10 shows the existence of a small peak in the electron density distribution at a point on the line joining the centres of the electrodes (electrode centre-line). This is a result of reduction of electron density near the centre of the segment due to convection, and upstream displacement of the high electron density region close to the wall, near to the downstream edge of the cathode.

This peak has an important effect on the Faraday voltage profile, as can be seen in figure 5.11. It can be seen in figure 5.9 that the current density near the cathode surface is small along the electrode centre-line, and the y-component of electric field depends mainly on the y-component of electron pressure gradient. The latter is large and the voltage gradient therefore positive, near the cathode surface where the electron density increases rapidly from small values at the wall. With increasing distance from the wall, the y-component of electron pressure gradient and, therefore, the voltage gradient decrease to negative values beyond the peak in electron density. As a result, the voltage rises to a maximum value and then decreases to negative values. The voltage reaches a negative minimum and begins to rise again where the y-component of electron pressure gradient is small and the x-component of current density is large, resulting in a positive voltage gradient. The latter becomes increasingly larger as the high electron density region near the anode is approached and the y-component of electron pressure gradient increases. Near the anode surface the current density along the electrode centre-line again decreases because of the concentration of current near the upstream edge of the anode. This, coupled with the negative y-component of electron pressure gradient in the region near the anode

surface beyond the peak in electron density, results in a reduction of the voltage gradient, the voltage profile becoming almost flat near the anode surface.

As can be seen in figure 5.11, the voltage gradient over much of the region near the centre of the electrode centre-line is positive and larger than t = 0 (see figure 5.7). This is due to the increased concentration of current near the downstream edge of the cathode, and to the downstream displacement of current lines near to the anode. This leads to an increased current density in a region near the centre of the electrode centre-line, and the increased x-component of current density results in an increased voltage gradient in the same region.

As at t = 0, the voltage gradient is positive at most points on the electrode centre-line due to the x-component of the current density, and the Faraday voltage across the channel is positive. Again, the system acts as a resistive load rather than as a generator of electrical power.

(ii) Overall generator parameters

Figure 5.12 shows the variation with time of the overall generator parameters $\sigma_{eff}/\langle\sigma_e\rangle$, $\beta_{eff}/\langle\beta_e\rangle$, β_{eff} and $\langle\sigma_e\rangle$; and figure 5.13 shows the variation in time of the Faraday voltage V_y, and the cathode and anode voltage drops δV_c and δV_a, which are defined by linearly extrapolating the Faraday voltages at the boundary layer edges. Thus, if $V_\delta^{(c)}$ and $V_\delta^{(a)}$ are the voltages with respect to the cathode at points on the electrode centre-line at the edges of the boundary layers on the cathode and anode walls, respectively, δV_c and δV_a can be written as follows:

$$\delta V_c = V_\delta^{(c)} - \frac{\left(V_\delta^{(a)} - V_\delta^{(c)}\right)}{(H - 2\delta)}\delta + \Delta V_c$$

and

$$\delta V_a = V_y - V_\delta^{(a)} - \frac{\left(V_\delta^{(a)} - V_\delta^{(c)}\right)}{(H - 2\delta)}\delta - \Delta V_a$$

The anode and cathode sheath voltage drops, ΔV_a and ΔV_c, make only small contributions to δV_c and δV_a at all times, except the instant at which δV_c changes sign (see figure 5.13).

The average Hall parameter $\langle \beta_e \rangle$ is approximately constant in time decreasing continuously from 1.39 at t = 0 to 1.37 at t = 8 x 10^{-6} sec.

It is clear from these plots that the time interval of the numerical integration is not of sufficient length for the plasma to be in at least a quasi-steady state by the end of the computation. For example, the cathode voltage drop is increasing towards positive values at the final time of the computation.

Figure 5.12 shows a continuous increase of $\langle \sigma_e \rangle$ with time. This is due to the continuous increase in time of the average electron density resulting from the spreading of the high electron density regions near the insulator segment upstream of the anode and near the downstream edge of the cathode. Due to convective displacement of the high electron density regions, the slope of the $\langle \sigma_e \rangle$ curve increases suddenly at a time of about 4.5 x 10^{-6} sec, which is the time taken for the gas to travel a distance equal to half the electrode length when the gas velocity is equal to the average gas velocity.

However, it can be seen in figure 5.12 that the effective conductivity σ_{eff} decreases at a rate greater than that at which $\langle \sigma_e \rangle$ increases, resulting in a continuous decrease of the ratio $\sigma_{eff}/\langle \sigma_e \rangle$ with time. This rapid decrease of σ_{eff} results from

the increase of the Faraday voltage V_y with time, which can be seen in figure 5.13. The positive value of V_y implies that the system behaves as a resistive load rather than as a generator; this has already been mentioned in discussions of the initial and final voltage distributions.

The increase of V_y with time is due to the simultaneous increase in current concentration near the downstream edge of the cathode and (to a lesser extent) near the upstream edge of the anode with time, together with downstream displacement of the current stream lines by the gas flow. These processes result in a decrease of effective area and an increase of effective path length of the current flow, and therefore an increase in internal impedance with time. The increase of effective path length by convection is the slower process and begins to have a large effect only after a time of about 4.5×10^{-6} sec has ellapsed; the significance of this time has already been indicated above.

These two processes also result in a decrease in time of the effective Hall parameter β_{eff} (see figure 5.12), because of the increase with time of the length of the region of the channel centre-line in which the x-component of the current density is significant, together with the increase with time of the magnitude of the x-component of the current density in that region.

The variation with time of the anode and cathode voltage drops is shown in figure 5.13. The continuous increase of the anode voltage drop with time is due to the continuous decrease with time of the conductivity in the low conductivity region near the anode

The initial decrease with time of the cathode voltage drop is due to the decrease with time of the electron pressure gradient in the region of the plasma opposite the cathode in which the magnitude of the current density decreases as the current becomes increasingly concentrated near the downstream end of the cathode. Eventually, the voltage drop becomes negative and then increases with time. The time at which the voltage gradient becomes positive is about 4.5×10^{-6} sec; the significance of this time has been mentioned above. The increase of the voltage drop with time is due to convection, which displaces the electron density peak downstream.

5.3 Comparison with Numerical Results of Uncles[8]

As stated in chapter 1, the present work may be regarded as an extension of the work of Uncles[8] to include the effects of turbulent boundary layers, turbulent transport processes, finite seed ion and seed atom diffusion and plasma-wall interactions, including seed-electrode interactions. In addition, by making the assumption of instantaneous electron temperature relaxation (see section 2.5), instead of Saha equilibrium as in reference (8), the numerically inconvenient fast thermal mode is eliminated without having to neglect the effects of finite ionization and recombination rates. However, the effects of Coulomb collisions, and finite interactions between external load circuitry and the plasma, considered in reference (8), have been neglected in the present work. These essential differences between the present theoretical model and that of Uncles must be considered in any detailed attempt to compare the numerical results presented in this chapter with those obtained by Uncles.

Comparison with results obtained by Uncles is made difficult by the different method used here to initiate the computations. In the present method the distributions of plasma parameters are first obtained by assuming a local balance between Joule heating and energy loss by electrons in elastic collisions with heavy particles (see equation (1.9)), together with local Saha equilibrium with a constant seeding fraction; the current field is first taken to be governed by Laplace's equation $\nabla^2\psi = 0$. Having obtained the initial electron density and seed atom density distributions the coupled current stream function and electron energy equations are solved consistent with the boundary conditions to obtain the initial electron temperature and current stream function distributions, together with the wall boundary values of electron density and seed atom density.

In the work of Uncles, the generator fluid is assumed to consist of argon slightly seeded with caesium; the seeding fraction is 0.001. The gas temperature and initial electron temperature are assumed to be uniform with $T = 1500^{o}K$ and $T_e = 3000^{o}K$, and the initial electron density is obtained from the Saha equation. The plasma state is assumed to be maintained by a uniform discharge along the channel. At $t = 0$ this discharge is removed, and external voltage sources applied to each electrode pair. The voltage sources are chosen to provide an average current density approximately equal to that sustaining the original non-equilibrium state.

Comparison shows there to be some similarities between the results obtained by Uncles for initial Hall parameters $0.3 < \beta_{e_o} \leq 1.6$ and the results obtained here for which the initial average Hall parameter $\langle \beta_e \rangle = 1.39$. The average gas temperature is $1519^{o}K$, and the average and maximum values of the electron temperature are $1715^{o}K$

and 3192°K, respectively.

Both the present theory and that of Uncles predicts a continuous decrease with time of the generator parameters $\sigma_{eff}/\langle\sigma_e\rangle$ $\beta_{eff}/\langle\beta_e\rangle$ and β_{eff} . Uncles finds that the solutions saturate and steady-state conditions are reached after a time of about 10^{-4} sec. The computation in the present work is not continued for a sufficient length of time for the solutions to saturate.

Probably due to the absence of plasma non-uniformities in the initial state, the initial values of $\sigma_{eff}/\langle\sigma_e\rangle$ and $\beta_{eff}/\langle\beta_e\rangle$ predicted by Uncles' theory are larger than those predicted by the present theory, though this may to some extent be due to conditions being such that the initial average electron temperature is lower in the present case.

The main features of the current and electron density distributions in the final steady-state obtained by Uncles that can be compared with the numerical results presented here are found to be

(i) The existence of an asymmetry of the current distribution between the anode and cathode.

(ii) A rather more uniform electron density near the anode than that near the cathode.

(iii) A higher electron temperature at the current concentration point on the cathode than at the current concentration point on the anode.

The features (i)-(iii) owe their existence to the asymmetrical effect of the electron pressure gradient on the Ohmic heating. Similar features, though greatly complicated by the additional physical processes involved, have been discussed in this chapter.

In reference (8), it is demonstrated that there are two regimes of operation of the non-equilibrium segmented electrode generator, $<\beta_e> > \beta_{crit}$ and $<\beta_e> < \beta_{crit}$, where $\beta_{crit} \sim 2$ is the critical Hall paramater of the electrothermal instability. In the work of Uncles it is found that, when $L/H \sim 1$, nonuniformities introduced by finite segmentation can grow into streamers or high conductivity paths, transverse to the gas flow, along which the bulk of the current can flow. As a result, the ratio $\sigma_{eff}/<\ _e>$ increases to a value of about two.

In the present work conditions have been taken to be such that generator operation is initially stable as a whole, the growth time of the electrothermal instability having a maximum negative value of -1.3×10^{-6} sec and a minimum positive value of 2.15×10^{-6} sec. Whilst the growth time for the final state has a maximum negative value of -9.8×10^{-7} and a minimum positive value of 3.22×10^{-8} sec, the overall behaviour can be compared to that found by Uncles in the stable regime. As can be seen in figure 5.9, the discharge near the midpoint of the line joining the downstream edges of the electrodes is somewhat like a streamer. However, the growth time of the electrothermal instability at this point is -1.875×10^{-3} sec, so that this structure is not due to the instability.

5.4 Problems remaining to be solved

The following problems remain to be solved:

(i) As mentioned on page 178, convergence problems are encountered in the numerical solution of the coupled current stream function and electron energy equation at high magnetic fields due to concentrations of current at the downstream edge of the cathode and upstream edge of the anode. A possible approach to overcoming these problems is to allow for Coulomb collisions; these should result in reduction of conductivity in regions of high electron temperature, thereby reducing the above-mentioned current concentrations.

(ii) Also mentioned on page 178 was the problem of saturation occurring in the region of current concentration near to the downstream edge of the cathode. The initial value of J_y at the downstream edge of the cathode is estimated to be $-3468 A/m^2$; this is close to the saturation current $-e(\nu_e + \frac{1}{2} n_{ew} c_{iw})$ at the same point, which has a value of $-4083 A/m^2$. However, for an applied current of 0.1 A, the average current density $\langle J_y \rangle$ is about $-365 A/m^2$, which is much less in magnitude that the saturation current. Therefore, current concentration at the downstream edge of the cathode severely limits the maximum current which can be passed, at least for the initial state. As there is an enhancement of the surface coverage and, therefore, electron emission at later times, a possible approach to solving this problem might be to start the computation with an initial state calculated using a different method. Allowance for Coulomb collisions should also help to solve the problem by reducing current concentration.

(iii) As shown on page 96, the condition for electron and ion collision effects to be negligible in the sheath requires that the sheath voltage drop be restricted to values less than about 0.1 mV. The condition is less restrictive if the sheath is assumed collisional for the ions alone ($|\Delta\phi| < 0.9$ V) or completely collision dominated ($|\Delta\phi| >> 0.9$ V). This demands a reformulation of the electrode wall boundary conditions.

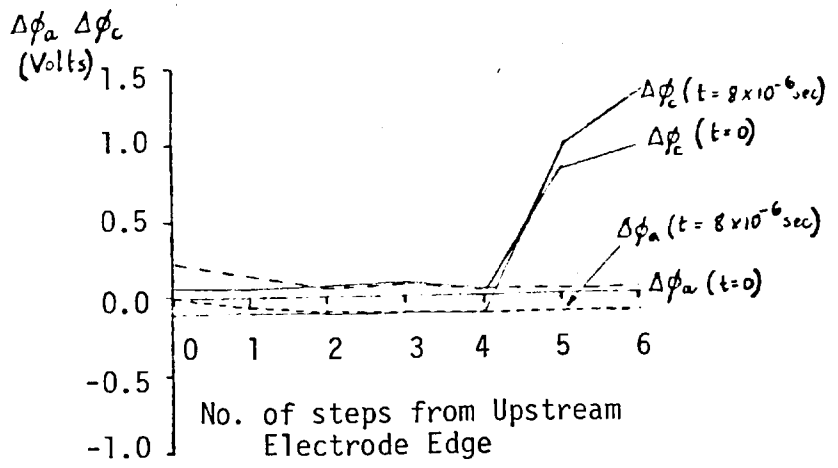

Anode and Cathode Sheaths Voltage Drop Profiles

Fig. 5.1

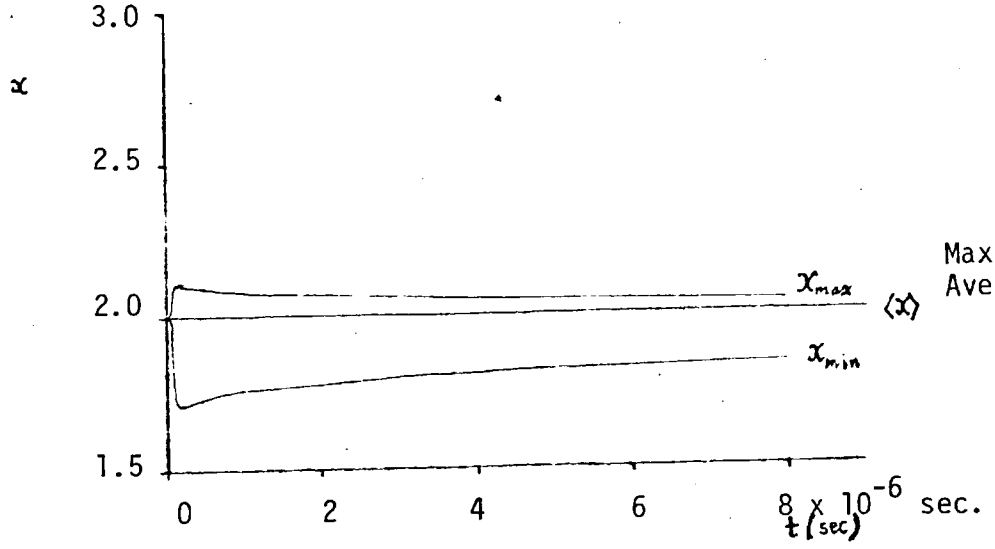

Maximum, Minimum and Average Seeding Fraction

Fig. 5.3

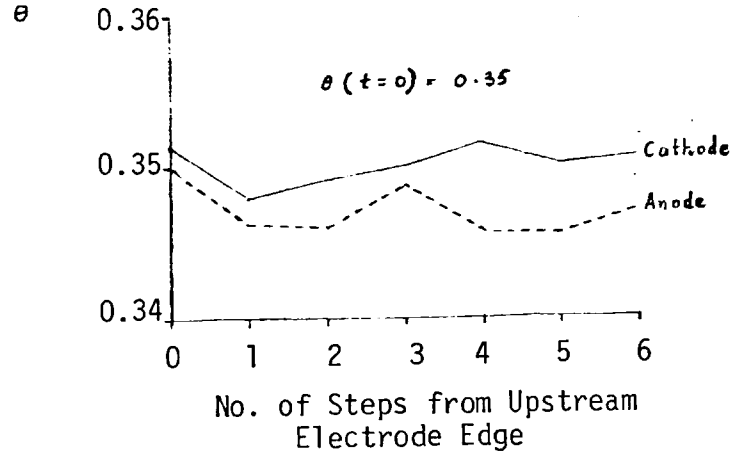

Surface Coverage Profiles

Fig. 5.2

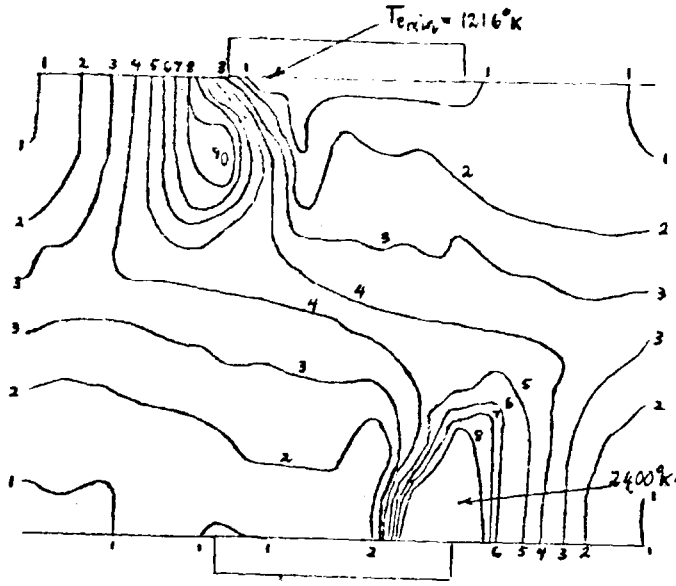

Contour Plot of T_e
Distribution in ζ-space
at t = 0
Countour Inverval = 150^0K

Fig. 5.4

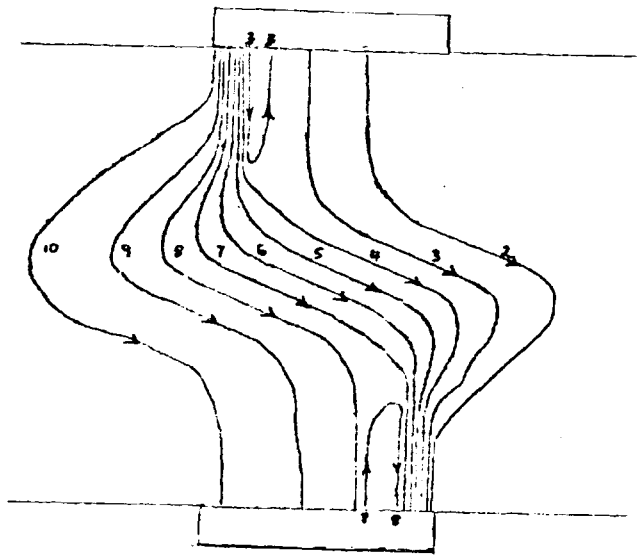

Contour Plot of ψ
Distribution in ζ-space
at t = 0
Contour Interval = 1 A/m

Fig. 5.5

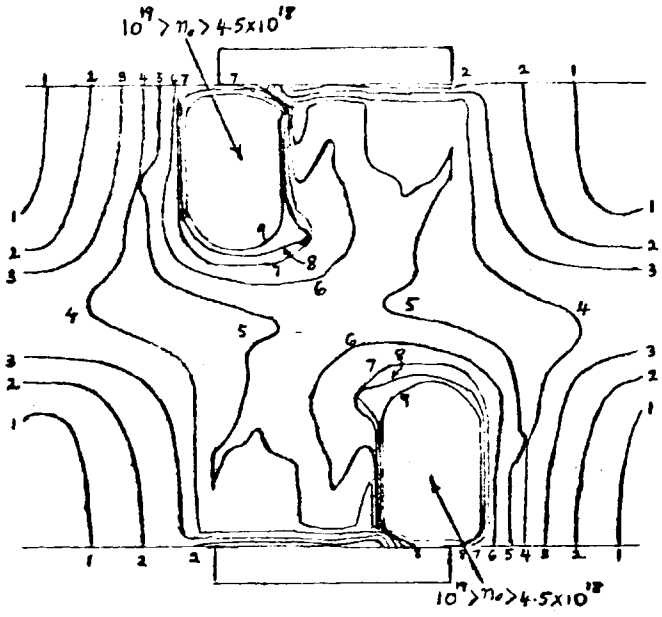

Contour Plot of n_e Distribution in ζ-space at t = 0
Contour Interval = $0.5 \times 10^{18}\ m^{-3}$

Fig. 5.6

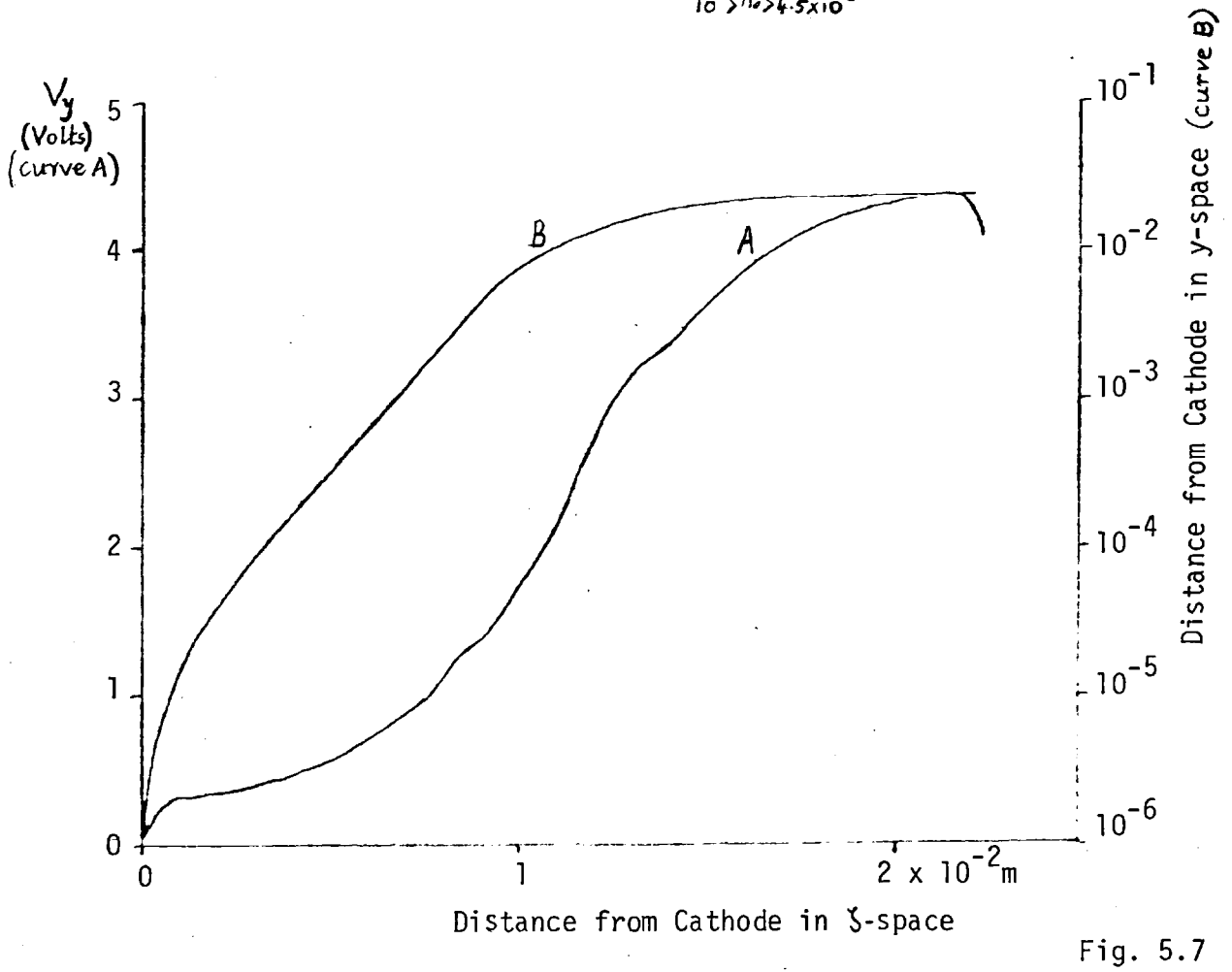

Fig. 5.7

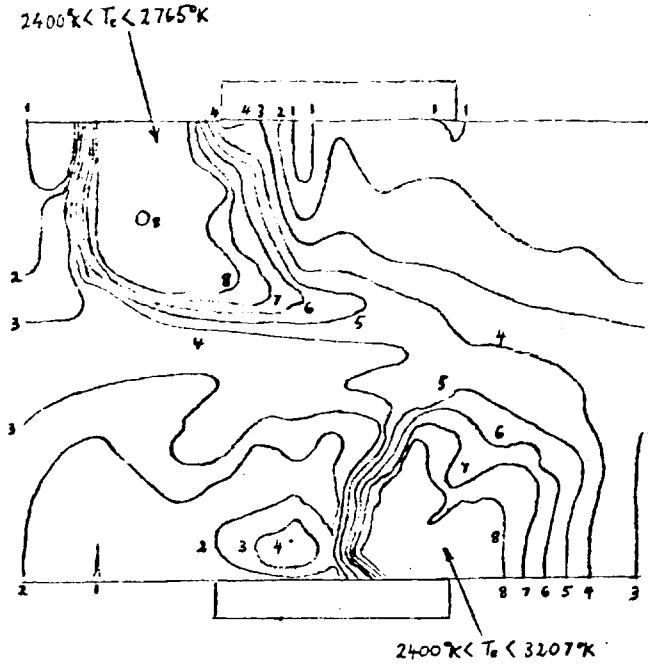

Contour Plot of T_e
Distribution in ζ-space
at $t = 8 \times 10^{-6}$ sec
Contour Inverval = 150^0K

Fig. 5.8

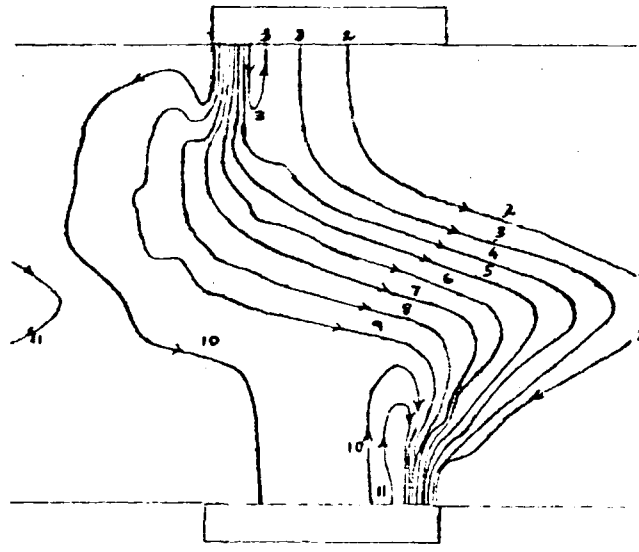

Contour Plot of ψ
Distribution in ζ-Space
at $t = 8 \times 10^{-6}$ sec
Contour Interval = 1 A/m

Fig. 5.9

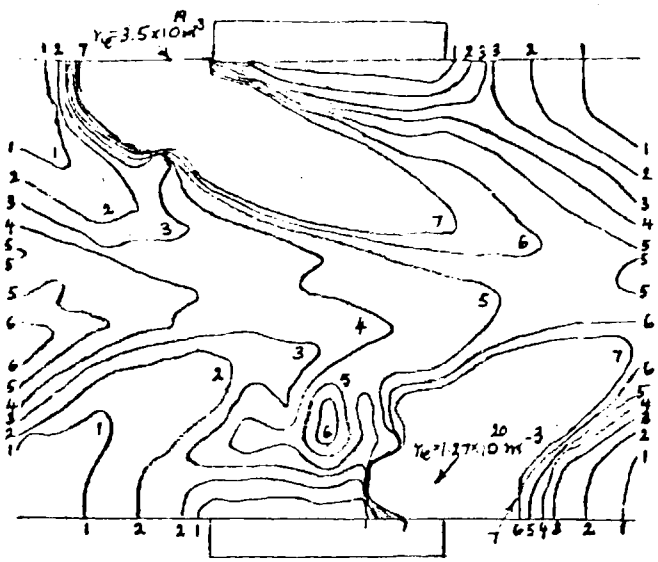

Contour Plot of n_e Distribution in ξ-space at $t = 8 \times 10^{-6}$ sec
Contour Interval

Fig. 5.10

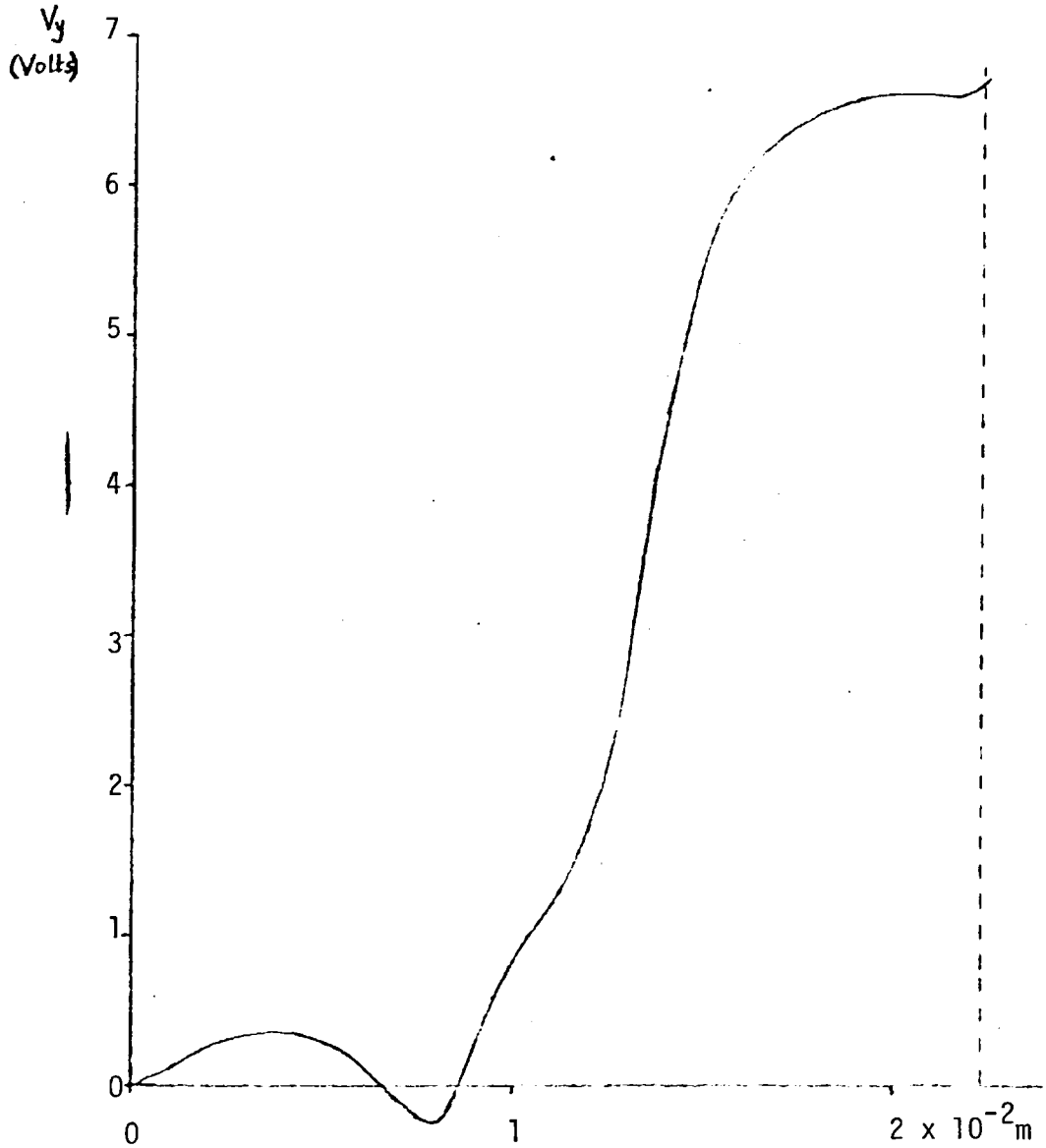

Distance from Cathode in ξ-space

Fig. 5.11

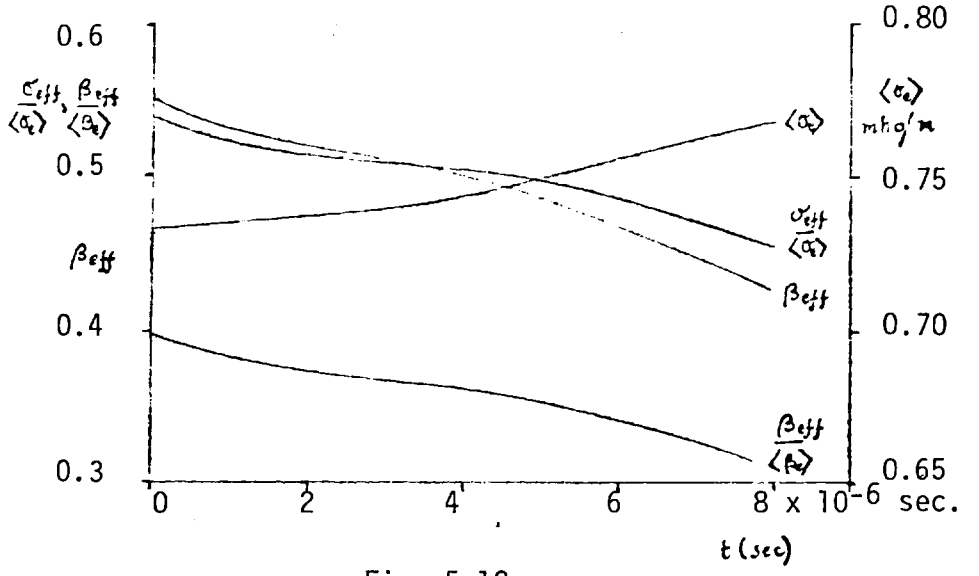

Fig. 5.12

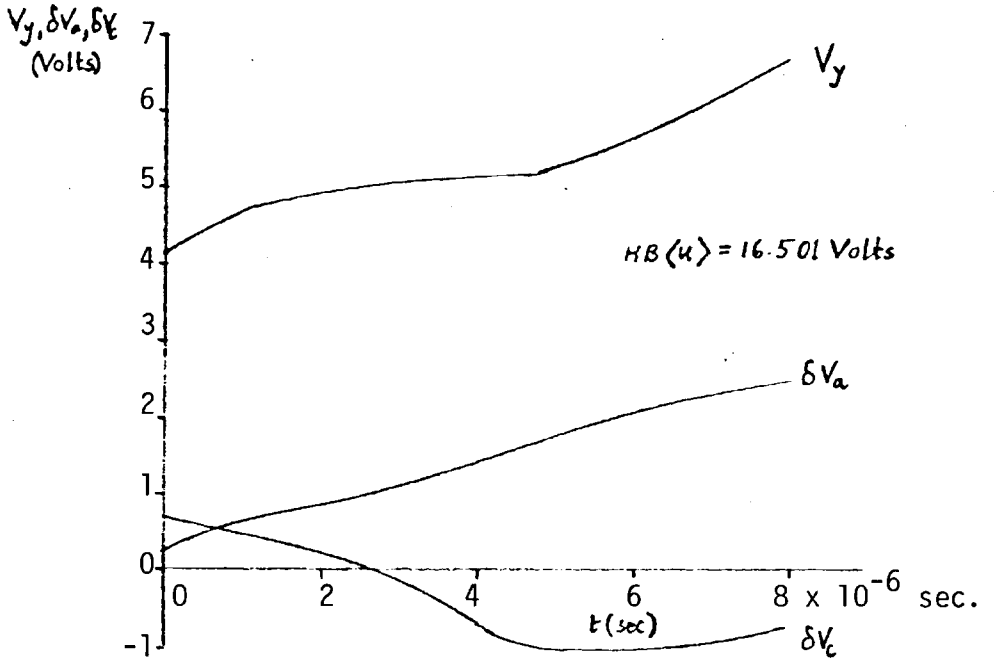

Fig. 5.13

APPENDIX A

DEFINITION OF FINITE DIFFERENCE MESH

The boundary layer equations are approximated by finite difference representations which are solved over a mesh in the x-y plane, the points of which are defined by the equations

$$x^n = x^{n-1} + \Delta x^{n-1}, \quad n = 2, 3, \ldots, N; \tag{A.1a}$$

$$y_1^n = 0; \tag{A.1b}$$

$$y_j^n = y_{j-1}^n + \Delta y_{j-1}^n, \quad j = 2, 3, \ldots, J. \tag{A.1c}$$

The mesh spacings Δx^n and Δy_j in equations (A.1) are completely arbitrary and may have large variations. This is important for turbulent boundary layer calculations where steep gradients near a wall necessitate the use of small mesh spacing, whilst relatively large spacing can be used away from the wall. Moreover, variations in the streamwise x-direction are usually rapid for small boundary layer thicknesses and relatively slow for larger boundary layer thicknesses, where the boundary layer thickness is defined as the distance from the wall of the point where the velocity is 0.99 of the centre-line value. Solutions show that boundary layers tend to grow as one advances along the channel from the initial position. Thus, it is desirable to employ a variable x-step which increases as the boundary layer thickens.. The x-step is here chosen to be a certain fraction f_1 of the local boundary layer thickness; that is

$$\Delta x^{n-1} = f_1 \delta^{n-1}, \quad n \geq 2. \tag{A.2}$$

where δ^{n-1} is the boundary layer thickness at $x=x^{n-1}$.

The step size in the y-direction is so defined that it is very small close to the wall and increases gradually towards the centre-line. The distribution of mesh rows for a given mesh column is defined by the formula

$$y_j^n = y_c^n \left[1 - \frac{\tanh \alpha^n (y_c^n - \zeta^n)}{\tanh (\alpha^n y_c^n)} \right], \qquad \text{(A.3)}$$

where, with a mesh of J-1 steps in the y-direction,

$$\zeta_j^n = y_c^n \left(\frac{j-1}{J-1} \right), \quad 1 \leq j \leq J. \qquad \text{(A.4)}$$

The quantity α appearing in equation (A.3) is chosen so that

$$\alpha^n y_c^n = \text{constant}, \qquad \text{(A.5)}$$

where the constant in (A.5) is determined from the assumed velocity profiles at the initial station $x=x^1$ (see section 3.3) as follows. From equations (A.3) and (A.4), we have

$$\begin{aligned} \Delta y_1^1 &= y_2^1 - y_1^1 \\ &= y_c^1 \left[1 - \frac{\tanh \alpha^1 y_c^1 \left(\frac{J-2}{J-1} \right)}{\tanh \alpha^1 y_c^1} \right]. \end{aligned}$$

The value of the quantity $\alpha^1 y_c^1$ is so chosen that Δy^1 is less than a fraction f_2 of the initial boundary layer thickness; that is,

$$\Delta y_1^1 < f_2 \delta. \qquad \text{(A.6)}$$

The mesh used in reference (32) is so constructed that step sizes in the y-direction are in a geometric progression; that is, $\Delta y_j = k \Delta y_{j-1}$, where $0<k<1$. This gives

$$y_j^n = \Delta y_1^n \frac{(k^{j-1} - 1)}{(k-1)}, \quad j = 1, 2, \ldots, J; \qquad \text{(A.7a)}$$

or, using the definition (A.4) of the distance ζ_j^n ,

$$y_j^n = \Delta y_1^n \frac{\left(k^{\zeta_j^n (J-1)/y_c^n} - 1\right)}{(k-1)} . \qquad \text{(A.7b)}$$

This method of mesh construction cannot be used here because the plasma and electrical equations must be solved on a mesh extending from the electrode at $y = 0$ to the opposite electrode at $y = H$. By symmetry, the gas-dynamic variables in the region $y_c \leq y \leq H$ are known from the solutions of the gas-dynamic equations for the region $0 \leq y \leq y_c$. If the mesh in the region $0 \leq y \leq y_c$ is defined by equations (A.7a), the mesh in the region $y_c \leq y \leq H$, on which the gas-dynamic variables are known, is defined by the equations

$$y_j^n = H - \Delta y_1^n \frac{\left(k^{N_J - j} - 1\right)}{(k-1)}, \quad J \leq j \leq N_J; \qquad \text{(A.8a)}$$

and

$$\zeta_j^n = \frac{(j-1)H}{(N_J - 1)}, \qquad \text{(A.8b)}$$

where $N_J = 2J-1$ is the total number of mesh point. Eliminating j from equation (A.8a) using (A.8b), we obtain

$$y_j^n = H - \Delta y_1^n \frac{\left[k^{(N_J-1)\left(1 - \frac{\zeta_j^n}{H}\right)} - 1\right]}{(k-1)} \qquad \text{(A.9)}$$

Considering y as a function of ζ it is clear from equations (A.7b) and (A.9) that this function is singular at $y = y_c$. It is necessary, however, that the function defining y_j be a continuous differentiable function of ζ_j^n because, due to their mixed elliptic-parabolic nature, the plasma and electrical equations can only be represented to second

order accuracy by finite difference forms on a mesh with constant step sizes. The y-variable in the plasma and electrical equations is therefore transformed to the ζ -variable defined above, derivatives being transformed as follows:

$$\frac{\partial}{\partial y} \rightarrow \frac{d\zeta}{dy}\frac{\partial}{\partial \zeta}$$

The function used to define the mesh here (see equation (A.3)) automatically defines the mesh in the region $y_c < y < H$ and is continuous and differentiable at $y = y_c$.

APPENDIX B

COEFFICIENTS IN LINEARIZED BOUNDARY LAYER EQUATIONS

The coefficients in the linearized boundary layer equations (3.10) can be written as:

$$r_{1,j} = 4\Delta x^{n-1} M^n_{j-1/2} - \frac{2\Delta x^{n-1}}{\Delta y^n_{j-1}} e_{1,j}\left(f_j u_j + T_j v_j\right) + \frac{2\Delta x^{n-1}}{\Delta y^n_{j-1}} e_{1,j-1}\left(f_{j-1} u_{j-1} + T_{j-1} v_{j-1}\right)$$

$$r_{2,j} = 4\Delta x^{n-1} H^{n-1}_{j-1/2} - \frac{2\Delta x^{n-1}}{\Delta y^n_{j-1}}\left(e_{2,j} f_j - e_{2,j-1} f_{j-1}\right) + 2T_{j-1/2} u_{j-1/2} - 2f_{j-1/2} v_{j-1/2}$$
$$- \frac{2R_g}{C_p}\frac{\left(p^n - p^{n-1}\right)}{p^{n-1/2}} T_{j-1/2} u_{j-1/2} - 2\Delta x^{n-1}\left(\frac{R_g}{C_p}\right)^2\left(\frac{1}{p^{n-1/2}}\right)^2\left[e_1\left(fu + Tv\right)^2\right]_{j-1/2}$$
$$+ 2\left(T_{j-1/2} u^{n-1}_{j-1/2} - T^{n-1}_{j-1/2} u_{j-1/2}\right) - 2\left(v_{j-1/2} f^{n-1}_{j-1/2} - v^{n-1}_{j-1/2} f_{j-1/2}\right)$$

$$r_{3,j} = \Delta y^n_{j-1} u_{j-1/2} + v_{j-1} - v_j$$

$$r_{4,j} = \Delta y^n_{j-1} v_{j-1/2} + u_{j-1} - u_j$$

$$r_{5,j} = \Delta y^n_{j-1} f_{j-1/2} + T_{j-1} - T_j$$

$$g_{1,j} = \left(fu + Tv\right)_{j-1/2} + \left(fu + Tv\right)^{n-1}_{j-1/2}$$

$$g_{2,j} = g_{1,j}$$

$$g_{3,j} = \frac{2\Delta x^{n-1}}{\Delta y^n_{j-1}} e_{1,j} f_j - \left(u_{j-1/2} T_j + \left(Tu\right)_{j-1/2}\right) + f_j v_{j-1/2}$$
$$- \left(\frac{p^{n-1}}{p^n}\right) u^{n-1}_{j-1/2} T_j + \left(\frac{p^n}{p^{n-1}}\right)\left(Tu\right)^{n-1}_{j-1/2} - v^{n-1}_{j-1/2} f_j$$

$$g_{4,j} = -\frac{2\Delta x^{n-1}}{\Delta y^n_{j-1}} e_{1,j-1} f_{j-1} - \left(u_{j-1/2} T_{j-1} + \left(Tu\right)_{j-1/2}\right) + f_{j-1} v_{j-1/2}$$
$$- \left(\frac{p^{n-1}}{p^n}\right) u^{n-1}_{j-1/2} T_{j-1} + \left(\frac{p^n}{p^{n-1}}\right)\left(Tu\right)^{n-1}_{j-1/2} - v^{n-1}_{j-1/2} f_{j-1}$$

$$g_{5,j} = \frac{2\Delta x^{n-1}}{\Delta y^n_{j-1/2}} e_{1,j} T_j + T_j\left(v_{j-1/2} - v^{n-1}_{j-1/2}\right)$$

$$g_{6,j} = -\frac{2\Delta x^{n-1}}{\Delta y^n_{j-1}} e_{1,j-1} T_{j-1} + T_{j-1}\left(v_{j-1/2} - v^{n-1}_{j-1/2}\right)$$

$$g_{7,j} = \frac{2\Delta x^{n-1}}{\Delta y^n_{j-1}}\left[\left(\frac{d\mu}{dT}\right)_j\left(f_j u_j + v_j T_j\right) + e_{1,j} v_j\right] - u_{j-1/2} u_j + v_j v_{j-1/2}$$
$$- \left(p^{n-1}/p^n\right) u^{n-1}_{j-1/2} u_j - v^{n-1}_{j-1/2} v_j$$

$$g_{8,j} = -\frac{2\Delta x^{n-1}}{\Delta y^n_{j-1}}\left[\left(\frac{d\mu}{dT}\right)_j (fu+Tv)_{j-1} + e_{1\,j-1} v_{j-1}\right] - u_{j-1/2}\,u_{j-1} + 2_{j-1/2} v_{j-1} - \left(\frac{p^{n-1}}{p^n}\right) u^{n-1}_{j-1/2} u_{j-1} - 2^{n-1}_{j-1/2} v_{j-1}$$

$$g_{9,j} = \frac{2\Delta x^{n-1}}{\Delta y^n_{j-1}} e_{1j}\,u_j + 2_{j-1/2} u_j - 2^{n-1}_{j-1/2} u_j$$

$$g_{10,j} = -\frac{2\Delta x^{n-1}}{\Delta y^n_{j-1}} e_{1\,j-1} u_{j-1} + 2_{j-1/2} u_{j-1} - 2^{n-1}_{j-1/2} u_{j-1}$$

$$S_{1,j} = f_{j-1/2} + f^{n-1}_{j-1/2}$$

$$S_{2,j} = S_{1,j}$$

$$S_{3,j} = -T_{j-1/2} + \frac{R_g}{c_p}\frac{(p^n - p^{n-1})}{p^{n-1/2}} T_{j-1/2} + T^{n-1}_{j-1/2} + 2\Delta x^{n-1}\frac{R_g^2}{c_p}\left(\frac{1}{p^{n-1/2}}\right)^2 e_{1j}\,(fu+Tv)_j\, f_j$$

$$S_{4,j} = -T_{j-1/2} + \frac{R_g}{c_p}\frac{(p^n - p^{n-1})}{p^{n-1/2}} T_{j-1/2} + T^{n-1}_{j-1/2} + \frac{2\Delta x^{n-1} R_g^2}{c_p}\left(\frac{1}{p^{n-1/2}}\right)^2 e_{1\,j-1}\,(fu+Tv)_{j-1}\, f_{j-1}$$

$$S_{5,j} = \frac{2\Delta x^{n-1} R_g^2}{c_p}\left(\frac{1}{p^{n-1/2}}\right)^2 e_{1j}\,(fu+Tv)_j\, T_j$$

$$S_{6,j} = \frac{2\Delta x^{n-1} R_g^2}{c_p}\left(\frac{1}{p^{n-1/2}}\right)^2 e_{1\,j-1}\,(fu+Tv)_{j-1}\, T_{j-1}$$

$$S_{7,j} = \frac{2\Delta x^{n-1}}{\Delta y^n_{j-1}} f_j \frac{1}{P_l}\left(\frac{d\mu}{dT}\right)_j - u_{j-1/2} + \frac{R_g}{c_p}\frac{(p^n - p^{n-1})}{p^{n-1/2}} u_{j-1/2} + \frac{2\Delta x^{n-1} R_g^2}{c_p}\left(\frac{1}{p^{n-1/2}}\right)^2 e_{1j}\,(fu+Tv)_j\, v_j - u^{n-1}_{j-1/2}$$

$$S_{8,j} = -\frac{2\Delta x^{n-1}}{\Delta y^n_{j-1}} f_{j-1}\frac{1}{P_l}\left(\frac{d\mu}{dT}\right)_{j-1} - u_{j-1/2} + \frac{R_g}{c_p}\frac{(p^n - p^{n-1})}{p^{n-1/2}} u_{j-1/2} + \frac{2\Delta x^{n-1} R_g^2}{c_p}\left(\frac{1}{p^{n-1/2}}\right)^2 e_{1\,j-1}\,(fu+Tv)_{j-1}\, v_{j-1} - u^{n-1}_{j-1/2} + \frac{\Delta x^{n-1} R_g^2}{c_p}\left(\frac{1}{p^{n-1/2}}\right)^2 (fu+Tv)^2_{j-1}\left(\frac{d\mu}{dT}\right)_{j-1}$$

$$S_{9,j} = \frac{2\Delta x^{n-1}}{\Delta y^n_{j-1}} e_{2j} + 2_{j-1/2} + \frac{2\Delta x^{n-1} R_g^2}{c_p}\left(\frac{1}{p^{n-1/2}}\right)^2 e_{1j}\,(fu+Tv)_j\, u_j - 2^{n-1}_{j-1/2}$$

$$S_{10,j} = -\frac{2\Delta x^{n-1}}{\Delta y^n_{j-1}} e_{2\,j-1} + 2_{j-1/2} + \frac{2\Delta x^{n-1} R_g^2}{c_p}\left(\frac{1}{p^{n-1/2}}\right)^2 e_{1\,j-1}\,(fu+Tv)_{j-1}\, u_{j-1} - 2^{n-1}_{j-1/2}$$

APPENDIX C

ELECTROTHERMAL WAVES AND THE TEMPERATURE RELAXATION APPROXIMATION

Simplified expressions for the growth and decay rates of electrothermal waves are presented here, and the validity of the assumption of instantaneous electron temperature relaxation for the range of conditions of interest in this work is considered. A simple expression for the growth rate of the electrothermal instability, useful for the stability theory of section 4.5 ,is derived. The analysis presented in this appendix is essentially that of Uncles[27] with simplifications made, consistent with the assumptions of slight seeding and negligible Coulomb collisions.

The electron energy equation is considered in the simplified form

$$\frac{D}{Dt}\left(n_e \frac{3}{2} k_B T_e\right) = \bar{J}^2/\sigma_e + n_e \frac{3}{2} k_B (T - T_e) \frac{2m_e}{m_h} \nu_{eh} - \dot{n}_e \mathcal{E}_i , \qquad (C.1)$$

which is obtained from equation (2.214) by neglecting compressional heating, thermal conduction, radiative energy loss, and the pressure gradient term in equation (2.132); turbulent fluctuations are neglected in the present analysis.

Neglecting the diffusion terms in equations (2.207) and (2.208), one obtains the electron and seed atom continuity equations in the simplified forms

$$\frac{Dn_e}{Dt} = \dot{n}_e \qquad (C.2a)$$

and

$$\frac{Dn_n}{Dt} = -\dot{n}_e \qquad (C.2b)$$

Equations(C.2) imply that the density of seed particles N_n (ions and neutrals) is constant in the rest frame of the plasma; that is,

$$N_n = n_i + n_n \doteq n_e + n_n = \text{constant}. \tag{C.3}$$

Neglecting the term dependent on the electron pressure gradient in equations (2.132) an approximate form of generalized Ohm's law is obtained:

$$\sigma_e \underline{E}' = \underline{J} + \beta_e (\underline{J} \wedge \underline{b}) , \tag{C.4}$$

which was used to obtain the ohmic heating term J^2/σ_e in equation (C.1).

Taken together with the change conservation equation

$$\nabla . \underline{J} = 0 , \tag{C.5}$$

and Faraday's Law

$$\nabla \wedge \underline{E} = 0 , \tag{C.6}$$

equations (C.1), (C.2a), (C.3) and (C.4) form the basis of an approximate description of a flowing plasma in an electromagnetic field.

It is well known that equations (C.1)-(C.6), when linearized, predict the growth and decay rates of electrothermal waves[7],[8]. These waves consist of two modes: the fast thermal mode, which is always severely damped and is of little physical interest, and the ionization mode which is unstable under certain conditions. The properties of these waves have been analyzed in detail by Nelson and Haines[7], who linearized and solved numerically the complete system of equations (2.132), (2.190), (2.194), (2.197), and (2.214), neglecting the ion current and turbulent fluctuations. It is sufficient for the present purposes to consider

a simple linear theory of these waves using equations (C.1)-(C.6), in which the effects of wave motion are neglected; this is justified in reference (8).

One-dimensional, small amplitude perturbations in n_e , $\overline{T_e}$, $\underline{J}$ and $\underline{E}$ about a uniform state are considered, and equations (C.1)-(C.6), which are transformed to the rest frame of the plasma, are linearized with respect to the perturbations. The uniform state is assumed to be in Saha equilibrium at the electron temperature, the Ohmic heating everywhere balancing the elastic collision losses.

As shown in figure (C.1), the direction of propagation of the small amplitude waves is assumed to be along the x-axis at an angle θ to the unperturbed current. Writing all perturbed quantities in the form

$$\chi = \chi_0 + \chi'$$

where χ_0 denotes the unperturbed value of the quantity χ , equations (C.1)-(C.6) can be linearized to give

$$\frac{Dn_e'}{Dt} = a_0 n_e' + a_1 T_e' \tag{C.7}$$

$$a_2 \frac{Dn_e'}{Dt} + a_3 \frac{D\overline{T_e}'}{Dt} = a_4 n_e' + a_5 T_e' \tag{C.8}$$

where the perturbed Ohmic heating has been evaluated from equations (C.4) (C.5) and (C.6), which are then eliminated from the system. The coefficients $a_0 - a_5$ are given by

$$a_0 = \left(\frac{\partial \dot{n}_e}{\partial n_e}\right)_0 = 1.09 \times 10^{-20} T_{e0}^{-9/2} n_{e0}^2 (n_{e0} - 2N_n) / (N_n - n_{e0}) \tag{C.9a}$$

$$a_1 = \left(\frac{\partial \dot{n}_e}{\partial T_e}\right)_0 = 1.09 \times 10^{-20} T_{e0}^{-9/2} n_{e0}^3 \left(\frac{\varepsilon_i}{k_B T_{e0}} + \frac{3}{2}\right) \frac{1}{T_{e0}} \tag{C.9b}$$

$$a_2 = \frac{3}{2} k_B T_{eo} + \mathcal{E}_i \qquad \text{(C.9c)}$$

$$a_3 = \frac{3}{2} k_B n_{eo} \qquad \text{(C.9d)}$$

$$a_4 = -\frac{1}{n_{eo}} \frac{J_o^2}{\sigma_{eo}} \left(\beta_{eo} \sin 2\theta + \cos 2\theta\right) - \frac{\partial}{\partial n_e} \left\{3 n_e k_B (T_e - T) \frac{m_e}{m_h} \nu_{eh}\right\} \qquad \text{(C.9e)}$$

$$= -\frac{1}{n_{eo}} \left(\frac{J_o^2}{\sigma_{eo}}\right) \left(\beta_{eo} \sin 2\theta + \cos 2\theta + 1\right)$$

$$a_5 = \frac{1}{2T_{eo}} \frac{J_o^2}{\sigma_{eo}} \cos 2\theta - \frac{\partial}{\partial T_e} \left\{3 n_e k_B (T_e - T) \frac{m_e}{m_h} \nu_{eh}\right\}$$

$$= \frac{1}{2T_{eo}} \frac{J_o^2}{\sigma_{eo}} \left\{\cos 2\theta - \frac{(3T_e - T)}{(T_e - T)}\right\} \qquad \text{(C.9f)}$$

Setting n_e' and T_e' equal to $n_e'(0) \exp(i\omega t)$ and $T_e'(0) \exp(i\omega t)$ respectively, equations (C.7) and (C.8) yield a dispersion relation for small amplitude electrothermal waves in the form of a quadratic for $i\omega$. This has two real roots, denoted by $g_\pm$, where

$$g_\pm = \frac{1}{2a_3} \left[\left(a_5 + a_0 a_3 - a_1 a_2\right) \pm \left\{\left(a_5 + a_0 a_3 - a_1 a_2\right)^2 + 4 a_3 \left(a_1 a_4 - a_0 a_5\right)\right\}^{1/2}\right] \qquad \text{(C.10)}$$

Equations (C.10) give the growth/decay rates for the ionization mode and the fast thermal mode, g_+ and g_- , respectively. The fast thermal mode is always severely damped, whilst the ionization mode can become unstable under certain conditions.

The decay time for the fast thermal mode $\tau_{FT} = |g_-^{-1}|$ is plotted as a function of T_e in figure (C.2); and the growth/decay time for the ionization mode $\tau_I = |g_+^{-1}|$ is plotted in figure (C.3a) as a function of T_e , and for magnetic field strengths of 0.7T and

1.4T. The gas temperature has been taken to be equal to 1519°K, which is the average value calculated from the computed gas temperature profile presented in section 3.5, and the seeding fraction has been taken to be 0.002. The angle θ between the zero order current flow and the direction of non-uniformity is taken to be $-\pi/4$, which is approximately the angle for maximum growth of an unstable wave[8]. The ionization mode is stable for a magnetic field strength of 0.7T, and unstable for a magnetic field strength of 1.4T.

It can be seen from figures (C.2) and (C.3a) that, for the range of electron temperatures considered, $\tau_{FT} \ll \tau_I$; for example, for $T_e \sim 2000°K$, $\tau_{FT} \sim 10^{-8}$ sec and $\tau_I \sim 10^{-4}$ sec. These values of the electrothermal time scales are compared with typical values of the covection time scale τ_u and the x-diffusion time scale τ_{dx}, which appear in the conditions (4.41) and (4.45) for numerical stability and accuracy of the explicit time integration scheme (see section 4.6). From conditions (4.41) and (4.45), τ_u and τ_{dx} are defined as follows:

$$\tau_u = \frac{\Delta x}{u_{xc}}$$

and

$$\tau_{dx} = \frac{m_{ih} \nu_{ih} \Delta x^2}{k_B T}$$

where Δx is the mesh step size in the x-direction. For a mesh of 49 columns, $\tau_u \sim 10^{-6}$ sec and $\tau_{dx} \sim 10^{-2}$ sec, again for the gas-dynamic parameters obtained from the solution of the boundary layer equations presented in section 3.5.

It is clear that the shortest time scale is that of the fast thermal mode. However, the fast thermal mode, being strongly damped, has little long term effect on the solutions of the equations, and therefore is of little practical importance. The short time scale of the fast thermal mode necessitates the use of an extremely small time step in the explicit numerical time integration of the equations if numerically stable and accurate solutions are to be obtained (see section 4.6). It is desirable, therefore, that removal of the fast thermal mode from the differential system be considered. Uncles[27] has shown that this can be done by assuming either Saha equilibrium $(\dot{n}_e = 0)$ or instantaneous electron temperature relaxation; that is, $\mathcal{D}T_e/Dt = 0$ in the electron energy equation (see section 2.5). The former assumption, which has been used before[8], is valid only at high electron temperatures and if the cross-stream diffusion terms in the continuity equations can be neglected. The assumption of instantaneous electron temperature relaxation, or the "temperature relaxation approximation", appears to have been used previously by Kolb[18] in a greatly simplified physical and numerical model. In addition to having a wider range of validity[27], this assumption does not require that the cross-stream diffusion terms in the continuity equations be neglected, thus allowing the coupling between plasma-surface interaction phenomena and plasma bulk phenomena, such as the electrothermal instability, to be studied; this possibility has so far not been considered.

The validity of the temperature relaxation approximation for the range of conditions of interest in the present work can be examined using the analysis of reference (27). Setting $\mathcal{D}T_e/Dt = 0$ in equation (C.8), expressions can be derived for the ratio n_e'/T_e' and

the growth rate g_+ for the ionization mode in the temperature relaxation approximation; these quantities are denoted by α'' and g_+'' respectively. Denoting the ratio n_e'/T_e' for the ionization mode in the more general case of equations (C.1) and (C.2) by α, the conditions of validity of the temperature relaxation approximation can be written as

$$\epsilon_\alpha'' = \left| 1 - \frac{\alpha''}{\alpha} \right| << 1 \qquad \text{(C.10a)}$$

and

$$\epsilon_g'' = \left| 1 - \frac{g_+''}{g_+} \right| << 1 \qquad \text{(C.10b)}$$

The functions ϵ_α'' and ϵ_g'' are plotted against T_e for magnetic field strengths of 0.7 Telsa and 1.4 Telsa in figure (C.3b). It can be seen from figure (C.3b) that, for the range of conditions of interest here, the conditions (C.10) are well satisfied, especially for $T_e \lesssim 2000°K$.

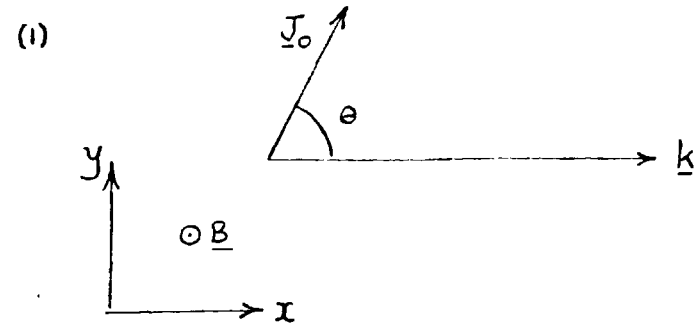

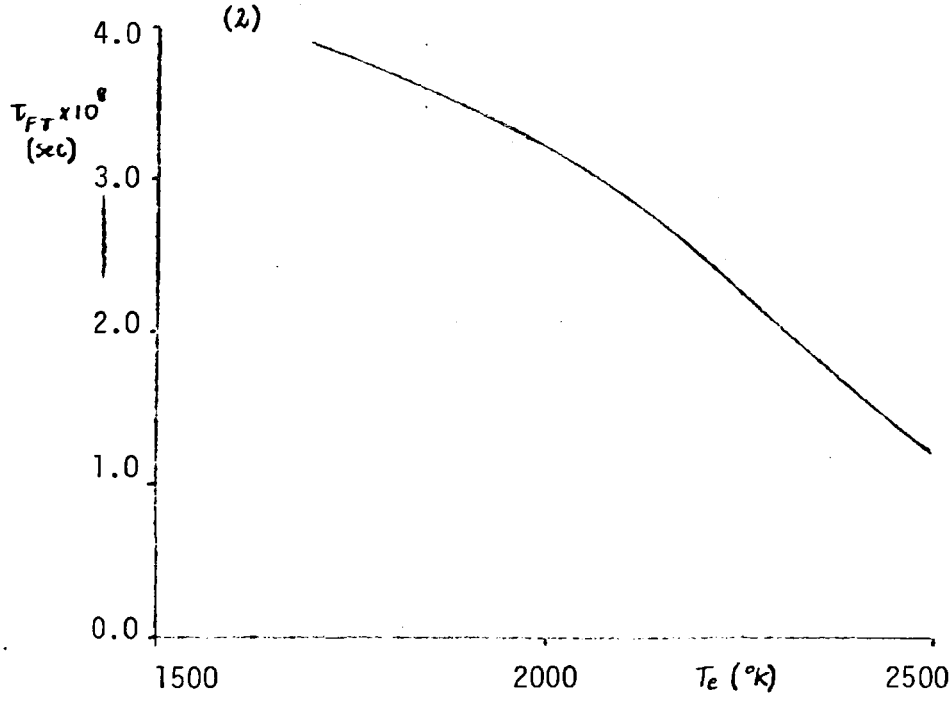

(1) Fig. C.1: Coordinate system for one-dimensional electrothermal wave theory.

(2) Fig. C.2: Decay time for the fast thermal mode τ_{FT} against T_e.

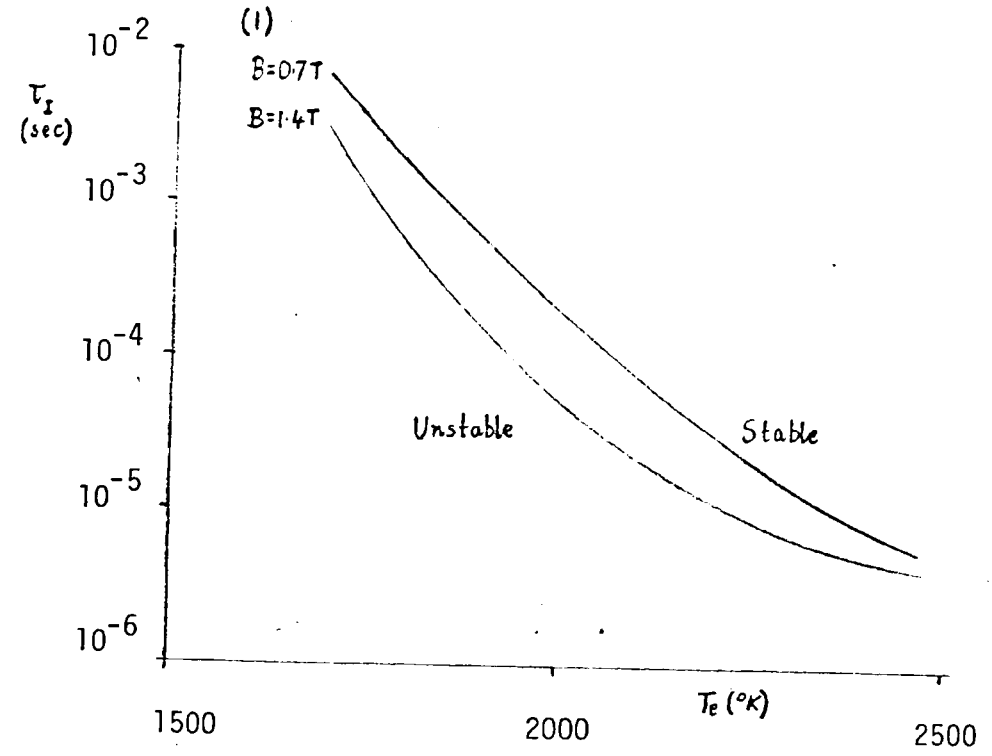

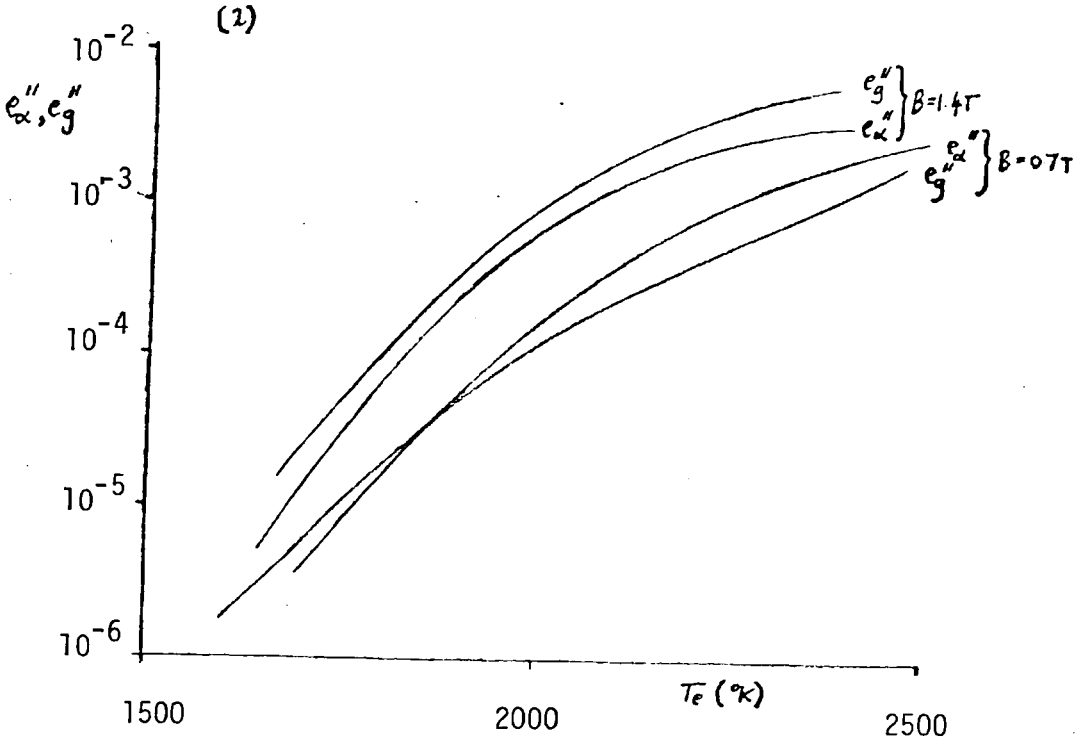

(1) Fig. C.3: Ionization mode growth/decay time τ_I against T_e for B = 0.7T and 1.4T.

(2) Fig. C.4: e''_α and e''_g against T_e for B = 0.7T and 1.4T.

APPENDIX D

RADIATIVE ENERGY LOSS

The main contribution to the radiation loss term $\dot{R}$ of the electron energy equation (2.227) comes from the lowest order caesium doublet ($6S_{1/2} - 6P_{1/2}$, $6S_{1/2} - 6P_{3/2}$), which comprises lines of wavelengths 8970Å and 8550Å. A general expression for $\dot{R}$ in terms of local values of plasma parameters and their derivatives can be derived, which is valid only if the plasma is optically thick to the radiation involved; that is, if $L_c \gg L_{a\nu}$, where L_c is the characteristic length scale of variation of plasma parameters, and $L_{a\nu}$ is a characteristic length scale for absorption of a photon. An expression for $L_{a\nu}$ is derived below in terms of the mean free path L_ν for absorption of a photon, which, for the ith line (i = 1,2), is shown in reference (1) to be given by

$$L_\nu^{(i)} = \frac{\Delta\nu_i}{a n_n f_i} \left[1 + \left\{ \frac{2(\nu - \nu_i)}{\Delta\nu_i} \right\}^2 \right] \qquad (D.1)$$

where $a = e^2/(2\pi\epsilon_0 m_e c)$, f_i is the oscillator strength for the transition corresponding to the ith line, and $\Delta\nu_i$ is the full width of the line at half maximum. The dominant line broadening mechanism is shown in reference (37) to be van der Waal's broadening by neutral atoms. Both the formula for $\Delta\nu_i$ and values for f_i in this case can be found in reference (38).

When the plasma is optically thick to radiation of frequency ν, photons tend to be trapped, having a small probability of escaping, and the specific intensity I_ν is close to the equilibrium value given by the Planck function

$$B_\nu \equiv \frac{2h\nu^3/c^2}{\left(e^{h\nu/k_B T_e} - 1\right)} \tag{D.2}$$

It is shown in reference (19) that an approximate solution of the equation of radiation transfer then yields the following expression for the radiation loss term $\dot{R}$:

$$\dot{R} = \nabla \cdot \underline{q}^R, \tag{D.3}$$

where $\underline{q}^R$ is given by

$$\underline{q}^R = -\sum_i \frac{4\pi}{3}\left(\int_0^\infty L_\nu^{(i)} \frac{dB_\nu}{dT_e}\, d\nu\right) \nabla T_e, \tag{D.4}$$

which can be written in the form

$$\underline{q}^R \equiv -\lambda^R \nabla T_e$$

where

$$\lambda^R = \sum_i \frac{4\pi}{3}\left(\int_0^\infty L_\nu^{(i)} \frac{dB_\nu}{dT_e} d\nu\right), \tag{D.5}$$

The sums in equations (D.4) and (D.5) are taken over the two lines. The quantity $\underline{q}^R$ may be interpreted as a radiative heat flux, and λ^R as the corresponding radiation thermal conductivity. Using equations (D.1) and (D.2) to express the integrands of the integrals in equations (D.4) and (D.5) in terms of ν and T_e, the following expression is obtained for λ^R:

$$\lambda^R = \sum_i \frac{\Delta\nu_i hc}{3\alpha f_i n_n} \int_0^\infty \nu \left\{1 + \left[\frac{2(\nu-\nu_i)}{\Delta\nu_i}\right]^2\right\} \frac{dn_\nu}{dT_e} d\nu \tag{D.6}$$

The condition for validity of equations (D.3)-(D.6) is given in reference (19). For the present case this condition can be expressed as

$$L_\nu^{(i)} \frac{T_e}{B_\nu} \frac{dB_\nu}{dT_e} \left| \nabla \ln T_e \right| \ll 1 . \qquad (D.7)$$

The lengths $(|\nabla \ln T_e|)^{-1}$ and $L_\nu^{(i)} (T_e/B_\nu)\, dB_\nu/dT_e$ are the characteristic length scales L_c and $L_{a\nu}^{(i)}$ introduced above, and the condition (D.7) is a quantitative expression of the conditions that the plasma be optically thick to the variation involved. For $\nu \sim \nu_i$, $h\nu/k_B T_e \gg 1$, for typical values of T_e, and, from equation (D.2),

$$\frac{T_e}{B_\nu} \frac{dB_\nu}{dT_e} \approx \frac{h\nu}{k_B T_e} \gg 1 \quad (\nu \sim \nu_i), \qquad (D.8)$$

so that

$$L_{a\nu}^{(i)} = L_\nu^{(i)} \frac{T_e}{B_\nu} \frac{dB_\nu}{dT_e} \approx \left(\frac{h\nu_i}{k_B T_e} \right) L_\nu^{(i)} \gg L_\nu^{(i)} .$$

Taking $n_n \sim 10^{22} m^{-3}$, $\Delta\nu_i \sim 10^{11} sec^{-1}$, $f_i \sim 1$, $\nu_i \sim 10^{15} sec^{-1}$, equation (D.1) yields for the mean free path of photons of frequency $\nu = \nu_i$,

$$L_\nu^{(i)} \sim 10^{-5} m ,$$

and, since for $T_e = 2000°K$, $h\nu_i/k_B T_e \sim 10$, the condition (D.7) requires that

$$L_c = \left(|\nabla \ln T_e| \right)^{-1} \gg 10^{-4} m$$

Since L_c is of the order of the boundary layer thickness, which for the gas-dynamic data used in chapter 4 is of the order of 10^{-3}m, the condition (D.7) is satisfied for $\nu \sim \nu_i$. However, it can be seen from equation (D.1) that, since $\nu_i \gg \Delta\nu_i$, the condition (D.7) rapidly becomes invalid for $\nu > \nu_i + \Delta\nu_i/2$ or $\nu < \nu_i - \Delta\nu_i/2$. This means that the plasma is not optically thick to radiation outside the frequency ranges of the lines and the total radiative energy loss cannot be represented by equations (D.3)-(D.6). Only the contribution to the radiative energy loss from frequencies in the line ranges can be represented by these equations, the integrations in equation (D.4)-

D.6) being taken over the frequency ranges of the lines. However, it is possible for this contribution to dominate the contribution from radiation to which the plasma is optically thin, since, for the latter radiation, $I_\nu << B_\nu$ (see reference (19)). If this is assumed to be the case, the radiation loss can be approximately represented by equations (D.3)-(D.6) in which the integrations are taken over the frequency ranges of the lines. Thus, equation (D.5) is replaced with

$$\lambda^R = \sum_i \frac{\Delta\nu_i h c}{3\alpha f_i n_n} \int_{\nu_1^{(i)}}^{\nu_2^{(i)}} \nu \left\{ 1 + \left[\frac{2(\nu-\nu_i)}{\Delta\nu_i} \right]^2 \right\} \frac{dn_\nu}{\alpha T_e} d\nu \qquad (D.9)$$

where the frequencies $\nu_1^{(i)}$ and $\nu_2^{(i)}$ are taken to be the extremities of the lines. Taking $\nu_1^{(i)} = \nu_i - \alpha\Delta\nu_i/2$ and $\nu_2^{(i)} = \nu_i + \alpha\Delta\nu_i/2$, and using the relation $n_\nu = 4\pi B_\nu/(ch\nu)$ where B_ν is given by equation (D.2), the integral I in equation (D.9) can be expressed in the form

$$I = \frac{8\pi h}{k_B T_e^2 c^3} \int_{\nu_1^{(i)}}^{\nu_2^{(i)}} \nu^4 \left\{ 1 + \left[\frac{2(\nu-\nu_i)}{\Delta\nu_i} \right]^2 \right\} \frac{e^{h\nu/k_B T_e}}{\left[e^{h\nu/k_B T_e} - 1 \right]^2} d\nu$$

$$\simeq \frac{8\pi h}{k_B T_e^2 c^3} \int_{\nu_1^{(i)}}^{\nu_2^{(i)}} \nu^4 e^{-h\nu/k_B T_e} \left\{ 1 + \left[\frac{2(\nu-\nu_i)}{\Delta\nu_i} \right]^2 \right\} d\nu \qquad (D.10)$$

since $h\nu/k_B T_e >> 1$ for $\nu \sim \nu_i$ (see equation (D.8)). Neglecting the variation of the factor $\nu^4 e^{-h\nu/k_B T_e}$ in equation (D.10) we have

$$I \simeq \frac{8\pi h}{k_B T_e^2 c^3} \nu_i^4 e^{-h\nu_i/k_B T_e} \int_{\nu_1^{(i)}}^{\nu_2^{(i)}} \left\{ 1 + \left[\frac{2(\nu-\nu_i)}{\Delta\nu_i} \right]^2 \right\} d\nu$$

$$= \left(\frac{8\pi h \Delta\nu_i}{k_B T_e^2 c^3} \right) \left(\alpha + \frac{1}{3}\alpha^3 \right) \nu_i^4 e^{-h\nu_i/k_B T_e} \qquad (D.11)$$

Inserting the integral I given by equation (D.11) into equation (D.9) we obtain

$$\lambda^R = \sum_i \frac{8\pi h^2 \Delta\nu_i^2}{(3\alpha f_i n_n k_B \bar{T}_e^2 c^2)} \left(\alpha + \frac{1}{3}\alpha^3\right) \nu_i^4 e^{-h\nu_i/k_B T_e} \qquad (D.12)$$

To fully define λ^R, a value of α must be specified. If we return to the above order of magnitude analysis, we see that, for $\alpha = 3$, $L_{\nu a} \sim L_e$ at $\nu = \nu_i \pm \alpha \Delta\nu_i/2$. Using this value of α equation (D.12) can be written as

$$\lambda^R = \sum_i \frac{32\pi h^2 \Delta\nu_i^2}{(\alpha f_i n_n k_B \bar{T}_e^2 c^2)} \nu_i^4 e^{-h\nu_i/k_B T_e} \qquad (D.13)$$

The electron thermal conductivity is given by (see equation (2.114))

$$\lambda_e = \frac{5 n_e k_B^2 T_e}{2 m_e \nu_{eh}}$$

$$= \frac{5 k_B^2 \sigma_e T_e}{2e^2} \qquad (D.14)$$

Taking $n_n \sim 10^{22} m^{-3}$, $\Delta\nu_i \sim 10^{11} sec^{-1}$, $f_i \sim 1$, $\nu_i \sim 10^{15} sec^{-1}$, $T_e = 2000°k$, $\sigma_e = 4 m h_0/m$ and $\beta_e \sim 1$, we find that

$$\frac{\lambda^R}{\lambda_e} \sim 10^{-5}$$

This result shows that, if equations (D.3)-(D.5) and equation (D.13) accurately describe the radiative energy loss from the plasma, the radiative loss term in the electron energy equation can be neglected.

It is interesting to note that the representation of radiative energy loss by equations (D.3)-(D.5), with λ^R given by equation (D.13), is consistent with that used by Uncles[8] who formulated the loss terms by regarding each rectangular cell of a two-dimensional finite difference mesh as a black body radiator, radiating to, and receiving energy from, the four neighbouring cells. Taking equal steps Δ in the x and y directions, Uncles derived an expression for λ^R of the form

$$\lambda^R = \sum_i \frac{2\pi h^2 \nu_i^4 \Delta\nu_i}{c^2 k_B T_e^2} \Delta e^{-h\nu_i/k_B T_e}$$

which is identical to equation (D.13) if the step size Δ is taken to be given by

$$\Delta = \frac{16\,\Delta\nu_i}{a f_i n_n} \qquad \text{(D.15)}$$

so that exact equivalence of the two formulations of the radiative energy loss exists only for one particular line, and if the step size is taken to have the value given by equation (D.15). Taking $n_n \sim 10^{22}\,m^{-3}$, $\Delta\nu_i \sim 10^{11}\,sec^{-1}$, $f_i \sim 1$, equation (D.15) yields $\Delta \sim 10^{-4}\,m$. The length scale defined by equation (D.15) is of the order of the absorption length $L_{AV}^{(i)}$ defined earlier.

REFERENCES

1. Mitchner, M. and Kruger, C.H. Jr.
Partially Ionized Gases, John Wiley, 1973

2. Haines, M.G. and McNab, I.R.
Physics in Technology. Magnetohydrodynamic Power Dynamics, Institute of Physics, vol. 5, 1974

3. McNab, I.R.
Electron Temperature Elevation in an MPD Generator. Ph.D. Thesis, 1974, University of Reading

4. Dvorak, K. and Haines, M.G.
Interim Report on the Experimental Results of the October 1977 Run of the MHD Closed Cycle Facility, IRD 78/45

5. Pei, R.Y. and Hess, R.W.
The Noble-Gas Closed-Cycle System of Magnetohydrodynamic Power Generation. Rand Report R-2128-ERDA, August 1977

6. Haines, M.G., Phil. Trans. Roy. Soc. London, A, vol. 261,44, 1967

7. Nelson, A.H. and Haines, M.G.
"Analysis of the Nature and Growth of Electrothermal Waves".
Plasma Physics 11, 811 (1969)

8. Uncles, R.J.
A Theoretical and Numerical Study of Electrothermal Instabilities and Non-equilibrium Phenomena in a Partially Ionized Plasma.
Ph.D. Thesis, 1972, University of London.

9. Nelson, A.H.
Ph.D. Thesis, 1969, University of London

10. Demetriades, S.T. and Argyropoulos, G.S.
"Ohm's Law in Multicomponent Nonisothermal Plasmas with Temperature and Pressure Gradients". The Physics of Fluids, vol. 9, no. 11, 1966

11. Cebeci, T.
"Calculation of Compressible Turbulent Boundary Layers with Heat and Mass Transfer". AIAA Journal, vol. 9, no. 6, June 1971, pp. 1091-1097

12. Sutton, G.W. and Sherman, A.
Engineering Magnetohydrodynamics. McGraw-Hill, 1965

13. Massey, H.S.W. and Burhop, E.H.S.
Electronic and Ionic Impact Phenomena, Oxford, 1952

14. Argyropoulos, G.S. and Casteel, M.A.
"Tables of Interaction Parameters for Computation of Ohm's Law Coefficients in Various Gases". Journal of Applied Physics, vol. 41, no. 10, 1970

15. Kruger, C.H., Mitchner, M. and Daybelge, U.
"Transport Properties in Partially Ionized Gases". AIAA Journal, vol. 6, p.1712, 1968

16. Cott, D.W.
"Ionizational and Electron Thermal Nonequilibrium in MHD Boundary Layers".AIAA Journal, vol. 9, no. 12, Dec. 1971, pp.2404-2410

17. High, M.D. and Felderman, E.J.
"Turbulent MHD Boundary Layers with Electron Thermal Non-equilibrium and Finite Rate Ionization". AIAA Journal, vol. 10, no. 1, Jan. 1972, pp.98-103

18. Kolb, G.
Proceedings of the 5th International Conference on MHD Electrical Power Generation, 1971, 175-190

19. Vincenti, W.G. and Kruger, C.H.
Introduction to Physical Gas Dynamics, John Wiley, 1965

20. Sears, F.W.
An Introduction to Thermodynamics, the Kinetic Theory of Gases and Statistical Mechanics. Second Edition, Reading (Mass.), Addison-Wesley, 1953

21. Schlichting, H.
Boundary Layer Theory, McGraw-Hill, 1979

22. Shapiro, A.H.
The Dynamics and Thermodynamics of Compressible Fluid Flow, vol. II, Ronald Press, New York, 1954

23. Argyropoulos, G.S., Demetriades, S.T. and Lackner, K.
"Compressible Turbulent Magnetohydrodynamic Boundary Layers". The Physics of Fluids, vol. 11, no. 12, Dec. 1968, pp. 2559-2566

24. Demetriades, S.T., Argyropoulos, G.S. and Maxwell, C.D.
"Progress in Analytical Modeling of MHD Power Generators". Proceedings of the 12th Symposium on the Engineering Aspects of MHD, March 1972

25. Doss, E.D., Dwyer, H.A. and Hoffman, M.A.
"Influence of Segmentation and Ambipolar Diffusion on MHD Nonequilibrium Boundary Layers". AIAA Journal, vol. 12, no. 2, Feb. 1974, pp.155-162

26. Doss, E.D., Argyropoulos, G.S. and Demetriades, S.T.
"Influence of Hall Currents on Flow Separation and Asymmetry in MHD Channels". Proceedings of the 14th Symposium on the Engineering Aspects of MHD, April 1974

27. Uncles, R.J.
"Removal of the Heavily Damped Mode from the Equations of a Partially Ionized Plasma".
Plasma Physics, vol. 16, 1974, pp.947-953

28. Gyftopoulos, E.P. and Levine, J.D.
"Work Function Variation of Metals Coated by Metallic Films".
Journal of Applied Physics, vol. 33, 1962, pp.67-73

Gyftopoulos, E.P. and Levine, J.D.
"Adsorption Physics of Metallic Surfaces Partially Covered by Metallic Particles".

I. Atom and Ion Desorption Energies

II. Desorption Rates of Atoms and Ions

III. Equations of State and Electron Emission S-Curves,
Surface Science, vol. 1, 1964

29. Sajben, M.
"Boundary Conditions for Adsorbing-Emitting Electrodes in Contact with Seeded Dense Plasmas". AIAA Journal, vol. 8, no. 3, March 1970

30. Koester, J.K., Sajben, M. and Zukoski, E.E.
"Analytical and Experimental Studies of Thermionically Emitting Electrodes in Contact with Dense, Seeded Plasmas". Proceedings of the 11th Symposium on the Engineering Aspects of MHD, 1970

31. Keller, H.B.
"A New Difference Scheme for Parabolic Problems". Numerical Solution of Partial Differential Equations, vol. II, edited by J. Bramble, Academic Press, New York, 1970

32. Keller, H.B. and Cebeci, T.
"Accurate Numerical Methods for Boundary-Layer Flows II: Two-dimensional Turbulent Flows". AIAA Journal, vol. 10, no. 9, Sept. 1972

33. Ames, W.F.A.
Numerical Methods for Partial Differential Equations. Nelson, 1969

34. Oliver, D.A.
"The Prediction of Interelectrode Breakdown in Magnetohydrodynamic Generators". 14th Symposium,Engineering Aspects of MHD, 1974

35. Lieberstein, H.M.
Overrelaxation for Nonlinear Elliptic Partial Differential Equations. Tech. Rep. No. MRC-TR-80, University of Wisconsin, Mathematics Research Center, Madison, Wisconsin, 1959

36. Roach, P.J.
Computational Fluid Dynamics, Hermosa, Albuquerque, 1972

37. Lutz, M.A.
"Radiation and Its Effect on the Nonequilibrium Properties of a Seeded Plasma". AIAA Journal, vol. 5, no. 8, 1416, 1967

38. Griem, H.R.
Plasma Spectroscopy, McGraw-Hill, 1964

39. Doss, E.D., Argyropoulos, G.S., Demetriades, S.T.
"Two-dimensional Flow inside MHD Ducts with Transverse Asymmetries". AIAA Journal, vol. 13, no. 5, May 1975, pp.545-546

40. Argyropoulos, G.S., Maxwell, C.D., Doss, E.D. and Demetriades, S.T.
"Results of Numerical Modeling of Some Recent MHD Generator Designs". 13th Symposium Engineering Aspects of MHD, 1973

41. Nelson, A.H.
"Development of the MHD Electrothermal Instability with Boundary Effects". AIAA Journal, vol. 8, no. 10, October 1970, pp. 1753-1759